LOAN DOCUMENT

PHOTOGRAPH THIS SHEET

AD-A283 636

DTIC ACCESSION NUMBER

LEVEL

INVENTORY

WL-TR-92-2022

DOCUMENT IDENTIFICATION

Dec 89

DISTRIBUTION STATEMENT

Approved for public release;
Distribution Unlimited

HANDLE WITH CARE

ACCESSION FOR

NTIS	GRA&I	☑
DTIC	TRAC	☐
UNANNOUNCED		☐
JUSTIFICATION		

BY

DISTRIBUTION/

AVAILABILITY CODES

DISTRIBUTION	AVAILABILITY AND/OR SPECIAL	
A-1		

DISTRIBUTION STAMP

DTIC ELECTE AUG 29 1994 S C D

DATE ACCESSIONED

DTIC QUALITY INSPECTED 1

DATE RETURNED

94 8 16 206

DATE RECEIVED IN DTIC

94-26447

REGISTERED OR CERTIFIED NUMBER

PHOTOGRAPH THIS SHEET AND RETURN TO DTIC-FDAC

DTIC FORM 70A JUN 94

DOCUMENT PROCESSING SHEET

PREVIOUS EDITIONS MAY BE USED UNTIL STOCK IS EXHAUSTED.

LOAN DOCUMENT

WL-TR-92-2022

LASER-BASED DIAGNOSTICS FOR TRANSIENT SPECIES IN HYDROCARBON FLAMES

RICHARD COPELAND

SRI
333 RAVENSWOOD AVE
MENLO PARK CA 94025

DECEMBER 1989

FINAL REPORT

AEROPROPULSION AND POWER DIRECTORATE
WRIGHT LABORATORY
AIR FORCE SYSTEMS COMMAND
WRIGHT PATTERSON AFB OH 45433-7251

NOTICE

When Government drawings, specifications, or other data are used for any purpose other than in connection with a definitely Government-related procurement, the United States Government incurs no responsibility or any obligation whatsoever. The fact that the government may have formulated or in any way supplied the said drawings, specifications, or other data, is not to be regarded by implication, or otherwise in any manner construed, as licensing the holder, or any other person or corporation; or as conveying any rights or permission to manufacture, use, or sell any patented invention that may in any way be related thereto.

This report is releasable to the National Technical Information Service (NTIS). At NTIS, it will be available to the general public, including foreign nations.

This technical report has been reviewed and is approved for publication.

JERRELL M. TURNER
Chief, Advanced Plasma Research Section
Power Components Branch
Aerospace Power Division
Aero Propulsion & Power Directorate

CHARLES W. ANDERSON
Chief, Power Components Branch
Aerospace Power Division
Aero Propulsion & Power Directorate

MICHAEL D. BRAYDICH, Lt Col, USAF
Deputy Chief
Aerospace Power Division

If your address has changed, if you wish to be removed from our mailing list, or if the addressee is no longer employed by your organization please notify WL/POOC-3, WPAFB, OH 45433-7919 to help us maintain a current mailing list.

Copies of this report should not be returned unless return is required by security considerations, contractual obligations, or notice on a specific document.

REPORT DOCUMENTATION PAGE

Form Approved
OMB No. 0704-0188

1a. REPORT SECURITY CLASSIFICATION Unclassified	1b. RESTRICTIVE MARKINGS N/A
2a. SECURITY CLASSIFICATION AUTHORITY N/A	3. DISTRIBUTION / AVAILABILITY OF REPORT Approved for public release, distribution is unlimited.
2b. DECLASSIFICATION / DOWNGRADING SCHEDULE N/A	
4. PERFORMING ORGANIZATION REPORT NUMBER(S) MP 89-219	5. MONITORING ORGANIZATION REPORT NUMBER(S) WL-TR-92-2022
6a. NAME OF PERFORMING ORGANIZATION SRI International 6b. OFFICE SYMBOL (If applicable)	7a. NAME OF MONITORING ORGANIZATION Aero Propulsion and Power Laboratory
6c. ADDRESS (City, State, and ZIP Code) 333 Ravenswood Avenue Menlo Park, CA 94025-3493	7b. ADDRESS (City, State, and ZIP Code) Wright Laboratory Air Force Systems Command Wright Patterson AFB OH 45433
8a. NAME OF FUNDING / SPONSORING ORGANIZATION 8b. OFFICE SYMBOL (If applicable)	9 PROCUREMENT INSTRUMENT IDENTIFICATION NUMBER F33615-86-C-2543
8c. ADDRESS (City, State, and ZIP Code)	10. SOURCE OF FUNDING NUMBERS PROGRAM ELEMENT NO. 61102 / PROJECT NO. 2301 / TASK NO. 51 / WORK UNIT ACCESSION NO. 28

11. TITLE (Include Security Classification)
LASER-BASED DIAGNOSTICS FOR TRANSIENT SPECIES IN HYDROCARBON FLAMES

12. PERSONAL AUTHOR(S)
Copeland, R.A.

13a. TYPE OF REPORT	13b. TIME COVERED	14. DATE OF REPORT (Year, Month, Day)	15. PAGE COUNT
Final	FROM 11/85 TO 11/89	890812	236

16. SUPPLEMENTARY NOTATION

17. COSATI CODES			18. SUBJECT TERMS (Continue on reverse if necessary and identify by block number)
FIELD	GROUP	SUB-GROUP	Laser-Induced Fluorescence, Photoacoustic Spectroscopy, Flames, Combustion, Hydrocarbons
21	2		
7	3		

19. ABSTRACT (Continue on reverse if necessary and identify by block number)

Detection of chemically important transient species is crucial to understanding the mechanism of hydrocarbon combustion. Though they often occur in low concentrations, these species determine the pathways and rates of many reaction steps. In this report we describe our efforts to develop and quantify diagnostic methods to measure these species in flames. We will describe methods to detect CH, CH_3, C_2H_2, CH_2, and HO_2; the first four species have successfully been observed in flames during this project. The detection techniques we use are laser-induced fluorescence (LIF) and absorption techniques including photoacoustic detection spectroscopy (PAD). The polyatomic molecules mentioned above are much more difficult to detect than the diatomic molecules CH and OH, and we have developed and used new variations on the basic techniques to achieve the desired sensitivity. In this research, we improved diagnostic techniques for the radicals mentioned above, detected species not previously observed in the flame environment, and increased our knowledge of the important species in hydrocarbon combustion.

20. DISTRIBUTION / AVAILABILITY OF ABSTRACT ☐ UNCLASSIFIED/UNLIMITED ☐ SAME AS RPT ☐ DTIC USERS	21. ABSTRACT SECURITY CLASSIFICATION Unclassified
22a NAME OF RESPONSIBLE INDIVIDUAL Dr. Sigmund Kizirnis	22b TELEPHONE (Include Area Code) 513-255-2923 / 22c OFFICE SYMBOL WL/POOC

DD Form 1473, JUN 86 Previous editions are obsolete.

CONTENTS

ACKNOWLEDGEMENT

I would like to thank Dave Crosley, Mark Dyer, Nancy Garland, Dave Huestis, Jay Jeffries, Katarina Kohse-Höinghaus, George Raiche, Karen Rensberger, Andy Sappey, Greg Smith, and Michael Wise for their contributions to the success of this project.

INTRODUCTION

Hydrocarbon combustion is the conversion of fuel and oxidant into water and carbon dioxide that produces heat. This simple definition masks the complex chemical reaction mechanism that underlies the macroscopic process. An extremely successful way to characterize this chemical mechanism is to apply species specific diagnostic methods directly to the combustion system of interest. In the past, most optical diagnostic methods have focused on the diatomic molecules, with OH being the most studied; however, much of the important chemistry involves transient species other than OH, some of which contain more than two atoms. In this work, we developed and improved diagnostic techniques to study several mechanistically important diatomic and polyatomic reactive species in hydrocarbon flames. The species selected during the early phases of this project (Contract No. F33605-85-C-2543) were chosen for their importance in the combustion chemistry and the feasibility of detecting them in the combustion environment. We investigated the species CH, CH_3, CH_2, and C_2H_2 and attempted to detect HO_2.

DETAILED COMBUSTION CHEMISTRY

Detailed chemical kinetic processes play an important role in many aspects of the hydrocarbon/air combustion in gas turbine engines. Among these processes are the formation of pollutants such as soot (with its associated radiative heat transfer problems) and NO_x, ignition (both cold starts and high-altitude relight), lean burnout, and the formation of exhaust plume emissions in the ultraviolet and visible light regions.

Although such processes are complex, involving dozens of molecular species and perhaps hundreds of reactions, they can be investigated by means of computer models if one has some insight into the relevant, important species and reactions (i.e., the crucial chemical pathways) that govern the processes in question. Such computer models have been constructed, but their accuracy is largely gauged by how well their results match experimental data on such bulk properties as flame speed, combustion efficiency, temperature, and formation of major stable products.

The key to a correct description of the chemical pathways for kinetically controlled processes lies in an *in situ*, direct identification of the transient intermediate species that are formed and consumed as a result of those reactions. Development of quantitative and

semiquantitative methods for the measurement and detection of such species is of primary importance. These methods can then be used for several purposes: determination of the needed reaction rate constants in controlled laboratory experiments; measurements on stable, laminar laboratory flames that provide a direct comparison with the computer model; and detection of important species in real-system flames. Detection of species in real-system flames will yield insight into the actual chemical mechanism operating in these systems and provide a crucial link to the laboratory experiments.

SELECTION OF DIAGNOSTIC METHODS

Many diagnostic techniques have been applied to the detection of transient species in the combustion environment. These include mass spectroscopic sampling, laser-induced fluorescence (LIF), scattering methods (Raman processes), direct absorption, and ionization methods.[1] The criteria we choose to apply are that the diagnostic techniques be strictly nonintrusive (i.e., no probe inserted into the flame) and sensitive enough to detect transient species in low concentrations. In the early stages of the project, we decided to emphasize LIF, mainly because of its inherent high sensitivity, and direct absorption techniques including photoacoustic (PAD) and photodeflection detection, because of their applicability to a wide range of transient species. These two methods are complementary in that LIF is not applicable to all species but is sensitive and selective, while absorption is less sensitive but applicable to many of the species that cannot be studied by LIF.

SELECTION OF SPECIES

Several criteria must be considered in choosing what hydrocarbon species to examine in detail: the species' ease of detection, concentration in the flame, and chemical significance. The selection process often involves trade-offs. The hydroxyl radical is one of the few that meets all the criteria. The choice of species was an important part of our research. The species selected as both chemically important and feasible for detection include CH, CH_3, C_2H_2, CH_2, and HO_2. C_3, C_2H, and HCO are less important or more difficult to detect. Almost all of these radical intermediates offer some potential for a laser-based method of detection; our successes and failures with these species and the specific reasons for selection of these species are discussed in the section entitled The Species.

THE TECHNIQUES

Several of the techniques briefly outlined below were considered for application to radical detection, and two were chosen for further study. This section describes why LIF and absorption were selected as complementary techniques for measuring the concentration of a wide variety of chemically important radicals.

LASER-INDUCED FLUORESCENCE (LIF)

LIF is an extremely sensitive method that can be applied to a wide variety of transient species in the flame.[2] Briefly, laser light excites the species to an electronic state that fluoresces. The basic procedure has many variations; where applicable, these are discussed below with the experiments on individual radicals.

Diatomic radicals such as OH, CH, CN, and NH with easily accessible electronic states can be observed in extremely low concentrations (i.e., <1 ppb for OH in a flame). In addition to the diatomic radicals, several chemically important polyatomic radicals had been observed before this project; for example, our laboratory had examined both NCO and NH_2 by LIF.[3] LIF is much more sensitive than other techniques and twice as molecule selective as most. Selectivity is obtained by varying both the excitation wavelength and the detection wavelength.[3] LIF is often the benchmark used for comparing other techniques, and LIF must be considered as one of the detection options in any detailed investigation of flame species.

For OH and most other diatomic radicals, the dual selectivity of LIF is merely convenient and increases the absolute detection sensitivity; however, for many polyatomic species it is an important advantage of the technique because in many instances there are strong overlapping transitions with other species or other vibrational "hot" bands of the same molecule in the excitation region of interest. For example, in our laboratory demonstration of NCO detection using the B electronic state in a CH_4/N_2O atmospheric pressure flame,[4] overlapping transitions from OH, NH, and CN all occurred in the same excitation wavelength region when we tried to observe the NCO. The only way we could selectively detect the molecules was by using the selectivity of the fluorescence wavelength to isolate one absorption from another; we were thus able to obtain interference-free excitation scans of OH, NH, CN, and NCO.

Other advantages of LIF are that its pointwise measurement provides better spatial resolution than most absorption methods and that it has the sensitivity necessary for single-shot measurements in turbulent systems. Single-shot LIF imaging is an important technique first developed in this laboratory.[5] All these properties make LIF a very good candidate for examining a number of species with optically accessible electronic states that fluoresce (for example, CH).

Although LIF is an extremely valuable tool, like all other analytical techniques it presents several experimental problems when one is trying to make the measurements quantitative. Making accurate quantitative measurements requires information on the quenching and lifetimes of the excited electronic state in the flame environment[6]; that is, the composition of the majority species must be well known and the quenching rates must be known or estimated at the temperature of interest. Such quenching rates and radiative lifetimes can be measured by experimental methods available in our laboratory. Recently, we have conducted extensive experiments to determine these properties for many flame radicals, such as OH,[7] NH,[8] and CH_3O.[9]

DIRECT ABSORPTION METHODS

Laser absorption detection techniques comprise several very different methods. The differences arise from the different ways the absorption is detected. In conventional absorption experiments, the decrease in the intensity of the light is monitored as the light passes through the absorbing flame. The major disadvantages of this technique are that the signal is usually small on a large background and thus sensitivity is limited, and that it is a line-of-sight measurement, so the spatial resolution is limited. The major advantage is that if the spectroscopic positions and oscillator strengths of the molecular transitions are known, absolute quantitative calibration is usually straightforward. Although conventional laser absorption is not sensitive enough for most molecules in this study, under some advantageous conditions it can be applied to transient species.

Two other absorption detection methods, photoacoustic (PAD)[10] and photo-deflection[11] spectroscopy, have recently been applied as combustion diagnostic techniques. Two spatially separated beams, the excitation beam and the probe beam, are used in photodeflection spectroscopy. When the excitation beam is resonant with an absorption in the system, a pressure wave is produced that deflects the probe beam. This deflection is in turn measured. In PAD spectroscopy only one laser is used, and when it is resonant with an absorption in the system, energy is put into the flame. The added energy produces a pressure burst that is detected on a microphone outside the flame.

Neither of these techniques has yet demonstrated a sensitivity equal to that of LIF, but they have been and will continue to be extremely useful for studying molecules that have a low fluorescence yield. The lack of spatial selectivity and molecule emission selectivity are two disadvantages of these absorption techniques. In regions of highly overlapping absorption bands from several species or from "hot" bands of the same molecule, it may be difficult to obtain the molecule selectivity needed to obtain a profile of the species of interest. A narrow laser bandwidth and extremely detailed spectroscopic information on all the molecules that absorb in the region of interest are necessary to associate different features with different molecules. These difficulties are more limiting in the detection of triatomic or larger molecules.

OTHER METHODS

Several other experimental methods were considered during the early phases of this project. These include resonance-enhanced multiphoton ionization (REMPI); Raman processes, including coherent anti-Stokes Raman spectroscopy (CARS) and resonant Raman techniques; and mass spectometric sampling (MS). Neither MS nor REMPI were applied because they require the insertion of a sampling probe into or near the combustion environment. If the probe perturbs the flame there is always a possibility that the concentration measurements are biased, and the environment is often so hostile that the probe could not withstand the extreme temperatures and conditions.

Raman techniques are not usually sensitive enough to detect trace species. They have been applied extensively and with great success to the major species; however, many of the chemically important trace species occur at much lower concentrations.

THE SPECIES

SELECTION OF THE SPECIES

Selection of the species to be studied was based on two critera: (1) the species' importance in the chemistry of hydrocarbon combustion and (2) the feasibility of detecting that species by the remote diagnostics described above. We determined the importance of various species by modelling the chemical mechanism of hydrocarbon combustion with a constant temperature kinetic model that included the important species. We determined the feasibility of detection by examining the available literature on spectroscopy of the molecules of interest.

We used an isothermal model of hydrocarbon/air combustion to evaluate the important intermediates and to determine which detection methods could be used in the combustion environment. The model, which consists of about 150 reactions and 30 species, incorporates a temperature jump to start the reaction. The time evolution of all the species can be monitored as the reaction proceeds. This time corresponds roughly to distance above the burner in a low-pressure flame. This model, while not quantitively correct, simulates the qualitative features of the reaction system. Figure 1 shows the time dependence of several potentially important species in the combustion. Figure 1(a) gives the predicted time evolution of the single-carbon species CH_4, CH_3, CH_2, CH, C, and CO at 2200 K and 40 Torr as well as stoichiometric initial conditions for the methane and oxygen mixture. This figure clearly shows that the CH_x radicals have very different profiles before they encounter the flame front and that the CH profile is significantly different from those of CH_2 and CH_3. Unfortunately, this difference implies that the CHconcentration cannot be used as a marker for CH_2 and CH_3; therefore, measurement of CH_3 and CH_2 concentrations takes on added significance. The methyl radical (CH_3) is one of the first species formed and is present in relatively high concentrations. Figure 1(b) shows several other species (HO_2, C_2H_2, HCO, C_2H, and C_3) under the same initial conditions. The HO_2 radical exhibits one of the more interesting profiles; it builds up

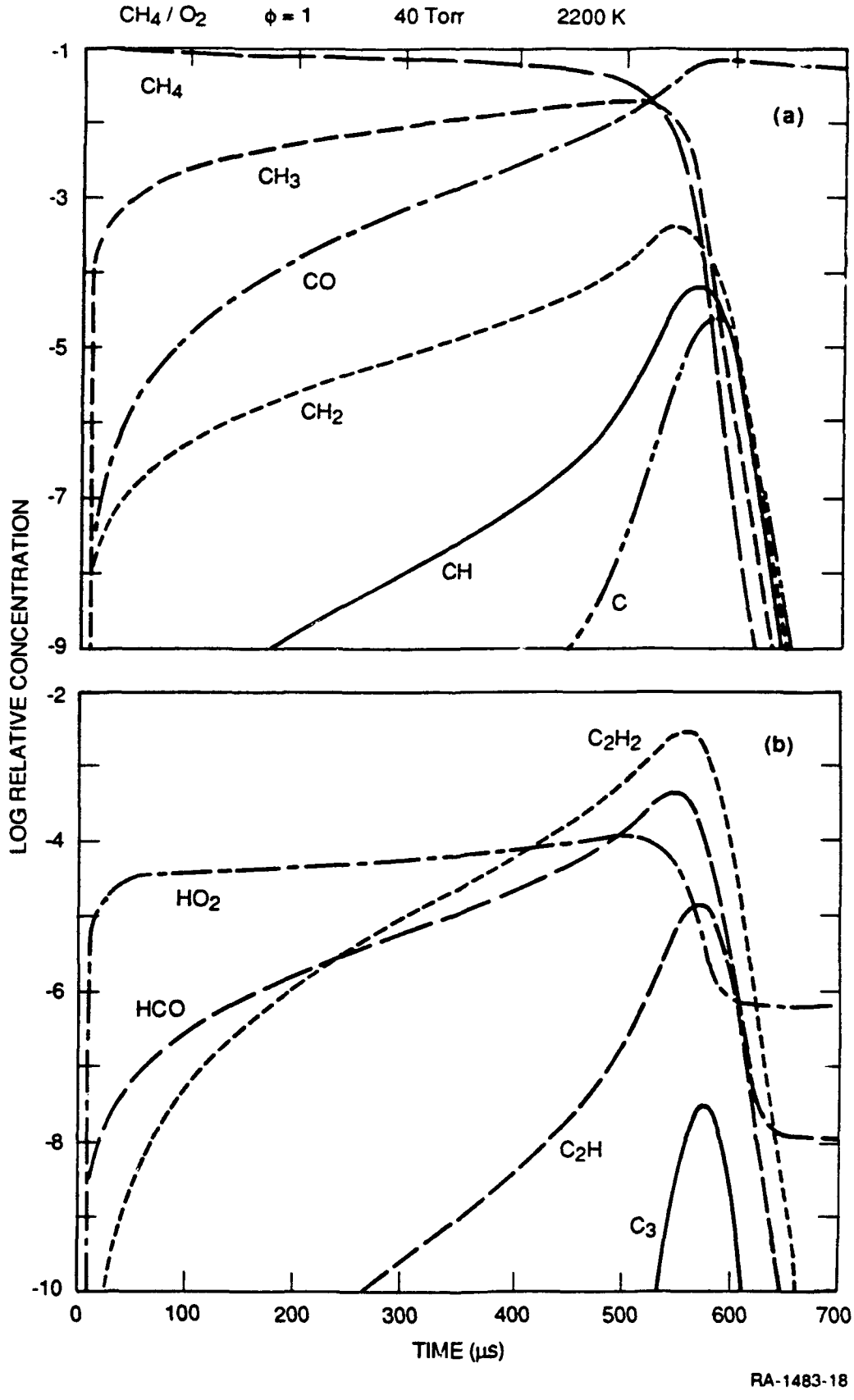

Figure 1. Model results for methane and oxygen combustion.

rapidly after the temperature jump and remains constant for a long time. Acetylene (C_2H_2) starts out at low concentrations, builds up slowly, and eventually reaches a relatively large concentration before it is abruptly consumed in the later stages of combustion.

From the model shown in Figure 1 and other models for other fuels and other temperatures, we selected the following five species for further study: CH, C_2H_2, CH_3, HO_2, and CH_2. We have attempted experiments on all five of these species and have successfully observed four in combustion systems. The reasons for selection of these species are detailed below in the sections describing the experiments performed on them. We considered detection of the species HCO, C_2H, and C_3 less feasible, less desirable, or both. As Figure 1(b) shows, the C_3 radical is present in extremely low concentrations and does not seem very important in the chemistry. On the other hand, the HCO radical is important in the production of ions in the flame, but the difficulty of using fluorescence methods to measure its concentration made its detection less feasible. The same problem exists for the C_2H radical. The literature contains insufficient spectroscopic data for evaluating whether detection of either HCO or C_2H is indeed possible. We believe detection of the two important radicals HCO and C_2H by LIF or absorption methods is several years in the future and will require futher basic studies. Investigations of some of these species by REMPI detection in flames are under way in other laboratories.[12,13]

CH

Studies on the CH radical formed a large part of the experimental work on this project, and all work on this radical is complete and published. This project has increased our knowledge of the collison dynamics of this species under combustion conditions to the extent that we can now make reasonable estimates for the fluorescence quantum yield under a variety of experimental conditions.

Although present in small concentrations, the CH radical can be observed in all hydrocarbon combustion. Its precise role in the combustion chemistry remains uncertain, largely because we do not yet know its reaction rate constants at high temperatures. Although the importance of the CH radical in the chemistry of combustion has not been verified, CH emission and LIF are often used to identify regions where combustion is occurring. CH concentration profiles are measured by absorption, saturated LIF, and REMPI techniques. Two-dimensional LIF imaging of CH has also been performed and undoubtedly will be applied to practical combustion systems in the future. The CH radical is a significant precursor in the emission from flames and therefore plays an important role in the plume emissions from rockets with carbon-containing fuels.

Room-Temperature Flow Cell Experiments

The CH experiments began with a brief study of CH collision dynamics in a room-temperature flow cell. We attempted to measure the collisional quenching rate constant for removal of the radical from the excited electronic state.

In a standard LIF experiment, a molecule is excited from the ground electronic state to the vibrational and rotational level of a higher lying electronic state. This excited molecule can either (1) radiate light, (2) undergo a collision and be removed without radiation in a process called quenching, or (3) undergo an energy transfer collision within the excited electronic state to another vibrational or rotational level. The competition between radiation and the collisional quenching processes determines the fluorescence quantum yield. If small effects due to the vibrational and rotational structure are neglected, the time dependence of the population in the excited electronic state N(t) is given by

$$N(t) = N_0 \exp\{-[\Sigma k_Q n_i + A]t\} \quad (1)$$

where N_0 is the population in the excited electronic state after the laser pulse, $k_Q(i)$ is the collisional quenching rate constant for species i, n_i is the concentration of species i, A is the Einstein spontaneous emission coefficient for the excited electronic state, and t is time. The LIF signal is proportional to N(t), so that a single exponential fit to the decay of the signal yields a decay constant τ^{-1} as given by

$$\tau^{-1} = \Sigma k_Q n_i + A \quad (2)$$

If the concentration of only one species is changed, a plot of the concentration of that species yields the quenching rate constant k_Q and the intercept of A plus the contributions from the other species. Often these contributions are small and the y-intercept corresponds only to A, which is the inverse of the radiative lifetime, τ_r. Under combustion conditions, a critical parameter is the fluorescence quantum yield, ϕ, given by

$$\phi = A\tau \quad (3)$$

ϕ is equal to 1 if the collisional quenching is negligible and approaches 0 as the collisional quenching begins to dominate.

In the room-temperature CH apparatus, the ground state radicals were generated from the sequential extraction of H atoms from CH_4 by microwave discharge generated

fluorine atoms. This is not a one-step process and must proceed through the reaction intermediates CH_3 and CH_2. This reaction took place in a flowing system with a typical total flow rate between 0.5 and 10 L/min. The total pressure in the system ranged from 2 to 10 Torr, with the majority of the gases being either He or Ar. Both of these rare gas species are inefficient at quenching A-state CH. With no other added gas, this source generated copious amounts of ground state CH. Light with a wavelength of about 440 nm from an excimer-pumped dye laser excited the CH molecules from the ground state to the $A^2\Delta$ excited electronic state. The fluorescence was monitored at right angles by an unfiltered phototube. We recorded the time dependence of the LIF with a 100-megasample transient digitizer. We added the various quencher species to the discharge flow of CH radicals, taking care that the added species were well mixed with the other discharge gases by the time the gases reached the observation region. Calibrated mass flow meters were used to measure the flow of the individual components so that we could obtain the partial pressures of each species.

Unfortunately, the CH LIF signal decreased significantly when we added only a small amount of quencher. With the quenchers H_2 and CO_2, we could not observe any change in the fluorescence lifetime before the CH signal disappeared completely. We believe the rapid disappearance of the CH LIF signal was due to rapid reaction of the ground state CH radicals with the quenchers or with one of the CH precursors during the long time required for thorough mixing of the species. These chemical reactions consume the ground state CH between the CH_4 injection site and the observation region. With the CO quencher, we observed changes in the CH fluorescence lifetime with added CO pressure and therefore attempted to shorten the distance between the CH production portion of the cell and the observation region. This procedure successfully increased the range of usable quencher pressures for CO, but the quenching rate constants and cross sections obtained using different flow and discharge configurations gave inconsistent results. The cross sections we obtained varied between about 3 and 16 $Å^2$ depending on the total flow rate, method of production of CH, and total pressure in the system. We believe this variation is due to poor mixing of the quencher with the bulk gas, reactions producing molecules that quench CH more rapidly than the quencher itself, or both. Both these experimental difficulties complicate the interpretation of the results of this technique.

The two major findings of the CH quenching work in room-temperature flow cells are that the quenching results for the CO collider are consistent with those of an earlier study of Nokes and Donovan,[14] and the quenching by CO_2 is smaller than 2 $Å^2$. Previous results of both room-temperature and high-temperature (1400 K) quenching are summarized in Reference 15.

Because of the importance of the flame measurements, we decided to proceed to time dependent measurements in a low-pressure flame. We feel that laser photodissociation is the best technique for measuring these quantities for CH at room temperature. Here, light from an excimer laser photodissociates a suitable precursor and then, after a variable delay, the CH quenching is measured with LIF. This method permits experiments to be performed with higher quencher pressures so that greater changes in the fluorescence decay constant can be observed. The photodissociation production mechanism has two important improvements over the setup described above. First, the quencher is thoroughly mixed with the radical precursor and the bulk gas, so the mixing problems encountered with the discharge flow production of CH are eliminated. Second, with laser photodissociation, the CH radicals are probed microseconds after their production, whereas the radicals in the discharge flow are probed milliseconds after production, during which time most of the ground state radicals are consumed by chemical reactions. CH quenching in the ground state can be measured by laser photodissociation; however, from a diagnostics perspective, the results are less important than initially anticipated.

Low-Pressure Flame Measurements

Although LIF measurements obtained by exciting the $A^2\Delta$ electronic state are commonplace, quantitative concentration measurements require knowledge of the fluorescence quantum yield, which depends on both the radiative and collisional processes that occur after electronic excitation.[15] Before our studies, little was known about collisional processes such as quenching (the total removal from the excited electronic state, which includes both reaction and energy transfer processes that change the CH electronic state) and rotational level specific processes at flame temperatures. Also, very little work had been performed on the $B^2\Sigma^-$ electronic state either at room temperature or in flames. We find that LIF measurement of the $B^2\Sigma^-$ state is an alternative detection method with sensitivity comparable to LIF measurement of the A state.

We examined the collisional energy transfer in the $A^2\Delta$ and $B^2\Sigma^-$ states of CH by directly measuring the time dependence of the LIF in several low-pressure, premixed flat flames. From direct observation of the fluorescence decay, we measured the fluorescence quantum yields needed for quantitative CH measurements and estimated limits on the collisional quenching rate constants for several key colliders. Both the concentrations of the major species and the temperature vary across the flame front in the combustion environment; these variations can alter the observed decay and change the fluorescence quantum yield. A quantitative understanding of the collisional quenching of CH by various

species in the flame permits extension of these measurements to flames where the time dependence cannot be observed, for example, as in high-pressure turbulent-flow systems.

Rotational level effects of quenching in the flames were also examined. In recent state-specific, room-temperature, flow cell studies of two simple hydrides, $OH(A^2\Sigma^+)$ and $NH(A^3\Pi_i)$, most colliders showed a significant decrease in the electronic quenching rate with increasing rotational level in the excited state.[16,17] To examine this relationship further, we evaluated the quantum state selectivity of the fluorescence quantum yield for different excited rotational levels and assessed its effect on LIF diagnostics at high temperatures. We found a small but measurable decrease in the quenching rate constants as the rotational quantum number increased in several flames.

We also examined the electronic-to-electronic energy transfer from the B-state of CH to the A-state. This nearly isoenergetic transfer has been observed in atmospheric pressure flames. From detailed position dependence studies on the signal, we found the signal could be used as a sensitive, versatile diagnostic tool, especially in particulate laden systems that generate scattered laser light at the excitation wavelengths.

The foregoing paragraphs briefly summarize the results on CH. With the information we have gained on CH fluorescence quantum yields in both the A- and B-states, accurate estimates of the fluorescence quantum yields are a reality. The results of this study are described in detail in publications resulting from this contract, which are included as appendices A through D and F.

C_2H_2

Although C_2H_2 (acetylene) is a stable species, it is an important intermediate in hydrocarbon combustion. Acetylene is considered a possible precursor in soot formation and production of higher hydrocarbons in methane combustion. It can also serve as a prototypical polyatomic molecule with which we can improve new methods. We have detected C_2H_2 in room-temperature and heated flows by means of both PAD in the infrared portion of the spectrum and LIF in the ultraviolet portion. In addition, the ultraviolet LIF method has proved successful in monitoring the decay of the C_2H_2 concentration in low-pressure flames.

Infrared PAD Studies

During the early part of this project, we examined pulsed photoacoustic detection of C_2H_2. Acetylene was selected as a good candidate for these initial PAD studies because of its absorption bands in the 9600 cm^{-1} region, where H_2O does not interfere at room temperature or high temperatures, as described below in the HO_2 section. C_2H_2 is also a

stable species that can be studied at high concentrations without elaborate preparations. We examined the C_2H_2 spectra at room temperature and elevated temperatures and in an atmospheric pressure flame.

In the experimental investigation of C_2H_2, we generated near-infrared radiation between 8400 and 12,700 cm^{-1} with a Nd:YAG-pumped dye laser. The fundamental dye output was focused into a high-pressure hydrogen cell, and the first or second Stokes stimulated Raman emission was collimated and separated from the other orders with a Pellin-Broca prism. The infrared beam, with a pulse of approximately 0.5 to 5 mJ, was then directed through a slowly flowing source of acetylene (at ~760 Torr) from the end of a 1/8"-I.D. tube. A Bruel & Kjaer type 4138 microphone was positioned 5 mm away from and orthogonal to the propagating laser beam and the flowing stream of C_2H_2. The microphone output was amplified and filtered through a Tektronix differential amplifier and sent into a PAR boxcar averager. Examples of the signal as a function of excitation wavelength are shown in Figure 2. The signal that is strongest and least complicated by possible overlapping H_2O bands is that near 9650 cm^{-1} (shown in the top panel of the figure). Figure 2 shows that C_2H_2 absorbs throughout the infrared in characteristic vibrational overtone bands. Many other molecules (for example, CH_4 and C_2H_6) also absorb light in this region and produce photoacoustic signals, and often these species can interfere. Therefore, one must have a good understanding of the spectroscopy and interference at room temperature and above.

To study acetylene at temperatures between room and flame temperatures, we constructed an atmospheric pressure, resistively heated, quartz-jacketed flow tube with a shroud of nitrogen surrounding the exit orifice for the heated C_2H_2. Using thermocouples positioned precisely at the point of C_2H_2-laser intersection, we achieved regulated temperatures as high as 900 K. We then performed several frequency scans on the $0030^00^0 \leftarrow 0000^00^0$ transition in C_2H_2 at temperatures ranging from 300 K to 900 K. The series of spectra in Figure 3 shows the striking differences in the rotational structure and signal intensity for higher temperatures and demonstrates why this particular acetylene band will be difficult to detect in a flame, where temperatures are higher and species

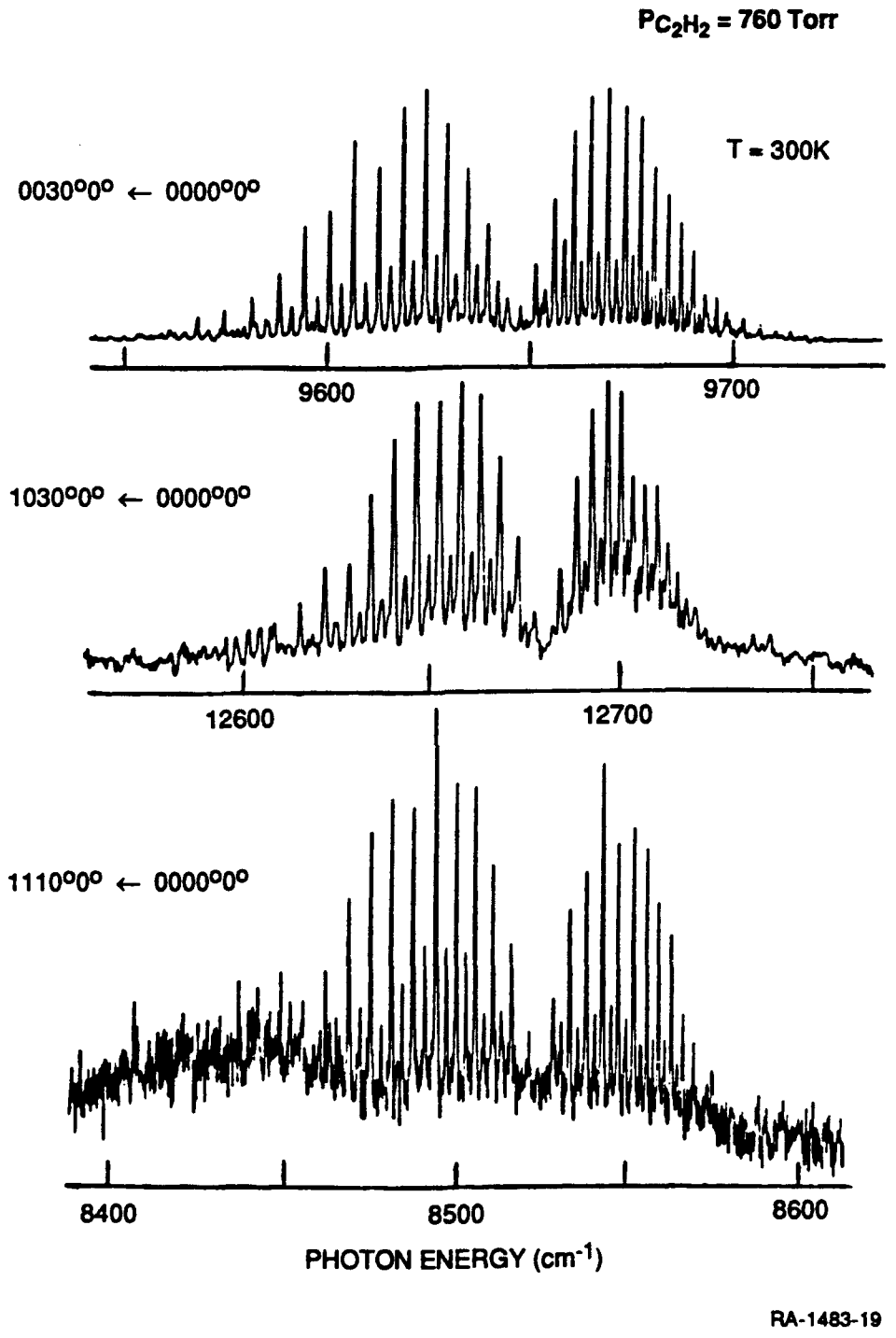

Figure 2. C_2H_2 PAD signal in the infrared.

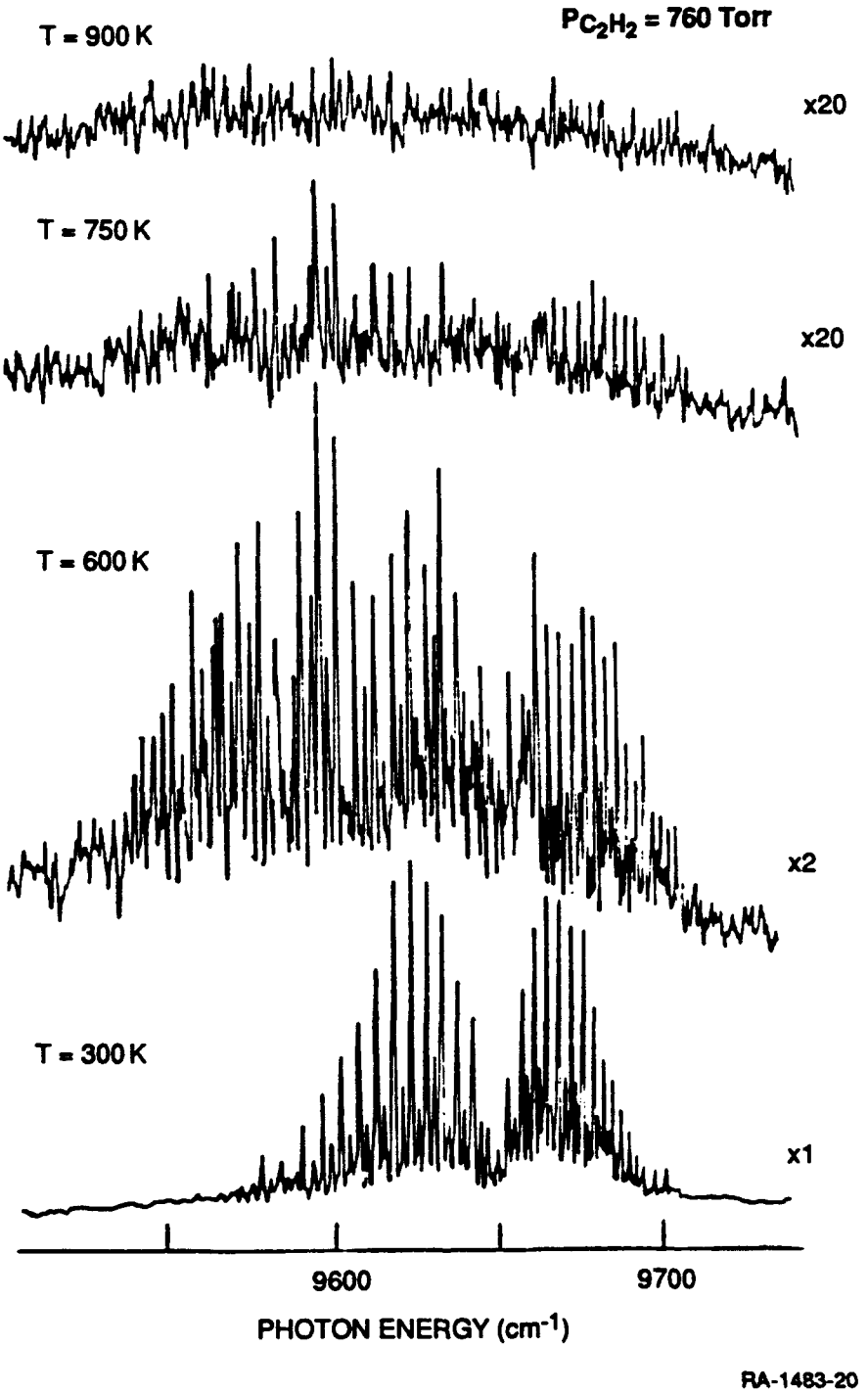

Figure 3. C_2H_2 PAD signal as a function of temperature.

TABLE 1

PERCENT OF THE MOLECULES IN THE GROUND VIBRATIONAL STATE AS A FUNCTION OF TEMPERATURE

T (K)	CH (%)	$C_2 H_2$ (%)
300	100	84
500	100	53
1000	98	13
1500	93	4
2000	86	1
2500	79	<1

concentrations lower. The temperature dependence of the C_2H_2 spectra is puzzling. With increasing temperature, the C_2H_2 signal decreased in magnitude and increased in complexity. The signal dropped by two orders of magnitude in going from 300 K (bottom panel) to 900 K (top panel). The increase in spectral congestion can be attributed to the population of vibrationally excited modes and the increased number of rotational levels populated. Table 1 shows the effect of temperature on the fractional population of the ground vibrational state of acetylene. Using the results in Table 1 and a simple calculation based on the rotational partition function, we estimate that the C_2H_2 signal decreases by about an order of magnitude on a representative rotational line as a result of this effect. The additional order-of-magnitude decrease must be due to either decomposition of the C_2H_2 in the heating region (which is significantly hotter than the exit temperature of 900 K) or some as yet uncharacterized process.

We made several attempts to detect acetylene in atmospheric pressure flames by PAD near 9600 cm^{-1}. Initially, an acetylene/oxygen flame burning on a glass blower torch was probed for C_2H_2. In the midst of significant acoustical background noise from the nozzle, we discovered a broad, apparently nonresonant photoacoustic signal that mimicked the dye laser energy in signal intensity, but there was no evidence of the strong acetylene band. This background signal persisted throughout and above the reaction zone but fell off in intensity well into the section containing burnt gases. The lack of identifiable structure in this type of flame compelled us to try a slot burner, which would allow a longer irradiated path, create almost negligible amounts of "nozzle" noise, and give somewhat more distinct flame zones than the conical plume produced by the acetylene torch. The flame zones from the slot burner could be clearly intersected by a focused laser beam.

The search for C_2H_2 recommenced in a methane/oxygen/nitrogen flame, but when no discernible peaks emerged above the noise, we seeded the flame with small amounts of acetylene. In the spectral scan of the C_2H_2-doped flame, we observed some low-level but distinct structures that somewhat resembled the C_2H_2 data at ambient temperature and pressure; however, these structures only appeared low in the rather thin reaction zone, and we feel they could be attributed to overlap of the laser beam with heated, unburnt acetylene in the premixed gases just below the reaction zone. The lack of adequate flame zone resolution in atmospheric flames and our failure to conclusively detect any notable acetylene features in various flames and flame regions indicated that, at least in high-pressure flame, PAD was probably not the method of choice for C_2H_2 detection. C_2H_2 was detected unambiguously only in the low-pressure burner system.

Ultraviolet LIF Studies at Room Temperature

Currently, the ultraviolet LIF method described below appears the most promising for sensitive and selective detection of C_2H_2. Before discussing the method itself, we will summarize the pertinent spectroscopic parameters. Acetylene absorbs light of specific wavelengths between 247 and 205 nm. These absorptions correspond to vibrational bands in the $\tilde{A}$ - $\tilde{X}$ electronic transition.[18,19] Although these bands are spectroscopically complex, they can be rotationally assigned; they exhibit a characteristic "fingerprint" for C_2H_2. Acetylene is linear in the ground electronic state and bent in the $\tilde{A}$-state. This geometry change causes long progressions in the vibrational bands, and the fluorescence is observed at wavelengths to the red of the excitation laser light.

We performed several experiments in a room-temperature flow cell or in the low-pressure burner without the flame in operation. The geometry was the same as for other LIF experiments; the fluorescence was imaged at right angles by a two-lens system onto the slits of a 0.3-m monochromator. Figure 4 shows a typical scan of C_2H_2 LIF as the excitation laser is scanned between 215.63 and 216.63 nm. The signal-to-noise ratio is extremely high, with the inset showing a small portion of the excitation spectrum slightly to the blue of the strong feature that can be attributed to the R-head of the ($v_3' = 4$, $K_a' = 1$) - ($v_4'' = 0$, $\ell_4'' = 0$) Π_u - Σ_g^+ subband (labeled $V_0^4 K_0^1$). This figure illustrates the complexity of the excitation features in this region, but in spite of the complexity, all the rotational transitions can be attributed to acetylene.[18] Vibrational bands similar to this are found throughout the ultraviolet. Thus far we have observed features between 210 and 230 nm.

The most surprising result occurred when we resolved the fluorescence. We observed extremely intense emission from C_2 after excitation of the A-state of C_2H_2. Figure 5 shows this strong fluorescence for excitation at ~215.9 nm in the V_0^4 K_0^1 band (see Figure 4). The top panel of Figure 5 shows the spectrum from 200 to 700 nm uncorrected for monochromator response, and the bottom panel shows a region between 250 and 350 nm that can be attributed to LIF from the A-state of C_2H_2 itself. To our surprise, when we looked into the cell containing the C_2H_2 with the laser beam going though, a green fluorescence corresponding to the C_2 emission was visible. This observation raises the question of how this electronically excited C_2 is being produced and suggests that C_2 production may be an extremely sensitive method of C_2H_2 detection. There are two obvious possibilities. Electronically excited C_2 could be the product of a chemical reaction, or it could be produced in a photophysical process by the laser itself. The pressure and power dependence of the various signals should reveal which process is the most important.

Before proceeding, we must comment on the origin of the C_2 emission. The largest features in the fluorescence spectrum, those at 430, 480, 520, and 560 nm, can be attributed to the $d^3\Pi_g$-$a^3\Pi_u$ Swan system. The spectrum clearly shows that many different vibrational levels are populated. The $C^1\Pi_g$-$A^1\Pi_u$ Deslandres-d'Azambuja system (DAS), with the Δv = -1, 0, and +1 progressions at 415, 380, and 360 nm, respectively, is also present. The Swan system is a triplet system, and the DAS system corresponds to singlet C_2. Because the C_2 emission occurs only when the laser is resonant with an acetylene transition in the low-pressure flow cell, the emission is probably not the result of an impurity in the acetylene. We have excited different bands in C_2H_2 and find that the vibrational structure in the Swan system does not change significantly but the vibrational structure in the higher energy DAS system is more sensitive to the energy of the excitation photon.

Other experiments examining the time dependence of the laser-induced C_2 emission as a function of pressure indicate that the emission is produced promptly during the laser pulse rather than from a reaction with a photodissociation product. Figure 6 is an example of the data showing the time dependence of the fluorescence at different wavelengths. We observed either the Swan, DAS, or C_2H_2 LIF itself. The zero pressure intercepts correspond to previously measured radiative lifetimes. The quenching rate constants obtained from the slopes of the lines are noticeably different. The Swan system is removed most slowly by added C_2H_2, which makes the Swan system a very promising candidate for detection of C_2H_2 at higher pressures; both the DAS system and C_2H_2 LIF are quenched much more rapidly. Such behavior with pressure must be taken into account in designing the best method for detecting C_2H_2 at atmospheric pressure. Quantitative aspects of these data are presented in appendices H, J, and K.

To understand the photophysics, we also examined the signal as a function of laser power for the different emissions, as shown in Figure 7. As expected, the C_2H_2 LIF has about a first-order correspondence with laser power, and the emissions from C_2 are of higher order. The slope of the C_2 line is about 2; this indicates that at least two photons are needed to reach the excited state.

Low-Pressure Flame Studies

Using the information obtained in the room-temperature studies described above, we set out to measure signals characteristic of C_2H_2 in several low-pressure flames. This search is complicated by the large number of species generated during the combustion.

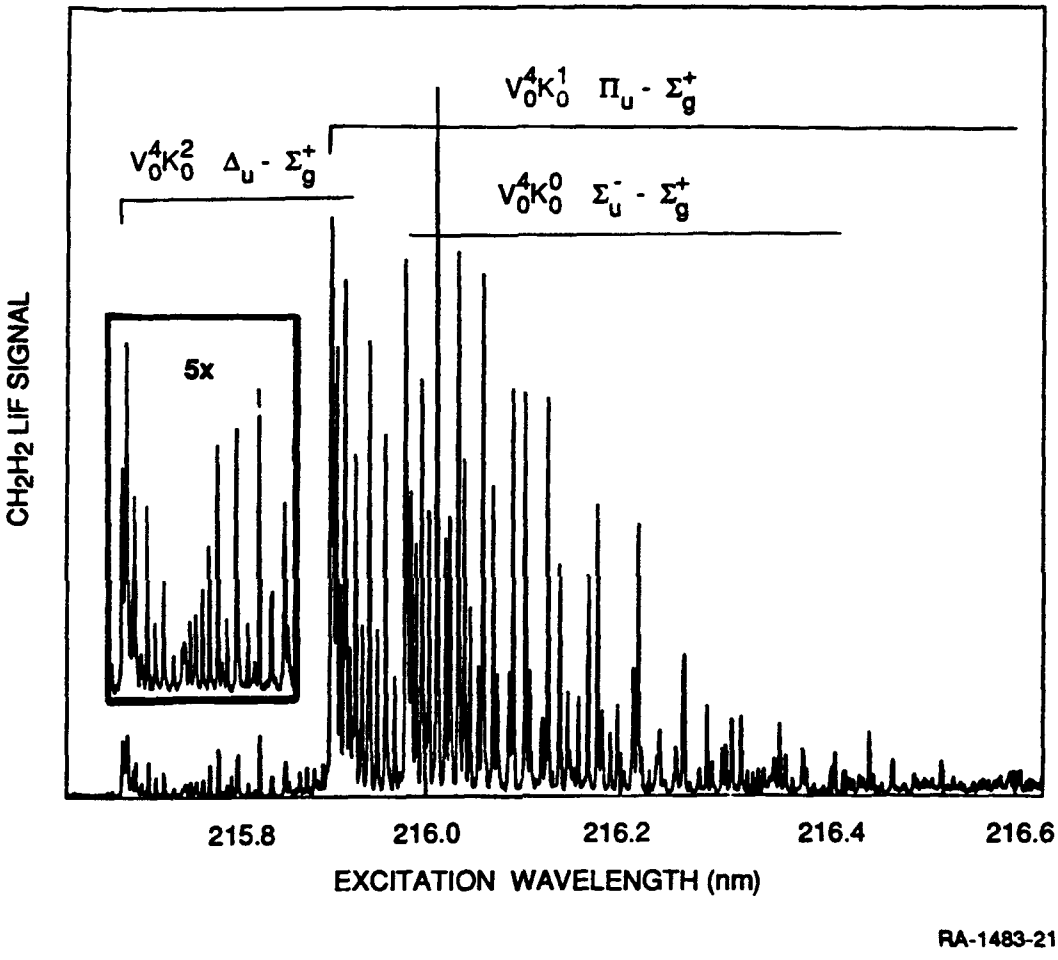

Figure 4. C_2H_2 LiF signal in the ultraviolet.

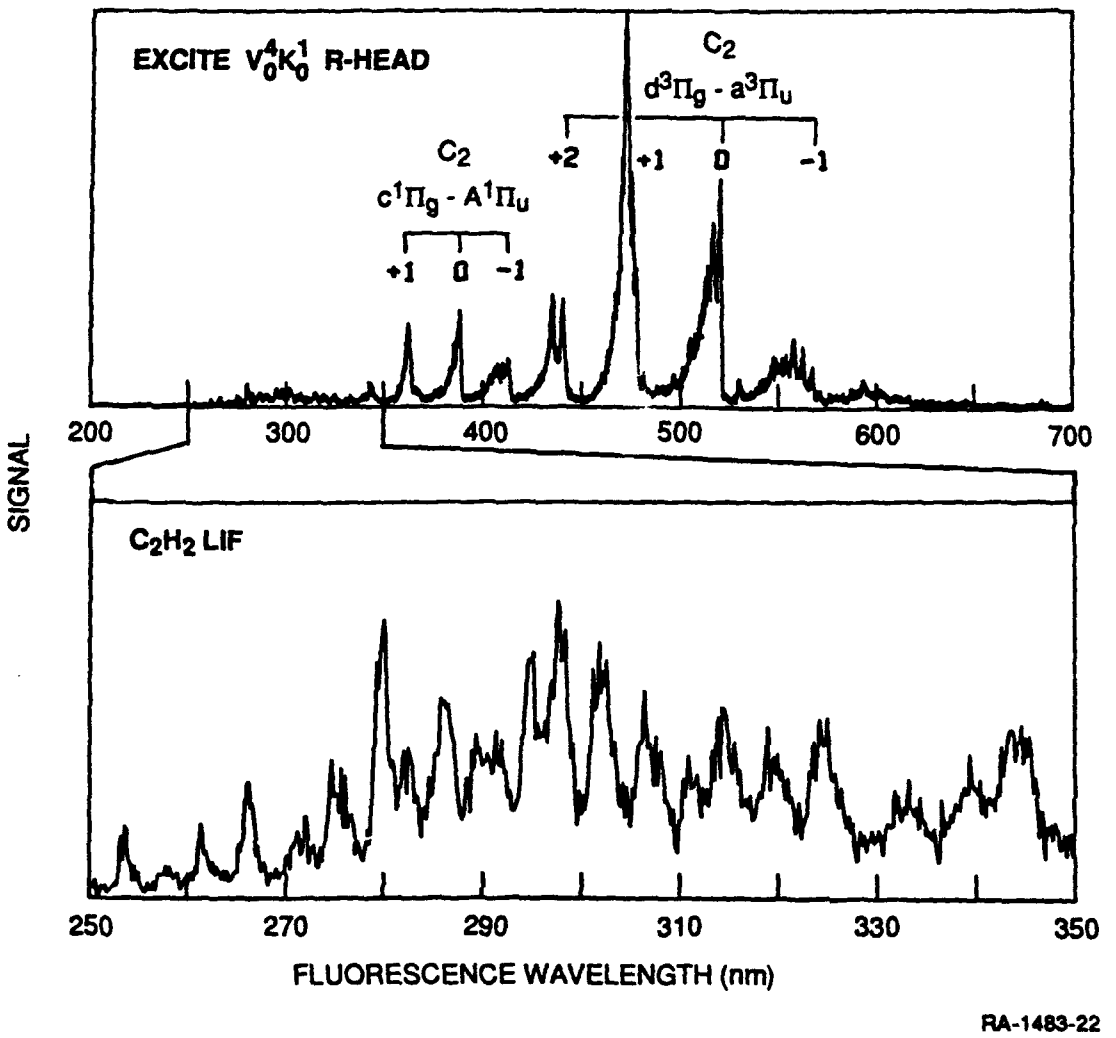

Figure 5. Fluorescence spectrum after excitation of C_2H_2.

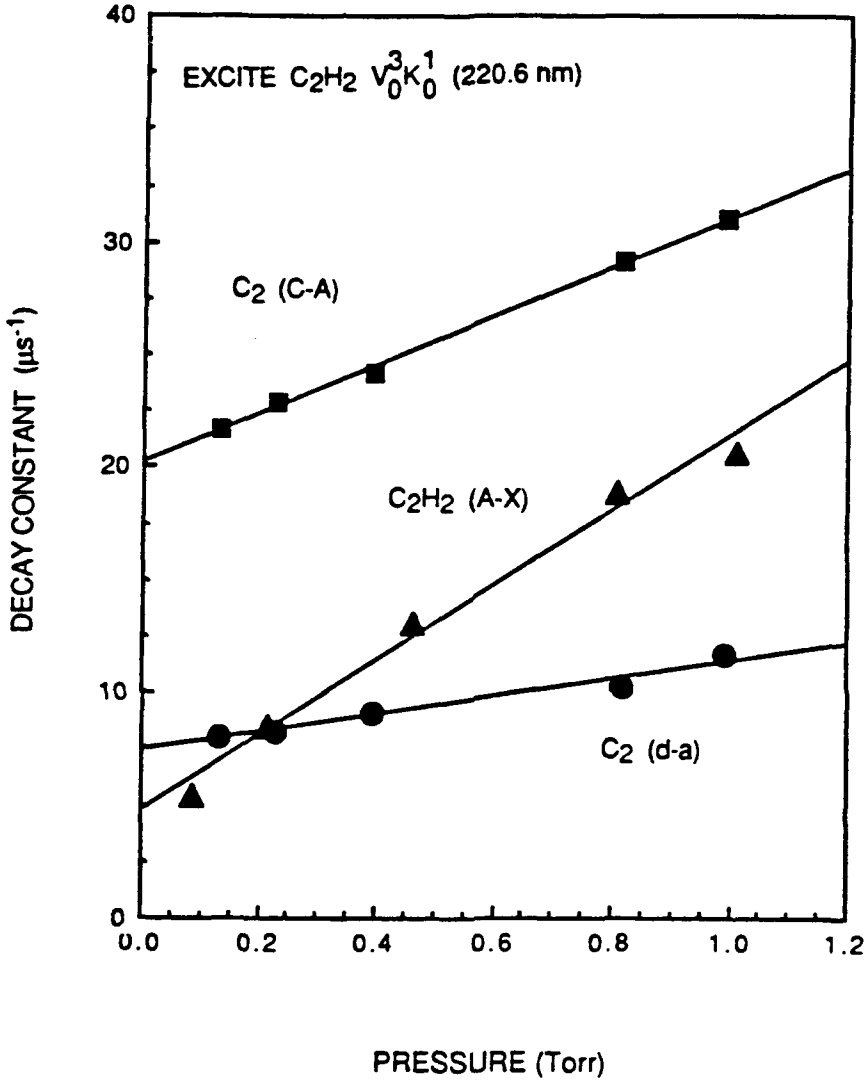

Figure 6. Pressure dependence of the time decay of the fluorescence signal.

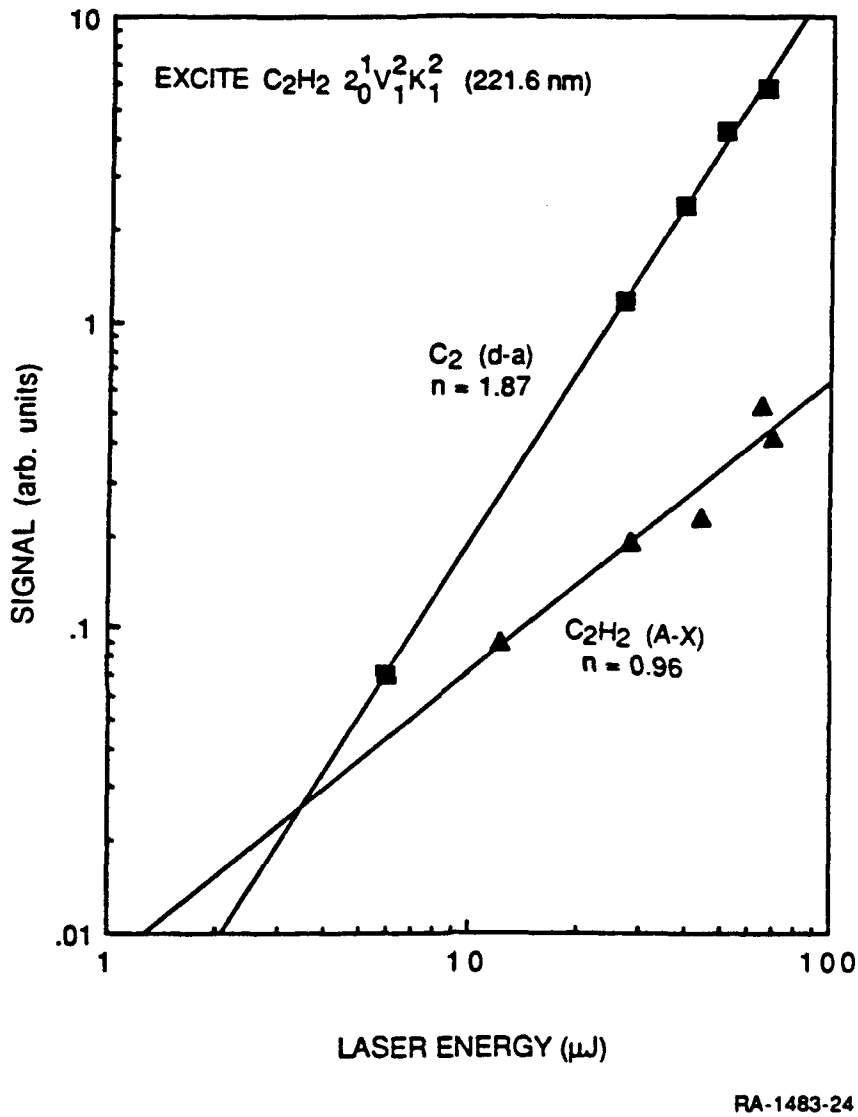

Figure 7. Laser power dependence of the C_2H_2 LIF signal and the C_2 Swan fluorescence.

To make the search for C_2H_2 easier, we began our investigation in a C_2H_2/O_2 flame. Because C_2H_2 is a fuel species, we would expect its concentration to be greatest near the burner surface and to decrease over the approach to the flame front as a result of decomposition and changes in temperature. By examining different excitation and detection wavelengths, we could decide which would be the most sensitive and least subject to interference from other species and processes. From the relative intensity of features in the fluorescence spectrum in Figure 5, the C_2 Swan emission will clearly generate the largest signals at typical laser powers. A large, continuous flame emission at the Swan (0,0) fluorescence wavelength presents an experimental difficulty; however, with time gating on the signal, the large background can be considerably reduced.

Figure 8 shows the fluorescence signal at ~520 nm, corresponding to the Swan (0,0) band after excitation at two wavelengths in the ultraviolet. The curve labeled "on resonance" corresponds to excitation of the $V_0^4\ K_0^1$ feature in C_2H_2, and the "off resonance" curve was taken at a wavelength where little acetylene is excited. Note that these two excitation features have very different profiles. The on resonance curve peaks near the burner, while the off resonance curve is negligible at the start, increases through the flame front, and decreases in the burnt gases. The difference between the two signals can be attributed to the concentration of C_2H_2 as corrected for the change in relative population of the rotational level we excite at the on resonance wavelength (shown in the bottom panel). Because the signals from the C_2H_2 and from the interference are of the same order of magnitude, the resonant component can be detected. To further investigate these signals, we seeded a small amount of C_2H_2 into a well characterized 7-Torr H_2/O_2 flame[7,20] for which temperature and OH concentration profiles had been measured. We were able to see strong C_2 signals similar to both the on and off resonance signals described above for the C_2H_2/O_2 flame. Although the profiles in this flame persisted higher off the burner, the relative amplitudes of on and off resonance components were very similar. When we dispersed the fluorescence in this flame, the C_2H_2 resonant and nonresonant signals showed very similar fluorescence spectra. The similarity indicates that no better detection wavelength exists for discriminating the interference from the desired signal and also points to the possibility that the two components can be produced by similar methods. Much more work is necessary before final conclusions can be drawn.

We have also estimated the amount of C_2H_2 we could detect with our very unoptimized system: near the burner we were able to observe about 200 ppm of C_2H_2. Several improvements can be made to lower this detection limit.

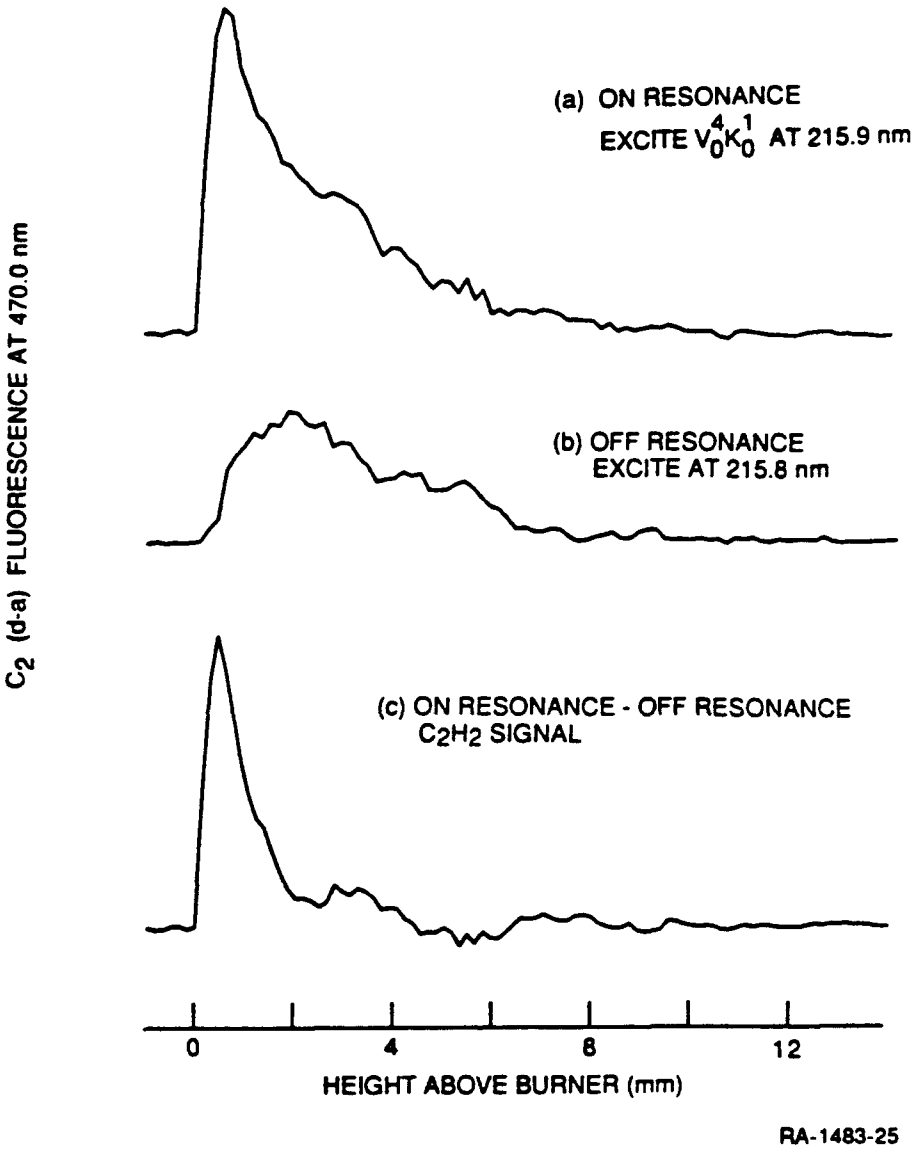

Figure 8. Position dependence of the C_2H_2 signal in a low-pressure flame.

CH_3

The methyl radical (CH_3) is a chemically important intermediate in the ignition and combustion of hydrocarbon fuels. CH_3 is less reactive than other hydrocarbon radicals, and often its decomposition or oxidation is a slow step in the combustion mechanism. Therefore, especially in the early stages of combustion, the CH_3 concentration would provide a crucial test of currently available combustion mechanisms. Unfortunately, the methyl radical has never been detected by LIF, and its only accessible electronic feature is unstructured and absorbs deep in the ultraviolet portion of the spectrum, near 216 nm.[21] This feature is unstructured because of the rapid predissociation of the excited state. The CH_3 radical has been detected by REMPI in low-pressure flames.[13,22]

We attempted to observe CH_3 by absorption in the 216-nm region. The first experiments were single-pass absorption studies, our ultimate goal being application of photoacoustic or photodeflection methods to this region of the spectrum. We have seen this absorption by directly measuring the power before and after the flame as a function of wavelength. The path length was 6 cm in a CH_4/O_2 flame at 100 Torr and $\phi = 1.5$. We observed an absorption of less than 5% with about a 2 to 1 signal-to-noise ratio, as can be seen in Figure 9. We were unable to observe an absorption signal in less rich flames because of the signal-to-noise level. However, this result is very encouraging, because we should be able to increase the sensitivity of the experimental apparatus both by multipassing the laser beam and by applying either photoacoustic or photodeflection techniques. All the possible interferences in the low-pressure burner system should be evaluated using different flames.

HO_2

The HO_2 radical is present in cool regions of the flame during the early stages of combustion. It is one of the few radical species in hydrogen combustion that has not been observed in the combustion environment. Both its low concentration and its unfavorable spectroscopic properties have contributed to its lack of detection. Because of the importance of this radical in the early ignition chemistry, an attempt to detect it was warranted.

Early in the project, we attempted to use PAD to detect HO_2 in a CH_4/O_2 flame at atmospheric pressure. Because HO_2 is not a stable species, we could not easily perform room-temperature experiments similar to those used in the infrared detection of C_2H_2. Infrared laser light was generated and the photoacoustic signal detected in the same manner as described above. As shown in Figure 10, we observed absorption features near 1.4 μm

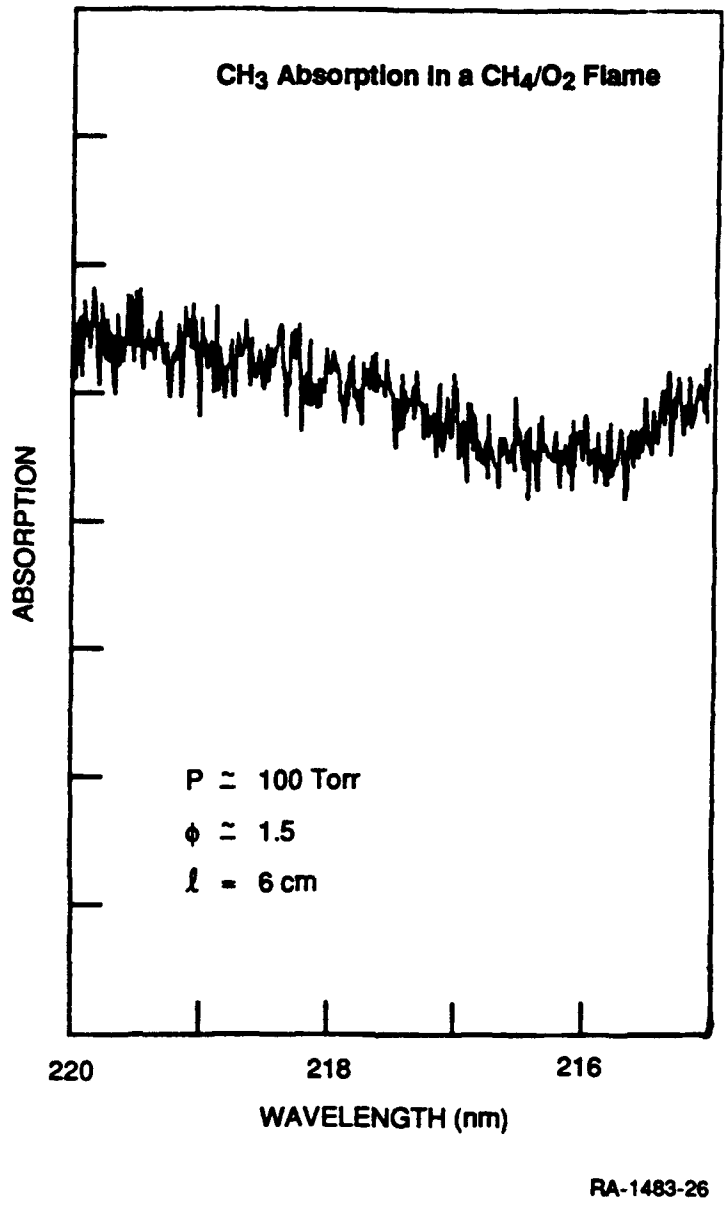

Figure 9. Methyl radical absorption in the ultraviolet.

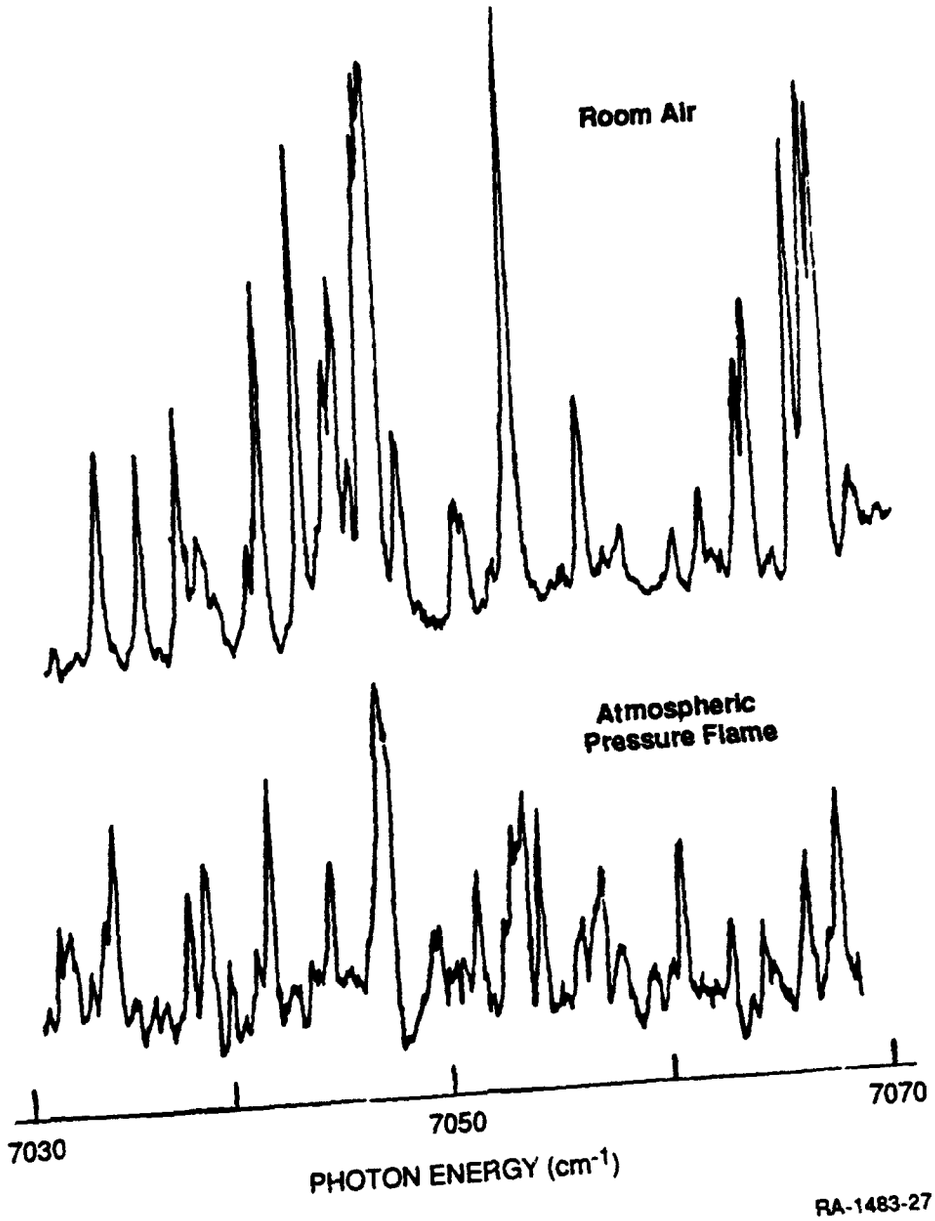

Figure 10. Water PAD spectra in the region of the HO_2 electronic transition.

in the area of a low-lying $^2A'$ excited state of HO_2, but all observed lines persisted out into the burnt gases and could be assigned to H_2O.[23] In retrospect, we concluded that, because of overlap with the major species (H_2O), HO_2 should be almost impossible to detect near the band origin of this transition by an absorption method.[24] This conclusion was verified by some simple kinetic modeling which showed that, even in low-pressure flames, the concentration of H_2O is always at least an order of magnitude greater than that of HO_2. Because of this difference in concentrations, any potentially successful detection method will be insensitive to background H_2O signals.

Two alternative methods may be feasible. The first involves exciting high vibration levels of the low-lying electronic state in the red and near infrared portions of the spectrum and observing the LIF with a red-sensitive photomultiplier tube. The other employs two lasers: one to photodissociate the HO_2 near 250 nm, and the second to probe the OH photofragment. The success of the second method hinges on the internal state distribution of the OH photofragment. If the OH photofragment comes out in high vibrational levels, we should be able to detect it above the thermal OH in the flame; but if the photofragment comes out in low vibrational levels, the signal will be masked by the thermal OH. Experiments in a room-temperature flow cell are needed to assess the feasibility of both techniques.

CH_2

The CH_2 diradical occurs during the early stages of fuel decomposition and is important in the chemistry of ignition, soot, and possibly NO_x formation. Methylene presented a unique experimental challenge. Methylene has a triplet ground state and a metastable singlet excited state lying about 3150 cm^{-1} higher. Unfortunately, the only known triplet excited state lies at such high energy[25] that excitation with lasers from the ground state is not feasible in the combustion environment. However, in room-temperature experiments, LIF has been observed in the $\tilde{b}^1B_1$ - $\tilde{a}^1A_1$ system of singlet CH_2 created directly in the $\tilde{a}$ state by the photodissociation of either acetic anhydride or ketene.[26-29] This system occurs in the visible region of the spectrum. Figure 11 shows the vibronic Boltzmann fraction for both the ground triplet state ($\tilde{X}$) and the singlet state ($\tilde{a}$) as a function of temperature. If these states are in equilibrium at combustion temperatures, about 1% of the CH_2 molecules will be in the $\tilde{a}^1A_1$ (0,0,0) state at 1600 K. At the start of this investigation we were unsure if this small fraction would be enough to detect CH_2 in the complex environment of a flame.

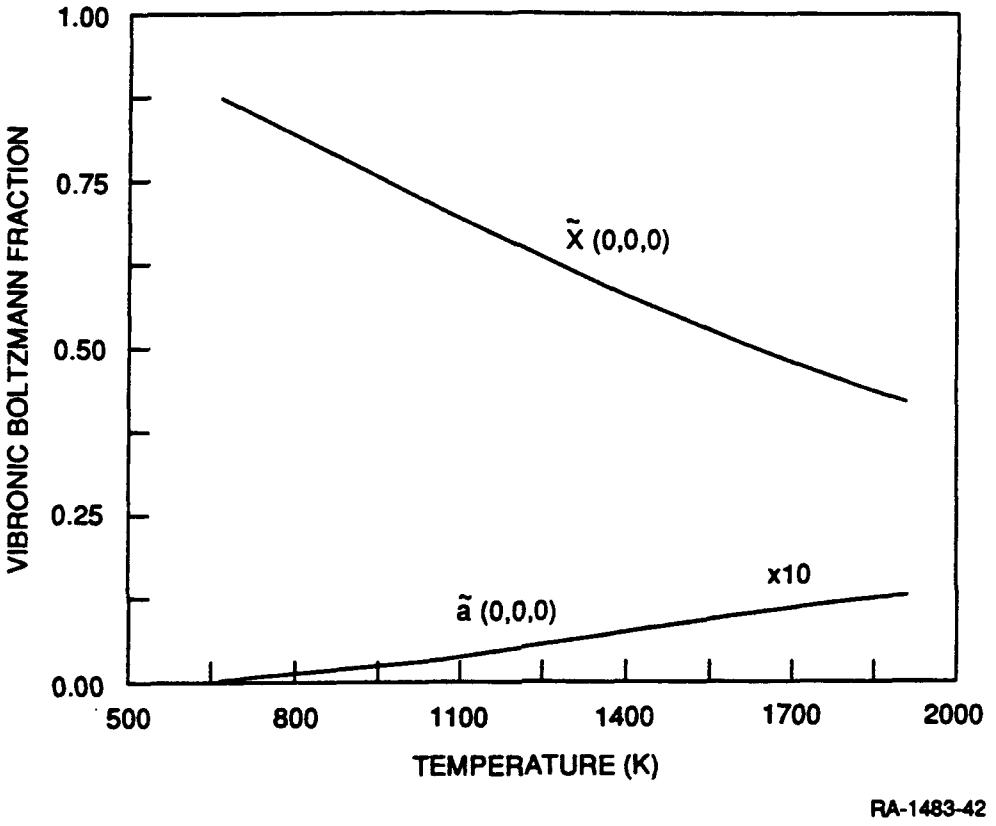

Figure 11. Plot of the vibronic Boltzmann fraction for the triplet ground state and lowest singlet state versus temperature.

On this project we performed the first optical detection of the chemically important methylene radical in a combustion system. The details of this observation are contained in Appendix I. What follows is a brief summary of that initial study.

Methylene absorbs light in vibrational bands between 400 and 800 nm[30]; initially, we chose to study the (0, 16, 0) - (0, 0, 0) vibrational band near 18,600 cm^{-1}. This investigation began in a low-pressure methane/oxygen flame because it was easy to operate at low pressures and the flame had a simpler chemistry than those containing higher hydrocarbons. The experimental setup was typical for LIF experiments. We observed the fluorescence at a right angle to the incoming laser beam and dispersed the fluorescence in a monochromator. From the start we knew that the signals would be small and thus the fluorescence would have to be detected away from the excitation laser wavelength to avoid scattered laser light. After several days of searching, we located an extremely weak signal in the correct wavelength region for both excitation and fluorescence. After all possible parameters were maximized, the signal corresponded to about 1 fluorescence photon every 5 laser shots. This extremely small signal made all the experiments difficult and time consuming. However, we unambiguously identified the detected species as methylene and went about examining different vibrational transitions by using other flame sources and looking at the time dependence of the fluorescence. We also obtained relative concentration profiles of CH_2, CH, and OH along with a temperature profile in a 5.6 Torr $\phi \approx 1.05$ methane/oxygen flame.

Attempts to make the measurements quantitative were hampered by uncertainty in the level of optical saturation in the methylene measurement and lack of available spectroscopic parameters. Since this was the first investigation of this species, many questions remain to be answered. Preliminary modeling studies[31] indicate that at these pressures the singlet and triplet manifold may not be in equilibrium and thus separate treatment of the two species would be required in any modeling effort. We also discovered the importance of knowing the level of saturation of the excitation laser. Finally, the spectroscopic parameters that require measurments were determined. These include vibrational band transition probabilities for the (0,16,0) level of the state.

Unfortunately, the signal levels for detection of CH_2 are extremely low, and thus extreme care must be used in its detection. Because of these low signal levels, this technique cannot be applied to a wide variety of combustion systems like detection of OH. However, detection is indeed feasible, and for a few well chosen laboratory flames it will

provide a good test of hydrocarbon combustion chemistry. Further work is required to make this technique quantitative.

CONCLUSIONS

In this project we have improved and quantified the LIF techniques used in measuring of the CH radical concentration and developed new methods for the detection of the chemically important transient species C_2H_2, CH_2, and CH_3. CH detection is now well understood and C_2H_2 detection shows promise as an extremely useful method applicable to several practical systems such as turbulent diffusion flames. We have demonstrated that detection of the chemically important polyatomic radicals is feasible and with additional development will provide useful information to help unravel the details of the chemistry of hydrocarbon combustion.

MANUSCRIPTS AND PRESENTATIONS SUPPORTED BY THIS CONTRACT

The following presentations have been supported by this contract:

1. R. A. Copeland and M. J. Dyer, "Time Dependence of CH Laser-Induced Fluorescence in Low-Pressure Flames," Paper 87-32, Western States Section of the Combustion Institute Spring Meeting, Provo, Utah, April 1987.

2. N. L. Garland, M. J. Dyer, R. A. Copeland, and D. R. Crosley, "Collisional Quenching of CH at Elevated Temperatures," Central States Section of the Combustion Institute Spring Meeting, Argonne, Illinois, May 1987.

3. R. A. Copeland, "LIF Detection of CH and NH in a Low-Pressure Burner," German Aerospace Research Establishment (DFVLR), Stuttgart, FRG, September 1987.

4 D. R. Crosley, "State Selectivity in Light Emission from Flames," N.A.T.O. Advanced Research Workshop on Selectivity in Chemical Reactions, Bowness-on-Windemere, England, September 1987.

5. R. A. Copeland, "Low-Pressure Burner Diagnostics" Max Plank Institut für Strömungsforschung, Göttingen, FRG, September 1987.

6. K. J. Rensberger, M. J. Dyer, and R. A. Copeland, "Time-Resolved Laser-Induced Fluorescence in Low-Pressure Flames," 1987 International Laser Science Conference, Atlantic City, New Jersey, November 1987. [Bull. Am. Phys. Soc. **32**, 1618 (1987).]

7. K. J. Rensberger, R. A. Copeland, J. B. Jeffries, K. Kohse-Höinghaus, M. L. Wise, and D. R. Crosley, "Laser-Induced Fluorescence Temperature Measurements in Low-Pressure Flames," Western Spectroscopy Association Thirty-Fifth Annual Conference on Modern Spectroscopy, Asilomar, California, January 1988.

8. D. R. Crosley, "Laser Detection of Reactive Intermediates in Combustion," U.S.-Israeli Workshop on Processes in Premixed Gas Combustion Systems, Ein Gedi, Israel, February 1988.

9. J. B. Jeffries, K. J. Rensberger, R. A. Copeland, K. Kohse-Höinghaus, M. L. Wise, and D. R. Crosley, "Laser-Induced Fluorescence Determination of Temperature in Low-Pressure Flames," Paper 88-57, Western States Meeting of the Combustion Institute, Salt Lake City, Utah, March 1988.

10. K. J. Rensberger, R. A. Copeland, M. L. Wise, and D. R. Crosley, "Time-Resolved Laser-Induced Fluorescence of CH and NH in Low-Pressure Flames," 41st Annual Summer Symposium on Analytical Chemistry, Stanford, California, June 1988.

11. G. A. Raiche, R. A. Copeland, and D. R. Crosley, "Laser-Induced Fluorescence Measurements of C_2H_2 and Absorption Studies of CH_3 in Low-Pressure Flames," Twenty-Second Symposium (International) on Combustion, Seattle, Washington, August 1988.

12. D. R. Crosley, "Laser-Induced Fluorescence in Flames," Ruhr-Universität, Bochum, FRG, October, 1988.

13. G. A. Raiche, R. A. Copeland, and D. R. Crosley, "Laser-Induced Fluorescence and Dissociation of Acetylene in Flames," Fourth International Laser Science Conference, Atlanta, Georgia, October 1988.

14. D. R. Crosley, "Detection of Radicals in Low-Pressure Flames Using Laser-Induced Fluorescence," Max Planck Institut für Strömungsforschung, Göttingen, FRG, November 1989.

15. A. D. Sappey, D. R. Crosley, and R. A. Copeland, "Laser-Induced Fluorescence Detection of Singlet CH_2 in Low-Pressure Flames," Western Spectroscopy Association Thirty-Sixth Annual Conference on Modern Spectroscopy, Asilomar, California, January 1989.

16. G. A. Raiche, D. R. Crosley, and R. A. Copeland, "Resonantly Enhanced Multiphoton Dissociation of C_2H_2 : Production of C_2 ($d^3\Pi_g$, $C^1\Pi_g$)," Western Spectroscopy Association Thirty-Sixth Annual Conference on Modern Spectroscopy, Asilomar, California, January 1989.

17. R. A. Copeland, "Laser-Based Diagnostics of Polyatomic Intermediates in Low-Pressure Flames: CH_2, C_2H_2, and CH_3" Stanford University High Temperature Gasdynamics Laboratory Seminar Series, Stanford, California, February 1989.

18. D. R. Crosley, "Combustion Diagnostics," Office National d'Etudes et de Recherches Aerospatiales, Chatillon, France, May 1989.

19. A. D. Sappey, D. R. Crosley, and R. A. Copeland, "Laser-Induced Fluorescence Detection of Singlet CH_2 in Low-Pressure Flames," Fifth Interdisciplinary Laser Science Conference, Stanford, California, August 1989. [Bull. Amer. Phys. Soc. **34**, 1682 (1989).]

20. G. A. Raiche, D. R. Crosley, and R. A. Copeland, "Optical Detection of Acetylene in Low-Pressure Flames," 1989 Fall Meeting of the Western States Section of the Combustion Institute, Paper 89-47, Livermore, California, October 1989.

21. A. D. Sappey, D. R. Crosley, and R. A. Copeland, "Laser-Induced Fluorescence Detection of Singlet CH_2 in Low-Pressure Methane/Oxygen Flames," 1989 Fall Meeting of the Western States Section of the Combustion Institute, Paper 89-48, Livermore, California, October 1989.

The following papers have been supported or partially supported by this contract:

1. D. R. Crosley, K. J. Rensberger, and R. A. Copeland, "State Selectivity in Light Emission From Flames," in *Selectivity in Chemical Reactions*, J. C. Whitehead, Ed. (Kluwer Academic Publishers, Dordrecht, 1988), p. 543.

2. K. J. Rensberger, M. J. Dyer, M. L. Wise, and R. A. Copeland, "Time-Resolved Laser-Induced Fluorescence in Low-Pressure Flames," in Advances in Laser Science-III, A. C. Tam, J. L. Gole, and W. C. Stwalley, Eds., AIP Conf. Proc. **172**, 750 (1988).

3. K. J. Rensberger, M. L. Wise, D. R. Crosley, and R. A. Copeland, "NH and CH Laser-Induced Fluorescence in Low-Pressure Flames: Quantum Yields from Time-Resolved Measurements," in *Twenty-Second Symposium (International) on Combustion*, (The Combustion Institute, Pittsburgh, 1988), p. 1867.

4. K. J. Rensberger, M. J. Dyer, and R. A. Copeland, "Time-Resolved CH ($A^2\Delta$ and $B^2\Sigma^-$) Laser-Induced Fluorescence in Low-Pressure Hydrocarbon Flames," Appl. Opt. **27**, 3679 (1988).

5. D. R. Crosley, "Semiquantitative Laser-Induced Fluorescence in Flames," Combust. Flame, **78**, 153 (1989).

6. K. J. Rensberger, J. B. Jeffries, R. A. Copeland, K. Kohse-Höinghaus, M. L. Wise, and D. R. Crosley, "Laser-Induced Fluorescence Determination of Temperatures in Low-Pressure Flames," Appl. Opt. **28**, 3556 (1989).

7. D. R. Crosley, "Rotational and Translational Effects in Collisions of Electronically Excited Diatomic Hydrides," J. Phys. Chem. **93**, 6273 (1989).

8. G. A. Raiche, D. R. Crosley, and R. A. Copeland, "Laser-Induced Fluorescence and Dissociation of Acetylene in Flames," in *Advances in Laser Science-IV*, J. L. Gole, D. F. Heller, M. Lapp, and W. C. Stwalley, Eds., AIP Conf. Proc. **191**, 758 (1989).

9. A. D. Sappey, D. R. Crosley, and R. A. Copeland, "Laser-Induced Fluorescence Detection of Singlet CH_2 in Low-Pressure Methane/Oxygen Flames," Appl. Phys. B., submitted.

10. G. A. Raiche, D. R. Crosley, and R. A. Copeland, "Resonance-Enhanced Multiphoton Photodissociation of C_2H_2," J. Phys. Chem, submitted.

11. G. A. Raiche, D. R. Crosley, and R. A. Copeland, "Optical Detection of C_2H_2 in Low-Pressure Flames" Applied Physics B, in preparation.

Copies of these works are included as the appendices.

REFERENCES

1 D. R. Crosley, Ed., *Laser Probes for Combustion Chemistry* (ACS Symposium Series, Vol. 134, 1980).

2. D. R. Crosley, High Temp. Mat. Proc. **7**, 41 (1986).

3. R. A. Copeland, D. R. Crosley, and G. P. Smith, *Twentieth Symposium (International) on Combustion,* (The Combustion Institute, Pittsburgh, 1984), p. 1195.

4. J. B. Jeffries, R. A. Copeland, G. P. Smith, and D. R. Crosley, *Twenty-First Symposium (International) on Combustion* (The Combustion Institute, Pittsburgh, 1986), p. 1709.

5. M. J. Dyer and D. R. Crosley, *Proceedings of the International Conference on Lasers '84,* (STS Press, McLean, Virginia, 1985), p. 211.

6. N. L. Garland and D. R. Crosley, *Twenty-First Symposium (International) on Combustion,* (The Combustion Institute, Pittsburgh, 1986), p. 1693.

7. K. Kohse-Höinghaus, J. B. Jeffries, R. A. Copeland, G. P. Smith, and D. R. Crosley, *Twenty-Second Symposium (International) on Combustion,* (The Combustion Institute, Pittsburgh, 1989) p. 1867.

8. K. J. Rensberger, M. L. Wise, D. R. Crosley, and R. A. Copeland, *Twenty-Second Symposium (International) on Combustion,* (The Combustion Institute, Pittsburgh 1989), p. 1867.

9. N. L. Garland and D. R. Crosley, J. Chem. Phys. **90**, 3566 (1989).

10. G. P. Smith, M. J. Dyer, and D. R. Crosley, Appl. Opt. **22**, 3995 (1983).

11. S. W. Kizirnis, R. J. Brecha, B. N. Ganguly, L. P. Goss, and R. Gupta, Appl. Opt. **23**, 3873 (1984).

12. J. S. Bernstein, X. Song, and T. A. Cool, Chem. Phys. Lett. **145**, 188 (1988).

13. U. Meier and K. Kohse-Höinghaus, Chem. Phys. Lett. **142**, 498 (1987).

14. C. J. Nokes and R. J. Donovan, Chem. Phys. **90**, 167 (1984).

15. K. J. Rensberger, M. J. Dyer, and R. A. Copeland, Appl. Opt. **27**, 3679 (1988).

16. R. A. Copeland, M. J. Dyer, and D. R. Crosley, J. Chem. Phys. **82**, 4022 (1985).

17. A. Hofzumahaus and F. Stuhl, J. Chem. Phys. **82**, 3152 (1985).

18. J. K. G. Watson, M. Herman, J. C. Van Craen, and R. Colin, J. Mol. Spectrosc. **95**, 101 (1982).

19. J. C. Van Craen, H. Herman, R. Colin, and J.K.G. Watson, J. Mol. Spectrosc. **111**, 185 (1985).

20. K. J. Rensberger, J. B. Jeffries, R. A. Copeland, K. Kohse-Höinghaus, M. L. Wise, and D. R. Crosley, Appl. Opt. **28**, 3556 (1989).

21. G. Herzberg, Proc. R. Soc. London A **262**, 291 (1961).

22. K. C. Smyth and P. H. Taylor, Chem. Phys. Lett. **122**, 518 (1985).

23. R. P. Tuckett, P. A. Freedman, and W. J. Jones, Mol. Phys. **37**, 379 (1979).

24. R. A. Toth and J. S. Margolis, J. Mol. Spectrosc. **55**, 229 (1975).

25 G. Herzberg and J. W. D. Johns, Proc. R. Soc. London A, **295**, 106 (1966).

26. D. Feldmann, K. Meier, R. Schmiedl, and K. H. Welge, Chem. Phys. Lett. **60**, 30 (1978).

27. J. Danon, S. V. Filseth, D. Feldmann, H. Zacharias, C. H. Dugan, and K.H. Welge, Chem. Phys. **29**, 345 (1978).

28. A. J. Grimley and J. C. Stephenson, J. Chem. Phys. **74**, 447 (1981)

29. M. N. R. Ashfold, M. A. Fullstone, F. Hancock, and G. W. Ketley, Chem. Phys. **55**, 245 (1981).

30. H. Petek, D. J. Nesbitt, D. Darwin, and C. B. Moore, J. Chem. Phys. **86**, 1172 (1987).

31. G. P. Smith, private communication.

Appendix A

STATE SELECTIVITY IN LIGHT EMISSION FROM FLAMES

STATE SELECTIVITY IN LIGHT EMISSION FROM FLAMES

David R. Crosley, Karen J. Rensberger and Richard A. Copeland
Molecular Physics Department
SRI International
Menlo Park
California 94025
USA

ABSTRACT. Chemiluminescence in flames is the result of energetic and highly specific reactions involving free radicals. If understood and linked to the major combustion chemical mechanism, it can be of use for monitoring the progress of that chemistry. Although there is firm evidence for certain reactions to form electronically excited OH and CH in hydrocarbon flames, the generally accepted chemiluminescence mechanisms cannot explain all of the observations, indicating the importance of other pathways. Some of the evidence for other pathways can be found in the highly nonequilibrium internal level distributions seen in flame chemiluminescence. An interpretation of these observed distributions in terms of the nascent results from the elementary reactions involves consideration of state-specific electronic quenching and energy transfer. We present some recent observations on chemiluminescent emission from CH and OH in hydrocarbon flames on a low-pressure flat flame burner, and summarize pertinent experiments in flames and other systems on excited state quenching and energy transfer in these two radicals.

1. INTRODUCTION

The light emitted as a result of chemiluminescent reactions of free radicals forms what we familiarly think of as a flame, even though those reactions constitute but a negligible pathway for the overall conversion of fuel and oxidant to combustion products. There have been numerous early studies of flame luminescence, as exemplified by Gaydon's book [1] on the topic, but in recent years the concentration on laser-based optical methods has generally superseded such studies. Nevertheless, an understanding of the process of chemiluminescence from flames can have practical benefits, for its use as a monitor of the progress of the flame chemistry under conditions where probing by lasers cannot be carried out. We can cite several such recent examples: the measurement of CH, C_2 and OH chemiluminescence to deduce spatial and temporal regimes of heat release in pulse combustors [2]; the use of CH emission to conditionally sample flame fronts in gas turbine engines [3]; and the observations of emission from C_2 and from both the $B^2\Sigma^-$ and $A^2\Delta$ states of CH as markers of shock fronts in detonation waves [4]. It can be noted, interestingly, that in this last study the radiation from these two states did not coincide temporally in the shock. Additionally, the chemiluminescence can be of direct significance such as

J. C. Whitehead (ed.), Selectivity in Chemical Reactions, 543–554.

its use in detecting rocket plumes through observations in visible and ultraviolet spectral regions [5].

Despite the many observations of these phenomena, there remain many unanswered mechanistic questions. Nearly all of the identifiable light emission from flames is from small free radicals, and the formation of the radicals in electronically excited states demands energetic precursors. Thus the reactants are also free radicals; many of the likely reactions form the highly stable CO molecule as one of the products. Only fairly recently [6] were any mechanistic pathways established for the production of excited OH and CH in one low-pressure flame, using absorption measurements of ground state radical concentrations; but, for at least CH, even that mechanism has been questioned in a different series of experiments [7].

In these reactions, there is often considerable energy deposited into internal degrees of freedom of the emitting, electronically excited radical. An illustrative example is shown in Fig. 1, which exhibits a Boltzmann plot of the rotational populations in the $v'=0$ level of the $A^2\Sigma^+$ state of the OH radical in the primary reaction zone of an atmospheric pressure methane/oxygen flame. The distribution appears bimodal, described by two "temperatures". At lowest N', the (poorly determined) value of 1700 K is not far from the rotational temperature of ground state OH, determined by absorption measurements. The highly nonequilibrium distribution at higher N', however, is far hotter than any possible flame temperature. It is the result of the nascent distribution from the chemiluminescent reaction forming [8] OH^* (possibly $CH + O_2$), together with rotational energy

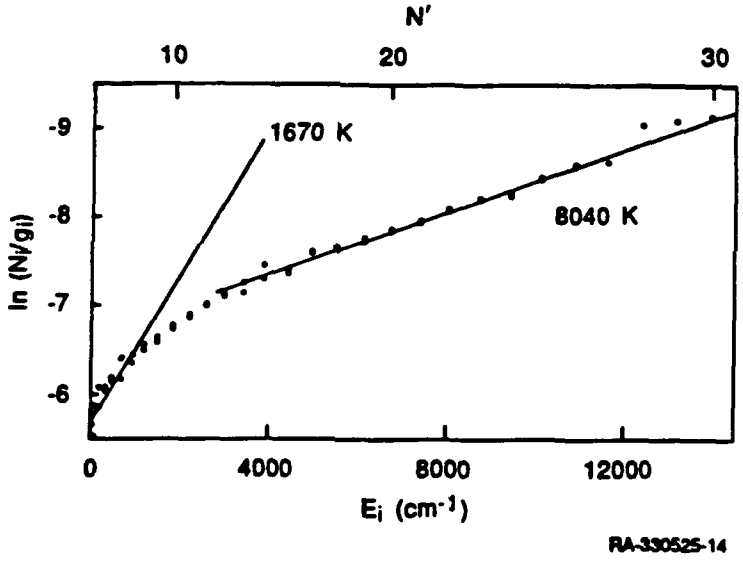

FIGURE 1. Rotational level Boltzmann plot: the logarithm of the state population divided by its degeneracy vs. its energy. Note that negative values increase to the top. This is for emission from the $v'=0$ level of the $A^2\Sigma^+$ state of the OH molecule, in the reaction zone of a stoichiometric, atmospheric pressure CH_4/O_2 flame. The distribution is bimodal, with the populations at low-N' close to that of the ground state OH rotational temperature, plus a nonequilibrium high-N' component reflecting the chemiluminescent reaction forming OH in the flame.

transfer, and rotationally state-specific collisional quenching which in this flame is the dominant removal mechanism from the excited state [9]. Similar distributions have been observed in other hydrocarbon flames [1,10].

It would be useful to relate the formation of the chemiluminescent, emitting radicals to the progress of the primary combustion reactions for a variety of flame conditions. In doing so, relationships among excited and ground state radical concentrations form important clues. So also do the particular state distributions (electronic, rotational and vibrational) populated by these reactions in the flames. Deducing those nascent distributions from the measured ones demands knowledge of collisional quenching and internal energy transfer in the flame environment. For several years we have been studying these collisional processes for a variety of small free radicals important in combustion, and have recently begun observations of the chemiluminescence itself in a low-pressure burner system. In this paper, we will concentrate on two species: OH and CH. We will describe some of the chemiluminescence results, which raise new questions (but do not yet resolve them!) concerning the mechanistic pathways, and shall summarize current knowledge of quenching and energy transfer for these radicals in flame environments.

2. CHEMILUMINESCENCE OF CH AND OH

It was long ago suggested [1] but only more recently established [11,12] that in hydrocarbon/oxygen flames the major, perhaps sole, means of formation of OH* is the reaction between CH and O_2. The evidence supporting this conclusion [11] comes from the constancy over various operating conditions, in a low-pressure C_2H_2/O_2 flame, of the relationship $[OH^*]nT^{1/2}/[CH][O_2]$, where n is the total density; this is as expected from a simple steady state balance between this formation reaction and collisional removal of the excited state. Further support is found in the results from a room temperature discharge flow system [12] of O + C_2H_2, which are in agreement with a complex computer model of the reaction network. This reaction yields rotationally hot distributions, as seen in Fig. 1, contrasting for example with the nonequilibrium vibrational distributions of $A^2\Sigma^+$ OH in a H_2/O_2 flame [1] (formed in that case via inverse predissociation).

Several spatial profiles of the intensities of chemiluminescence of CH* and OH* and laser-induced fluorescence (LIF) of CH and OH from the low-pressure burner experiments [13] are shown in Figs. 2 and 3. A sintered, porous disc flat flame burner of 5 cm diameter is housed in an evacuable chamber, permitting flames to be stabilized down to about 3 Torr. Measurements of excited state chemiluminescence are made with a small monochromator, here operated with a typical 10 nm bandpass and a wavelength fixed to the center of the emission band being monitored. The spatial resolution is governed by the slit width and is about 0.4 mm. Ground state measurements are made using LIF with an excimer-pumped dye laser, frequency doubled to detect OH or used directly in the ultraviolet or blue for exciting the CH B and A states respectively. Here, the pulsed laser produces pulsed LIF, which is time-resolved to discriminate against the flame emission.

Fig. 2 shows the spatial profiles for a stoichiometric propane/oxygen flame at 6.5 Torr. There are several salient features. First, the OH* emission profile peaks higher off the burner (i.e., later in the flow) than the ground state CH profile. The O_2 concentration, although not measured here, must continually decrease as a function of distance from the burner. Over this region, the temperature (measured

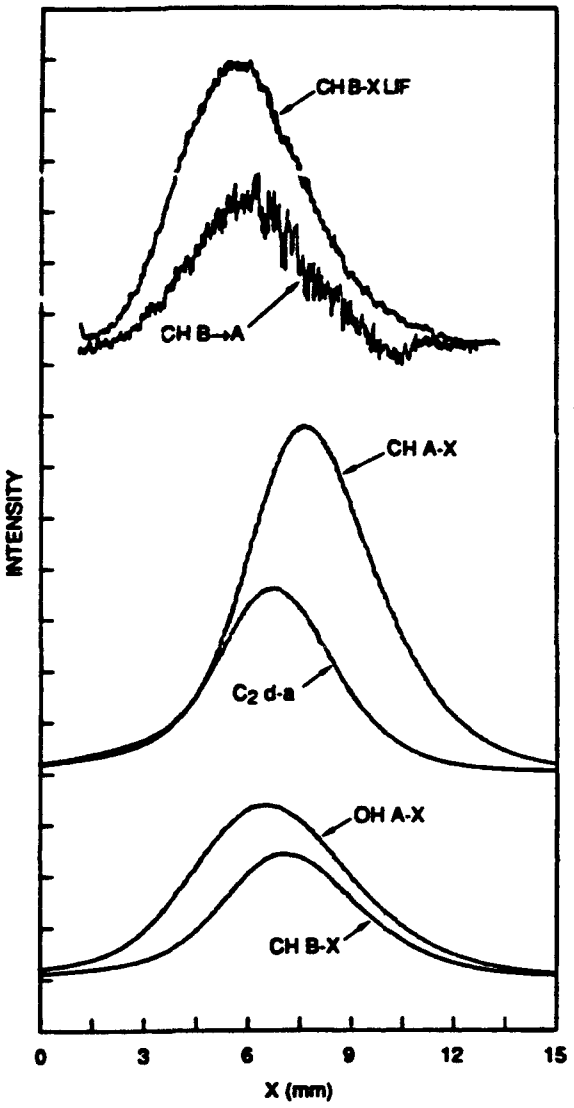

FIGURE 2. Spatial profiles of LIF and chemiluminescence for several flame radicals, taken in the low-pressure burner. The flame is C_3H_8/O_2 at a pressure of 6.5 Torr. Note that intensities, not radical concentrations, are plotted; the relationship between the two involves a quantum yield which is however nearly constant throughout this flame.

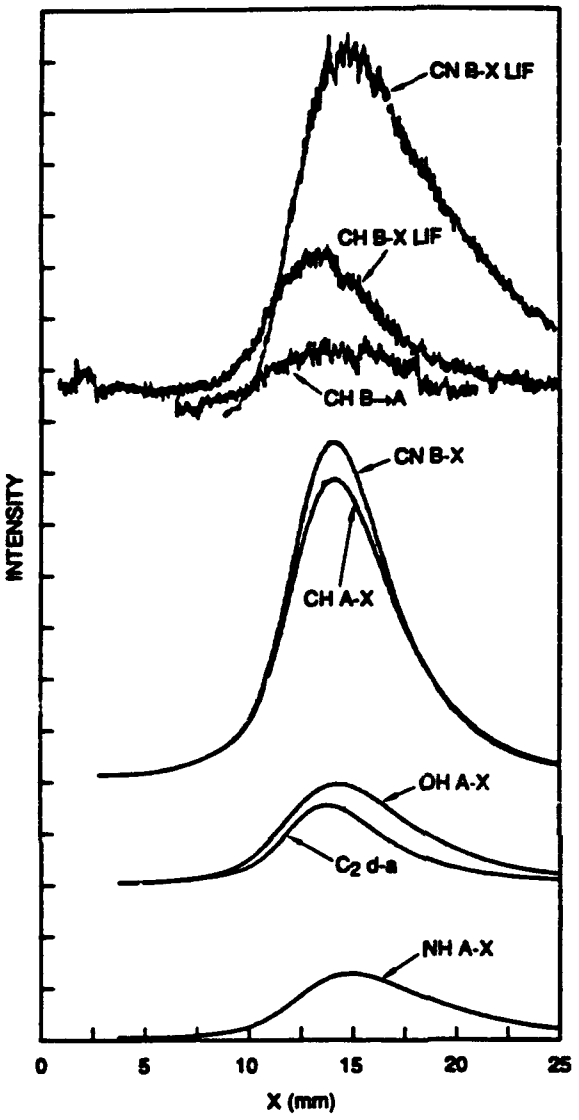

FIGURE 3. As Fig. 2 for a C_3H_8/N_2O flame.

separately in CH rotational excitation scans) varies from ~1500 K to 2000 K. Using temperature-dependent quenching cross sections [9], described below, we expect that the OH quantum yield should vary only about 5% through the flame; direct measurements [14] of CH quenching on the same burner show that its quantum yield too is constant. Thus these intensity profiles can be taken as equivalent to concentration profiles of OH* and ground state CH. Taken together, they do not match that expected from the CH + O_2 reaction. Consequently, there must here be some additional mechanism responsible for the production of OH*. This is also evident from the strong OH* emission in a C_3H_8/N_2O flame (Fig. 3). Again, the hydroxyl emission peaks later than the CH ground state, even though here there is little molecular oxygen present.

Evidence concerning the CH* production mechanism comes from the state selectivity observed. In the oxygen-based flame, Fig. 2, the CH $B^2\Sigma^-$ chemiluminescence has a slightly different profile from that of the $A^2\Delta$ emission. This suggests either that these two states are formed via different reactions, or else that the emission quantum yield varies markedly with position through the flame, differing for each state. The latter possibility can be addressed from the quenching study [14] on both states of CH made in the burner. Although the B state quenches more rapidly and the B → A transfer rate varies slightly (perhaps 10%) with burner position (see below), that cannot explain the difference in profiles. This can be concluded from an energy transfer experiment in an atmospheric pressure methane/oxygen flame [15], which showed that only about 20% of the B-state molecules are quenched to the emitting A-state. Thus we conclude that there are (at least) two mechanisms for producing excited CH. Similar results are seen for methane flames. (The N_2O-based flames provide no evidence of this nature because strong chemiluminescence from CN masks the CH B-X emission, as seen in Fig. 3). On the other hand, the differences are small (see Fig. 2) and disappeared when the propane flame was diluted with N_2. Thus there is a state selectivity indicating at least two production reactions, although the reaction which produces the difference in A and B state profiles may be only a fraction of the total CH* formation mechanism.

Previous evidence for the mechanism of formation of CH* comes from two experiments. A measurement [6] of spatial profiles in low-pressure C_2H_2/O_2 flames showed the ratio $[CH^*]/[C_2][OH]$ to be remarkably constant with variation in many different flame parameters. Only the $A^2\Delta$ state was observed, however. In a more recent study [7] in a low pressure discharge flow at room temperature, emission spatial profiles, measured downstream from mixing of O + C_2H_2, were compared with the results of a computer calculation, varying many discharge parameters. Here it was concluded that CH* was produced from the reaction O + C_2H, not the reaction C_2 + OH deduced from the flame study. The present profiles suggest that neither mechanism is solely responsible for the formation of electronically excited CH.

Another pertinent observation is that of a third excited state of CH, $C^2\Sigma^+$, which lies some 6300 cm^{-1} or 9000 K higher than $B^2\Sigma^-$. It is not seen in low pressure discharges [7,16] of acetylene and oxygen but is observed in atmospheric pressure flames of those two reactants [16]. This is significant in that the energetics of the two proposed CH* formation reactions are considerably different; O + C_2H has just enough energy at threshold to populate the $v'=0$ level of $B^2\Sigma^-$ whereas OH + C_2 is energetic enough to directly produce $C^2\Sigma^+$. We find the argument in Ref. 7, that the C-state is formed in flames from vibrationally excited C_2H, to be questionable, in view of the very large amounts of excess energy required above threshold.

3. COLLISIONAL QUENCHING OF CH AND OH IN FLAMES

It can be seen from the above that it is necessary to account for collisional effects on the emission quantum yields when interpreting chemiluminescence profiles to deduce mechanistic information. In this section, we summarize the results of a series of experiments on quenching and energy transfer in electronically excited OH and CH, which are pertinent to such flame studies.

We have made OH measurements in discharge flow cells and a laser pyrolysis/laser fluorescence (LP/LF) apparatus [16] for T = 230 to 1400 K, and on CH in the burner, at T ~ 1700 K. The measurements of quenching were made from the pressure dependence of the direct time decay of LIF signals; an example of such a decay trace from the CH experiments is shown in the upper panel of Fig. 4. Energy transfer has been studied using fluorescence scans following laser excitation of an individual upper state level.

The OH room temperature results showed a key finding [17,18]: that the quenching cross section σ_Q varied markedly with rotational level N', for some 20 collision partners studied. This state-specific effect can be seen because individual rotational levels are excited by the laser, and they do not rotationally thermalize before undergoing a significant amount of quenching. In some cases, σ_Q drops as much as twofold as N' increases from 0 to 5. This has important implications for interpreting distributions such as in Fig. 1, because the OH in the flame also does not become rotationally thermalized before quenching [19]. On the other hand, neither the rotational level dependence at high N', nor the temperature dependence of the N'-dependence is known, so at present the effects of this variation of σ_Q can only be estimated. Recent experiments in the burner [14] have shown the quenching of both the B- and A-states of CH vary with N', although the variation in the flames is less marked, 20% at most. The degree varies with flame; it is flat for CH_4/O_2 and decreases similarly for C_3H_8/O_2 and C_2H_2/O_2. This can be ascribed to the different collisional environments in these flames. We can make analogy with both the OH results [18] as well as with recent room temperature studies [20] of σ_Q for $A^3\Pi_i$ NH, which show a degree of rotational level dependence similar to that for OH. We then expect a large N' variation for CO_2 and little for H_2O, although this does not offer a full explanation of the variation with flame.

Room temperature σ_Q values for OH are large, ranging from 10 to 100 $Å^2$, indicating [18] that attractive forces are involved in the collision. (The rotational level dependence is then ascribed [18] to anisotropies in this attractive surface). A governing attractive interaction is in accord with studies [21] of the temperature dependence of OH quenching, measured in both the flow and LP/LF systems. In all cases, σ_Q decreases as the temperature increases. There is a further decrease in the cross section averaged over a thermal rotational distribution, because of the shift with increasing temperature to higher N', having lower state-specific σ_Q. This must also be taken into account in interpreting chemiluminescence data, which exist over a range of temperature near the flame front.

The average cross section for a rotationally thermal distribution in the v'=0 level of the $A^2\Delta$ state of CH has also been measured at elevated temperature in the LP/LF apparatus [22]. Here, a comparison could be made with cross sections determined from a photodissociation method at room temperature [23]. For the four colliders common to both experiments, σ_Q increased from 25% to tenfold, in going from 300 K to 1300 K. This behaviour is markedly different from that of OH. This indicates a quenching mechanism for CH involving some kind of barrier or repulsive surface.

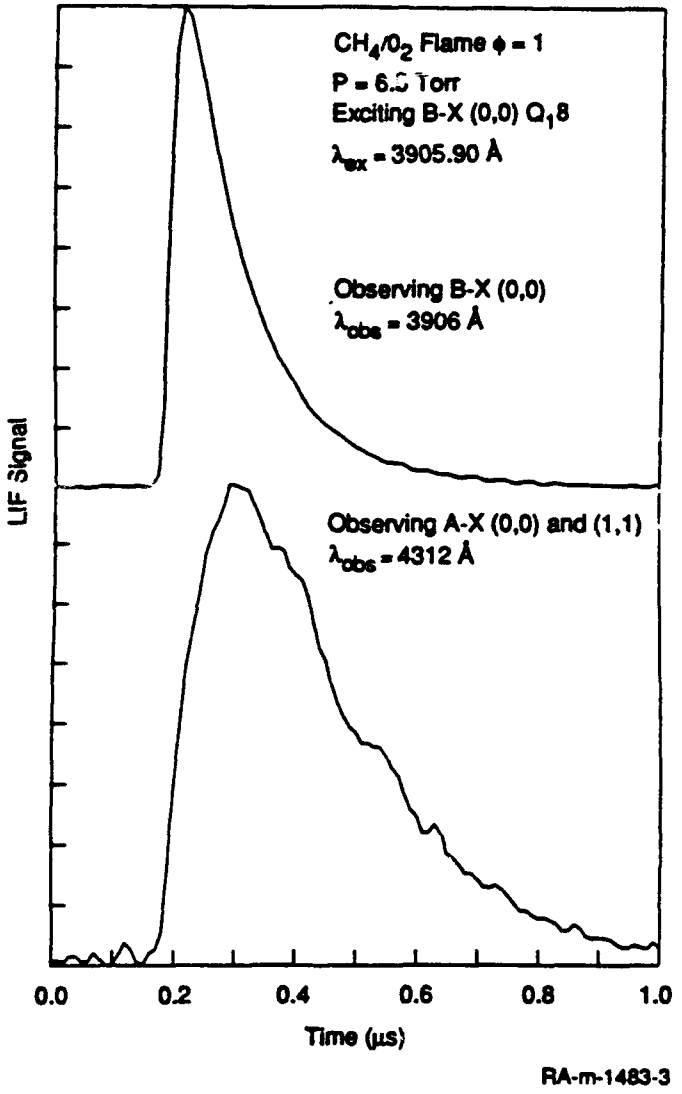

FIGURE 4. Time dependence of fluorescence from the CH molecule in a CH_4/O_2 flame at 6.5 Torr. The laser, with a pulse length of 10 ns, excites the $B^2\Sigma^-$ state. The upper panel shows the fluorescence from this state; the decay time is governed by both quenching and radiation. The bottom panel shows the fluorescence from $A^2\Delta$, populated by collisional energy transfer from B. Its rise time is the same as the B decay time, and this trace decays due to quenching and radiation from A.

Quenching of both the $B^2\Sigma^-$ and $A^2\Delta$ states of CH has also been studied in the low-pressure burner [14]. Unlike the flow or LP/LF systems, flames do not offer an environment consisting of only one collision partner. Nonetheless, some collider-specific cross sections can be obtained for important flame gases. Operating in an H_2/O_2 flame at about 1500 K (with trace amounts of CH_4 added to produce CH), σ_Q for H_20 could be measured. Results for N_2 and CO_2 were obtained by diluting flames with these chemically inert gases, and extrapolating the quenching rate to 100% added diluent. An example of this method is shown in Fig. 5. For these two colliders the quenching cross sections are larger than those from the LP/LF experiments. The LP/LF experiments were performed at 1300 K while these flame measurements are at 1700 K. This thus shows an increase in cross section with increasing temperature for these two colliders, for which no room temperature measurements exist. For H_20, this represents the first quenching determination for this important collision partner. The cross sections are collected in Table 1.

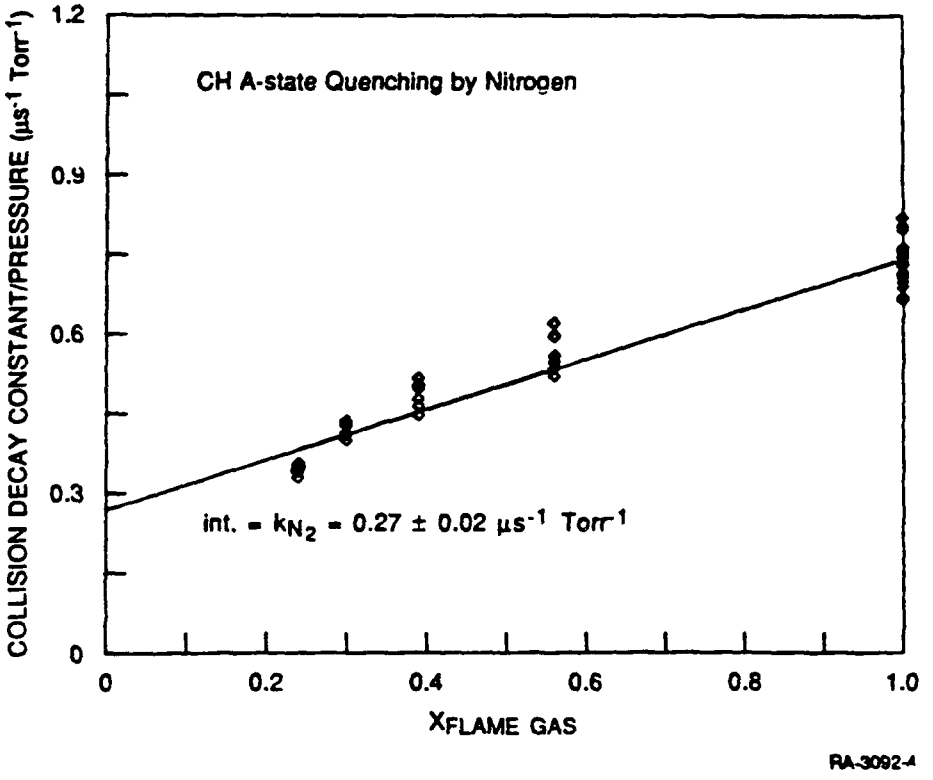

FIGURE 5. Plot of the collisional rate constant in CH_4/O_2 flames diluted with N_2, as a function of mole fraction of flame gas. X=0.0 corresponds to 100% N_2, so that the intercept is the rate constant due to nitrogen quenching.

This table replaces Table 1 in the text. Subsequent studies have shown we can only set upper limits on the collisional cross sections. See K. J. Rensberger, M. J. Dyer, and R. A. Copeland, Appl. Opt. 27, 3679 (1988) for a complete discussion.

CH $A^2\Delta$ and $B^2\Sigma^-$ collisional cross sections/$Å^2$.

Collider	N_2	CO_2	H_2O
Flame			
CH B	<4	<4	<18
CH A	<3	<4	<13
LP/LF (Ref. 22)			
CH A	1.4	2.1	

The decay trace shown in the upper part of Fig. 4 is obtained following laser excitation of a specific N' level in the v'=0 level of the $B^2\Sigma^-$ state of CH in the burner. Here, the spectrometer which viewed the fluorescence was tuned to 390 nm, the location of the (0,0) band of the B-X system. If the spectrometer wavelength is changed to 413 nm, the trace in the lower panel results. This is fluorescence in the (0,0) and (1,1) bands of the A-X system, produced by CH molecules which have been collisionally transferred from the B to the A state. Note that the risetime of the A-X emission is the same as the decay of the B-X trace, whereas the A state dies out more slowly, having smaller σ_Q for all flame conditions and the three individual collision partners for which measurements were made. Spatial profiles showing the fluorescence from A caused by collisional transfer from B are given in Figs. 2 and 3.

4. SUMMARY

Observations on chemiluminescence of OH and CH in hydrocarbon flames have been summarized, and new experimental results suggesting possible multireaction pathways have been described. The possible reactions for the production of CH* have very different energetics, and the nascent distributions of populations within internal levels of the emitting radical may provide clues concerning the important pathway. A proper interpretation of the observed rotational distributions must include considerations of the competing collisional routes of quenching and rotational energy transfer. Experiments performed over a large temperature range have shown that for these two radicals the quenching cross section depends markedly on both rotational quantum state and temperature.

ACKNOWLEDGMENTS

M.A. DeWilde of the Ballistic Research Laboratory took the OH emission scan resulting in Fig. 1; M.J. Dyer, N.L. Garland, J.B. Jeffries and G.P. Smith took part in the quenching and energy transfer studies on OH and CH described in the paper. We thank all of these researchers for their help and numerous discussions. The assembly of this summary was funded by the Gas Research Institute; the research described has received support from GRI, the Air Force Aeropropulsion Laboratory, NASA and the Department of Energy.

REFERENCES

[1] A.G. Gaydon, The Spectroscopy of Flames, Second Edition, Chapman and Hall, London, 1974.

[2] J.M. Corliss, D.D. Paul, R.H. Barnes and W.A. Ivanic, Proceedings of the International Gas Research Conference, in press, 1987; D. Reuter, B.R. Daniel, J. Jagoda and B.T. Zinn, Comb. Flame, 65 (1986) 281.

[3] L.P. Goss, B.G. MacDonald, D.D. Trump and G.L. Switzer, AIAA Paper 831480, Eighteenth Thermophysics Conference, Montreal, Canada, June 1983.

[4] K. Saito and I. Murakami, Comb. Flame, 34 (1979) 331.

[5] W.L. Shackleford, JANAF Exhaust Plume Technology Meeting, San Antonio, Texas, May 1985; R.B. Lyons, J.B. Wormhoudt and C.E. Kolb, Prog. Astron. Aero., 83 (1982) 128.

[6] E.M. Bulewicz, P.J. Padley and R.E. Smith, Proc. Roy. Soc., A315 (1970) 129.

[7] J. Grebe and K.H. Homann, Ber. Bun. Phys. Chem., 86 (1982) 587.

[8] An asterisk is used to denote an electronically excited molecule.

[9] N.L. Garland and D.R. Crosley, Twenty-First Symposium (International) on Combustion, The Combustion Institute, Pittsburgh, 1987, in press.

[10] M.A. DeWilde and D.R. Crosley, NBS Special Publication 561, (1979) 1171.

[11] R.P. Porter, A.H. Clark, W.E. Kaskan and W.E. Browne, Eleventh Symposium (International) on Combustion, The Combustion Institute, Pittsburgh, 1967, p. 907.

[12] J. Grebe and K.H. Homann, Ber. Bun. Phys. Chem., 86 (1982) 581.

[13] K.J. Rensberger and R.A. Copeland, unpublished results.

[14] K.J. Rensberger, M.J. Dyer and R.A. Copeland, Appl. Opt., to be published.

[15] N.L. Garland and D.R. Crosley, Appl. Opt., 24 (1985) 4229.

[16] G.P. Smith, P.W. Fairchild, J.B. Jeffries and D.R. Crosley, J. Phys. Chem., 89 (1985) 1269.

[17] I.S. McDermid and J.B. Laudenslager, J. Chem. Phys., 76 (1982) 1824.

[18] R.A. Copeland, M.J. Dyer and D.R. Crosley, J. Chem. Phys., 82 (1985) 4022.

[19] G.P. Smith and D.R. Crosley, Eighteenth Symposium (International) on Combustion, The Combustion Institute, Pittsburgh, 1981, p. 1511.

[20] N.L. Garland and D.R. Crosley, J. Chem. Phys., to be published.

[21] R.A. Copeland and D.R. Crosley, J. Chem. Phys., 84 (1986) 3099; J.B. Jeffries, R.A. Copeland and D.R. Crosley, J. Chem. Phys., 85 (1986) 1898; G.P. Smith and D.R. Crosley, J. Chem. Phys., 85 (1986) 3896.

[22] N.L. Garland and D.R. Crosley, Chem. Phys. Lett., 134 (1987) 189.

[23] C.J. Nokes and R.J. Donovan, Chem. Phys., 90 (1984) 167.

Appendix B

TIME-RESOLVED LASER-INDUCED FLUORESCENCE IN LOW-PRESSURE FLAMES

AMERICAN INSTITUTE OF PHYSICS
CONFERENCE PROCEEDINGS NO. 172
NEW YORK 1988

OPTICAL SCIENCE AND ENGINEERING SERIES 9

SERIES EDITOR: RITA G. LERNER

ADVANCES IN LASER SCIENCE–III

PROCEEDINGS OF THE THIRD INTERNATIONAL LASER SCIENCE CONFERENCE

ATLANTIC CITY, NJ 1987

EDITORS:

ANDREW C. TAM
IBM ALMADEN RESEARCH CENTER

JAMES L. GOLE
GEORGIA INSTITUTE OF TECHNOLOGY

WILLIAM C. STWALLEY
UNIVERSITY OF IOWA

TIME-RESOLVED LASER-INDUCED FLUORESCENCE IN LOW-PRESSURE FLAMES

Karen J. Rensberger, Mark J. Dyer, Michael L. Wise,
and Richard A. Copeland
Molecular Physics Department, SRI International
Menlo Park, California 94025

ABSTRACT

Time-resolved laser-induced fluorescence measurements of the total removal rate constants of electronically excited states of the NH and CH radicals have been obtained in a variety of low-pressure (5 to 20 Torr) flames. The NH($A^3\Pi$) removal rate constants have been examined for flames containing N_2O as an oxidizer and source of nitrogen. The NH fluorescence quantum yields decrease significantly in the early portion of the flame where the temperature is lower, and become constant farther away from the burner. For CH, the $B^2\Sigma^-$ removal rate constant is about 70% faster than that of the $A^2\Delta$ in several hydrocarbon/oxygen stoichiometric flames; both rates do not vary significantly from flame to flame. The CH removal rate constants for both electronic states are constant or show a slight increase from the burner surface into the burnt gases for all the flames. Temperature profiles are obtained using excitation scans over several rotational levels for CH and NH.

INTRODUCTION

Laser-induced fluorescence (LIF) is a sensitive, selective and non-intrusive spectroscopic diagnostic technique for the detection of minor species in flames.[1] Radical intermediates such as CH and NH are ideal candidates for LIF detection because of their relatively low concentration (ppm) and easily accessible electronic states. Quantitative concentration measurements using LIF require knowledge of both the radiative and the collisional processes that occur following electronic excitation.[2]

In this work, we examine the collisional energy transfer of the $A^2\Delta$ and $B^2\Sigma^-$ states of CH and the $A^3\Pi$ state of NH by direct measurement of the time dependence of the LIF in several low-pressure premixed flat flames. At atmospheric pressure, the LIF of these radicals follows the time profile of the excitation laser because of the rapid collisional quenching; in the low-pressure flame, the quenching rate is reduced so that the fluorescence decays are significantly slower than that of the laser light and can be directly observed.

EXPERIMENTAL APPROACH

For these LIF experiments, the pulsed output of an excimer-pumped dye laser excites the radicals from the ground state to a specific level (v, J) in an excited electronic state. The radicals are generated in a premixed low-pressure laminar flame burning on a

McKenna Products flat porous plug burner of 6 cm diameter. Flames of many different fuels, oxidizers, and fuel equivalence ratios are burned in the study. The burner can be scanned vertically to examine different regions of the flame. The LIF is imaged onto the entrance slit of a monochromator acting as a wide bandpass tunable filter. A photomultiplier tube monitors the dispersed light and its output is amplified and captured using either a 100 megasample/sec transient digitizer or a boxcar integrator. The time dependent fluorescence signal is fit from 90% to 10% of its peak value to a single exponential decay constant.

NH($A^3\Pi$) QUENCHING

Until this study, the collisional removal rate constants of the $A^3\Pi$ state of NH in flames were unknown; however, we have now directly measured fluorescence decay constants in a number of low-pressure flames containing N_2O. Figure 1 is a typical summary plot of the data for a C_2H_4/N_2O flame at 14 Torr with a fuel equivalence ratio of $\phi = 1.06$. The bottom solid line is the NH LIF signal from excitation of the $P_3(7)$ transition in the (0,0) vibrational band of the $A^3\Pi$-$X^3\Sigma^-$ electronic transition as a function of height above the burner. At this pressure the signal peaks near 5 mm and persists out past 12 mm. The boxes above the LIF signal correspond to the right-hand vertical axis and give the temperature profile extracted from NH excitation spectra. Details will be given in a future publication. The diamonds show the decay constants extracted from the temporal evolution as a function of height above the burner. They change considerably from early times in combustion (near the burner) to the burnt gases (> 10 mm). Each decay constant is composed of a pressure independent term due to the NH radiative lifetime of 2.3 μs^{-1} and a pressure dependent term due to collisional quenching. The decrease in the decay constants shown in Figure 1 for NH is typical for all the flames studied. This behavior can be explained by the change in density and relative collision velocity that results from the differences in the temperature. This accounts for most of the change in the decay constant. We therefore conclude that the effective cross section for collisional removal is roughly the same over the entire flame.

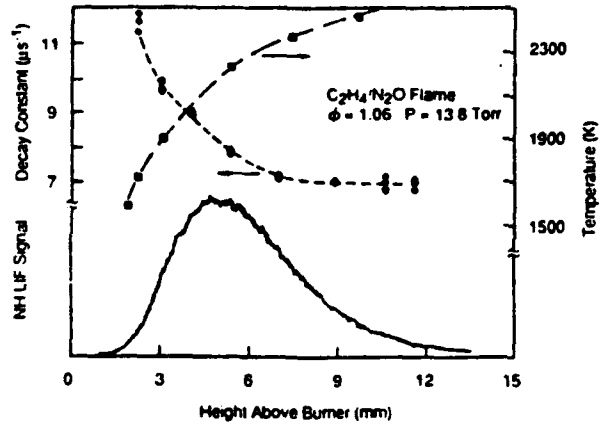

Figure 1

$CH(A^2\Delta)$ AND $CH(B^2\Sigma^-)$ QUENCHING

The electronic quenching of the $A^2\Delta$ state of CH has been studied previously for a 20 Torr methane/oxygen flame by Cattolica et al.[3]; we have now made temporally resolved measurements in several different hydrocarbon/oxygen flames for both the $A^2\Delta$ and the $B^2\Sigma^-$ electronic states of CH. We find these notable aspects of the data. The CH fluorescence quantum yields for both the B- and A-states extracted from the decay constants remain constant or decrease slightly with distance from the burner surface, in marked contrast to NH. As CH is found primarily in the region of the flame front where the temperature is increasing, a quenching cross section that also increases with distance from the burner is suggested from the data. We observe that the B-state is removed about 70% faster than the lower lying A-state for all the flames, even though the position dependences are similar. This difference in quenching was anticipated from indirect measurements in an atmospheric pressure flame by Garland and Crosley.[4] Both electronic states show a slight decrease of 10 to 20% in quenching with increasing rotational level $N' = 2$ to 14.

CH B→A ELECTRONIC-TO-ELECTRONIC ENERGY TRANSFER

In addition to the total removal rates described above, we obtain information on the pathways of the removal of the CH B-state by wavelength resolution of the fluorescence. We find that a significant fraction of the molecules initially excited to the B-state fluoresce at a later time from the A-state of CH. This effect, previously observed in atmospheric pressure flames,[4] can be used advantageously to eliminate scattered laser light from the detection of CH. Exciting the B-state and observing the A-state about 50 nm away could eliminate many detection problems in systems with significant particulate scattering. The signal profiles for the B-state LIF and the B→A transferred emission show that the relative amount of electronic energy transfer is constant throughout the changing collision environment across the flame. All flames studied to date show this energy transfer effect.

ACKNOWLEDGEMENTS

We thank Dave Crosley for many helpful discussions on both the experiment and interpretation. This research is supported by the Aero Propulsion Laboratory of the Air Force Wright Aeronautical Laboratories and the National Science Foundation.

REFERENCES

1. D. R. Crosley, High Temp. Mat. and Proc. 7, 41 (1986).
2. N. L. Garland and D. R. Crosley, Twenty-First Symposium (International) on Combustion, The Combustion Institute, Pittsburgh, in press (1987).
3. R. J. Cattolica, D. Stepowski, D. Puechberty, and M. Cottereau, J. Quant. Spectrosc. Radiat. Transfer 32, 363 (1984).
4. N. L. Garland and D. R. Crosley, Appl. Opt. 24, 4229 (1985).

Appendix C

NH AND CH LASER-INDUCED FLUORESCENCE IN LOW-PRESSURE FLAMES: QUANTUM YIELDS FROM TIME-RESOLVED MEASUREMENTS

Twenty-Second Symposium (International) on Combustion/The Combustion Institute, 1988/pp. 1867–1875

NH AND CH LASER-INDUCED FLUORESCENCE IN LOW-PRESSURE FLAMES: QUANTUM YIELDS FROM TIME-RESOLVED MEASUREMENTS

KAREN J. RENSBERGER, RICHARD A. COPELAND, MICHAEL L. WISE AND DAVID R. CROSLEY

Molecular Physics Laboratory
SRI International
Menlo Park, California 94025

Time-resolved laser-induced fluorescence measurements of the total removal rate constants for the $v' = 0$ vibrational level of electronically excited states of the NH and CH radicals are obtained in a variety of low-pressure (5 to 25 Torr) flames. The NH($A^3\Pi_i$) removal rate constants are examined for flames containing N_2O as an oxidizer and source of nitrogen. The NH fluorescence quantum yields decrease in the early portion of the flame where the temperature is lower, and become constant farther away from the burner. For CH, the $B^2\Sigma^-$ removal rate constant is about 70% faster than that of the $A^2\Delta$ in several hydrocarbon/oxygen stoichiometric flames; both rates do not vary significantly from flame to flame. The CH removal rate constants for both electronic states are constant or show a slight increase from the burner surface into the burnt gases for all the flames. Temperature profiles are obtained using excitation scans over several rotational levels for CH and NH. Upper limits and estimates for collider specific quenching cross sections for H_2O, N_2, CO_2, and several fuel species are extracted. Collisional energy transfer is observed from the $B^2\Sigma^-$ to the $A^2\Delta$ state of CH. Quantitative measurements show this process has useful diagnostic applications.

Introduction

Laser-induced fluorescence (LIF) is the most sensitive and selective nonintrusive technique for the detection of many diatomic radicals in flames.[1] LIF is generally straightforward to apply to a wide variety of combustion environments, furnishing detailed species concentrations to help unravel complicated chemistry and transport phenomena. Since its inception, however, researchers have realized that quantitative LIF concentration measurements are complicated by collisional processes that occur in the excited electronic state.[2] Only a fraction of the molecules excited by the laser fluoresce and are detected; the rest are removed by collisions (i.e., quenched). Knowledge of this fraction, the fluorescence quantum yield Φ, is needed to relate the measured signals to the desired ground state radical concentrations. Absolute concentration measurements are directly impacted, but even relative measurements can be affected under conditions of varying major species concentration and temperature. One approach[3,4] attempts to minimize the effects of collisions by using a high laser fluence (saturation), but has several drawbacks among which are the difficulty of estimating the probed volume[4] and the complexity of the model used for data analysis. In this work, we attempt to understand the collisional effects for a variety of conditions in sufficient detail to provide enough insight to estimate Φ and its accuracy for different flame conditions.

We examine the NH and CH radicals in low-pressure premixed laminar flat flames via direct measurement of the time evolution of LIF signals. There are significant unanswered questions concerning the quantum yields of these frequently observed radicals. This was pointed out in a study in the preceding symposium,[5] in which estimates of Φ under typical flame conditions were attempted, beginning from available literature on bimolecular quenching rate constants. Much important information, particularly the temperature dependence of quenching and the value of the water quenching cross section, are lacking. In the work presented here, results on total removal rate constants, as functions of position in the flame and of rotational level, are presented for both radicals in several different hydrocarbon flames. Importantly, the variation with flame position is smooth, can be extrapolated, and is generally understood. Some information on collider-specific quenching rate constants is obtained, and small effects of rotational level dependence can be discerned. Collisional transfer between two excited states in CH, $B^2\Sigma^- \rightarrow A^2\Delta$,

is observed and may have useful diagnostic applications.

Experimental Approach

The apparatus can be divided into three parts: the low-pressure burner system, the excitation laser, and the fluorescence detection system. Major features of each are outlined below; a complete description can be found in Ref. 6.

The burner system is composed of a vacuum chamber with electronic, mechanical, and optical components for positioning and probing the flame. The burner is a flat-flame porous-plug McKenna design. Flames of many different fuels and oxidizers are burned between 5 and 25 Torr total pressure.

The output of a pulsed excimer-pumped dye laser (~15 ns, ~0.2 cm^{-1}) excites the radical from the ground state to a specific quantum level in the excited electronic state. All measurements are made on the $v' = 0$ vibrational level; excitation is to $NH(A^3\Pi_i)$, $CH(B^2\Sigma^-)$, or $CH(A^2\Delta)$ at 336, 385, and 413 nm respectively. An aperture limits the beam diameter to less than 1 mm. Pulse energies between 1 μJ and 1 mJ are obtained using beamsplitters and attenuators. A laboratory computer controls the laser wavelength and records the signal. An $f/3$ lens collects the LIF and an $f/4$ lens focuses the light onto a filter or the entrance slit of a monochromator, where it is detected by a photomultiplier whose amplified output is captured using either a 100 megasample s^{-1} transient digitizer or a boxcar integrator, averaging between 30 and 2000 laser shots.

The wavelength dependence of the response of the detection system is crucial to the interpretation of the results. LIF populates a single rotational level N′ in the excited state. In NH and CH, like OH, rotational equilibration is not achieved prior to quenching. If the fluorescence is viewed with a narrow band detector (≤10 nm) rotational energy transfer to levels whose fluorescence is not viewed in that bandpass can be a significant removal mechanism.[7] If all rotational levels are observed with equal sensitivity, many possible complications arising from rotational energy transfer, and from the rotational level dependence of both the radiative lifetime[8] and the quenching are minimized. All results and interpretations are based upon using a detection system with a flat response over the entire vibrational band monitored.

The decay trace following excitation of a single N′ appears to be a single exponential, but is actually composed of a combination of many exponentials similar in magnitude. We fit the time-dependent signals from 90% to 10% of the peak to a single exponential to obtain a decay constant τ^{-1}, which is the sum of the radiative rate and a collisional removal rate Q. The single exponential fits and the experimental data agree to within the noise level in the signal.[6] Under these conditions, some rotational relaxation has occurred and the values obtained represent the behavior of the distribution of rotational levels following excitation of N′. This distribution strongly peaks near the initially excited N′ as can be seen for CH from fluorescence scans under steady-state conditions in both atmospheric pressure[9] and low-pressure[10] flames, and is true for NH as well. Subtracting the known radiative rate for the initially excited N′ from the measured value of τ^{-1} yields the collisional removal rate Q, which when divided by the pressure gives the total removal rate constant k_Q^P in units of μs^{-1} $Torr^{-1}$. When converted into density units by knowledge of the temperature, these rate constants furnish quenching rate constants k_Q in units of cm^3 s^{-1}, which can be divided by the average collision velocity to give quenching cross sections $\sigma_Q(k_Q = \langle v \rangle \sigma_Q)$.

Profiles of radical concentrations as a function of height above the burner are obtained using the boxcar integrator. The laser wavelength is set to a transition originating from a rotational level whose relative population does not change significantly over the temperature region sampled; in CH this is $R_2(7)$ for the B-state and P(7) (overlap of two lines) for the A-state, and in NH $P_3(8)$. The burner is scanned using a dc motor and the position read via a potentiometer attached to the drive mechanism.

Precise knowledge of the temperature is important for the interpretation of the LIF profiles and the quenching data. It is determined at a given burner position through unsaturated excitation scan spectra which are fit directly to a single temperature parameter. In NH we scan the very congested Q-branch region. It contains many lines of high and low N″ in a small wavelength range. For CH A-state excitation, we scan the Q- and R-branches and for CH B-state only the R-branches. Excitation scans have also been taken with CN and with OH. In most cases the temperatures agree to about ±200 K. Further details on the temperature measurements, including a discussion of sources of error, can be found in Ref. 11.

Quenching of $NH(A^3\Pi_i)$

Prior to this investigation, Φ for NH in flames was estimated[5] from quenching data at room temperature[12,13] and at 1400 K.[14] The higher temperature study, using laser pyrolysis/laser fluorescence (LP/LF), provides the best guide for flame estimates. However, the list of colliders investigated did not include the important rapid quencher H_2O or hydrocarbons with more than one carbon.

The effect of these species could only be estimated by analogy with the behavior of other similar colliders, and the more extensive studies on OH. Here, we measure the time dependence of the NH LIF in flames of hydrogen and various hydrocarbons burning in N_2O near 14 Torr and fuel equivalence ratios $\phi \sim 1$.

Figure 1 shows the data obtained in a H_2/N_2O flame. The diamonds show the position dependence of the decay constant τ^{-1} while the boxes denote the temperature; the bottom portion displays the NH LIF intensity. As the temperature increases from about 1000 K at 1.5 mm to over 2200 K near 9 mm, the decay constant decreases, largely due to the corresponding decrease in the density. This corresponds to a slight increase in Φ, 0.19 at the point nearest the burner to 0.22 in the burnt gases (420 ns radiative lifetime). The rate constant k_Q has increased, from 0.7 to 1.3×10^{-10} cm^3 s^{-1}, an amount slightly more than the increase in the collision velocity, indicating that the average cross section σ_Q has increased as well. This likely reflects the changing composition of the flame gases over this spatial region.

The flames we investigate containing NH all use N_2O as the oxidant and the fuels H_2, CH_4, C_3H_8, C_2H_4, and C_2H_2 at 13.8 ± 0.3 Torr and ϕ near 1. Figure 2 summarizes the k_Q dependence on temperature, which is estimated from the measured temperature profiles at the position where the decay constants are obtained. In the different flames

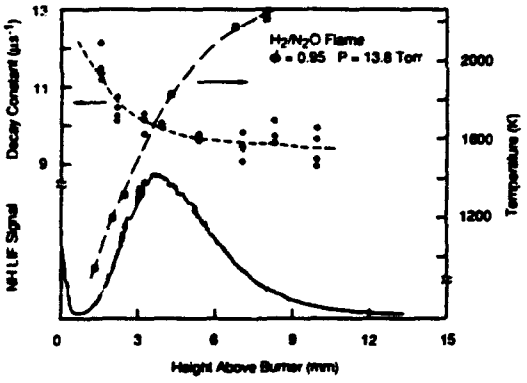

FIG. 1. Summary of NH data obtained in a 13.8 Torr, ϕ = 0.95, H_2/N_2O flame. The bottom curve is the NH LIF signal as a function of height above the burner following excitation of the $A^3\Pi_i - X^3\Sigma$ (0,0) $P_3(8)$ rotational line. The increase near the burner surface is due to laser light scattered off the burner surface. The boxes illustrate the NH rotational temperatures (right vertical axis) and the diamonds the fluorescence decay constants (left vertical axis) as functions of position. The dashed lines have been added to guide the eye through the experimental data points.

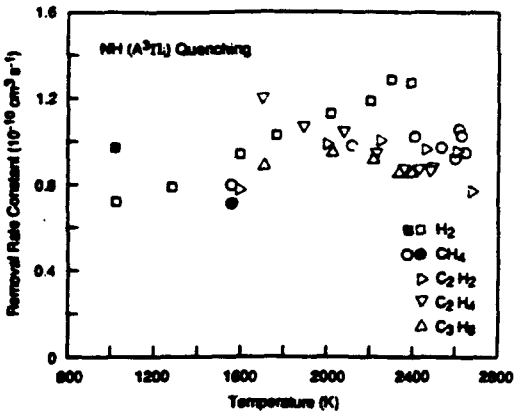

FIG. 2. Temperature dependence of the NH($A^3\Pi_i$) total quenching rate constants for several flames. The oxidizer in all cases is N_2O and the fuel equivalence ratios are 0.95, 1.04, 1.01, 1.06, and 1.04 for H_2, CH_4, C_3H_8, C_2H_4, and C_2H_2, respectively. The open symbols show the experimental data points while the closed symbols show the calculated rate constants from the cross sections given in Ref. 14 (see text). The rate constants at a particular temperature are recorded at different positions in the different flames and therefore under different collison environments.

these positions can correspond to very different collision environments. However, the rate constants in the hydrocarbon flames are remarkably similar, varying only about 10% from flame to flame. Note that k_Q in the H_2/N_2O flame are 10% to 30% faster than those at the same temperature in the hydrocarbon flames, save for C_2H_4 near the burner.

We can compare the results for the H_2 and CH_4 flames with k_Q calculated from the cross sections of Ref. 14. There, σ_Q for H_2, N_2O and CH_4 were determined to be 4.5, 2.8 and 7.8 Å^2, respectively, at 1400 K. Fortunately, this temperature is similar to those for the flame data taken closest to the burner. At this point, some reaction of the fuel and oxidizer has occurred, and a small amount of water and nitrogen is present due to diffusion back to the burner surface. However, in order to estimate quenching rates from the 1400 K σ_Q, we ignore these processes and assume that the fuel and oxidizer concentrations can be approximated by the initial values and use the σ_Q directly. To gauge this assumption, we examine the results of a computer model[15,16] and experimental measurements[17] for low-pressure H_2/N_2O flames. (Results for such flames at atmospheric pressure[18] are inapplicable because of different conditions.) We do find partial decomposition but note that the k_Q results in Fig. 2 vary smoothly and only little at low temperatures. The calculated k_Q for the H_2 and CH_4 flames are shown

in Fig. 2 as the solid box and solid circle. In the H_2 case, k_Q is overestimated by 20%, while that for CH_4 is only slightly lower than measured. This agreement, together with the smooth variation of k_Q in this region, suggests that we can describe NH quenching in the cooler regions of these two flames.

Thus encouraged, we use the experimental k_Q to estimate the approximate magnitude of the quenching cross sections for the other fuel species. In the CH_4 flame, about half the quenching is by N_2O and the rest is by the CH_4. Assuming the same amount of fuel and oxidizer reaction and diffusion at the first appearance of NH near 1600 K for all the flames, we estimate a cross section for C_2H_2 that is 1–3 times that of CH_4 and those for C_2H_4 and C_3H_8 are 2–5 times that of CH_4. The trends agree with results on NH at room temperature[19] and expectations based on quenching of OH by hydrocarbons.[20]

Perhaps the most important unknown quenching cross section is that for H_2O. From our data we can currently generate a reasonable upper limit. (Further measurements and detailed flame modeling are needed for a more accurate value.) The limit is obtained as follows. We follow k_Q as far into the burnt gases of the H_2/N_2O flame as possible. If the combustion were complete we would have about 50% H_2O and 50% N_2, but we know from preliminary modeling studies[16] that this is not the case. The flame contains unburnt fuel, radicals such as H, O, and OH, and NO at the highest point where we can measure NH. From Refs. 12 and 14 we know that N_2 quenching is so slow that for this purpose it can be set to zero. For the other species, the σ_Q are unknown; however, assuming they also do not contribute leads to an upper limit for H_2O. The minimum possible H_2O mole fraction in this region of the flame[14] is about 30%. Using this concentration yields the value $\sigma_Q(H_2O) \leq 17$ Å^2 at 2200 K. This upper limit is consistent with a combination of room temperature[13] and LP/LF[14] results for the polar colliders water and ammonia: at 300 K, $\sigma_Q(N' = 7)$ for H_2O is about 35 Å^2, half the value of 65 Å^2 for NH_3, while at 1400 K, $\sigma_Q = 26$ Å^2 for NH_3. Thus with our estimations of the flame temperature hydrocarbon and water cross sections, a consistent set of values for NH quenching contained in Table I is emerging.

The rotational level dependence of k_Q has also been examined in several flames, at the peak of the NH concentration where the signal is largest. Experiments at room temperature, both NH emission following photodissociation of NH_3[12] and direct LIF decay,[13] have shown that σ_Q depends on N′. Here, the initial N′ is varied between 2 and 16. Recall that some rotational energy transfer occurs, so the signal is actually a sum of exponentials with slightly different decay constants; however, the results realistically represent the N′-specific dependence. In the H_2/N_2O, C_3H_8/N_2O, and CH_4/N_2O flames we find a consistent, albeit small, decrease in σ_Q with increasing rotation, ranging from 3 to 8% from $N' = 2$ to 12.

TABLE I
Cross sections for NH and CH quenching at high temperatures.

	NH($A^3\Pi_i$)		CH($A^2\Delta$)	CH($B^2\Sigma^-$)	
	σ(Å^2)	T(K)	σ(Å^2)	σ(Å^2)	T(K)
N_2	<0.1[a]	1400	1.4[b]		1300
			<3[c]	<4[c]	1800
CO_2	1.2[a]	1400	2.1[b]		1300
			<4[c]	<4[c]	1800
H_2O	<17[c]	2200	<13[c]	<18[c]	1200

[a]Results of Ref. 14.
[b]Results of Ref. 24.
[c]Upper limits from this work.

This rotational level dependence is too small to have meaningful implications for concentration measurements, but can affect LIF temperature determinations.[11] Levels with higher N′ live longer due to the slower quenching and longer radiative lifetime.[8] (The ratio determines the overall quantum yield Φ, which increases slightly with N′ in these flames.) A narrow gate on the peak of the signal can be used under low-pressure conditions where the time dependence of the decay is resolved to avoid effects of the rotational relaxation, but at high pressures such time resolution is not possible. In our flames, the variation from $N' = 2$ to 12 is typically only 5%. The effect on the temperature determination is investigated by a simple calculation assuming all of the fluorescence is detected by a wide boxcar gate. We find that a 5% variation corresponds to a systematic temperature error of 120 K at 1800 K, enough to render questionable some detailed comparisons with flame chemistry models. Consequently, the effects of rotational level dependent quenching on excitation scan temperature determinations in NH cannot be completely ignored.

We can summarize these results for quantum yields in the $A^3\Pi_i$ state of NH. This radical is quenched more slowly than CH (see below) or OH[15] in flames, and Φ is some 50 to 100% larger. As a guide, we recommend that a general value for the quenching rate constant of 1×10^{-10} cm^3 s^{-1} should be used to extract the absolute concentration in N_2O-based flames with ϕ near unity. All of the measurements we performed clustered between ±30% of this value. Interestingly, the values near the peak of the NH concentration have significantly less variation. Within 25% of the peak, the k_Q differ only by 10% from flame to flame. We are encouraged

that the collider-specific rate constants describe quenching in the H_2 and CH_4 flames realistically. From information on other collider-specific σ_Q, we expect richer flames to have slightly faster rate constants and leaner flames slightly slower. Flames of N_2O diluted by N_2 should have slower quenching in that the N_2 diluent causes no quenching. In flames containing NH_3 and O_2, NH should be quenched slightly faster since both of these molecules have large σ_Q.[12-14] Such differences perhaps account for as much as, but no more than, a two-fold difference in Φ and thus the absolute concentration. Differences appear to be greater at low NH values compared to the signal maximum (see Fig. 2).

Quenching of CH $A^2\Delta$ and $B^2\Sigma^-$

In the CH radical there are three different electronically excited states which can be conveniently accessed by LIF in flames. The origin of the electronic transitions to the $A^2\Delta$, $B^2\Sigma^-$, and $C^2\Sigma^+$ lie at 431, 387, and 314 nm, respectively. (The $C^2\Sigma^+$ predissociates so rapidly that direct time resolved measurements on this state are beyond the capabilities of our detection system.) The time evolution of the $A^2\Delta$ state has been observed in low-pressure acetylene/oxygen[21] and methane/oxygen[22] flames; however, the time evolution of the $B^2\Sigma^-$ state has not been previously investigated.

Here we study both states in flames of CH_4, C_3H_8, and C_2H_2 burning in O_2 and in H_2/O_2 flames seeded with 10% methane to produce the radical. The $A^2\Delta$ state is also investigated in C_3H_8 burning in N_2O flames, but intense flame emission in the B-X system of the CN radical interfered with the CH B-X LIF, preventing a study of the $B^2\Sigma^-$ state in that flame. For CH, the rate constants are obtained from the slope of the pressure dependence of the quenching decay constants, measured at the peaks of the CH signal; the intercepts correspond to the radiative rates. Data for five different flames are shown in Fig. 3.

We consider first the results for the $A^2\Delta$ state. The decay constants in all the hydrocarbon/oxygen flames have a similar pressure dependence, whereas those for the propane/nitrous oxide flame are somewhat lower, and those for the hydrogen/oxygen flame seeded with 10% methane higher. These differences could be due either to differences in temperature or composition at the position of the CH signal maxima. The H_2/O_2 flame is coolest and C_3H_8/N_2O is hottest, with highest and lowest density, respectively. However, there is also more H_2O (a good quencher) in the former flame and more of the poor quencher N_2 in the latter. The data of Fig. 3 are not sufficient to distinguish which is more important. An average k_Q for CH($A^2\Delta$) quenching in all the hydrocarbon/O_2 flames is obtained from the slope of a linear least-squares fit to the CH_4/O_2, C_3H_8/O_2, and C_2H_2/O_2 flame data. The result is 0.77 ± 0.04 μs^{-1} $Torr^{-1}$; using an average flame temperature of 900 K, we calculate a rate constant of 1.4×10^{-10} cm^3 s^{-1}.

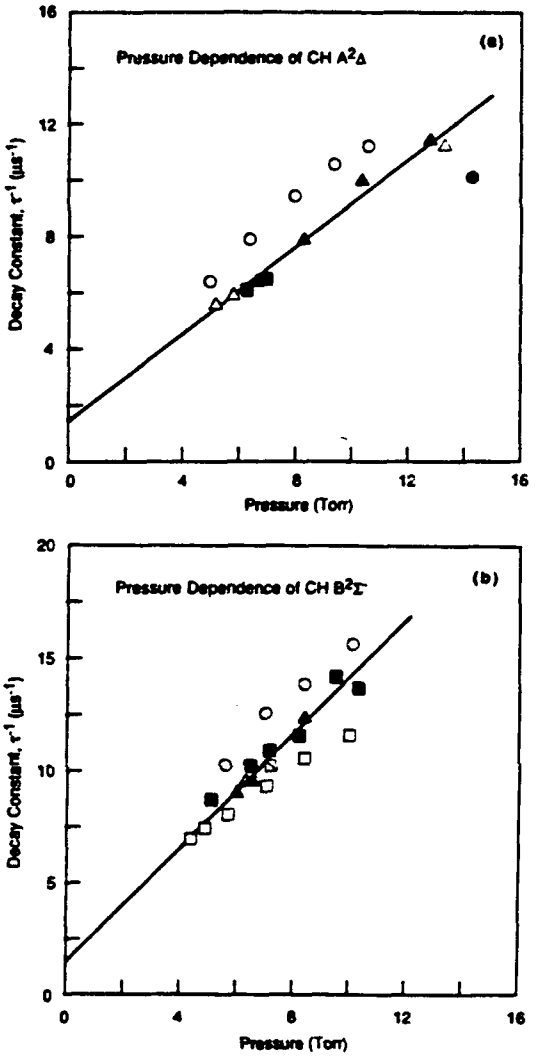

FIG. 3. Pressure dependence of the decay constants for (a) CH ($A^2\Delta$) and (b) CH ($B^2\Sigma^-$) quenching in the following flames: ○, H_2/O_2 seeded with CH_4; ■, CH_4/O_2 $\phi = 1$; □, CH_4/O_2 $\phi = 0.66$; ⧅, CH_4/O_2 $\phi = 1.2$; △, C_2H_2/O_2 $\phi = 1$; ▲, C_3H_8/O_2 $\phi = 1$; ●, C_3H_8/N_2O $\phi = 1$. The slopes of the linear least-squares fits to the data for the CH_4, C_2H_2, and C_3H_8/O_2 $\phi = 1$ flames give the quenching rate constants k_Q and the intercepts correspond to the radiative rates.

Similar results have been obtained for the $B^2\Sigma^-$ state in the oxygen-based flames. From the slope

of the pressure dependence plot we obtain a rate constant of 1.3 ± 0.14 μs^{-1} $Torr^{-1}$ or, using a flame temperature of 1800 K, 2.5×10^{-10} cm^3 s^{-1}. Thus, under identical flame conditions, the B-state of CH is quenched about 70% faster than the A-state. This is in accord with the implications of results of multiphoton ionization of CH in flames, using the A- and B-states as resonant intermediates,[23] and with atmospheric pressure flame measurements of energy transfer processes.[9]

The quenching for both states as a function of position in the CH_4/O_2 flame is displayed in Fig. 4. These data are representative for this flame, but for the propane and acetylene flames the decay constants are unchanging across the entire profile. (This stands in marked contrast to the results previously described for NH, Fig. 1.) Because the temperature change across the flame leads to a density decrease, this means that the quenching cross section must be increasing with increasing temperature. This also contrasts with results for both OH and NH, but is in accord with collider-specific measurements on $CH(A^2\Delta)$. For four colliders common to both studies, σ_Q measured with LP/LF at 1300 K[24] were larger than those measured in a photodissociation/emission experiment at 300 K.[25]

From the data in the H_2/O_2 flame at the peak CH signal, we obtain upper limits for the H_2O quenching in both the A- and the B-states. The reasoning is similar to that used for NH. We assume all the other species present have a zero quenching rate and that H_2O makes up 40–50% of the total gases. This leads to upper limits on the H_2O quenching cross sections of 13 and 18 $Å^2$ for the A- and B-state respectively.

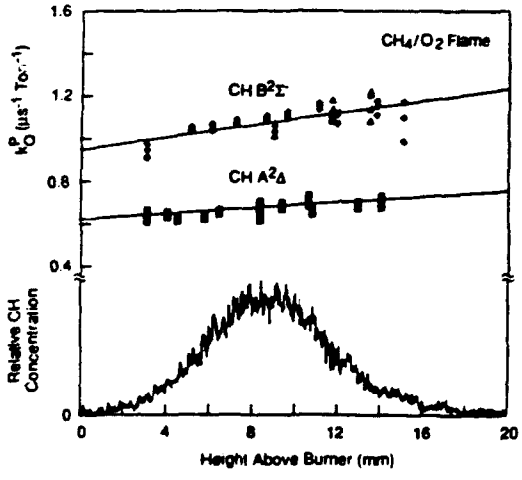

FIG. 4. Position dependence of the CH ($A^2\Delta$) and ($B^2\Sigma^-$) quenching rate constants for a methane/oxygen flame. The lower trace is the CH ground state relative concentration profile. The different symbols for the quenching data indicate data taken on different days. The lines are linear least-squares fits to the data.

Upper limits for the contributions of N_2 and CO_2 to the quenching are estimated by adding known amounts of each gas to a propane and oxygen flame gas mixture. Addition of the gas may cool off the flame, but we did not measure the temperature for each flame composition. The greatest effect will be seen for a constant temperature flame. For both gases, we see that the quenching at the peak CH signal decreases significantly with each further addition. The change is due to the addition of a less efficient quencher, but counterbalanced somewhat by the increase in density by cooling. The addition of CO_2 may also influence the flame chemistry. Extrapolation of the measured quenching rate constants to 100% added N_2 or CO_2 gives an upper limit to the rate constants for quenching by each gas. Cross sections derived from these limits using a temperature of 1800 K are $\sigma_Q < 3$ $Å^2$ and < 4 $Å^2$ for N_2 for the A- and B-state, respectively, and $\sigma_Q < 4$ $Å^2$ for CO_2 for both states. The A-state cross sections are larger than those measured[24] at 1300 K: σ_Q is 1.4 $Å^2$ and 2.1 $Å^2$ for N_2 and CO_2. No collider specific quenching cross sections are available for comparison for the B-state. Table I summarizes all of the high temperature cross sections.

We can use the collider-specific cross sections to calculate quenching rates for comparison with the other reported direct decay measurements on $A^2\Delta$ in low-pressure flames. (Disagreement of nearly a factor of two in a similar comparison in Ref. 5 was attributed to the estimate of $\sigma_Q(H_2O)$ used there, 23 $Å^2$, being too large.) In a CH_4/O_2 flame at 20 Torr, $k_Q^P = 0.8$ μs^{-1} $Torr^{-1}$ was measured,[22] agreeing with our experimental value of 0.77 μs^{-1} $Torr^{-1}$. Using reported major species concentrations, the upper limit for σ_Q of H_2O, and the σ_Q for CO, CO_2 and O_2 from Ref. 14, we calculate 0.91 μs^{-1} $Torr^{-1}$. In a C_2H_2 flame at 10 Torr,[21] $k_Q^P = 1.0$ μs^{-1} $Torr^{-1}$. Our measured value is 0.77 in a somewhat leaner flame; the calculated result is also 0.8 μs^{-1} $Torr^{-1}$.

For CH there is also a rotational level dependence of the quenching rate constant. The decay constants at the peak of the CH signal are measured as a function of N'. In the CH_4/O_2 flame, there is no dependence (within ±5%) as N' varies from 2 to 12. In the C_3H_8/O_2 flame, k_Q decreases 16 and 18% for the A- and B-states over the same range of N'; in C_2H_2/O_2 the respective decreases for A and B were 9 and 18%. This variation can affect temperature measurements[11] in the same way as for NH, although the effects are more severe. Calculations such as those described for NH indicate a similar amount of error for the same degree of rotational level dependence of the quenching. For

CH, there are no meaningful effects in the methane flame, but in the propane and acetylene flames, errors of 200 to 400 K at 2000 K can result. The direction is the same, that is, the apparent temperatures are larger than the actual due to the increased signal when exciting high rotational levels.

Quantitative LIF measurements of the CH radical using either the A- or B-state thus turns out to be easier than initially anticipated. This is due to the fact that the time decay of the emission does not change significantly over the entire region of the flame where the CH is present in detectable quantities. This is especially important in two-dimensional LIF imaging of the CH radical,[26] for the intensity pattern may then be directly equated to a map of relative ground state CH concentration. From the measurements of the rate constants for the electronic quenching, we can estimate fluorescence quantum yields for the excitation of the two states. The B-state of CH quenches more rapidly than the A-state, but its radiative lifetime is shorter, at about 340 ns compared to the A-state radiative lifetime of about 540 ns. The two effects almost cancel, giving essentially the same fluorescence quantum yield upon excitation of either state. The selection of the excitation transition will therefore depend only on the excitation laser and the detection system.

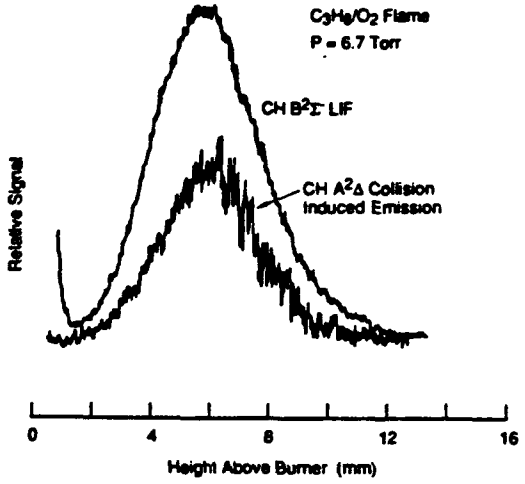

FIG. 5. CH ($B^2\Sigma^-$) LIF and CH ($A^2\Delta$) collision-induced emission profiles in a propane/oxygen flame. Both traces are obtained using excitation of the B-$XR_2(7)$ transition. The upper curve is the CH B-X LIF profile obtained from observation of the B-X band. The increase at small height is from laser scatter off the burner surface. Observation of the A-X band under the same excitation conditions yields the lower curve, evidence for the collisional transfer of CH B-state molecules to the CH A-state.

CH $B^2\Sigma^- \rightarrow A^2\Delta$ Electronic Energy Transfer

When the $B^2\Sigma^-$ state of CH is collisionally quenched, some of the molecules are transferred to the $A^2\Delta$ state from which they then emit. If the quantum yield for this particular process can be estimated accurately, this electronic energy transfer could be exploited as a useful monitor of CH radicals. Excitation of B and observation of emission from A could avoid interferences from other fluorescers and scattered light, especially where particulates are present. (A similar scheme involving excitation of the $C^2\Sigma^+$ state and observation of emission from B and A was studied earlier[27] as a means of detecting OH and CH with the same laser.)

Electronic energy transfer from the $B^2\Sigma^-$ state of CH to the $A^2\Delta$ state has been observed in atmospheric pressure flames[9] but only under steady state conditions and averaged over all of the flame front. Here we have spatially resolved the signals to investigate the dependence of this energy transfer for different flame conditions. Figure 5 shows the profile of the directly observed B → X LIF together with the profile of the collision-induced A → X emission following excitation of the B-state in a C_3H_8/O_2 flame. The profiles are very similar even though the flame gas composition and temperature are changing. This strongly suggests that many collision partners cause this electronic energy transfer with approximately equal efficiency, and with little temperature dependence. Similar results are found for all the hydrocarbon/oxygen flames. Direct observation of the time dependence of the A → X emission following excitation of the B-state[28] confirms this collisional population mechanism, in that the A → X signal rises with a rate characteristic of the disappearance of the B-state, and decays at a slower rate corresponding to the slower A-state quenching. From Ref. 9, 20% of the collisionally quenched B-state CH molecules are transferred to the A-state; our results are consistent with that measurement.

The similarity of the profiles in Fig. 5, and corresponding data for other flames, suggests that the B → A transfer can be used accurately as a monitor of CH. The rate of this process, like the overall quenching rates of both states, does not vary greatly with flame composition or temperature, making its use in imaging experiments an attractive possibility.

Acknowledgments

We thank Mark Dyer, Katharina Kohse-Höinghaus, Jay Jeffries and Greg Smith for many helpful discussions, and particularly Mark Dyer for his experimental help during the early stages of the CH work, and Greg Smith for pertinent combustion modeling. The participation of Michael Wise was

made possible by a grant from the National Science Foundation program for Research Experiences for Undergraduates. This work is supported by the Thermal Systems and Engineering program of the National Science Foundation and by the Aero Propulsion Laboratory of the Air Force Wright Aeronautical Laboratories.

REFERENCES

1. Crosley, D. R. and Smith, G. P.: Opt. Engr. 22, 545 (1983); Lucht, R. P.: Laser Spectroscopy and Its Applications, (L. J. Radziemski, R. W. Solarz, and J. A. Paisner, Eds.), p. 623, Marcel Dekker, 1986; Crosley, D. R.: High Temp. Mat. Proc. 7, 41 (1986).
2. Crosley, D. R.: Opt. Engr. 20, 511 (1981).
3. Daily, J. W.: Appl. Opt. 15, 955 (1976); Lucht, R. P., Sweeney, D. W., Laurendeau, N. M., Drake, M. C., Lapp, M. and Pitz, R. W.: Opt. Lett. 9, 90 (1984).
4. Kohse-Höinghaus, K., Heidenreich, R. and Just, Th.: Twentieth Symposium (International) on Combustion, p. 1177, The Combustion Institute, 1985.
5. Garland, N. L. and Crosley, D. R.: Twenty-First Symposium (International) on Combustion, p. 1693, The Combustion Institute, 1988.
6. Rensberger, K. J., Dyer, M. J. and Copeland, R. A.: Appl. Opt., in press, 1988.
7. Smith, G. P. and Crosley, D. R.: Eighteenth Symposium (International) on Combustion, p. 1511, The Combustion Institute, 1981; Crosley, D. R and Smith, G. P.: Comb. Flame 44, 27 (1982).
8. Fairchild, P. W., Smith, G. P., Crosley, D. R. and Jeffries, J. B.: Chem. Phys. Lett. 107, 181 (1984); Garland, N. L. and Crosley, D. R.: J. Quant. Spectr. Radiat. Transf 33, 591 (1985).
9. Garland, N. L. and Crosley, D. R.: Appl. Opt. 24, 4229 (1985).
10. Joklik, R. G. and Daily, J. W.: Comb. Flame 69, 211 (1987).
11. Rensberger, K. J., Copeland, R. A., Jeffries, J. B., Kohse-Höinghaus, K., Wise, M. L., Crosley, D. R.: Appl. Opt., to be published.
12. Hofzumahaus, A. and Stuhl, F.: J. Chem. Phys. 82, 3152 (1985).
13. Garland, N. L. and Crosley, D. R.: J. Chem. Phys., to be published, 1988.
14. Garland, N. L., Jeffries, J. B., Crosley, D. R., Smith, G. P. and Copeland, R. A.: J. Chem. Phys. 84, 4970 (1986).
15. Kohse-Höinghaus, K., Jeffries, J. B., Copeland, R. A., Smith, G. P. and Crosley, D. R.: Twenty-Second Symposium (International) on Combustion, in press, 1988.
16. Smith, G. P.: SRI Report MP 88-006.
17. Balakhnine, V. P., Vandooren, J. and Van Tiggelen, P. J.: Comb. Flame 28, 165 (1977).
18. Vanderhoff, J. A., Bunte, S. W., Kotlar, A. J. and Beyer, R. A.: Comb. Flame 65, 45 (1986); Coffee, T. P.: Comb. Flame 65, 53 (1986); Dixon-Lewis, G. and Islam, S. M.: Tenth Symposium (International) on Combustion, p. 495, The Combustion Institute, 1965.
19. Sasaki, S.-i., Kano, A., Tsunashima, S. and Sato, S.: Bull. Chem. Soc. Jpn. 59, 1675 (1986).
20. Copeland, R. A., Dyer, M. J. and Crosley, D. R.: J. Chem. Phys. 82, 4022 (1985); Smith, G. P. and Crosley, D. R.: J. Chem. Phys. 85, 3896 (1986).
21. Kohse-Höinghaus, K., Perc, W. and Just, Th.: Ber. Bunsen Phys. Chem. 87, 1052 (1983).
22. Cattolica, R. J., Stepowski, D., Puechberty, D. and Cottereau, M.: J. Quant. Spectr. Radiat. Transf 32, 363 (1984).
23. Tjossem, P. J. H. and Cool, T. A.: Twentieth Symposium (International) on Combustion, p. 1321, The Combustion Institute, 1985.
24. Garland, N. L. and Crosley, D. R.: Chem. Phys. Lett. 134, 189 (1987).
25. Nokes, C. J. and Donovan, R. J.: Chem. Phys. 90, 167 (1984).
26. Dyer, M. J. and Crosley, D. R.: Proceedings of the International Conference Lasers '84, p. 211, STS Press, 1985; Hanson, R. K.: Twenty-First Symposium (International) on Combustion, p. 1677, The Combustion Institute, 1988.
27. Jeffries, J. B., Copeland, R. A., Smith, G. P. and Crosley, D. R.: Twenty-First Symposium (International) on Combustion, p. 1709, The Combustion Institute, 1988.
28. Crosley, D. R., Rensberger, K. J. and Copeland, R. A.. Proceedings of the NATO Advanced Research Workshop on Selectivity in Chemical Reactions, in press, p. 543, D. Reidel, 1988.

COMMENTS

L. A. Melton, Univ. of Texas, USA. The total quench rates you have shown vary slowly as a function of position in the flame. Is this a result of all flame species having roughly the same quench rates or of fortuitous averaging?

Author's Reply. The major species in the flame have very different quenching rate constants for both CH and NH. For example, water and propane are efficient quenchers while nitrogen is inefficient for both radicals (see Table I for values for N_2, H_2O,

and CO_2). Also, the temperature (i.e., the density) is increasing with height above the burner, resulting in changes in the collision frequency.

The major species concentration, quenching rate constants and temperature all affect the observed fluorescence decay. However, in general, the decay constant changes only slightly with height, indicating that a fortuitous averaging must be occurring. In most flames the relatively efficient quenching of the fuel molecules near the burner surface is compensated by the buildup of the combustion product water further from the burner. The small changes in the total decay constant mask the dramatic changes in the contributions from individual major species.

●

K. Schofield, Univ. of California, USA. As scientists we become obsessed with making measurements with as much care and minimal errors as possible. However, it is always worthwhile to remember that flames generally are not a media for such accurate measurements. Moreover, results often are obtained for species concentrations that change by many orders of magnitude and even a factor of two becomes quite minor when plotted on a logarithmic concentration scale. As a result of your work and others it appears now that flame electronic quenching does not vary significantly between similar type flames or throughout a flame for numerous species. In many cases, ignoring quench variations totally, or not invoking the other experimental techniques devised to minimize such variations, becomes a significant possibility for many applications especially those aimed at trying to resolve flame chemistry or test kinetic models. It might be useful to compare your fully corrected data with that resulting solely from the case in which the raw fluorescence data are adjusted solely for the temperature effects on the pumped level densities. This would indicate the possible magnitides of error which might be quite acceptable for certain applications.

Author's Reply. For many minor species concentration measurements in a flame, this factor of two accuracy for a given radical is adequate to learn more about flame chemistry and test kinetic models. For example, a great deal of chemical insight can often be obtained by examining the region or slope of the concentration profile of one reactive intermediate compared to another. However, for comparison with quantitative computer models of the flame chemistry, temperature must be determined accurately. Changes of ±100 K (<10%) can drastically alter the chemistry and minor species concentrations at a given point. A determination with a systematic temperature error of this degree can preclude meaningful comparison with models. Understanding the interplay between temperature and minor species concentrations is important in determining the level of accuracy required for both.

For a particular excited state of a given radical (OH, CH, and NH) we find the fluorescence quantum yields vary at most ±50% from flame to flame and with position. The largest deviations appear in regions of relatively low concentrations. Differences between one radical and another can be much greater, for example, the quantum yield for NH is about 5 times greater than that for OH. In most cases, a difference of this magnitude would be significant, and one must know the value for each species.

As with most scientific investigations, the researchers must determine what is the accuracy required to answer the important fundamental or practical questions. With our current knowledge of the quenching of diatomic hydride radicals we can estimate the quantum yield to a factor of two under almost all experimental conditions.

Appendix D

TIME-RESOLVED CH ($A^2\Delta$ AND $B^2\Sigma^-$) LASER-INDUCED FLUORESCENCE IN LOW PRESSURE HYDROCARBON FLAMES

Reprinted from Applied Optics, Vol. 27 page 3679, September 1, 1988

Time-resolved CH ($A^2\Delta$ and $B^2\Sigma^-$) laser-induced fluorescence in low pressure hydrocarbon flames

Karen J. Rensberger, Mark J. Dyer, and Richard A. Copeland

Total collisional removal rate constants for the CH $A^2\Delta$ and $B^2\Sigma^-$ electronic states are obtained in low pressure (<20-Torr) hydrocarbon flames. The B state is consistently removed ~70% faster than the A state. Variations of ±50% are observed for different rotational levels and positions in the flame. For these flames, A-state emission following excitation of the B state indicates a rapid electronic-to-electronic energy transfer pathway that is insensitive to collision environment. Upper limits to the collider specific cross sections are obtained for H_2O, N_2, and CO_2. The CH concentration and temperature profiles are measured and parametrized using a unique method.

I. Introduction

Laser-induced fluorescence (LIF) is a sensitive, selective, and nonintrusive spectroscopic diagnostic technique for the detection of minor species in flames.[1] Radical intermediates present at relatively low concentration (ppm) but with easily accessible electronic states, such as OH, C_2, NH, and CN, are ideal candidates for LIF detection.[2] The CH radical is included in those easily studied via LIF; however. unlike OH, its precise role in the combustion chemistry remains uncertain due in large part to the lack of knowledge of its reaction rates at high temperatures. Even though the importance of the CH radical in the chemistry of combustion has not been verified, CH emission[3-5] and LIF[6-10] are often used as diagnostics for regions where combustion is occurring. CH concentration profiles are measured via absorption,[11-15] saturated LIF,[14-19] and resonance enhanced multiphoton ionization.[20] In addition, 2-D imaging of CH using LIF has been demonstrated[6,7] and undoubtably will be applied in practical combustion systems in the future.

Quantitative LIF concentration measurements of CH require knowledge of the fluorescence quantum yield, which depends on both the radiative and collisional processes that occur following electronic excitation.[21] The radiative lifetimes and relative vibrational band emission strengths are reasonably well characterized for the $A^2\Delta$, $B^2\Sigma^-$, and $C^2\Sigma^+$ electronic states.[22-26] Collisional processes such as quenching (the total removal from the excited electronic state, which includes both reaction and energy transfer processes, that change the CH electronic state) and rotational energy transfer are understood to a lesser degree. Recently, several studies have examined these important collisional processes for the $A^2\Delta$ and $B^2\Sigma^-$ electronic states in atmospheric pressure flames[27] and for the $A^2\Delta$ state in low pressure flames.[8,9,14-16] In addition to the flame studies, the collisional removal rates of the $A^2\Delta$ electronic state have been measured at room temperature[28-30] and 1300 K.[31]

In this work, we examine the collisional energy transfer of the $A^2\Delta$ and $B^2\Sigma^-$ states by direct measurement of the time dependence of the LIF in several low pressure premixed flat flames. From the direct observation of the fluorescence decay, we measure the fluorescence quantum yields needed for quantitative CH measurements and estimate upper limits for the collisional quenching rates for several key colliders.[21] Both the major species concentrations and the temperature vary across the flame front in the combustion environment; these can alter the observed decay and change the fluorescence quantum yield. A quantitative understanding of the collisional quenching of CH by various species in the flame permits extension of these measurements to flames where the time dependence cannot be observed, such as in high pressure turbulent flow systems.

Rotational level effects of quenching in the flames are also examined. In recent state-specific room-temperature flow-cell studies of two simple hydrides, OH($A^2\Sigma^+$) and NH($A^3\Pi_i$), a significant decrease in the electronic quenching rates with increasing rotational level in the excited state is observed for most co-

The authors are with SRI International, Molecular Physics Department, 333 Ravenswood Avenue, Menlo Park, California 94025.
Received 29 February 1988.
0003-6935/88/173679-11$02.00/0.

liders.[32-36] Will this effect persist in the flame environment? To address this question, we evaluate the quantum state selectivity of the fluorescence quantum yield for different excited rotational levels and assess its effect on LIF diagnostics at high temperatures. We find a small but measurable decrease in the quenching rate constants as the rotational quantum number increases in several flames.

During this study we examined the electronic-to-electronic energy transfer from the B state of CH to the A state. This nearly isoenergetic transfer has been observed in atmospheric pressure flames.[27] We investigated this interesting dynamic process in several different flames to test its applicability as a sensitive versatile diagnostic technique.

The CH radical ground state concentration profiles and CH rotational temperatures are obtained for several of the flames. Preliminary attempts to parametrize the radical and temperature profiles are presented to simplify presentation of the data and allow for a straightforward comparison to other flames. These methods, while only discussed briefly here, will be the basis for a more complete description of the parametrization method.[37]

These flame measurements are of both practical interest in quantitative diagnostics of the CH radical by LIF in combustion systems and fundamental interest in the collision dynamics of radicals at high temperature. The attempts to unravel the details of the collisional energy transfer in both CH electronic states are aided by a judicious choice of flames and pressures in this unique collision environment where collisions of relatively large kinetic energy are sampled.

II. Experimental Approach

The LIF signal in flame experiments is affected by the temperature, collision environment, excitation transition, and optical detection system. These properties of the system can affect both the precision and accuracy of LIF concentration measurements; however, seldom are they examined in a systematic and well-controlled manner.

Low pressure flames have several distinct advantages over atmospheric pressure flames for such a study. In low pressure flames, the combustion region is expanded to several millimeters when the pressure is kept below 50 Torr. At these pressures, fluorescence decays persist after the laser light pulse and may be measured at different locations across the flame profile. This detailed position and time information are difficult to obtain at high pressures with conventional LIF methods. Most of the information obtained from the low pressure studies with insight can be extended to high pressure diagnostic studies.

In this experiment, we choose the CH radical as a test case to examine these effects in the controlled environment of a low pressure flame. Various flames are examined to sort out many of the complications in LIF measurements. Since this work is the first in a series of such experiments, we will describe the apparatus in detail.

A. Apparatus

The LIF experimental apparatus shown in Fig. 1 can be conveniently divided into three parts: the low pressure burner system, the excitation laser, and the fluorescence detection system.

The low pressure burner system is composed of a vacuum chamber with the associated electronic, mechanical, and optical components for positioning and probing in the low pressure environment. The burner is a McKenna Products flat-flame porous-plug burner 6 cm in diameter. An inert gas often flows through a shroud surrounding the burner to create a well-controlled interface between the flame and the residual gases in the chamber. The burner and exhaust manifold are water cooled to maintain safe operating temperatures for all the components. Fine metering valves control and calibrated mass flow meters monitor the flow of the gases. The pressure is measured with a Wallace and Tiernen 200-Torr gauge and compared with a 1000-Torr Baratron pressure gauge. The burner can be positioned via three dc motors mounted in the vacuum chamber, and the position of the burner can be read out via potentiometers that are mounted on all the translation components. We have examined both the accuracy and hysteresis of the vertical drive and find that the relative position can be measured to $\sim$100 μm when approaching from one direction and $\sim$200 μm when scanning in both directions. This resolution is sufficient for these studies with a laser beam diameter a factor of $\sim$3–5 larger. Both the intensity and position of the LIF signal profiles are reproducible over several hours and from day to day.

The flames for most of the studies are hydrocarbon/oxygen flames with a fuel equivalence ratio ϕ near one and vary in pressure between 5 and 20 Torr. The total flows of fuel, oxidizer, and shroud for each flame (1)–(7) are given in Table I. Also listed is the pressure range over which the measurements are obtained. For two flames not listed, extra nitrogen or carbon dioxide is added to a propane/oxygen flame to measure the CH quenching in different conditions. Major species profiles have not been measured. Measured temperature profiles using CH, CN, and NH excitation scans are briefly described below and in a subsequent publication.[38]

The excitation laser is a pulsed excimer-pumped dye laser ($\sim$15 ns, $\sim$0.3 cm^{-1}) that excites the CH radicals from the $X^2\Pi$ ground state to a specific level (v',J',N') in either the $A^2\Delta$ or $B^2\Sigma^-$ excited electronic state. QUI dye dissolved in dioxane and coumarin 120 dye dissolved in methanol generate light near 390 and 430 nm for the B and A states, respectively. An aperture limits the diameter of the excitation beam to be <1 mm as it traverses the flame. The optical transitions are easily saturated; thus a beam splitter and filters attenuate the laser beam power to minimize scattered light signals. For the temperature measurements, we attenuate the beam so that the LIF signal is linearly proportional to the laser power. For the time dependence measurements described below, the linearity of the signal with laser power is less critical, and often we

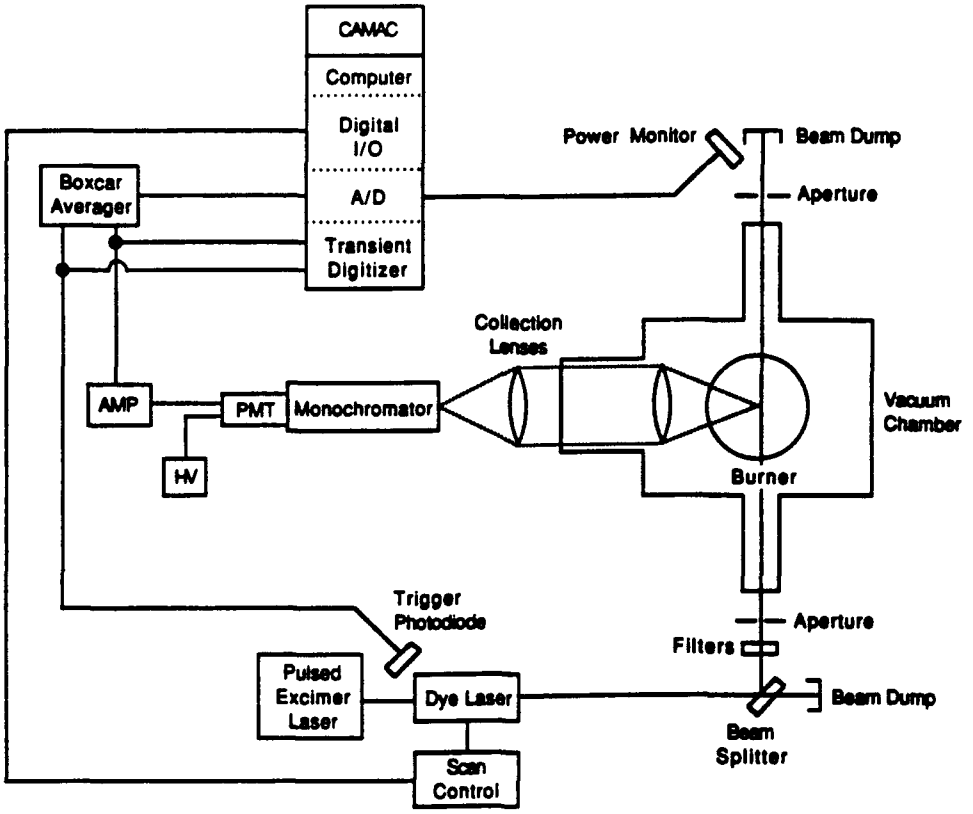

Fig. 1. Schematic of the LIF low pressure burner apparatus.

use more laser power. The laser wavelength can be controlled through an interface to the laboratory computer.

A two-lens system collects the CH LIF and focuses the light onto the entrance slit of a wide bandpass monochromator or filter. As discussed below, these measurements require a detection system with a response which is relatively uniform over the fluorescence region of the band under investigation. A small monochromator (Spex, Minimate-1) with an entrance slit of 0.4 mm and an exit slit of 10 mm is used in the quenching measurements. This arrangement transmits a bandpass that is relatively flat across its peak response for 10 nm. For both the A and B states, fluorescence from the upper electronic state rotational levels of >10 is attenuated with this system. For some of the CH B-state quenching measurements, only a filter (Corion, S40-400-S, incident angle of 15°) is used. Angle tuning of the interference filter permits selection of the appropriate wavelength range. For all the temperature measurements, a Jarrell-Ash monochromator with entrance slits of 500 μm and exit slits of 4 mm transmits a 20-nm bandpass, which is wide enough to detect the entire band. A 1P28 photomultiplier tube monitors the transmitted light, and its output is amplified and captured using either a transient digitizer (100 Msample s^{-1}) or a boxcar integrator with a 1-μs gate. With this detection system, lifetimes as short as 50 ns can be accurately measured. A CAMAC-based laboratory computer controls the detection electronics.

Table 1. Flame Conditions for the Observation of the CH Radical

Flame	Flow rates[a] Fuel	Oxidizer	N_2 Shroud	Pressure range (Torr)	ϕ[b]
(1) CH_4/O_2	0.55	1.05	0.4	5–10	1.0
(2) CH_4/O_2	0.55	1.68	0.9	4–10	0.66
(3) CH_4/O_2	0.65	1.05	0.8	7	1.2
(4) C_3H_8/O_2	0.21	1.05	0.9	6–13	0.98
(5) C_2H_2/O_2	0.5	1.3	0.5	3–7	1.0
(6) $H_2/CH_4/O_2$	2.3, 0.1	1.3	0.6	5–11	1.0
(7) C_3H_8/N_2O	0.2	2.0	0.5	8–15	1.0

[a] Units of standard liters per minute.
[b] Fuel equivalence ratio.

B. Spectroscopy and Data Analysis

The CH $A^2\Delta$–$X^2\Pi$ transition near 430 nm and the $B^2\Sigma^-$–$X^2\Pi$ transition near 390 nm can both be used for CH LIF measurements. The $X^2\Pi$, $A^2\Delta$, and $B^2\Sigma^-$ electronic states are similar in that they all have an electronic spin of one-half; however, the electron orbital angular momenta of the states differ. All three states have two different spin-orbit rotational manifolds labeled F_1 and F_2, and the X- and A-state rotational levels are also split by λ-doubling. The line positions, labeling of λ-doublet components, and assignments are taken from Ref. 39. Often the fine structure is resolved in excitation scans by the laser light, but in most cases, it only plays a very minor role in the phenomena in this study and can be safely neglected.

The laser light excites the molecules to a single rotational level in the excited state, and we observe the temporal evolution of the resulting fluorescence. The decay of the fluorescence is affected by electronic, vibrational, and rotational energy transfer, which occur simultaneously. In the hydrides, OH, NH, and CH, partial rotational equilibration within a vibrational state is achieved prior to electronic quenching. Thus the observed total fluorescence following excitation of one level is composed of the fluorescence from many different levels. However, if all rotational levels are observed with equal sensitivity, many complications arising from the rotational level dependence of the radiative lifetime, the rotational energy transfer rate, and the quenching can be eliminated. The rotational dependence of the radiative lifetime is small and well characterized.[24] However, the rotational dependence of the quenching at flame temperatures is unknown for most colliders; OH and NH show dramatic changes with most colliders at room temperature.[32-36] The observed decay of the fluorescence is a combination of many exponentials similar in magnitude. We choose to fit all the time-dependent data from 90 to 10% of the peak of the signal to a single exponential. We call this the decay constant τ^{-1}, which is the sum of the radiative rate τ_r^{-1} and the collisional rate Q, where the quantities are the average values for the average rotational distributions occurring between 90 and 10% of the peak signal and will be specific to the initially excited rotational level. The limits of 90–10% are somewhat arbitrary but are selected to minimize the effects of scattered laser light at early times and minimize the effects of rotational energy transfer at later times.

Figure 2 shows a typical time dependence of the fluorescence signal obtained when exciting the overlapped fine structure components of the $P(7)$ rotational line of the $A^2\Delta$–$X^2\Pi$ (0,0) electronic transition in a 6.7-Torr propane/oxygen flame (flame 4). Typically the signals from 100 to 2000 laser pulses are summed to obtain the time-dependent signals. The squares are the data points, while the line is the best single exponential fit to the data from 90 to 10% of the peak value. This fit gives a decay constant of 6.37 μs^{-1}, which corresponds to a fluorescence lifetime of 157 ns. Little deviation is seen between the best fit single exponential and the experimental data, suggesting that the single exponential description is adequate.

The decay constants are related to the fluorescence quantum yield Φ by the relationship

$$\Phi = \tau_r^{-1}\tau = \tau_r^{-1}(\tau_r^{-1} + Q)^{-1}. \quad (1)$$

Since the collisional rate Q depends directly on the number of colliders, the fluorescence quantum yield decreases at higher pressures. The collisional rate Q is the product of the quenching rate constant k_Q^P and the pressure, where the superscript P indicates a rate constant in units of (μs^{-1} Torr^{-1}), or equivalently Q is the product of the quenching rate constant k_Q and the density n, where k_Q is in units of cm^3 s^{-1}. This notation will be used throughout this paper. Transformation of the experimentally derived k_Q^P into the more fundamental k_Q requires a temperature measurement to convert from pressures to densities. Extraction of collision cross sections from the rate constants also requires a temperature measurement as well as the reduced mass of the collision pair. The thermally averaged cross section σ is defined from $k_Q = \sigma_Q \langle v \rangle$, where $\langle v \rangle$ is the average relative collision velocity [$\langle v \rangle = (8kT/\pi\mu)^{1/2}$].

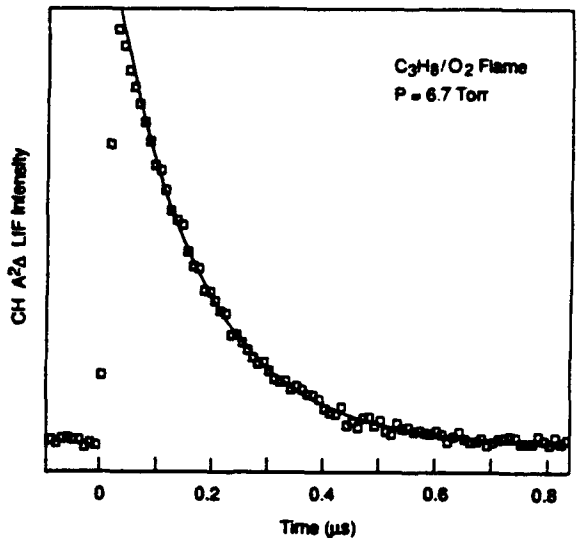

Fig. 2. Typical time dependence of the fluorescence signal (squares) and single exponential fit (line).

III. Results

A. CH $A^2\Delta$ and $B^2\Sigma^-$ Quenching

In these experiments, we measure decay constants for CH ($A^2\Delta$ and $B^2\Sigma^-$) quenching in the flames listed in Table I. We survey several hydrocarbon/oxygen flames, a propane/nitrous oxide flame, and a hydrogen/oxygen flame seeded with a small amount of methane. We make the measurements at the peak CH LIF signal and vary the pressure and excitation transition and also examine different positions across the CH concentration profile. For all these flames, which have a variety of collision partners and temperatures, the quenching varies by <50% for different flames, positions, and excitation transitions when a comparison for one electronic state at the same pressure is made.

The average rate constant for CH A-state quenching is obtained from the pressure dependence of the CH A-state quenching decay constants. The data for five flames taken at the peak CH signal for each flame is shown in Fig. 3(a). The decay constants for the hydrocarbon/oxygen flames have the same pressure dependence, whereas those for the hotter propane/nitrous oxide flame (flame 7) are somewhat slower and those for the cooler hydrogen/oxygen flame seeded with 10% methane (flame 6) are faster. We take the rate constant for CH A-state quenching to be the slope of the linear least-squares fit to the methane/oxygen, pro-

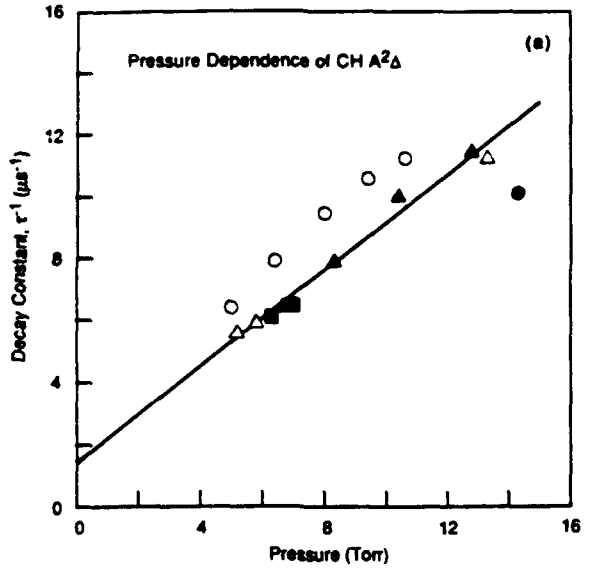

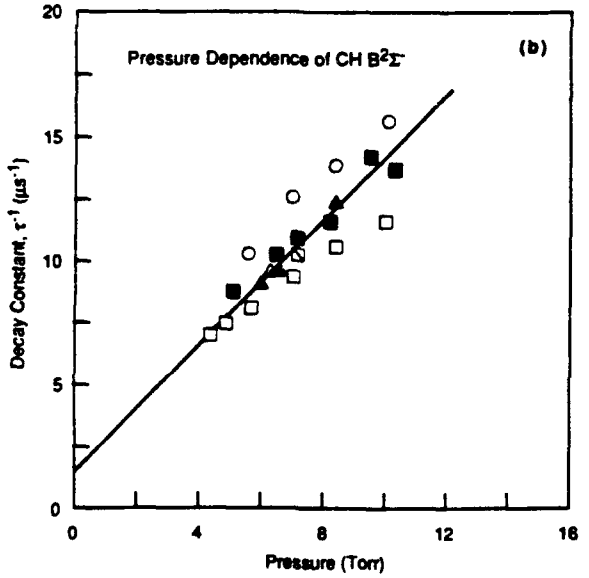

Fig. 3. Pressure dependence of the decay constants for (a) CH($A^2\Delta$) and (b) CH($B^2\Sigma^-$) quenching in the following flames: ○, H_2/O_2 seeded with CH_4; ■, CH_4/O_2, $\phi = 1$; □, CH_4/O_2, $\phi = 0.66$; ⧅, CH_4/O_2, $\phi = 1.2$; △, C_2H_2/O_2, $\phi = 1$; ▲, C_3H_8/O_2, $\phi = 1$; ●, C_3H_8, N_2O $\phi = 1$. The slopes of the linear least-squares fits to the data for the CH_4, C_2H_2, and C_3H_8/O_2, $\phi = 1$ flames give the quenching rate constants k_Q^P, and the intercepts correspond to the radiative rates.

pane/oxygen, and acetylene/oxygen flames data, which is $k_Q^P = 0.77 \pm 0.04$ μs^{-1} $Torr^{-1}$ or, using an average flame temperature of 1800 K, is $k_Q = (1.44 \pm 0.18) \times 10^{-10}$ cm^3 s^{-1}. The uncertainties given above and throughout are two statistical standard deviations.

The pressure dependence of the CH *B*-state quenching decay constants for seven flames taken at the peak CH signal for each flame is shown in Fig. 3(b). The decay constants for the hydrogen/oxygen flame seeded with 5% methane are again higher than those for the hydrocarbon/oxygen flames. At higher pressures, the lean methane/oxygen flame decay constants are somewhat below the rest. Attempts to measure CH *B*-state decay constants in a propane/nitrous oxide flame were unsuccessful, as CN *B*–*X* emission in the same wavelength region interfered with the CH *B*–*X* LIF detection. The rate constant for CH *B*-state quenching is taken to be the slope of the linear least-squares fit to the methane/oxygen, propane/oxygen, and acetylene/oxygen flames decay constants and is $k_Q^P = 1.32 \pm 0.14$ μs^{-1} $Torr^{-1}$ or, using a flame temperature of 1800 K, is $k_Q = (2.47 \pm 0.38) \times 10^{-10}$ cm^3 s^{-1}. In general, the CH *B* state is quenched 70% faster than the CH *A* state in these flames.

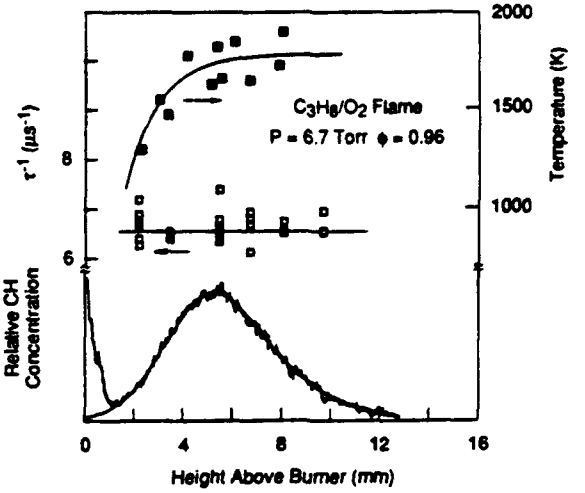

Fig. 4. Summary of CH data obtained in a 6.7-Torr propane/oxygen flame. The bottom curve is the CH ground state relative concentration profile. The line through the curve is the two Gaussian fit. The increase near the burner surface is due to laser light scattered off the burner surface. The open boxes are the CH($B^2\Sigma^-$) decay constants (left vertical axis), and the solid boxes are the CH rotational temperatures (right vertical axis) as functions of position. The lines through the data points are linear and exponential fits to the data as described in the text.

In the flame environment, both the temperature and major species concentrations vary greatly across the CH profile. We investigate what effect this has on the quenching and thus the fluorescence quantum yield by measuring decay constants at different regions in each flame. Figure 4 shows the decay constants τ^{-1} as a function of height above the burner for a propane/oxygen flame. For CH we find that the fluorescence decays are relatively constant over the flame profiles for all the flames, giving quantum yields that are almost independent of position. For example, the propane/oxygen flame shown in Fig. 4 has a quantum yield that is constant at 0.28 across the flame profile. The data for a methane/oxygen flame shown in Fig. 5 show a slight increase in the quenching for both states. For this flame, the quantum yield changes from 0.30 to 0.25 across the flame. For all the flames, the quantum yields for the *A* state are similar to those for the *B* state. Even though the quenching is less in the *A* state, the natural radiative rate is also slower. To facilitate a comparison of the quenching for different flames and both electronic states, we report in Table II the slope and intercept of the pressure independent total remov-

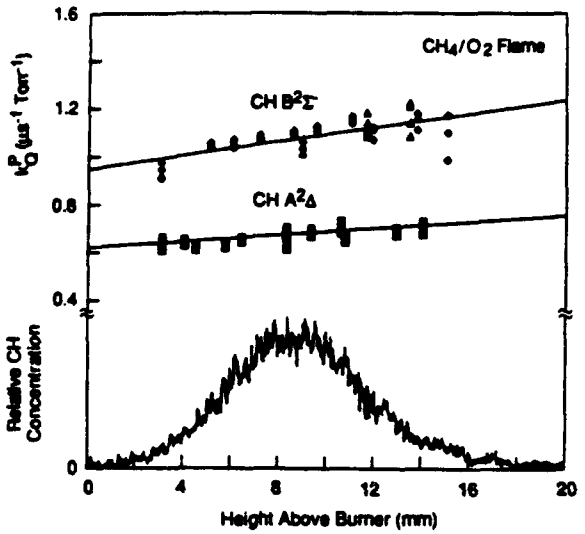

Fig. 5. Position dependence of the CH($A^2\Delta$) and ($B^2\Sigma^-$) quenching rate constants k_Q^P for a methane/oxygen flame. The lower trace is the CH ground state relative concentration profile. The different symbols for the quenching data indicate data taken on different days. The lines are linear least-squares fits to the data.

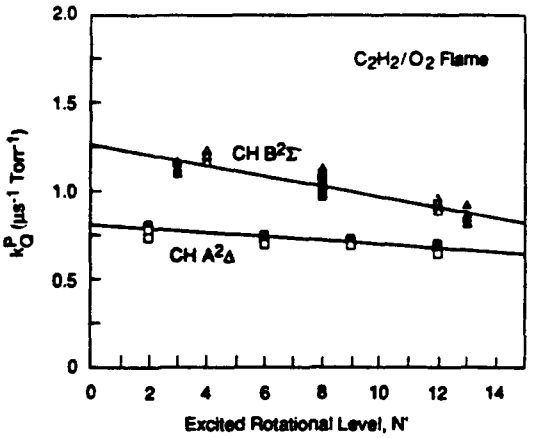

Fig. 6. Rotational level dependence of the CH($A^2\Delta$) and ($B^2\Sigma^-$) quenching rate constants k_Q^P in acetylene/oxygen flames. The different symbols indicate data taken on different days. The lines are linear least-squares fits to the data.

al rate constant k_Q^P vs height above the burner surface, as given by the equation

$$k_Q^P = k_Q^P(0) + k_\alpha^P x, \qquad (2)$$

where x is the height above the burner, $k_Q^P(0)$ is the rate constant extrapolated to the burner surface, and k_α^P is the change in the rate constant with height. The parametrized form can be used to calculate fluorescence quantum yields for a given pressure, temperature, and position in similar low pressure flames for the conversion of LIF profiles to radical profiles (see below). We later describe use of these data to obtain the quenching rate constants k_Q and collision cross sections.

All the results presented thus far have been for one excited rotational level, but several rotational levels must be used for excitation scans for temperatures. We measure the rotational level dependence of the quenching by recording the time evolution of the signal following excitation of different rotational levels at the position of the peak CH signal. Data for the CH A- and B-state quenching for acetylene/oxygen flames are shown in Fig. 6, where N' is the initially excited rotational level. We find that the quenching decay constants do not vary significantly (15%) over rotational levels $N' = 2$–13, in contrast to the strong dependence shown by OH and NH at room temperature.[32–36] This dependence is similar to that for OH and NH seen in other flame experiments in this laboratory.[40,41] Data for rotational levels $N' = 12$ and 13 should be considered with caution, as fluorescence from these levels is attenuated by the detection system; however, from the lower rotational levels, the trend is clear.

Table III contains a summary of the rotational level dependence for all the flames. The data are presented in a fashion similar to the position dependence as an intercept and slope for a fit of k_Q^P vs initially excited rotational level. The methane/oxygen flame quenching shows essentially no dependence on rotational level, while the propane/oxygen and acetylene/oxygen show a slight dependence. The small change we observe has a minimal impact on concentration measurements, but it can affect temperature measurements as discussed below.

B. Electronic Energy Transfer from $B^2\Sigma^-$ to $A^2\Delta$

One of the pathways for the quenching of the B state is by electronic-to-electronic energy transfer to the A state, as evidenced by collision-induced emission from the A state after B-state excitation. Figure 7 shows the time dependence of the wavelength-resolved LIF following excitation of the $Q_1(8)$ rotational line of the B–X (0,0) electronic transition in a 6.5-Torr methane/oxygen flame (flame 1). The upper curve is the time dependence of the fluorescence at 3906 Å (B-state fluorescence), while the lower curve is that at 4312 Å (A-state fluorescence). The temporal evolution of the LIF at the two wavelengths is clearly different. The B-state fluorescence shows a single exponential decay

Table II. Distance Dependence of the Total Removal Rate Constant k_Q^P

	CH B		CH A	
Flame	$k_Q^P(0)$ (μs^{-1} Torr^{-1})	k_α^P (μs^{-1} Torr^{-1} mm^{-1})	$k_Q^P(0)$ (μs^{-1} Torr^{-1})	k_α^P (μs^{-1} Torr^{-1} mm^{-1})
(1) CH_4/O_2	0.95 ± 0.02	0.014 ± 0.002	0.610 ± 0.007	0.009 ± 0.001
(4) C_3H_8/O_2	1.08 ± 0.03	−0.003 ± 0.004	0.700 ± 0.020	0.000 ± 0.003
(5) C_2H_2/O_2	1.05 ± 0.02	−0.003 ± 0.007	0.720 ± 0.020	0.003 ± 0.006

Table III. Rotational Level Dependence of the Total Removal Rate Constant k_Q^o at the Peak of the CH Signal

Flame	CH B Intercept (μs^{-1} Torr^{-1})	CH B Slope (μs^{-1} Torr^{-1})	CH A Intercept (μs^{-1} Torr^{-1})	CH A Slope (μs^{-1} Torr^{-1})
(1) CH_4/O_2	1.07 ± 0.02	0.000 ± 0.002	0.706 ± 0.008	−0.007 ± 0.001
(4) C_3H_8/O_2	1.38 ± 0.07	−0.033 ± 0.008	0.833 ± 0.027	−0.017 ± 0.003
(5) C_2H_2/O_2	1.26 ± 0.02	−0.029 ± 0.002	0.800 ± 0.010	−0.010 ± 0.001

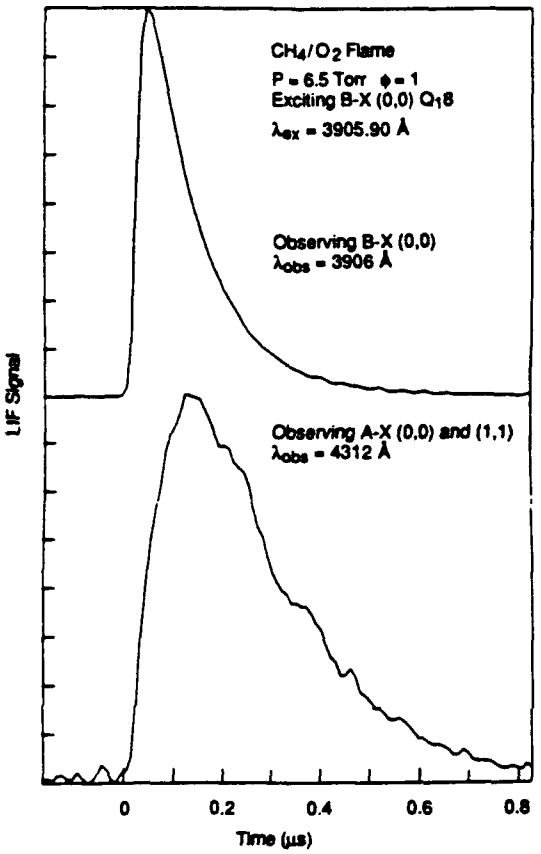

Fig. 7. Time dependence of the CH fluorescence following excitation of the $B^2\Sigma$–$X^2\Pi$ (0,0) $Q_1 8$ transition. The upper curve is obtained observing only B–X fluorescence, while the lower curve is observing only A–X fluorescence.

corresponding to depopulation of the $B^2\Sigma^-$ electronic state in collisions with the flame gases that is significantly faster than the decay of the $A^2\Delta$ state for the same flame conditions. The A-state fluorescence arises from electronic energy transfer from the B state to the A state as observed in the atmospheric pressure flame in Ref. 27. The two exponentials of the A-state fluorescence signal reflect the rapid collisional population of the A state from the B state and the slower collisional removal of the A state. A single exponential fit for the upper curve from 90 to 10% of the peak value yields a CH B-state quenching decay constant of 9.5 μs^{-1}, corresponding to a fluorescence lifetime of 105 ns.

A comparison of profiles of the collision-induced emission for each flame to the B-state LIF profiles shows a slight variation between flames, but the size of the collision-induced emission is between 30 and 50% of the CH B-state signal. We did not calibrate the detector response, but the ratio of electronic energy transfer to quenching was found to be ~0.2 in an atmospheric pressure flame.[27] The major species concentrations in the flame change over this region, but that change does not result in a significant change in the relative amount of signal.[42]

C. Temperature and CH Profiles

Temperature profiles are needed to extract rate constants and cross sections for collisional quenching from the measured decay constants and are also needed to obtain the ground state CH concentrations from the observed LIF signal intensity. A complete discussion of the method we use to extract temperatures from LIF excitation scans will be given in a subsequent publication.[38] We perform excitation scans over a spectral region that contains both low and high rotational levels and fit the spectrum to a synthesized spectrum using known wavelengths and line strengths and using a Gaussian shape linewidth and the temperature as variables. Excitation scans are taken using the $B^2\Sigma^-$–$X^2\Pi$ or the $A^2\Delta$–$X^2\Pi$ electronic transitions. (Examples of the data and fits can be found in Ref. 38.) As a consistency test, we compare the results for the temperatures obtained from CH excitation scans to those from NH and CN excitation scans for the same flame, a rich propane/nitrous oxide flame. The NH and CN spectra are fit in a similar fashion as the CH spectra and all agree to within 200 K of each other. We have observed a systematic trend in which the temperatures from CH B scans are 100–200 K lower than those from CH A scans but currently have no explanation.[38]

Rather than graphically presenting the experimental data points as a function of position for all the flames studied, we choose to use a simple algebraic formula to parametrize the measurements so that they can be easily tabulated.[37,38] An example of the data and the fit is shown in Fig. 4 for a propane/oxygen flame: we fit the data points obtained using A- and B-state excitation scans to the exponential equation

$$T = T_B + T_a \exp(-\alpha x). \quad (3)$$

The baseline temperature T_B is the temperature extrapolated out to the burnt gases. The parameters for all the flames are given in Table IV. As can be seen in Fig. 4, a linear function, such as used for the quenching, does not reproduce the shape of the temperature profile. These parameters adequately characterize the temperature over the region of significant CH concentration; however, using the equation to extrapolate

ıtside the experimental range should not be attempt-
l (as negative values at $x = 0$ indicate). The tem-
ɛratures at the peak of the CH signal are close to the
$_B$ value. The baseline temperatures for the hydro-
ırbon flames are quite similar, reaching values near
300 K, while the hydrogen/oxygen flame is much cool-
, reaching only 1200 K. The propane/nitrous oxide
ame is significantly hotter (2500 K), possibly because
sits higher off the cooled burner element.

To monitor the distribution of the CH concentration
the flame, we obtain CH LIF signal profiles as a
ınction of height above the burner surface. The
aximum of the CH concentration appears in the
ame front and lies relatively close to the burner sur-
ce. The position of the burner surface is determined
om where laser scatter starts to be seen in the profile.
most cases a 500-μm laser beam radius is used.

The LIF signal profiles can be directly related to the
H ground state concentration profiles by applying
veral corrections. First, since the fluorescence is
llected perpendicular to the laser beam, near the
ırner surface some of the light is obscured by the
ırner, and the profiles must be corrected for the
ange in the amount of light getting to the detector.[43]
ıe correction factor as a functior of burner height
n be calculated using geometry. Another correction
r the change in population of the rotational level
cited in the ground state with temperature can be
plied using the parametrized temperatures given
ove. This can be minimal with an appropriate
oice of excited rotational level. We chose to excite
om the $N'' = 7$ level, as its relative population does
t change significantly for large changes in tempera-
re through the flame front. For all the profiles
ported, the temperature correction is negligible.

The effect of the fluorescence quantum yield on the
ofiles depends on how the signal is collected. If the
tire time evolution of the fluorescence is captured
th a long boxcar gate, the observed profile must be
vided by the position dependence of the fluorescence
antum yield as given above. However, if a very
ort gate (10 ns) is used at early times in the fluores-
nce decay, the population is not significantly re-
ced by quenching. Changes in the fluorescence
antum yield arising from differences in quenching
te constants across the flame profile will be small,
d a constant fluorescence quantum yield can be
ed. For most of the profiles we report, we use a gate
at integrates over the entire time dependence, and,
erefore, the position dependence of the quantum
yield is used. However, our data on the position dependence of the quenching show that only for the methane/oxygen flame is there noticeable change in the quenching with position.

The accurate reproduction of radical profiles by flame models is an important test of their ability to predict the chemistry occurring throughout the flame. The temperature profiles from Table IV and the pressures and flow rates from Table I are necessary input data to the current models. We have selected a method of presenting our CH ground state concentration profiles whereby representative profiles can be reproduced for comparison with other experimental and modeling profiles. Our parametrization has six independent variables and well represents the shape of the CH profiles. Simpler forms may be applicable; however, this form is the best we have found to date.[37] The parametrization consists of fitting the profile to an equation, which adequately reproduces the profiles:

$$N = N_1 \exp[-\alpha_1(x - d_1)^2] + N_2 \exp[-\alpha_2(x - d_2)^2]. \quad (4)$$

This equation is the sum of two independent Gaussian functions. The parameters for all the flames studied are given in Table V. Each profile has been scaled to have a maximum peak of 1000 units. Figure 4 shows a two Gaussian fit to the CH concentration profile obtained in a propane/oxygen flame. In a number of the CH profiles with scattered laser light, the fit is restricted to distances >1 mm above the burner surface. The above representation, although reasonably accurate, does not make for an easy comparison from one flame to another using the parameter values. Qualitatively, the C_2H_2/O_2 profile peaks significantly closer to the burner (~2.5 mm) with the CH_4/O_2 peaking the farthest at ~9 mm. The width of the profile generally correlates with the distance above the burner in that the higher the CH radical is produced, the wider the profile. A more quantitative description of these features can be found in a subsequent publication.[37]

IV. Rate Constants and Collider-Specific Cross Sections

A. Estimates of Cross Sections for Quenching

The rate constants k_Q^P show an unexpected independence with position in the flame as given in Table II. However, a closer examination of the underlying collision dynamics reveals that this independence actually results from two things: both the collision cross section and the temperature increase with distance above

able IV. Parameters Describing the Temperature Profile in Several Flames

Flame	T_B(K)	$T_$(K)	α(mm^{-1})	Pressure (Torr)
) CH_4/O_2	1856	−962	0.197	7.0
) C_3H_8/O_2	1788	−2545	0.722	6.7
) C_2H_2/O_2	1718	−854	0.402	6.4
) $H_2/CH_4/O_2$	1227	−3128	0.898	10.6
) C_3H_8/N_2O	2576	−2473	0.265	14.3

Table V. Parameters of a Two Gaussian Fit Used to Reproduce the CH Ground State Concentration Profile[a]

Flame	N_1	α_1 (mm^{-1})	d_1 (mm)	N_2	α_2 (mm^{-1})	d_2 (mm)	Pressure (Torr)
(1) CH_4/O_2	841	0.083	8.79	227	0.246	10.11	7.0
(4) C_3H_8/O_2	714	0.141	4.99	343	0.075	7.22	6.7
(5) C_2H_2/O_2	551	1.200	1.79	506	0.268	2.66	6.4
(6) $H_2/CH_4/O_2$	559	0.374	4.41	477	0.121	5.12	10.6

[a] All data normalized to give a maximum value of 1000 in arbitrary units.

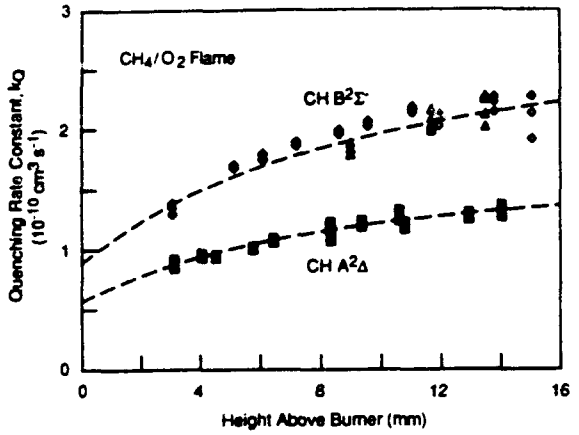

Fig. 8. Position dependence of the quenching rate constants k_Q for $CH(A^2\Delta)$ and $(B^2\Sigma^-)$ in a methane/oxygen flame. The data and lines are calculated using the temperature profile tabulated in Table IV and the quenching rate constants k_Q^P shown in Fig. 5.

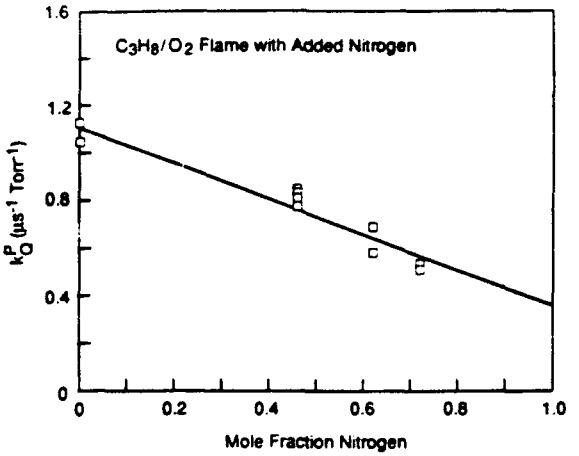

Fig. 9. Dependence of the quenching rate constants k_Q^P for $CH(B^+\Sigma^-)$ in a propane/oxygen flame with added nitrogen. A mole fraction of 0.72 approximates a propane/air flame. The line is a linear least-squares fit to the data, and the intercept at a mole fraction of 1.0 gives the upper limit of the rate constant for quenching by nitrogen.

the burner. Over the flame profile, the pressure remains constant, but as the temperature increases, the density and collision frequency decrease. By converting the measured k_Q^P to k_Q using our temperature profiles, we remove the effect of the changing density and can compare quenching at different temperatures and flame gases. Figure 8 shows the data for a methane/oxygen flame that has been corrected for the changing density.

We use the parametrized form for the temperature profile as given in Table IV. The rate constants increase slightly moving from the burner surface toward the burnt gases. Further reduction of the data to a collision cross section requires an approximation on the reduced mass of the collision pair μ, which is needed to estimate the average relative collision velocity $\langle v \rangle$. Assuming μ changes only slightly, the cross sections increase but to a lesser extent than the rate constants, moving from the burner to the burnt gases.

Perhaps the most important unknown collider specific quenching cross section is that for H_2O. We measure the total removal rate constant for the A state in the H_2/O_2 flame with a small amount of CH_4 to be 0.86 μs^{-1} $Torr^{-1}$. From our data we can currently generate a reasonable upper limit for water. (Further measurements and detailed flame modeling are needed for a more accurate value.) The limit is obtained using this reasoning. We have measured the value of the removal at the peak of a H_2/O_2 flame with small quantities of CH_4. We assume, albeit incorrectly but accurately for a limit, that all the other species do not contribute to the quenching at that point. From typical models of this flame[41] we assume H_2O makes up 40–50% of the total gases. This leads to upper limits on the H_2O quenching cross section of 13 and 18 $Å^2$ for the A and B state, respectively. Interestingly, this upper limit is significantly below the best estimate (equal to the NH_3 quenching value) made for CH previously.[21]

Upper limits for the contributions of N_2 and CO_2 to the quenching are estimated by adding known amounts of each gas to a C_3H_8/O_2 flame. The addition of the gas may cool off the flame, but we did not measure the temperature for each flame composition. The greatest effect on the quenching will be seen for a constant temperature flame. For both gases, we see that the quenching at the peak CH signal decreases significantly with each further addition of N_2 or CO_2. The change is due to the addition of a less efficient quencher but counterbalanced somewhat by the increase in density by cooling. Figure 9 shows the influence of the addition of N_2 on the fluorescence decay of the B state. The addition of CO_2 may also influence the flame chemistry by creating more CO, which is a more rapid quencher than CO_2.[31] Extrapolation of the measured quenching rate constants to 100% added N_2 or CO_2 gives an upper limit to the rate constants for quenching by each gas. Cross sections derived using a temperature of 1800 K are $\sigma_Q < 3$ $Å^2$ and < 4 $Å^2$ for N_2 for the A and B states, respectively, and $\sigma_Q < 4$ $Å^2$ for CO_2 for both states. The A-state cross section limits are larger than the values[31] at 1300 K: σ_Q is 1.4 and 2.1 $Å^2$ for N_2 and CO_2. This is consistent with the upper limits given above. No collider-specific quenching cross sections are available for comparison for the B state. Our data show that these species are not very efficient quenchers for this state.

B. Comparison with Other Studies

The $A^2\Delta$ state has been examined via time-resolved LIF in two other studies both in low pressure acetylene/oxygen[19] and methane/oxygen[8] flames; however, the time evolution of the $B^2\Sigma^-$ state has not been previously investigated. We can use the collider-specific cross sections to calculate quenching rates for comparison to the other reported direct measurements. Disagreement of nearly a factor of 2 in a similar comparison in Ref. 21 can be attributed to their estimate of $\sigma_Q(H_2O)$ from the cross section for quenching by ammonia. The value used for H_2O was a factor

of ~2 greater than the upper limit determined in this work. Cattolica *et al.*[8] in a CH_4/O_2 flame at 20 Torr measured a rate constant of 0.8 μs^{-1} $Torr^{-1}$, agreeing with our experimental value for the *A* state of 0.77 μs^{-1} $Torr^{-1}$. Using reported major species concentrations, the upper limit for H_2O, and the σ_Q for CO, CO_2, and O_2 from Ref. 31, we calculate a maximum value of 0.9 μs^{-1} $Torr^{-1}$. In a C_2H_2/O_2 flame at 10 Torr, Kohse-Hoeinghaus *et al.*[17-19] measure 1.0 μs^{-1} $Torr^{-1}$. Our measured value is 0.77 in a somewhat leaner flame; the calculated result is also 0.8 μs^{-1} $Torr^{-1}$.

The comparisons presented above are encouraging. From the above discussion and similar comparisons for the OH radical in Ref. 21, and with knowledge of the major species concentration and temperature, fluorescence quantum yields for CH *A*-state LIF can be estimated to about ±25%. This is a significant improvement over the factor of 2 estimates for CH from two years ago.[21]

We believe the *B*-state measurements also provide a consistent picture; however, we know of no other flame data for direct comparison. Our measurements directly confirm other indirect measurements in atmospheric pressure flames[20,27] that the *B* state of CH does quench significantly faster than the *A* state. For a wide variety of flames we observe a 70% faster rate in *B* than *A*.

V. Implications for CH Diagnostics

Quantitative measurement of CH using the *A* or *B* states may turn out to be much easier than initially anticipated. The time decay of the fluorescence does not change significantly over the entire region of the flame where the CH is present. This means that a single value of the fluorescence quantum yield can be used for most applications that do not make stringent requirements on the accuracy of greater than ~25%. But this also means that the fluorescence quantum yield is independent of the temperature, and a correction for the temperature, which in most circumstances would be required when using a constant cross section (as in the case of NH[40] and OH[41]), would reduce the accuracy of the CH profile for all the flames examined in this study.

From the measurements of the rate constants for electronic quenching of the *A* and *B* states of CH, we can estimate the fluorescence quantum yield for excitation of the two states. The *B* state of CH quenches more rapidly than the *A* state by ~70%; however, the *B*-state lifetime is ~340 ns, which is ~60% shorter than the *A*-state radiative lifetime of ~540 ns. The two effects almost entirely cancel, making, for example, a fluorescence quantum yield of ~10% in a 20-Torr hydrocarbon/oxygen flame for the *B* state and 11% for the *A* state. In almost all applications, such a small difference is insignificant, and selection of the most advantageous excitation transition will depend on the excitation laser and detection system.

The rotational level dependence described above for CH is in most cases too small to have meaningful implications for concentration measurements but can affect LIF temperature determinations.[38] Levels with higher N′ live longer due to the slower quenching and longer radiative lifetime. This ratio determines the overall quantum yield, which increases slightly with N′ in these flames. For CH, there are no measurable effects in the methane flame, but in the propane and acetylene flames assumption of a constant fluorescence quantum yield for all rotational levels can result in errors of 200–400 K at 2000 K. The apparent temperatures recorded from time-integrated LIF excitations scans would always be higher than the actual due to the increased signal when exciting high rotational levels. These errors in temperature could have a considerable impact on the ability to compare measured profiles to the result of flame chemistry model predictions. All our reported temperature measurements are obtained from excitation scans in which a very short boxcar gate is used to minimize this effect.

The results on the electronic-to-electronic energy transfer from the $B^2\Sigma^-$ to the $A^2\Delta$ are encouraging for detection of the CH radical in particulate-laden systems. Exciting the *B* state near 390 nm and observing the fluorescence near 440 nm from the *A* state would eliminate almost all scattered light problems. Since we find the amount of transfer relatively independent of flame conditions, the signal obtained will be a adequate representation of the CH ground state concentration profile. When combined with the quantitative results of Ref. 27, which show that 20% of the initially excited *B* state fluoresces in the *A* state, absolute CH concentrations can be estimated.

We thank Dave Crosley, Katharina Kohse-Hoeinghaus, Jay Jeffries, and Greg Smith for many helpful discussions on both the experiment and interpretation. We gratefully acknowledge support for this research by the Aero Propulsion Laboratory of the Air Force Wright Aeronautical Laboratories.

References

1. D. R. Crosley and G. P. Smith, "Laser-Induced Fluorescence Spectroscopy for Combustion Diagnostics," Opt. Eng. 22, 545 (1983).
2. D. R. Crosley, "Laser-Induced Fluorescence Measurement of Combustion Chemistry Intermediates," High Temp. Mat. Proc. 7, 41 (1986).
3. J. M. Corliss, D. D. Paul, R. H. Barnes, and W. A. Ivancic, "Species and Fluid Mechanic Measurements in an Operating Pulse Combustor," in *Preprints, 1986 International Gas Research Conference, Vol. 2: Residential and Commercial Utilization*, T. L. Cramer, Ed. (Government Institutes, Rockville, MD, 1986), p. 10.
4. D. Reuter, B. R. Daniel, J. Jagoda, and B. T. Zinn, "Periodic Mixing and Combustion Processes in Gas Fired Pulsating Combustors," Combust. Flame 65, 281 (1986).
5. L. P. Goss, B. G. MacDonald, D. D. Trump, and G. L. Switzer, "CARS Thermometry and N_2 Number Density Measurements in a Turbulent Diffusion Flame," AIAA paper 83-1480, AIAA Eighteenth Thermophysics Conference, Montreal (June 1983).
6. M. J. Dyer and D. R. Crosley, "Fluorescence Imaging for Flame Chemistry," in *Proceedings, International Conference on Lasers '84*, K. M. Corcoran, D. M. Sullivan, and W. C. Stwalley, Eds. (STS Press, McLean, VA, 1985).

7. M. G. Allen, R. D. Howe, and R. K. Hanson, "Digital Imaging of Reaction Zones in Hydrocarbon-Air Flames using Planar Laser-Induced Fluorescence of CH and C_2," Opt. Lett. 11, 126 (1986).
8. R. J. Cattolica, D. Stepowski, D. Puechberty, and M. Cottereau, "Laser-Induced Fluorescence of the CH Molecule in a Low-Pressure Flame," J. Quant. Spectrosc. Radiat. Transfer 32, 363 (1984).
9. R. G. Joklik and J. W. Daily, "LIF Study of CH $A^2\Delta$ Collision Dynamics in a Low Pressure Oxy-Acetylene Flame," Combust. Flame 69, 211 (1987).
10. M. C. Branch, A. Alfarayedhi, and M. Sadeqi, "Structure of Flames Associated with Nitramine Solid Propellants," Western States Section/Combustion Institute Spring Meeting, Paper 87-20, Provo, UT (1987).
11. R. P. Porter, A. H. Clark, W. E. Kaskan, and W. E. Browne, "A Study of Hydrocarbon Flames," in *Eleventh Symposium (International) on Combustion* (The Combustion Institute, Pittsburgh, PA, 1967), p. 907.
12. E. M. Bulewicz, P. J. Padley, and R. E. Smith, "Spectroscopic Studies of C_2, CH and OH Radicals in Low Pressure Acetylene+Oxygen Flames," Proc. R. Soc. London Ser. A 315, 129 (1970).
13. R. G. Joklik, J. W. Daily, and W. J. Pitz, "Measurements of CH Radical Concentrations in an Acetylene/Oxygen Flame and Comparisons to Modeling Calculations," Paper 85-34, Western States Section of the Combustion Institute, Davis, CA (Oct. 1985).
14. P. A. Bonczyk and J. A. Shirley, "Measurement of CH and CN Concentration in Flames by Laser-Induced Saturated Fluorescence," Combust. Flame 34, 253 (1979).
15. J. F. Verdieck and P. A. Bonczyk, "Laser-Induced Saturated Fluorescence Investigations of CH, CN, and NO in Flames," in *Eighteenth Symposium (International) on Combustion* (Combustion Institute, Pittsburgh, PA, 1981), p. 1559.
16. Y. Takubo, H. Yano, H. Matsuoka, and M. Shimazu, "Saturation Behavior of Laser-Induced CH Fluorescence in a Propane-Air Flame," J. Quant. Spectrosc. Radiat. Transfer 30, 163 (1983).
17. K. Kohse-Hoinghaus, W. Perc, and Th. Just, "Laser-Induced Saturated Fluorescence as a Method for the Determination of Radical Concentrations in Flames," Ber. Bunsenges. Phys. Chem. 87, 1052 (1983).
18. K. Kohse-Hoeinghaus, R. Heidenreich, and Th. Just, "Determination of Absolue OH and CH Concentrations in a Low Pressure Flame by Laser-Induced Saturated Fluorescence," in *Twentieth Symposium (International) on Combustion* (The Combustion Institute, Pittsburgh, PA, 1984), p. 1177.
19. K. Kohse-Hoeinghaus, S. Kelm, U. Meier, J. Bittner, and Th. Just, "Concentration Profiles of Flame Radicals Determined by Laser-Induced Fluorescence," in *Second Workshop, Modeling of Chemical Reaction Systems*, Heidelberg, Aug. 1986, J. Wasnek, Ed. (Springer-Verlag, Berlin, 1987).
20. T. A. Cool and P. J. H. Tjossem, "Direct Observations of Chemi-Ionization in Hydrocarbon Flames Enhanced by Laser Excited $CH^*(A^2\Delta)$ and $CH^*(B^2\Sigma^-)$," Chem. Phys. Lett. 111, 82 (1984).
21. N. L. Garland and D. R. Crosley, "On the Collisional Quenching of Electronically Excited OH, NH and CH in Flames," in *Twenty-First Symposium (International) on Combustion* (The Combustion Institute, Pittsburgh, PA, 1988), p. 1693.
22. N. L. Garland and D. R. Crosley, "Relative Transition Probability Measurements in the A-X and B-X Systems of CH," J. Quant. Spectrosc. Radiat. Transfer 33, 591 (1986).
23. J. B. Jeffries, R. A. Copeland, and D. R. Crosley, "Transition Probabilities in the $C^2\Sigma^+$-$X^2\Pi$ System of CH," J. Quant. Spectrosc. Radiat. Transfer 37, 419 (1987).
24. J. Brzozowski, P. Bunker, N. Elander, and P. Erman, "Predissociation Effects in the A, B, and C States of CH and the Interstellar Formation Rate of CH via Inverse Predissociation," Astrophys. J. 207, 414 (1976).
25. K. J. Becker, H. H. Brenig, and T. Tatarczyk, "Lifetime Measurements of Electronically Excited $CH(A^2\Delta)$ Radicals," Chem. Phys. Lett. 71, 242 (1980).
26. W. Ubachs, G. Meyer, J. J. ter Meulen, and A. Dymanus, "Hyperfine Structure and Lifetimes of the $C^2\Sigma^+$, $v = 0$ State of CH," J. Chem. Phys. 84, 3032 (1986).
27. N. L. Garland and D. R. Crosley, "Energy Transfer Processes in CH $A^2\Delta$ and $B^2\Sigma^-$ in an Atmospheric Pressure Flame," Appl. Opt. 24, 4229 (1985).
28. C. Nokes, G. Gilbert, and R. J. Donovan, "Direct Kinetic Study of $CH(A^2\Delta)$," Chem. Phys. Lett. 99, 491 (1983).
29. C. J. Nokes and R. J. Donovan, "Time-Resolved Kinetic Studies of Electronically Excited CH Radicals. II. Quenching Efficiencies for $CH(A^2\Delta)$," Chem. Phys. 90, 167 (1984).
30. F. L. Tabares and A. Gonzalez Urena, "Electronic Quenching of $CH(A^2\Delta$-$X^2\Pi)$ and $OH(A^2\Sigma^+$-$X^2\Pi)$ by N_2 and O_2," J. Photochem. 21, 281 (1983).
31. N. L. Garland and D. R. Crosley, "Collisional Quenching of CH $A^2\Delta$, $v' = 0$ at 1300 K," Chem. Phys. Lett. 134, 189 (1987).
32. I. S. McDermid and J. B. Laudenslager, "Radiative Lifetimes and Quenching Rate Coefficients for Directly Excited Rotational Levels of OH ($A^2\Sigma^+$, $v' = 0$)," J. Chem. Phys. 76, 1824 (1982).
33. R. A. Copeland and D. R. Crosley, "Rotational Level Dependence of Electronic Quenching of $OH(A^2\Sigma^+$, $v' = 0)$," Chem. Phys. Lett. 107, 295 (1984).
34. R. A. Copeland, M. J. Dyer, and D. R. Crosley, "Rotational-Level-Dependent Quenching of $A^2\Sigma^+$ OH and OD," J. Chem. Phys. 82, 4022 (1985).
35. A. Hofzumahaus and F. Stuhl, "Electronic Quenching, Rotational Relaxation, and Radiative Lifetime of $NH(A^3\Pi$, $v' = 0,N')$," J. Chem. Phys. 82, 3152 (1985).
36. N. L. Garland and D. R. Crosley, "Rotational-Level-Dependent Quenching of the $A^3\Pi_i$ State of NH," J. Chem. Phys., in preparation.
37. R. A. Copeland, K. J. Rensberger J. B. Jeffries, and D. R. Crosley, "Parametrization of Species and Temperature Profiles in Low Pressure Flames," to be published.
38. K. J. Rensberger, J. B. Jeffries, R. A. Copeland, K. Kohse-Hoeinghaus, M. L. Wise, and D. R. Crosley, "Laser-Induced Fluorescence Determination of Temperatures in Low Pressure Flames," in preparation.
39. C. E. Moore and H. P. Broida, "CH in the Solar Spectrum," J. Res. Natl. Bur. Stand. U.S. Sec. A 63, 19 (1959).
40. R. A. Copeland, M. L. Wise, K. J. Rensberger, and D. R. Crosley, "Time-Resolved Laser-Induced Fluorescence of the NH Radical in Low-Pressure N_2O Flames," in preparation.
41. K. Kohse-Hoeinghaus, J. B. Jeffries, R. A. Copeland, G. P. Smith, and D. R. Crosley, "The Quantitative LIF Determination of OH Concentrations in Low Pressure Flames," in *Twenty-Second Symposium (International) on Combustion* (The Combustion Institute, Seattle, 1988), in press.
42. K. J. Rensberger, M. L. Wise, D. R. Crosley, and R. A. Copeland, "NH and CH Laser-Induced Fluorescence in Low-Pressure Flames: Quantum Yields from Time-Resolved Measurements," in *Twenty-Second Symposium (International) on Combustion* (The Combustion Institute, Seattle, 1988), in press.
43. W. R. Anderson, L. J. Decker, and A. J. Kotlar, "Concentration Profiles of NH and OH in a Stoichiometric CH_4/N_2O Flame by Laser Excited Fluorescence and Absorption," Combust. Flame 48, 179 (1982).

Appendix E

SEMIQUANTITATIVE LASER-INDUCED FLUORESCENCE IN FLAMES

COMBUSTION AND FLAME 78: 153–167 (1989)

Semiquantitative Laser-Induced Fluorescence in Flames

DAVID R. CROSLEY

Molecular Physics Laboratory, SRI International, Menlo Park, CA 94025

Laser-induced fluorescence (LIF) provides a selective, sensitive, and nonintrusive means of measuring reactive intermediates in combustion chemistry. This article examines ways in which LIF can be used in a semiquantitative manner to gain insight into certain features of flame chemistry mechanisms, through concentration estimates accurate to within perhaps a factor of three. Experiments detecting NH and NS are described, and extensions of semiquantitative LIF to multiple-species detection including two-dimensional imaging are discussed.

INTRODUCTION

Chemical kinetic processes govern or play a major role in several key combustion problems, including pollutant formation (NO_x, SO_x, soot), ignition and inhibition phenomena, and the emission of radiation in the ultraviolet and visible. An understanding of the details of the pertinent mechanisms is best achieved through detection of molecules that are the reactive intermediates in those chemical steps. This can be accomplished through sampling probe methods that do not destroy those intermediates, such as molecular beam sampling mass spectrometers, or through spectroscopic techniques, often involving lasers. Each has advantages and disadvantages, as described in another article in this issue [1]. The main differences are the generality afforded by mass spectrometry compared with the limited number of molecules detectable with lasers, but on the other hand the exclusive ability of the laser techniques to make instantaneous, nonintrusive measurements including the simultaneous mapping of an entire two-dimensional field.

For the detection of intermediates present in low concentration, laser-induced fluorescence (LIF) is generally the method of choice [2]. The laser is tuned so that its wavelength matches that of an absorption line of some species of interest, elevating it to an electronically excited state that fluoresces. The emitted photons, which may be detected through a filter or monochromator to provide further species differentiation, form the signal. In addition to a high degree of molecular selectivity, LIF is quite sensitive. Measurements of small molecules at the parts-per-million level are performed with relative ease, and meaningful measurements at the parts-per-billion level can be made. The range of applicability of LIF is limited by the fact that the molecule of interest must possess an electronic transition in a wavelength region accessible to available lasers. In spite of this, a large number of combustion intermediates are detectable by LIF. Those containing one to four of the atoms H, C, O, N, and S and which have been observed with the method are listed in Table 1.

Measurements of combustion intermediates are most often used in the form of concentration profiles as a function of distance above a burner. In the past, concentration gradients were used to calculate fluxes and deduce selected reaction rates [3]. More typically now, the profiles are compared with those predicted using large-scale computer models [4] of the chemical reaction networks, sometimes adjusting the rate constants to achieve agreement. Quantitative comparisons such as these often require accurate absolute concentration de-

Published by Elsevier Science Publishing Co., Inc.
655 Avenue of the Americas, New York, NY 10010

0010-2180/89/$03.50

TABLE 1

Molecules (1–4 Atoms) Detectable by Laser-Induced Fluorescence That Are Intermediates in Combustion Chemistry

Molecule[a]	Excitation wavelength (nm)	Molecule[a]	Excitation wavelength (nm)
H*	206	NCO*	440
C	280	HCO	615
O*	226	HCN	189
N	211	HNO*	640
S	311	NH_2*	598
OH*	309	C_3	405
CH*	413	C_2O	665
NH*	336	S_2O	340
SH*	324	SO_2*	320
CN*	388	NO_2*	590
CO*	280	HSO	585
CS	258	CS_2	320
NO*	226	N_3	272
NS*	231	NCN	329
SO*	267	CCN	470
O_2*	217	HCCO	310
S_2*	308	NO_3	570
C_2*	516	C_2H_2*	220
		CH_2O*	320

[a] An asterisk denotes that LIF detection has been performed in a flame.

terminations, which must be approached with considerable care [5].

LIF can also be used in a semiquantitative manner. The simple presence of an intermediate species in some flame, at an estimated concentration, can signal important concepts concerning the flame chemistry. The relative concentrations of two (or more) species can provide choices among alternative reaction mechanisms. For such purposes, the accuracy of the measurement need not be high: knowing the concentration to within a factor of 3 or 5 can be quite adequate in the hands of an insightful chemist.

LIF has, however, seldom been used in this way. The purpose of this article is to illustrate where a single, approximate LIF measurement has yielded important flame chemical mechanistic information, using two simple cases from work in our laboratory. Extensions of these ideas to the simultaneous detection of two or more species, including two-dimensional imaging measurements, are also discussed.

We emphasize that it is often necessary to detect species other than the OH molecule in order to generate useful ideas about the flame chemistry. OH is the most important molecular radical in most flames and its measurement is crucial to an understanding of the chemistry. However, it alone tells very little about that chemistry, because its concentration often rises slowly through the reaction zone and remains relatively high (several parts per thousand or greater) far into the burned gases. Those intermediates that rise and then fall before or within the reaction zone of the flame, where the high-temperature gradient occurs, are much more revealing. These can include all other species (save for H and O) in Table 1. Because OH is important, is present often at high concentration, and is easy to detect, it has been the focus of most LIF flame studies. To really understand the chemistry, however, other species must be measured besides this popular molecule.

LIF SIGNAL ANALYSIS

Most LIF experiments have been performed at atmospheric pressure. The collision processes occur so quickly that, during the laser pulse, the excited state population N_e remains in a steady-state ratio to that of the ground state. The LIF signal S is given by

$$S = N_e A \tau_L G V \Omega, \tag{1}$$

where A is the Einstein coefficient for emission into the spectral region detected by the phototube, V is the volume probed by the laser, Ω is the solid angle collected, and τ_L is the laser pulse length. G is an apparatus factor comprising filter transmission, photodetector efficiency and gain, and electronic amplification. (The product $GV\Omega$ can often be calibrated using Rayleigh or Raman scattering, with proper attention to wavelength-dependent factors.) The excited state population is determined by a balance between the rates at which it is pumped by the laser and is removed due to

radiative, nonradiative, and collisional processes:

$$N_e = N_g f \frac{BI}{[g_l/g_u]BI + k_r + k_{pre} + \sum_i k_{Qi} n_i} . \quad (2)$$

B is the Einstein absorption coefficient, I the laser intensity, and k_r and k_{pre} the rates for radiation and (if present) predissociation. The sum over $k_{Qi}n_i$ is the rate of collisional quenching in the mixture of species, each having bimolecular quenching rate coefficients k_{Qi} and densities n_i. N_g is the ground state concentration and f the fraction of molecules in the absorbing vibrational-rotational level. The term $[g_l/g_u]BI$, with lower and upper electronic degeneracies g, represents stimulated emission.

The spectroscopic coefficients A and B in Eqs. 1 and 2 contain factors for Franck–Condon vibrational overlap, rotational line strength, and the total radiative rate k_r. Generally, these are known or can be measured in separate experiments (usually not in flames). It is the quenching contribution [6] to the denominator of Eq. 2 that is the most difficult to know accurately. Collisional quenching has been investigated thoroughly for the $A^2\Sigma^+$ excited state of the OH radical, and found to exhibit a marked dependence on collision partner, temperature, and vibrational and rotational level. The combustion diagnostics implications of these studies, many of which were performed in our laboratories, are discussed in ref. 7. There, quenching rate coefficients k_{Qi}, calculated using a reasonable collision model, are given for several colliders of combustion interest as a function of temperature. It was concluded that, for OH, the quenching can be estimated to within some 30%, given some knowledge of the collisional environment, for example, from the initial mixing ratio between fuel and oxidant plus the temperature at the point the measurement was taken. Calculated quenching rates agree to within this uncertainty with the direct measurements made in flames at atmospheric and reduced pressure. For other molecules the situation is not so good, in part because few quenching measurements have been made at elevated temperature. Estimates of $\Sigma k_{Qi}n_i$ to within a factor of 2 or 3 are realistic to expect for H, O, NH, CH, and NO; for the other atomic and molecular species, too little appears generally known at present to do even this well. Nonetheless, these levels of accuracy should be quite adequate for the purposes of semiquantitative LIF, as described below.

LIF SPECTRA IN FLAMES

In a stable laminar flame, LIF data are often taken as so-called excitation scans, in which the laser is tuned throughout some spectral region where the molecule of interest absorbs. All (or some fixed fraction) of the fluorescence is detected each time the laser, which has a typical bandwidth of 0.3 cm^{-1}, overlaps an absorption line. The resulting pattern is characteristic of the absorbing molecule and is used to provide unambiguous identification. An example is given in Fig. 1, which shows an excitation scan taken in the reaction zone of a methane–oxygen flame burning at 7 torr pressure. This is the R branch head of the (0,0) band of the $B^2\Sigma^- - X^2\Pi$ electronic transition of the CH molecule near 387 nm. CH is present in many hydrocarbon flames, although the role it plays is not known, due in large part to a lack of knowledge of its reaction rates at high temperature. Emission from CH has been used to mark reaction zones and it has been suggested as an important participant in prompt-NO production through the CH + N_2 reaction.

The fluorescence in the entire (0,0) B–X band of CH, including the Q and P branches, was detected. Note that for this light diatomic hydride, all the rotational lines are well resolved and clearly identifiable even in this bandhead region. In this case, the excitation scan has been used to determine the temperature at the point of measurement of the radical: the dashed line shows a fit of the entire spectrum [8, 9] to a single temperature, using a spectral simulation computer code [9] including the appropriate spectroscopic data base on line positions and intensities. Accurate determination of the temperature, even for relative radical concentration measurements, is crucial for any comparison with chemical mechanisms due to the

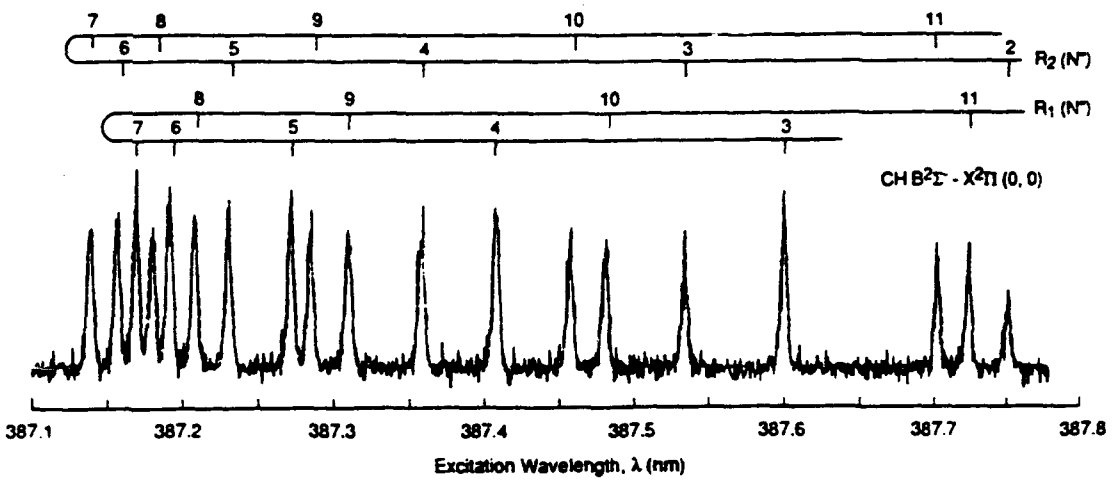

Fig. 1. Excitation scan through the R-branch region, as labeled, of the (0,0) band of the $B^2\Sigma^- - X^2\Pi$ transition of the CH molecule. The flame is CH_4/O_2 burning at 7 torr; the detected emission is that of the entire band including also the P and Q branches at longer wavelengths. The scan is fit to two parameters, a temperature and a linewidth (assumed the same for all lines) using a simulated spectrum calculated with a population distribution corresponding to that temperature. The fit is shown by the dashed line.

highly nonlinear temperature dependence of chemical reaction rate coefficients [9].

As we move to a polyatomic radical, the spectra rapidly become more complex. The simplest such situation is that of a linear triatomic, exemplified by the NCO molecule, for which an excitation spectrum over the range of a single laser dye is exhibited in Fig. 2. This $A^2\Sigma^+ - X^2\Pi_i$ transition has a rotational structure very similar to diatomics with the same state symmetries; however, the vibrational pattern is much more complicated [10]. These excitation spectra were taken in the reaction zone of a CH_4/N_2O flame burning at atmospheric pressure, where NCO appears in copious quantity; the radical has also been suggested as an important intermediate in fuel nitrogen production of NO_x. Detection was through a monochromator at 440 nm, to filter out strong LIF signals due to CH, C_2, and CN, which are concomitantly excited. Note that the top two spectra are noise-free at the sensitivity illustrated.

The top scan shows the overall pattern, which increases sharply in intensity as one scans to shorter wavelengths through the (000–000) electronic origin band near 440 nm. Toward shorter wavelengths, the spectrum quickly becomes much more congested due to the appearance of hot bands, that is, absorption of the laser by excited vibrational levels of NCO in the hot flame. The drop in laser power for wavelengths less than 430 nm accounts for the decrease in apparent intensity of bands moving to yet shorter wavelengths. In the middle spectrum, a 4-nm portion showing the four bandheads of the (000–000) band is exhibited; the bottom panel is a further expanded section, 0.45 nm in extent, which shows individual rotational lines of the $^QP_{12}$ satellite branch. (Interestingly, this $^QP_{12}$ head is barely discernible in room temperature LIF spectra of the radical; this is because the rotational levels contributing in the head region have $J \sim 70$ and are sparsely populated at 300 K.)

The overall pattern throughout this region is complex, in large part because vibrationally excited levels contain significant fractions of the total NCO population. In order to make measurements of NCO, even semiquantitative ones, it is necessary to have at hand assignments of the vibrational bands and rotational lines contributing to the absorption and fluorescence at the laser and detection wavelengths. In the case of this triatomic molecule, detection in hot bands to the red, such at

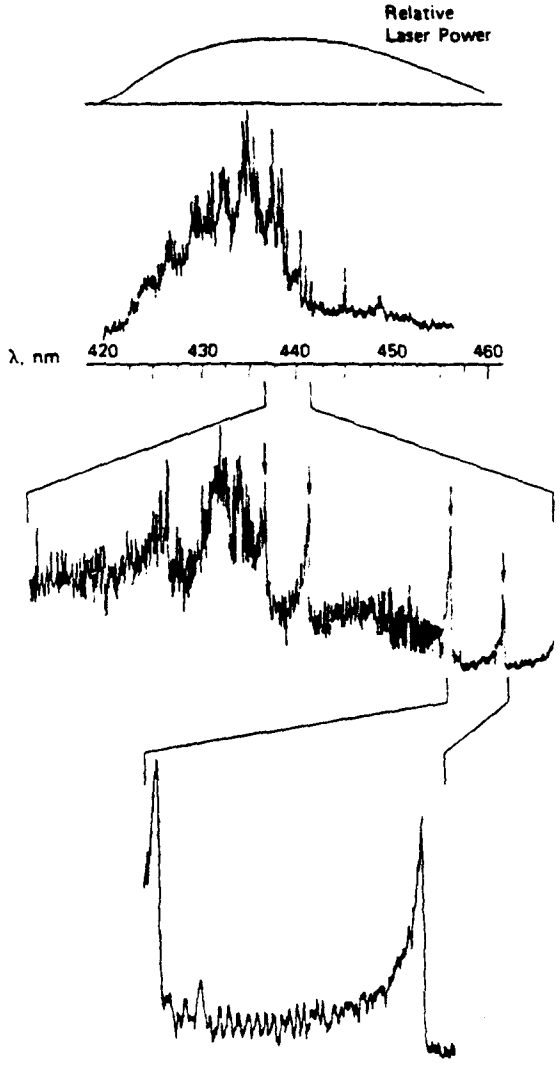

Fig. 2. Excitation scans for the $A^2\Sigma^+$-$X^2\Pi_i$ system of the linear triatomic radical NCO, in the reaction zone of an atmospheric pressure CH_4/N_2O flame. The fluorescence is detected at 465 nm (the 000 → 100 band region) with a 4-nm bandpass. Top spectrum: total scan over the entire range of one laser dye (Coumarin 440), unnormalized to laser power. Middle: 4-nm portion showing the region of the 000 ← 000 band, with the (right to left) Q_1, P_1, P_2, and $^oP_{12}$ heads marked by arrows. Hot bands begin to appear at wavelengths shorter than the Q_1 head. Bottom: Region 0.45 nm in extent showing the rotationally resolved $^oP_{12}$ branch, with a head having $J \sim 70$.

(000)–(100) at 466 nm, offers less congestion and therefore less ambiguity in individual line assignments [10].

The situation continues with other polyatomics, placing limits on the detectivity and selectivity which can be obtained. In Fig. 3 are seen two excitation scans [11] of the CH_2O molecule, seeded into an atmospheric pressure CH_4–air flame at a mole fraction of 0.5%. This excitation is the $2_0^1 5_0^1$ band at 305 nm; a few rotational subband heads are marked. The bottom panel shows the spectrum in the unburnt gases, just above the burner and below the reaction zone of the flame. The top scan was taken higher in the flame, where the signal-to-noise ratio can be seen to be much smaller.

Although some formaldehyde has been consumed by reaction, a major cause of the much smaller signal levels (as witnessed by the lower signal-to-noise ratio) is the dilution of the population over the much larger number of levels. In particular, the distinct bandheads in the lower spectrum arising from rotational levels highly populated at room temperature become less pronounced in the flame because those levels contain a much smaller fraction of the total population at high temperatures. This fact can be considered quantitatively by an examination of the partition functions for these molecules at different temperatures in Table 2. (Both CH and NCO have $^2\Pi$ ground states, with fourfold electronic degeneracy, which accounts largely for the fact that the total partition function for NCO is larger than that of CH_2O at the lower temperatures.) Note that there are some 500 times as many levels populated for the polyatomics compared to CH at 2000 K; for similar absorption strengths and quantum yield (which is approximately the case) typical polyatomic signals will be that much smaller for the same radical concentration.

Another type of LIF flame experiment involves "fluorescence scans." For these, the laser wavelength is fixed upon one excitation line, and a monochromator dispersing the fluorescence is scanned to reveal the spectrum of the emitted fluorescence. This spectrum arises only from the initially excited level pumped by the laser, if no collisional redistribution has occured in the excited

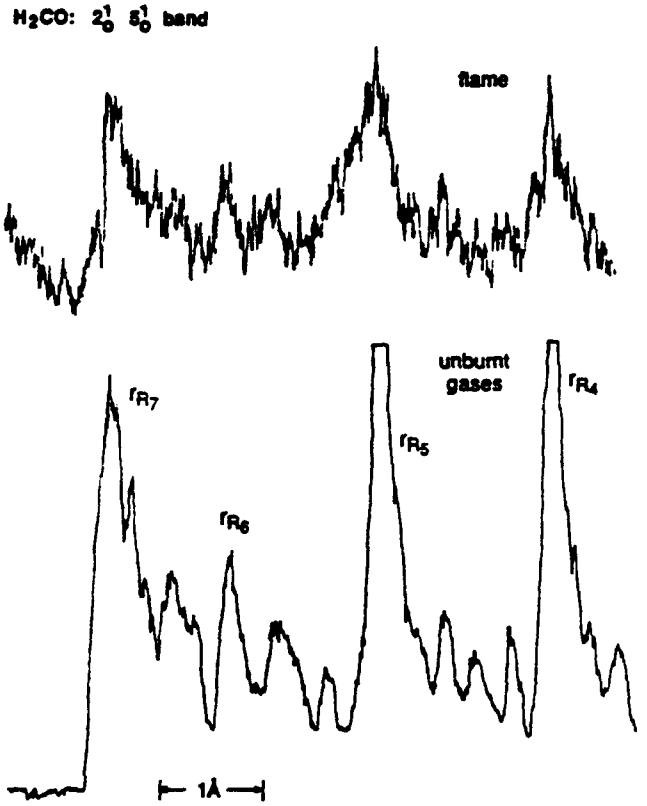

Fig. 3. Excitation scans of the CH_2O molecule near 318 nm, exciting the $2^1 5^1$ level of the $\tilde{A}^1A_2$ electronic state. The marked peaks are R-branch subband heads, formed from a sequence of rotational levels J each having a common value of K, the projection quantum number along the figure axis of the molecule; always, $J \geq K$. Bottom: scan in the cool unburned gases below an atmospheric pressure CH_4/O_2 flame, in which CH_2O is seeded at a concentration of 0.5%. Top: scan in the reaction zone of the flame. The signals are much weaker due to the shift in population with the increase in temperature. Many more levels are populated and there is less population in levels with smaller J, K that form the bandheads prominent in this region.

state. It then consists of the (typically three) strong rotational branches emitted by that level, appearing in a series of vibrational bands. An example is shown in Fig. 4, for the NCO molecule. The bottom spectrum is a fluorescence scan in a low-pressure discharge flow, in which NCO is the only radical of consequence present. The spectrum shown is obtained by exciting the $v_1v_2v_3 = 000$ level of the $B^2\Pi_i$ state, an electronic state different from that involved in the scans of Fig. 2. Long progressions in the three ground state vibrations can be seen. In the upper panel is a fluorescence scan exciting at the same wavelength, but this time in the CH_4/N_2O flame. The same progression of bands can be seen, providing a definitive spectroscopic identification of the molecule in this flame. (The larger breadth of the bands in the flame is due to wider monochromator slits.) However, lines arising from simultaneous excitation of the OH and CN molecules are also present in the flame.

TABLE 2

Partition Functions for Some Combustion Intermediates

Temperature	CH	NCO	CH_2O
300 K	50	4.6×10^3	1.4×10^3
1000 K	170	1.7×10^4	3.4×10^4
2000 K	400	1.8×10^5	2.1×10^5

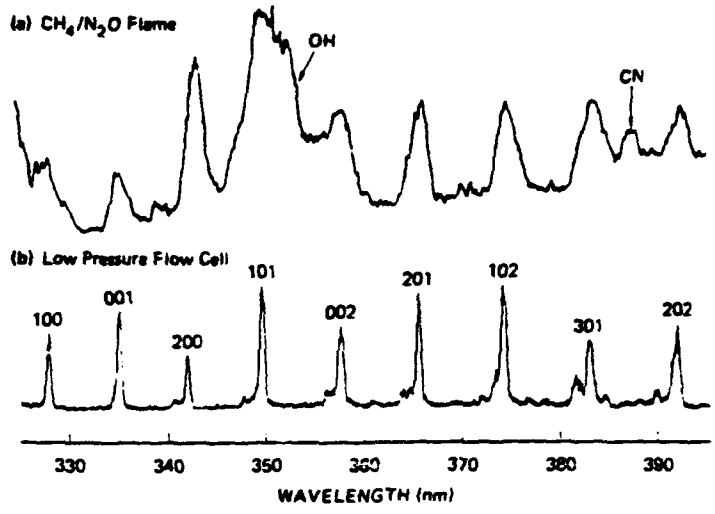

Fig. 4. Fluorescence spectra of the NCO molecule. Excitation is to the $v_1v_2v_3 = 000$ level of the $B^2\Pi$ electronic state of the radical near 315 nm, and a monochromator dispersing the fluorescence is scanned, showing a series of transitions to vibrational levels (as numbered) in the lower electronic state. *Bottom*: fluorescence scan in a low-pressure discharge flow system in which NCO is the only radical present in appreciable quantity. *Top*: fluorescence scan in an atmospheric pressure CH_4/N_2O flame, with the same excitation. By the characteristic fluorescence pattern NCO can be distinguished even though there are interferences due to OH and CN absorbing at the same wavelength. Observation of the 201 or 102 band at 366 or 374 nm, respectively, appears the best for detection of NCO in the presence of these diatomics.

Tuning the monochromator to, for example, the 201 band or the 102 band will permit the detection of NCO without interference from the diatomics. This can be necessary because of the much stronger signal from the diatomics for comparable line strengths, as noted above. Without selective detection the diatomic signals can mask those of the polyatomics. Later, however, we shall see how this overlap in excitation might be exploited to learn about flame chemistry.

During the time the molecule resides in the upper electronic state, it may suffer collisions that leave it excited but in a different internal (vibrational-rotational) level from the one originally pumped by the laser. In this case fluorescence scans can be used to study that collisional redistribution of the excited state population. An example is shown in Fig. 5, which is a rotationally resolved fluorescence scan for the B state of the CH radical in an atmospheric pressure CH_4/O_2 flame [12]. The initially excited rotational level remains the most highly populated. There is competition between rotational energy transfer (which redistributes the population) and quenching (which removes it from the excited state and freezes the distribution). Similar studies on OH [13, 14], CH(A) [12, 15], and CN [16] show that rotational thermalization is also not achieved in those molecules. Such effects must be taken into account to determine the effective quantum yield within the spectral bandpass employed to obtain quantitative measurements of concentration and temperature [6].

Semiquantitative Detection of NH and NS

Equations 1 and 2 contain the parameters necessary to obtain measurements of molecular species in flames using LIF. The Einstein coefficients for absorption and emission contain Franck-Condon vibrational overlap and rotational line strength factors that are available from spectroscopic measurements in flow cells and/or flames. The overall radiative rate k_r and bimiolecular quenching rate coefficients k_{Qi} are usually obtained from low pressure experiments if available, although only for OH and to a lesser degree NH and CH does sufficient information [7] exist to permit a calcula-

tion of the sum for actual flame conditions. It is generally the quenching contribution to Eqs. 1 and 2 that is most uncertain; in spite of that fact, useful information can still be obtained from intermediate species LIF measurement. We illustrate this point with two examples.

The first consists of measurements on the NH radical made in a CH_4/N_2O flame [6]. Because the N–N bond strength in N_2O, 4.93 eV, is much stronger than the 1.68 eV bond strength of the N–O bond, the most obvious chemical mechanism would involve splitting off an oxygen atom to oxidize the hydrocarbon. Now it has long been known [17] that the emission spectrum of hydrocarbon–nitrous oxide flames includes band systems of the molecules NO, CN, NH, and NH_2 in addition to those from OH and CH; the former set

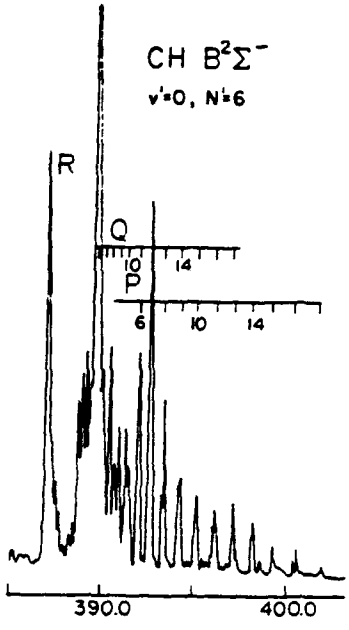

Fig. 5. Rotationally resolved fluorescence spectrum of the CH B–X (0,0) band following excitation of the $N' = 6$ rotational level in the excited state. The P and Q branch lines emitted by the initially pumped level can be distinguished. The other levels, most evident in the P branch, have been populated by collisional rotational energy transfer with the gases of this rich atmospheric pressure $CH_4/N_2/O_2$ flame. Quenching, which removes the emitting B-state altogether, occurs competitively with rotational energy transfer. Thus, the distribution is neither that of the initially excited level alone nor a rotationally thermal distribution.

of molecules can be produced only through breakage of the much stronger N–N bond. On the other hand, such emission may well arise from direct chemiluminescent formation of the excited emitting states within the flame, and may not be a valid indicator of the chemically important ground state concentrations.

LIF can supply the proper measure of the chemically relevant ground state, for it is that state that absorbs the laser radiation. Excitation scans were taken of both OH and NH in the luminous zone of the flame. At the time (early 1980) that this experiment was performed, little was known concerning the quenching of $A^3\Pi_i$ NH and nothing was known about high-temperature quenching of either radical. Nonetheless, the simple assumption was made that the quantum yield at atmospheric pressure, $Q/A = \Sigma k_{Qi} n_i / A$, was the same for both species. Together with known spectroscopic data, the concentration ratio [NH]/[OH] ~ 0.04 was obtained. A separate absorption measurement showed that OH was, as usual, present at high levels, $\sim 7 \times 10^{15}$ cm^{-3}. The inferred concentration of NH is then 3×10^{14} cm^{-3}, quite ample to be of chemical significance. This finding has been important in setting the entire stage for the consideration of the chemistry of hydrocarbon–nitrous oxide flames, showing that it would be imprudent to ignore the role of radicals produced following breakage of the N–N bond of the N_2O.

Subsequent to this simple experiment and analysis [6], a measurement [18] of NH in such a flame was performed using absorption, which does not rely on a quenching estimate. The result, also 3×10^{14} cm^{-3}, agrees better with our determination than the approximation on Q/A warrants. In fact, a much more recent set of measurements in low-pressure flames [5, 19] indicates that Q/A is probably smaller for NH than for OH by about a factor of 3. Nonetheless, chemical models of such flames now include pathways for generation and reaction of NH, as they should. (What such pathways should be is not yet clear; it was in fact ambiguity among the possibilities which led to the postulation and successful search for NCO in such flames [10, 20].)

A more recent example is that of the NS

molecule [21]. NS had been observed previously only in spectroscopic experiments in discharges, and never in flames; it had only rarely [22] been considered as a potential flame intermediate. We wondered whether NS might be present in flames of hydrocarbons containing fuel sulfur and fuel nitrogen, which are often combined in coals. If so, it could be a link between the cycles that produce NO_x and SO_x.

Our studies of NS began with a series of spectroscopic [23] and quenching measurements [24], in a microwave discharge in N_2 mixed with SCl_2 in a flow cell at low pressure and room temperature. An excitation scan through the (0,0) vibrational band of the $C^2\Sigma^+ - X^2\Pi$ transition is shown in the upper panel of Fig. 6. The individual rotational lines can be assigned and analyzed; the four-headed pattern is the same as those seen in the similar Σ–Π transitions of NCO and CH illustrated earlier.

A small burner was then positioned in place of the flow system and used to burn a CH_4/N_2O mixture seeded with SF_6. The resulting excitation scan, with the laser beam focused into the flame-front region, is shown in the lower panel of Fig. 6. This is, unambiguously, the same molecule that had been detected under well-controlled conditions in the flow system, clearly illustrating the selectivity of the LIF method. The larger number of lines in the flame spectrum is due to the higher temperature and consequently larger fractional population in higher rotational levels.

For more careful measurements, we formed a simulated coal flame from methane burning in

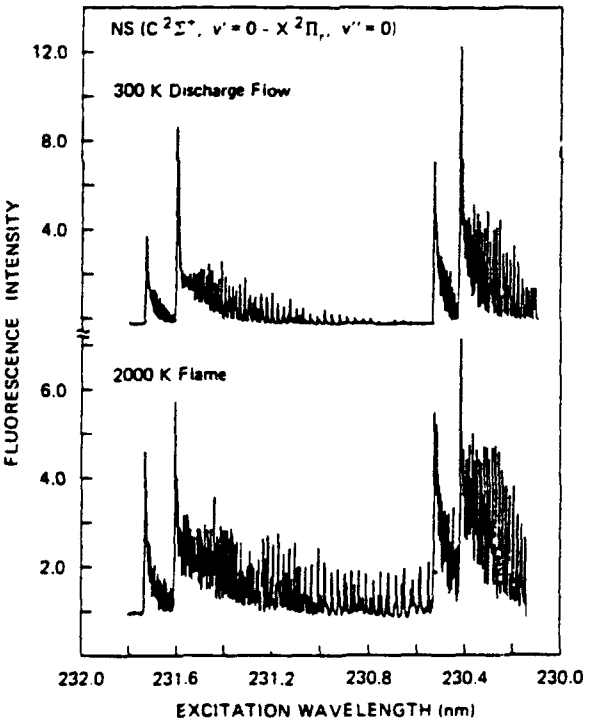

Fig. 6. Excitation scans for the NS molecule, in the (0,0) vibrational band of the *C–X* transition. Four prominent band heads and many individual rotational lines are evident. *Top*: NS in a room temperature flow system, produced in a microwave discharge in N_2 and SCl_2. *Bottom*: NS in an atmospheric pressure CH_4/N_2O flame seeded with SF_6. Scans in CH_4/O_2 flames seeded with H_2S and NH_3 appear identical. The flame species can be unambiguously identified as NS by the characteristic spectrum; the larger number of rotational lines in the flame scan is due to the higher temperature.

oxygen containing minor amounts of NH_3 and H_2S to represent fuel nitrogen and sulfur. NS was observed in all such flames, and even in a flame of pure natural gas burning in N_2O; here, the sulfur source was the 2 ppm of methyl mercaptan added by the utility company to produce a noticeable odor.

Just finding the NS raises interesting questions, but even more useful would be estimates of its absolute concentration. For this purpose, it was necessary to estimate many of the parameters in Eqs. 1 and 2, including seeking analogies with the collisional behaviour of other molecules. The choices are described in detail in ref. 21. The Einstein A emission coefficient was taken from an ab initio quantum chemical calculation; together with our measured Franck–Condon factors [23] and calculated rotational line strengths, these also furnished absorption coefficients B. The decay of the $C^2\Sigma^+$ state of NS is governed by predissociation, with an effective lifetime of 6 ns measured by magnetic depolarization (Hanle effect), which is too fast for direct observation by our detection electronics. The major uncertainty, however, is posed by the fact that quenching of the C state of NS has never been measured. We estimated it by analogy to quenching results on NO and PO, as well as our measurements [24] on the $B^2\Pi$ state of NS itself.

A careful consideration of all the uncertainties involved in the estimates, together with experimental error bars, led to an overall uncertainty of a factor of three in the absolute concentrations of NS measured in these flames. How good is a measurement to within a factor of three? When the molecule has never before been observed in a flame, it can be quite revealing. In some of the flames, the steady-state NS concentration was measured to be as much as 5% of the total added sulfur. Even with a range of 2%–15%, this means that a very large fraction of the fuel sulfur is being processed through this one radical. With this estimate of the total concentration, together with the fact that the NS signal disappeared rapidly when the laser beam was moved into the burned gases, we deduced that NS was removed primarily by a reactant present at a few tenths of a mole percent, and produced by a reaction between some radical present at 10 ppm or more and a stable species present at 0.1% or greater. The conclusion is that NS may be an important reaction intermediate in the reducing atmosphere of rich hyrocarbon flames with fuel nitrogen and fuel sulfur. It may play a major role in NO_x–SO_x interaction chemistry. This simple observation of NS does not prove that role, but clearly indicates further measurements of reaction rates and studies in flames are needed.

This observation of NS, a new radical in combustion chemistry, illustrates the type of ideas and insights that one can obtain using semiquantitative LIF in flames. Although estimates were necessary for some parameters in the analysis, the concentration values deduced are accurate enough to raise, if not answer, important questions about the flame chemical mechanism.

MULTIPLE SPECIES LASER-INDUCED FLUORESCENCE

The detection of a single species in a flame can provide valuable insight into the flame chemistry, as shown by the preceding examples of NH and NS. Even more informative can be the detection of more than one type of molecule at the same point and the same time. For example, whether CN precedes NH in a CH_4/N_2O flame may disclose the rate of attack of nitrogen atoms or nitric oxide molecules on methane compared with that of hydrogen atoms reacting with the nitrous oxide. In those few cases in which such measurements have been made, the approach has been the sequential use of different excitation wavelengths, even different lasers, each optimized for one of the desired species. Because beam sizes and divergences are different, considerable care must be taken to ensure that the same volume is probed by each laser. An imprecise match can render meaningless any comparison with calculated flame chemistry models. This problem can be greatly exacerbated in attempts to make measurements in turbulent flames, where each laser must be fired simultaneously and sample the same spatial region of the flame despite severe optical inhomogeneities.

We took a different approach [25], seeking

particular laser wavelengths at which more than one species could be excited. The objective is to use one laser at one wavelength to detect two or more molecules in, necessarily therefore, the same probed volume. This series of experiments was performed in a CH_4/N_2O flame burning at atmospheric pressure on a small glassblowing torch. We have already seen that in this flame there exist many different reactive radicals, so it provided a fertile test system to develop the method.

In the spectral region near 315 nm exist electronic transitions of the intermediates OH, NH, CH, CN and NCO. Several of the individual absorption lines of these molecules overlap within the Doppler width of typically 0.2 cm^{-1}, which approximately matches the 0.3-cm^{-1} bandwidth of typical commercial lasers. This permits the concurrent detection of these species using spectrally dispersed or filtered fluorescence. We have already seen an example of such overlap in the flame fluorescence spectrum in Fig. 4, in which OH and CN were excited together with NCO. Between 280 and 320 nm, there are many wavelengths at which two molecules of the set of diatomics absorb and a few where three can be detected. NCO is also included near 315 nm.

At one wavelength, 312.22 nm, there exists an overlap of absorptions by the important hydrides NH, CH and OH; CN can also be observed nearby. Figure 7 exhibits five repeated excitation scans over the same wavelength region, selectively detecting in turn each of these species. In Fig. 7a, the OH (0,1) A–X band is observed in the monochromator; the largest feature is the $P_1(7)$ line of the (0,0) excitation. The smaller lines belong to (1,1) and are observed following $v' = 1 \rightarrow 0$ energy transfer in the flame. This is clear from Fig. 7b, where the (1,2) band is detected and these (1,1) excitation lines stand out prominently. In Fig. 7c, CN fluorescence near 388 nm is detected. Most of this spectrum tracks that of OH in Figs. 7a and 7b and is due to a transfer of electronic energy from excited OH to CN in the flame. Some of the excitations mapped are those of the so-called tail bands of the CN B–X system. These two causes of CN excitation can be separated by the choice of detection wavelength, as seen below. In Fig. 7d, the A–X system of NH at

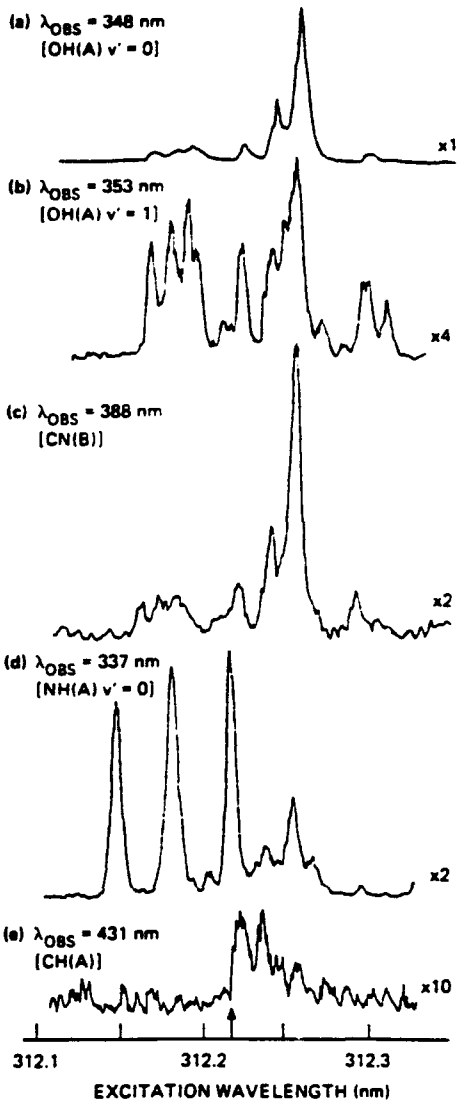

Fig. 7. Excitation spectra over the same laser wavelength region but detecting at different fluorescent wavelengths to measure various radicals in the reaction zone of an atmospheric pressure CH_4/N_2O flame. The arrow at the bottom denotes the wavelength where all excitations overlap, used for the fluorescence scan in Fig. 8. (a) Detection at λ_d = 348 nm to observe excitation in the (0,0) band of OH. (b) λ_d = 353 nm to observe excitation in the (1,1) band of OH. (c) λ_d = 388 nm to observe the (0,0) and (1,1) bands of CN, created by excitation transfer from OH; compare with Figs. 7a and 7b. The much smaller lines between 312.10 and 312.15 nm are direct excitation of the tail bands of CN. (d) λ_d = 337 nm to observe excitation in the NH A–X system, with the most prominent lines seen the $P(N'' = 12)$ triplet of the (2,1) band. (e) λ_d = 431 nm to observe A–X emission from CH resulting from energy transfer following excitation in the (0,0) and (1,1) bands of the C–X transition.

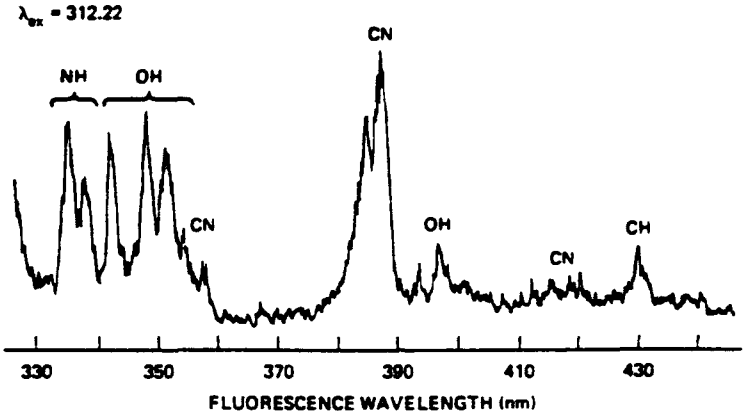

Fig. 8. Fluorescence scan following excitation in the CH_4/N_2O flame at 312.22 nm, as denoted by the arrow in Fig. 7e. Directly excited LIF from OH, NH, and CN can be seen. The CH emission results from $C \rightarrow A$ collisional energy transfer following excitation of the C state. The large CN feature has two peaks: that at shorter wavelength is direct excitation of the $v' = 3$ and/or 4 levels of the B state, and the emission at 388 nm results from energy transfer from OH excited by the laser.

336 nm is selectively detected; the prominent excitation here is the P branch triplet for $N'' = 12$ in the (2,1) band. In Fig. 7e, an excitation scan of the CH C–X system is seen, monitored via energy transfer of the radical into the emitting $A^2\Delta$ state. The doublet is the R branch set for $N'' = 7$ in (0,0) and the weaker lines belong to (1,1). Attempts to directly detect CH $C^2\Sigma^+$ emission near 314 nm were swamped by signal from OH in the same region, and the electronic-to-electronic energy transfer was exploited to selectively observe CH.

At 312.22 nm, denoted by the arrow in Fig. 7e, all four of these species are resonantly excited. With the laser tuned to this wavelength, the fluorescence scan of Fig. 8 was taken. Emission from each of the diatomic species can be seen. In the tallest feature, labeled CN, the direct excitation is the peak at shorter wavelength, while the higher one to the red results from energy transfer from OH.

These spectroscopic coincidences will permit instantaneous correlation measurements among different species in pointwise or imaging (see below) flame experiments. They avoid the complications of alignment of two separate laser beams and the accompanying variation in spatial and temporal profiles of each pulse. This can be useful in a stable, laminar flame, and is probably essential in the study of the chemistry of turbulent combustion. A single optical system could be used to collect the fluorescence. The light emitted by each species would be directed onto a separate detector using beamsplitters and appropriate filters. The throughput of such a system is much higher than that of the monochromator used for the scan in Fig. 8, and will yield correspondingly higher signal levels.

In turbulent flames, where the conditions at a given point change rapidly with time, measurements made upon successive laser pulses can be related only in a statistical fashion. This is true of course for measurements of one as well as several intermediate chemical species. Because of the complex and highly nonlinear aspects of flame chemistry, attempts to relate statistical averages of one radical, e.g., CN, to another such as OH are not likely to be very useful for developing insight into that chemistry. The technique of two-dimensional fluorescence imaging [26] was developed in order to provide an instantaneous spatial distribution of the measured radical, avoiding ambiguities in a statistical analysis. By tuning the laser so that more than one species is excited, and focusing the

light through beamsplitters onto different diode array detectors, one could obtain correlated spatial distributions of different radicals, results that should be extremely informative concerning the chemical mechanism involved.

A simple example of what one might do is illustrated by two-dimensional LIF imaging of the CH radical in a flame [27]. This experiment was performed in a stable laminar flame using two different lasers and the data were taken sequentially, not simultaneously. Nonetheless, the technique of multiple species detection at a single laser wavelength could be used for the purpose. Each laser beam was formed into a sheet of radiation in a now-standard fashion [26], slicing through a small atmospheric pressure CH_4/O_2 flame on a glassblowing torch. The data are plotted as concentration profiles in Fig. 9. Each line, or track, shows the distribution across the flame at a particular height above the burner. The lines extending to the edge of the frame are OH, whereas those profiles filled-in (for distinction) are CH. A spatial point consists of a box 0.1 mm in the x direction and 1 mm in the y direction.

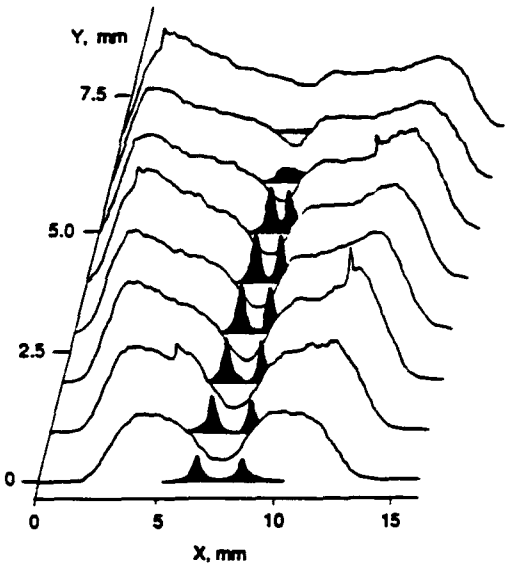

Fig. 9. Composite results from OH and CH two-dimensional LIF imaging experiments in the tip of a glassblowing torch flame, burning CH_4 and O_2 at atmospheric pressure. Each track represents the intensity across a horizontal segment of the vidicon face. The distances marked are those in the flame; the y axis is stretched and skewed for clarity. Each track represents a sum over 1 mm vertical spatial resolution while the horizontal resolution is 0.1 mm. The lines represent the OH distribution, with a maximum in the burned gases, and the filled-in profiles are those of CH, which exists primarily in the flame front region. These are sequential experiments, each averaging over seven laser pulses; for measurements in a time-varying system such as a turbulent flame, a single pulse of a laser tuned to overlapping transitions of the two species would be used.

It is clear from these distributions that measurements of OH and of CH provide very different information about the flame chemistry. The OH tells us primarily where the burned gases are, that is, where the chemical reactions have already occurred. On the basis of OH alone, it is very difficult to distinguish the reaction zone. CH, in contrast, is near the flame front and reveals where the combustion chemistry is now taking place. To obtain a complete picture of the flame chemistry, one that is both current and historical, the measurement of both species is necessary.

This distinction between OH and CH was evident from prior knowledge about the conical flame shape in this stable, laminar system. In dealing with a time-varying system like turbulent combustion or explosion, this simple information concerning where the flame chemistry is occurring and has taken place could be valuable in comparing with models of turbulent combusting flows [27]. For these conditions, a single laser tuned to a CH/OH overlap and a pair of array detectors are needed to obtain properly correlated measurements.

The data exhibited in Figs. 7–9 are LIF signals uncorrected for quenching. To be carefully quantitative, one would need to know the flame environment for each point at which the measurement is made. Obviously, this cannot be done for the case of an instantaneous image in a time-varying flame. The situation can be ameliorated by operating under optical saturation conditions [28], although problems are then introduced concerning the size and shape of the volume probed. Nonetheless, relating an instantaneous LIF image to the desired radical ground state concentrations will remain semiquantitative. As we learn more about quenching under differing flame conditions [5, 7, 19], we

can place closer limits on the uncertainties introduced by such estimates.

CONCLUSION

Laser-induced fluorescence measurements of radical intermediates are usually obtained in the form of profiles, often solely for OH but sometimes including other species, for comparison with computer calculations of detailed flame chemical mechanisms. We have seen that LIF can also be used in a quite different way, to detect and make semiquantitative measurements of one or more particular reactive species. Such information, even the presence alone of some radical, can lead to insight into the flame chemistry. Examples were offered by the detection of the NH radical in CH_4/N_2O flames, showing that the chemistry involves breakage of the N–N bond in the oxidant, and the finding of NS in copious quantity in simulated coal flames, raising important questions about its role in interactions between the NO_x–SO_x formation mechanisms. Particularly useful would be the measurement of more than one intermediate species simultaneous in position, and also in time for rapidly varying processes. The successful search for wavelengths at which more than one radical can be detected using selectively filtered fluorescence detection provides the means for such an experiment. The method could even be extended to simultaneous two-dimensional imaging in time-variant systems, to obtain correlations concerning the chemical mechanism and the flow dynamics; an example of very simple information of that type was afforded by images of CH, which mark the zone of reaction in a CH_4/O_2 flame, and OH, which show where the reaction has already occurred.

As our chemical knowledge advances, one wishes of course to improve the level of accuracy of the corresponding LIF measurements. Where possible, quantitative comparison with mechanistic predictions is the goal. Continued investigations of the spectroscopy and collisional behavior of key radical species ensure that such progress will occur. However, it is important to identify those key species on which to concentrate such efforts. This can be done by careful considerations of the flame chemistry, coupled with semiquantitative detection of new species as discussed here. Such measurements will not merely identify new species as for NS; they can also help formulate questions leading to a search for other intermediates from mechanistic considerations, e.g., the detection of NH leading to an inquiry about NCO. Progress in our understanding of combustion chemistry will result from a thoughtful combination of both semiquantitative and quantitative measurements of reactive flame intermediates.

I gratefully acknowledge the experimental efforts of and many useful discussions with several coworkers involved in the experiments described: Richard Copeland, Mark Dyer, Nancy Garland, Jay Jeffries, Karen Rensberger, and Gregory Smith. The work described has received support from several sources: U.S. Army Research Office, Basic Energy Sciences Division of the Department of Energy, Air Force Wright Aeronautical Laboratories, and Physical Sciences Department of the Gas Research Institute.

REFERENCES

1. Seery, D. J., *Combust. Flame*, (1988, in press).
2. Crosley, D. R., and Smith, G. P., *Opt. Eng.* 22:545 (1983); Bechtel, J. H., Dasch, C. J., and Teets, R. in *Laser Applications* (R. K. Erf and J. F. Ready, Eds.), Academic, New York, 1983; Lucht, R. P., in *Laser Spectroscopy and Its Applications* (L. J. Radziemski, R. Solarz and J. A. Paisner, Eds.), Marcel Dekker, New York, 1986; Crosley, D. R. *High Temp. Mat. Proc.* 7:41 (1986).
3. Fristrom, R. M., and Westenberg, A. A. *Flame Structure*, McGraw-Hill, New York, 1965.
4. Gardiner, W. C., Ed., *Combustion Chemistry*, Springer-Verlag, New York, 1984.
5. Kohse-Höinghaus, K., Jeffries, J. B., Copeland, R. A., Smith, G. P., and Crosley, D. R., *Twenty-Second Symposium (International) on Combustion*, The Combustion Institute, Pittsburgh, in press.
6. Crosley, D. R., *Opt. Eng.* 20:511 (1981).
7. Garland, N. L., and Crosley, D. R., *Twenty-First Symposium (International) on Combustion*, The Combustion Institute, Pittsburgh, 1988, p. 1693.
8. Anderson, W. R., Decker, L. J., and Kotlar, A. J., *Combust. Flame* 48:163 (1982).
9. Rensberger, K. J., Copeland, R. A., Jeffries, J. B.,

Kohse-Höinghaus, K., Wise, M. L., and Crosley, D. R., *Appl. Opt.* (in press).
10. Copeland, R. A., Crosley, D. R., and Smith, G. P., *Twentieth Symposium (International) on Combustion*, The Combustion Institute, Pittsburgh, 1984, p. 1195.
11. Garland, N. L., unpublished data.
12. Garland, N. L., and Crosley, D. R., *Appl. Opt.* 24:4229 (1985).
13. Smith, G. P., and Crosley, D. R., *Eighteenth Symposium (International) on Combustion, The Combustion Institute*, Pittsburgh, 1981, p. 1511; Crosley, D. R., and Smith, G. P., *Combust. Flame* 44:27 (1982).
14. Chan, C., and Daily, J. W. Appl. Opt. 19:1357 (1980); Stepowski, D., and Cottereau, M. J. J., *Chem. Phys.* 74:6674 (1981); Lucht, R. P., Sweeney, D. W., and Laurendeau, N. M., *Appl. Opt.* 25:4086 (1986).
15. Kohse-Höinghaus, K., Perc, W., and Just, Th., *Ber. Bunsen Ph. Ch.* 87:1052 (1983).
16. Vanderhoff, J. A., Beyer, R. A., Kotlar, A. J., and Anderson, W. R., *Combust. Flame* 49:197 (1983).
17. Gaydon, A. G., *The Spectroscopy of Flames*, 2nd ed., Chapman and Hall, London, 1974.
18. Anderson, W. R., Decker, L. J., and Kotlar, A. J., *Combust. Flame* 49:179 (1982); 51:125 (1983).
19. Rensberger, K. J., Wise, M. L., Crosley, D. R., and Copeland, R. A., *Twenty-Second Symposium (International) on Combustion*, The Combustion Institute, Pittsburgh, in press.
20. Anderson, W. R., Vanderhoff, J. A., Kotlar, A. J., DeWilde, M. A., and Beyer, R. A., *J. Chem. Phys.* 77:1677 (1982).
21. Jeffries, J. B., and Crosley, D. R., *Combust. Flame* 64:55 (1986).
22. Wendt, J. O. L., Wootan, E. C., and Corley, T. L., *Combust. Flame* 49:261 (1983).
23. Jeffries, J. B., Crosley, D. R., and Smith, G. P., *J. Phys. Chem.* 93:1082 (1989).
24. Jeffries, J. B., and Crosley, D. R., *J. Chem. Phys.* 86:6839 (1987).
25. Jeffries, J. B., Copeland, R. A., Smith, G. P., and Crosley, D. R., *Twenty-First Symposium (International) on Combustion*, The Combustion Institute, Pittsburgh, 1988, p. 1709.
26. Dyer, M. J., and Crosley, D. R., *Opt. Lett.* 7:382 (1982); Kychakoff, G., Howe, R. D., Hanson, R. K., and McDaniel, J. C., *Appl. Opt.* 21:3225 (1982); Hanson, R. K., *Twenty-First Symposium (International) on Combustion*, The Combustion Institute, Pittsburgh, 1988, p. 1677.
27. Dyer, M. J., and Crosley, D. R., *Proceedings of the International Conference Lasers '84*, STS Press, McLean VA, 1985, p. 211.
28. Kohse-Höinghaus, K., Heidenreich, R., and Just, Th., *Twentieth Symposium (International) on Combustion*, The Combustion Institute, Pittsburgh, 1984, p. 1177; Kohse-Höinghaus, K., Koczar, P., and Just, Th., *Twenty-First Symposium (International) on Combustion*, The Combustion Institute, Pittsburgh, 1988, p. 1719; Salmon, J. T., and Laurendeau, N. M., *Appl. Opt. 24:1313 (1985).*

Received 8 April 1988; revised 26 September 1988

Appendix F

LASER-INDUCED FLUORESCENCE DETERMINATION OF TEMPERATURES IN LOW-PRESSURE FLAMES

Laser-Induced Fluorescence Determination of Temperatures in Low-Pressure Flames

Karen J. Rensberger, Jay B. Jeffries, Richard A. Copeland,
Katharina Kohse-Höinghaus,[a] Michael L. Wise, and David R. Crosley

SRI International
Molecular Physics Laboratory
Menlo Park, California 94025

ABSTRACT

Spatially resolved temperatures in a variety of low-pressure flames of hydrogen and hydrocarbons burning with oxygen and nitrous oxide are determined from OH, NH, CH, and CN laser-induced fluorescence rotational excitation spectra. Systematic errors arising from spectral bias, time delay, and temporal sampling gate of the fluorescence detector are considered. In addition, we evaluate the errors arising from the influences of the optical depth and the rotational level dependence of the fluorescence quantum yield for each radical. These systematic errors cannot be determined through goodness-of-fit criteria, and they are much larger than the statistical precision of the measurement. The severity of these problems is different for each radical; careful attention to the experimental design details for each species is necessary to obtain accurate LIF temperature measurements.

[a]On leave from Institut für Physikalische Chemie der
Verbrennung, DFVLR, Stuttgart, West Germany

MP 88-248
October 28, 1988

I. Introduction

Laser-induced fluorescence (LIF) is an ideal diagnostic technique for the measurement of the concentrations of a variety of small free radical molecules which are important reaction intermediates in combustion chemistry.[1] Diatomic hydride radicals such as OH, NH, and CH, with their easily accessible excited electronic states, are readily observed by LIF in flame experiments. Although the OH radical has been the subject of the largest number of studies, simultaneous measurements of other species are needed to answer detailed questions about the flame chemistry. For example, the NH radical, unlike OH, is present only in the reaction zone and is an important intermediate in the production of NO_x in flames containing either fuel nitrogen or oxidizers such as NO_2 or N_2O. Prompt NO production is initiated by the reaction of CH with N_2. In addition, CH emission and fluorescence are often used for diagnostics of the reaction zone of hydrocarbon flames. Besides the hydride radicals, the CN radical is another important intermediate species in NO_x production.

The spatial variation of the concentration of diatomic radicals in stable laminar flames can be predicted by computer model calculations and measured by LIF.[2] A comparison of the predicted and measured variations of radical concentrations with position in the flame provides a sensitive test of the chemical mechanism used in the model. Quantitative comparisons, whether on an absolute or relative basis, require knowledge of the gas temperature with precise spatial correlation to the LIF concentration measurement. There are two reasons for this. First and most important, the predictions of the model calculation at each point in the flame can be markedly different for temperature changes of 100 to 200 K because of the non-linear effects of temperature upon a chemical reaction sequence. Second, the temperature is needed to relate number density in a particular

rotational and vibrational level, as measured by the LIF intensity, to the total mole fraction of the radical species.

There are many methods to measure the gas temperature in flames, including both intrusive probe measurements and nonintrusive light scattering techniques.[3] Included among the laser-based nonperturbative techniques are LIF, coherent and spontaneous Raman scattering, and Rayleigh scattering.[4] Laser-induced fluorescence provides an excellent way to measure both the concentrations of the reactive intermediate radicals and spatially correlated temperatures. In this work, we discuss the use of LIF rotational excitation spectra for temperature measurement.

To obtain a rotational temperature, the radical is excited from several different rotational levels in the ground electronic state to an excited electronic state, from which it radiates. The fluorescence signal intensity for each individual transition is a measure of the population in that particular rotational level of the ground electronic state. In turn, the population distribution in the rotational levels is governed by the temperature. From the measured intensities and knowledge of the rotational line strengths (B_i), the population in each level N_i is determined. The temperature can be obtained from the slope of a Boltzmann plot of $\ln(N_i/g_i)$ versus E_i, where g_i and E_i are the degeneracy and energy, respectively, of the ground state level i. Alternatively, a portion of a rotational excitation spectrum may be directly fit to determine a temperature. This technique has the obvious advantage in being able to use complex, overlapped spectra.

In this paper, we describe in detail experiments on OH performed in stable, laminar, low-pressure flames of H_2 burning in O_2 and N_2O. These experiments investigate the influence of rotational-level-dependent quantum yield and detector wavelength response function (spectral bias) on the apparent gas temperature. For OH we also investigate the effects of optical depth, manifest as significant absorption of the laser beam and

fluorescence across the burner. Low-pressure flames offer special advantages for these purposes. First, the temperature gradients are gradual compared with the laser spatial cross section. Second, collisional quenching is reduced so that the excited state lifetime is significantly longer than the duration of the laser pulse, and the direct time decay of the fluorescence can be used to study collisional effects. We find that the detector spectral bias, the optical depth, and the rotational-level-dependent quantum yield can produce significant systematic errors in addition to the statistical precision of the LIF temperature determination. We will demonstrate for OH that even if the influence of these parameters is neglected, the rotational spectra (or Boltzmann plots) are still satisfactorily fit to a temperature. This temperature can deviate by as much as several hundred degrees from the true value, i.e., that correctly determined by properly taking all these effects into account. The magnitude of these systematic errors cannot be determined by statistical measures of precision but often must be evaluated experimentally.

Measurements on NH, CH, and CN in hydrogen or propane flames burning with oxygen or nitrous oxide allow comparisons of the temperatures obtained in the same flame with different radicals. The optical depth problem is not observed for these radicals, but the detector spectral bias and the rotational level dependence of the quantum yield is still a concern.

The section below on the experimental technique includes a brief description of the low-pressure flame apparatus and a discussion of the detection considerations for each of the radicals: OH, NH, CH, and CN. The influence of rotational energy transfer, the rotational dependence of the transition moment, and the optical depth on the LIF temperature are studied in detail for OH. In the following section, temperature measurements on each of the radicals are then compared.

In addition to their direct applicability to low-pressure flames, the present results provide guidance for temperature measurements at atmospheric pressure using LIF of radicals. Our use of a narrow (10-30 ns) detector gate placed at the signal peak minimizes the effects of rotational energy transfer and rotational-level-dependent quantum yields seen when integrating the entire fluorescence decay over time. In contrast, at atmospheric pressure, detector temporal bandwidth greater than 1 GHz and picosecond laser pulses are necessary to time resolve the fluorescence. The effects on the measurement due to rotational-level-dependent quantum yields must be carefully taken into account when applying this work to higher pressure flames.

II. Experimental Technique

1. Experimental Apparatus

The low-pressure burner apparatus is discussed in detail elsewhere,[5] and only the aspects important to temperature measurements will be discussed here. Flames of hydrogen or propane are burned with either oxygen or nitrous oxide. These flames are supported on a 6 cm diameter porous-plug McKenna burner, which resides in an evacuated chamber, and can be scanned vertically with an accuracy and reproducibility of 0.1 mm. For most experiments, the pressure ranges between 6 and 15 Torr. The laser beam usually traverses the burner horizontally at the center, resulting in a detection path length through the flame of 3 cm. For the OH measurements, because absorption of the beam is substantial (9% for the strong lines in the R branch) the burner is positioned with the laser beam closer to the burner edge, yielding a detection path length of 1.25 cm. The collimated laser beam is apertured with a measured beam diameter of ~0.5 mm, which corresponds to a temperature spread of about 100 K in the region of the largest temperature gradient in the hottest flames, and proportionately less in the cooler flames.

Light from a pulsed XeCl excimer-pumped dye laser with a pulse length of ~12 ns excites the radicals from the v" = 0 level in the ground state to v' = 0 in the excited state. Table I lists the specific band system for each radical and the laser dye used. In all cases, the laser intensity is attenuated to insure that the excitation transition is not saturated and the LIF signal is linear with laser power.

The LIF is collected with f/3 optics and focused at f/4 into a 0.3 m monochromator used as an adjustable bandpass optical filter. The light is detected with a 1P28 photomultiplier, amplified, and captured with a boxcar integrator. Typically, between 10 and 100 laser shots at each wavelength are summed to obtain the signal. The time delay between the excitation laser and the detection gate, and the time width of that gate are discussed in detail below. For reasons discussed below, the detector must have a constant response over the entire wavelength region of the vibrational band detected. A 0.3 m monochromator with 0.5 mm entrance and 4 mm output slit provides a trapezoidal shaped spectral response function with a 20 nm bandpass at the top of the trapezoid and a 23 nm bandpass at the base.

2. Spectral Fitting

To obtain a rotational temperature, the wavelength of the excitation laser is scanned to excite the radical from several different rotational levels and/or fine structure levels of the ground electronic state. The signal intensity I_i obtained when exciting from level i in the ground state to level f in the excited state and collecting all the fluorescence is

$$I_i = G\Phi_f B_{fi} N_i, \qquad (1)$$

where G is a constant related to the light collection efficiency, B_{fi} is the excitation line strength for the respective rotational line, and N_i is the population in level i. The

fluorescence quantum yield Φ_f is $A_f/(A_f + Q + k_{pre})$, where A_f is the Einstein A coefficient, Q is the total collisional quenching rate, and k_{pre} is the predissociation rate. The fluorescence quantum yield depends on the rotational transition and collision environment. In low pressure flames, it may be quite high, around 0.2 or so, while at atmospheric pressure it is greatly reduced by collisional quenching. A recent approach applicable to O_2 and OH attempts to avoid the quenching problem by exciting transitions which are strongly predissociated.[6-8] In this case, the quantum yield depends only on the predissociation rate, but at a significant cost in signal levels. For the temperature measurements described here, the quantum yields may be directly measured. From the LIF line intensities and knowledge of the rotational line strengths and fluorescence quantum yields, the relative N_i can be determined. The population in each rotational level is proportional to $g_i\exp(-E_i/kT)$. The temperature can be obtained from the slope of a Boltzmann plot of $\ln(N_i/g_i)$ versus E_i.

Alternatively, a portion of the rotational excitation spectrum can be directly fit by a least-squares procedure to determine a temperature; here, the line positions, rotational line strengths, and energy levels are input data. There are only two free parameters in such a fit: the temperature and linewidth. Direct spectrum fitting to determine temperature is the accepted technique for CARS,[9] and has been done elsewhere for LIF.[10] The advantage of such direct fits is that individual intensities do not need to be extracted from overlapping transitions in the spectrum. For example, Fig. 1 shows the excitation spectrum in the Q-branch region of the NH A-X system which we use to obtain NH temperatures. Here we scan only 0.5 nm and excite more than 50 transitions with N" between 1 and 20. At this laser resolution, this region is too congested to determine straightforwardly individual N_i and obtain the temperature from Boltzmann plots. Table I contains the scan ranges and other pertinent data for OH, NH, CH, and CN.

The experimental spectrum is fit by comparing it to a synthesized spectrum and varying the fit parameters (temperature and Gaussian linewidth) to minimize the sum of the

squares of the residuals. The line positions and line strengths of the transitions and the ground state energy levels are the necessary input to the fit. The remainder of this section will describe how these are obtained and will describe some details of the fitting procedure.

The line positions, as well as the spectroscopic labeling, for the OH (A-X) transitions are obtained from Dieke and Crosswhite[11] and for NH (A-X) from Brazer, Ram, and Bernath.[12] The line positions for CH (A-X) and CH (B-X) are from Moore and Broida;[13] the labeling is as suggested in Ref. 14. The line positions for CN are calculated as described below from the molecular constants given by Colket.[15] The calculated spectrum for the CN radical agrees to within 0.01 Å with published wavelengths for N" from 1 to 49.[16] No tabulated line positions were found for N" from 52 to 58, so the calculated line positions for N" from 52 to 58 are adjusted to match the experimental spectrum as described next.

The experimental spectrum as it is obtained is not linear in wavelength. The laser stepping motor drive shows an oscillatory behavior that is evident when the experimental wavelengths of the transitions are compared to known line positions. For the short scan regions needed here, the nonlinearity appears to be a slow curve and can be fit to a three-term polynomial, which is used to adjust the synthesized line positions to match the experimental line positions. Each scan region is calibrated separately, as the nonlinearity varies from region to region.

The linewidth determined by the spectral fitting procedure is a convolution of the laser linewidth and the Doppler width of the transition. Our measured linewidth for the doubled laser output at 310 nm is 0.2 cm^{-1} and is not sufficiently narrow to accurately determine the temperature just from the Doppler width of the transitions. The linewidths from the CH and CN spectra are generally twice as wide, due to a larger laser linewidth, than those for the OH and NH spectra. The fit to determine the temperature is not highly

dependent on the value for the linewidth, as the sum of squares of the residuals from the fit changes less than 1% for a change in the linewidth of 0.002 Å.

The rotational line strengths for each radical are calculated after the approach developed by Zare et al.[17] A computer program calculates the position and line strength of rotational lines of an electric-dipole-allowed transition from molecular constants using a model Hamiltonian described by Zare et al. Some of the molecular constants needed are the term origin, the rotational constants, the spin-orbit splitting constants, and the spin-rotation splitting constants. A note of caution is deserved here. Depending on which set of molecular constants is used, large differences on the order of 1 to 2 Å between the calculated and tabulated line positions are seen, especially for CH and NH. The differences appear to be the greatest when there is significant λ-doubling in a Π state. It is preferable to use a set of constants for both the excited and ground states obtained using the same Hamiltonian used to calculate the line positions and line strengths. Since tabulated line positions are readily available for all the radicals but CN, we use these in the temperature fitting. The rotational line strengths calculated are not as sensitive to the molecular constants as the line positions, and are used in the spectral fitting program. The constants for NH are given in the same reference as the line positions. Those for CH are given in Ref. 18 to 20. The constants for OH are obtained from fitting the tabulated line positions in Dieke and Crosswhite with the Zare et al. method.

The rotational line strengths calculated in the program assume that the electronic transition moment is independent of the internuclear separation. This is a poor assumption for OH.[21] The variation in the electronic transition moment with internuclear distance seen for OH manifests itself in a rotational level dependence of the electronic transition moment.[22] The magnitude of the error in the temperatures for spectra fit to rotational line strengths neglecting this can be estimated from

$$T_{corrected} = T_{observed}(1-\gamma T_{observed})^{-1}. \quad (2)$$

The parameter γ is 3.24×10^{-5} for OH, calculated from spectroscopic considerations including the internuclear distance dependence of the transition moment.[21] For OH, we fit some of the rotational excitation spectra with line strengths neglecting the rotational variation of the electronic transition moment. A flame at 2300 K produces an apparent temperature low by 180 K and at 1200 K low by 35 K, in excellent agreement with the prediction of Eq. (2). All of the OH temperatures discussed in this work are obtained using the corrected line strengths.[22] The NH and CH radicals have substantially less variation of the transition moment with rotational level: $\gamma = 5.4\times10^{-6}$ for NH ($A^3\Pi_i$), $\gamma = 3.2\times10^{-6}$ for CH ($A^2\Delta$), and $\gamma = 5.2\times10^{-6}$ for CH ($B^2\Sigma^-$). The error thus produced for these radicals is estimated to be less than 30 K for the highest temperatures. This systematic error is less than the precision of the measurements discussed here. For non-hydride radicals, γ is generally too small to influence temperature measurements.

A list of the ground state energy levels needed to calculate rotational populations at a given temperature is obtained from the computer program used to calculate rotational line strengths. Each rotational level is split to give F_1 and F_2 components for OH, CH, and CN, and into three analogous components for NH. For our purposes, for NH and CN, the splitting is small and is ignored. The λ-doublet splitting for OH and CH is also small and is neglected.

The scan ranges listed in Table I cover a range of low and high rotational levels. For OH, NH, and CH (B-X), the rotational levels cover a range through which temperatures from room temperature to 2500 K and higher can be measured. The CH (A-X) scan range that is listed covers low rotational levels and very high ones. It is best for flames above 1500 K; a different range that covers intermediate rotational levels is necessary for cooler flames, such as for measurements on the H_2/O_2 flame seeded with

CH_4. The CN scan range is similar, in that a different set of rotational levels may be necessary to measure temperatures lower than 1900 K.

It is difficult to assess how noise-free a spectrum must be in order for it to yield a meaningful temperature. The OH and NH (Fig. 1) spectra are of much higher quality than the CH and CN spectra. Examples of spectra for CH(A-X) and CN are shown in Fig. 2 and 3 and for CH(B-X) in Ref. 23. The signal to noise ratio for the CN spectrum for the small peaks, which correspond to high rotational levels and are most sensitive to the temperature, is about 3 and becomes worse at lower temperatures. The CH spectra, in general, are of lower quality than those for OH and NH, mainly due to a much smaller concentration of the CH radical in the flames.

3. Detector Response Requirements

To determine the bandpass necessary to detect the LIF without spectral bias requires a discussion of the spectroscopy and collisional energy transfer of the radical. The spectral bias problem has been discussed in detail for atmospheric pressure flames[24] and is summarized here. In LIF, the laser light excites the radical to a particular rotational and vibrational level of the excited electronic state. The initially excited level can radiate, undergo energy transfer to other rotational or fine structure levels of the same electronic state which subsequently radiate, or be collisionally removed from the manifold of radiating levels to another electronic state. All radiation emitted in the detector spectral bandpass forms the LIF signal. Each level radiates with characteristic transitions (P, Q, R) to the ground electronic state. The line strengths and selection rules governing these transitions vary with each molecule; however, the emission in each vibrational band occurs over a finite range of wavelengths. The large rotational constant of the hydride radicals extends the spread of wavelengths. For example, the calculated (0,0) bands for the radicals

OH (A-X), NH (A-X), CH (A-X), CH (B-X), and CN (B-X), at 2500 K are illustrated in Fig. 4. The spectra in this figure show that if the excited electronic state is rotationally equilibrated at 2500 K, fluorescence from each radical will extend over a wide (15-25 nm) range; the width of the spectrum for each of the radicals is given in Table I.

In these experiments with flames between 5 and 15 Torr, we estimate the average time between rotational energy transfer collisions to be about 30 ns. Thus, if we use a narrow detector (boxcar) gate of 10 ns during or promptly after the 15 ns laser pulse, the excited state population distribution of the radiating molecule will be dominated by the initial level. Significant additional population will be found in only those levels adjacent to it. For this case, the required bandpass is dictated by the range of rotational levels excited and the wavelength of their P-, Q-, and R-branch transitions. For the OH rotational levels excited here, $3 \leq N' \leq 16$, the required bandwidth to detect all the light becomes 13 nm. The requirements for the other radicals are listed in Table I.

Alternatively, if energy transfer collisions create a thermal population distribution in the excited electronic state before the fluorescence is detected, then this light will have the same spectral distribution for any initially excited level, and can be detected with any broad or narrow bandpass spectral response. However, this case also requires a delay between the excitation laser pulse and the detector time gate to permit sufficient rotational relaxation. For the hydride radicals, collisional quenching is competitive with rotational energy transfer.[24-28] Thus, the delay while waiting for thermalization of the excited state population also reduces the signal at least a factor of ten. Such a scheme was applied[2] to low-pressure flames where the fluorescence lifetime of the radical is long compared to the laser pulse length. In an atmospheric pressure flame, the collision rates become so fast that the fluorescence is quenched rapidly compared to the 12 ns laser pulse and thermalization is never achieved.[24-26] Only the time-integrated fluorescence, which has a rotational distribution far from thermal, can be easily detected.

To test the effects of spectral bias, we shift the 20 nm bandpass detector to be centered at 320 nm. This is about 8 nm to the red of the optimum for the OH detection. The detector will then collect the light from the P- and Q-branch transitions with high rotational quantum number with greater efficiency than from those with lower N. Most of the R-branch ($J < 19.5$) and some of the Q_1 branch ($J < 6$) will not be detected. The rotational excitation spectrum listed in Table I is then scanned in the burnt gases of a 7.2 Torr, stoichiometric H_2/N_2O flame. Instead of the 2300 K temperature measured with the optical bandpass properly adjusted, the rotational excitation spectrum is fit by a temperature of 3770 K with a statistical precision of ~150 K. Note the goodness of fit shown in the Boltzmann plot in Fig. 5, even though the resulting temperature is clearly not possible in such a flame. The adiabatic flame temperature is 2600 K. The spectral fit also does not show any obvious bias. The use of a narrow bandpass detector (1.3 nm), centered on the low N region of the Q-branch bandhead, has been previously demonstrated[24] in atmospheric flames to give precise temperatures as much as 800 K lower than those detected without spectral bias. For similar reasons, the use of a 10 nm bandwidth for the detection centered on the Q-branch fluorescence of the CH B-X rotational excitation spectrum in Table I results in a temperature ~400 K too cold. Switching to the 20 nm bandwidth solved this problem for the CH B-X system. These examples clearly show that statistical measures of precision do not provide warnings of possible systematic errors which can severely limit the accuracy of the measured temperature. Rather, the collisional energy transfer and spectroscopy for each radical must be considered.

4. Laser-Detector Timing

Changes in the fluorescence quantum yield with rotational level can effect the measured temperatures. There are three rotational-level-dependent terms in the quantum yield: the oscillator strength, noted above for the absorption transition, the collisional quenching rate, and the predissociation rate. The radiative lifetimes of OH, NH, and CH depend on rotational level, although this variation is the largest in OH.[29] The higher rotational levels have a longer radiative lifetime. In addition, at room temperature, the collisional quenching rates of both OH and NH decrease with increasing rotation of the electronically excited radical.[30] Consequently, moving the detector gate to longer delays will increase the relative amount of fluorescence from higher rotational levels, and the apparent temperature will become higher. For OH, we tested this in the burnt gases of a 7.2 Torr H_2/N_2O flame near 2300 K; here the fluorescence lifetime is ~100 ns. Several boxcars recorded the rotational spectrum simultaneously, each with a 10 ns gate at different gate delays. The spectra obtained in this way are compared to one obtained from a prompt 10 ns gate. The systematic error ΔT increases smoothly from 80 K at 50 ns delay to 240 K at 250 ns. When a wide (300 ns) gate is used to integrate all the fluorescence, the error is + 100 K. All of the fits to the spectra have satisfactory statistical precision, again much smaller than this systematic deviation.

A rotational-level-dependent quantum yield for the LIF has been observed for OH,[31] CH,[5,32] and NH[32,33] in low-pressure flames. However, for the flames studied here, the 10 ns detector gate is short compared to the fluorescence lifetime of all the radicals studied except CN. By using such a short gate promptly after the laser pulse, the quantum yield variation with rotational level can be neglected since very little quenching has occurred. However, if the detector gate is delayed to permit rotational equilibration or is sufficiently wide to integrate the entire signal, then rotational-level-dependent quantum

yields may produce significant errors in the temperature. For OH in a stoichiometric 7.2 Torr H_2/N_2O flame, the quantum yield has significant dependence on rotational level only in the reaction zone.[31] In the burnt gases, this dependence can be safely neglected at the ± 50 K precision. However, without a short, prompt detector gate in the reaction zone, errors of 100 to 200 K may result. For NH, the rotational-level-dependent quenching can cause errors of ~150 K, and for CH such effects can cause systematic errors as large as 400 K in propane and acetylene flames. Again these problems are avoided in low-pressure flames with a short, prompt detector gate.

5. Optical Depth

In these low-pressure flames, OH is the only radical for which we see significant (>1%) absorption. For OH in a 7.2 Torr stoichiometric H_2/N_2O flame, we see as much as 9% absorption on the strongest lines of the R-branch. This absorption must be considered quantitatively. The boundary between the flame and the background gas is cooler than the flame itself. The OH radicals in this boundary layer have more population in the lower rotational levels. Thus, there is more absorption by the low rotational levels both of the excitation laser beam as it traverses to the uniform probed region of the burner and of the subsequent fluorescence on its way to the detector. Recall that the upper electronic state does not thermalize, so low initially-excited rotational levels will radiate through transitions absorbed by low levels. With increased absorption of both the laser and the fluorescence by lower rotational levels, the apparent temperature from the excitation scan becomes too high. Both the absorption and boundary layer effects are evident in the rotational excitation scan for OH displayed in Fig. 6. The spectrum is taken from the burnt gases of a 7.2 Torr stoichiometric H_2/N_2O flame. The top trace shows an absorption spectrum along the line of sight through the flame, and the bottom trace is the corresponding LIF excitation

spectrum from the uniform flat flame. The absorption spectrum is fit to a temperature of 1990 K, reflecting a concentration weighted average over the flame and its cooler boundary. Without correcting for absorption, the LIF spectrum is fit to a temperature of 2330 K. The absorption correction to the LIF spectrum as described below results in a temperature of 2250 K, corresponding to an error of + 80 K.

The horizontal position of the burner for most of the OH measurements has a 5 cm traverse of the flame by the laser beam and a detection path length of 1.5 cm through the flame. In these experiments, the absorption correction is made by a particularly expedient normalization of the LIF signal by the laser intensity, as monitored by a postflame photodiode which measures absorption of the laser beam over the entire 5 cm path length. The excitation is in the R-branch and the prompt detector gate ensures that most of the observed fluorescence originates from the initially excited rotational level. The fluorescence is emitted and reabsorbed in all three rotational branches, which have different line strengths. Thus, we need to correct for the absorption of the laser beam in the R-branch over the 2.5 cm from the edge of the flame to the center of the flame, where we image the LIF, and we need to correct for the absorption of the fluorescence in all three branches over the shorter 1.5 cm out of the flame. For the path lengths in this experiment, the absorption of the laser in the R-branch over the longer path length (2.5 cm) is equivalent to the absorption of the fluorescence in the P-, Q-, and R-branches of the shorter path. Thus, the laser absorption over the entire path through the flame provides a measure of the total absorption. For a different experimental set up with different path lengths, the proper absorption correction must be recalculated. The temperatures and radical profiles, corrected for absorption, measured at the center of the burner agree with those taken at the position closer to the edge, ensuring that the flame is sufficiently flat for a meaningful comparison.

One method that we did not explore, but deserves further study, is to use the OH (A-X) (1,0) band for excitation. Absorption of the excitation laser beam by the ground state radical is less, by a factor of three, because of the reduced transition probability for this band. However, excitation to v' = 1 introduces further complications in the detection scheme. The (1,1) and (0,0) bands overlap each other, so neither can be cleanly detected without collecting fluorescence from the other. The (1,0) band could be used for detection; about a third of the fluorescence from v' = 1 is in this band. However, a further complication is that the rotational level dependence of the amount of vibrational relaxation from v' = 1 to v' = 0 versus electronic quenching varies with collision partner,[34] and will therefore change throughout the flame profile. In our low-pressure flames where we can use a short detector gate, this would not be a severe problem.

III. Temperature Comparisons

Rotational temperatures of both NH and OH are measured in a 7.2 Torr H_2/N_2O stoichiometric (fuel equivalence ratio $\phi = 1.0$) flame, and the values are plotted versus height above the burner in Fig. 7. The wavelength regions scanned are given in Table I. The measured NH and OH temperatures agree to $\pm$ 50 K. The good agreement indicates that the method described above properly accounts for the influence of rotational-level-dependent oscillator strength and optical depth problems possible for the OH measurements. The temperature at the point 46 mm above the burner, in the burnt gases, was measured 13 times over a period of two weeks. The average temperature measured is 2320 $\pm$ 30 K, which is indicative of the statistical precision of the OH measurements.

Figure 7 also shows the temperature profile of a 7.2 Torr, $\phi = 1$, H_2/O_2 flame as measured from OH excitation spectra. Note that temperature measurements are possible at temperatures as low as 400 K, at a height 1 mm above the burner. Despite the large heat

release available for H_2 and O_2, this low-pressure flame burns at a very low temperature. The burnt gas temperature is only 1200 K; this difference with $T_{adiabatic}$ has been observed previously.[35] By seeding (<10%) methane into an H_2/O_2 flame, a temperature measurement using the A-X system of CH is made; it agrees with this low OH LIF flame temperature.

In a second series of experiments, the CH, NH, and CN radical are all used to measure the temperature in the same 15 Torr, *rich* ($\phi = 1.33$) C_3H_8/N_2O flame. The measured temperature and radical LIF profiles for each species are given as a function of height above the burner in Fig. 8. The intense CN fluorescence overwhelms that of the CH B-X system which is in the same spectral region, so only the CH A-X system can be used in this flame. The relevant scan parameters are given in Table I. Most of the measurements with CH A-X agree within 100 K with those using NH A-X. Thus, we have observed agreement for temperature measurements from NH, CH(A-X), and OH excitation scans. However, the measurements for CN in the burnt gases are consistently 200 K high. One reason may be rotational-level-dependent quantum yields. There is no collisional quenching data for CN in this flame, and the radiative lifetime is too short (65 ns)[36] for the quantum yield to be neglected with our 10 ns detection gate. This discrepancy deserves further study.

In another comparison, the temperatures are determined in a 6.8 Torr, $\phi = 1$, C_3H_8/O_2 flame using both the A-X and B-X systems of CH. The regions scanned are given in Table I. The temperature and CH radical concentration profiles in this flame are presented in Fig. 9. CH is present only in the reaction zone. For reasons we do not understand, temperatures measured using the B-X excitation spectra are systematically 150-200 K lower than those obtained with the CH A-X system. Note that CH ($B^2\Sigma^-$) predissociates[29c] rapidly for $N \geq 15$. If rotational energy transfer from the higher levels excited in the rotational excitation spectrum can rapidly transfer >10% of their population to

these predissociating levels, such a discrepancy could be explained. However, experiments with varying detector gate delays, as described above for OH, will be necessary to test this hypothesis.

IV. Summary

We have assessed the systematic temperature measurement errors from the detector spectral bias, temporal gate width, and rotational-level-dependent oscillator strength for the hydride radicals OH, NH, and CH. For low-pressure flames where the fluorescence lifetime is long compared to the excitation pulse length and detector gate, we have agreement for the temperatures measured from the excitation spectra of the three radicals to ~100 K. Even with the careful measurement methods described above for these laminar laboratory low-pressure flames, we do not obtain this reasonable agreement for measurements using the B-X system of CH or the B-X system of CN. This points to additional rotational-level-dependent effects which might influence LIF measurements of temperature with these radicals.

Acknowledgements

The participation of Michael Wise was made possible by a grant from the National Science Foundation program for Research Experiences for Undergraduates. The work on OH was supported by the Division of Basic Energy Sciences of the Department of Energy. That on NH was supported by the Thermal Systems and Engineering program of the National Science Foundation. The measurements on CH and CN were supported by the Aero Propulsion Laboratory of the Air Force Wright Aeronautical Laboratories.

References

1. D. R. Crosley and G. P. Smith, "Laser-induced fluorescence spectroscopy for combustion diagnostics," Opt. Engr. 22, 545 (1983); J. H. Bechtel, C. J. Dasch and R. Teets, "Combustion Research with Lasers" in *Laser Applications*, R. K. Erf and J. F. Ready, Eds., Academic, New York, 1983; R. P. Lucht, "Applications of Laser-Induced Fluorescence Spectroscopy for Combustion and Plasma Diagnostics" in *Laser Spectroscopy and Its Applications*, L. J. Radziemski R. Solarz and J. A. Paisner, Eds., Marcel Dekker, New York, 1986; D. R. Crosley, "Laser-induced Fluorescence Measurement of Combustion Chemistry Intermediates," High Temp. Mat. Proc. 7, 41 (1986); A. C. Eckbreth, *Laser Diagnostics for Combustion Temperature and Species*, Abacus, 1987.

2. K. Kohse-Höinghaus, P. Koczar and Th. Just, "Absolute Concentration Measurements of OH in Low-Pressure Hydrogen-Oxygen, Methane-Oxygen and Acetylene-Oxygen Flames," in *Twenty-First Symposium (International) on Combustion* (The Combustion Institute, Pittsburgh, 1988), p. 1719.

3. A. G. Gaydon and H. G. Wolfhard, *Flames, Their Structure, Radiation and Temperature*, Fourth Edition, Chapman and Hall, London, 1979.

4. S. S. Penner, C. P. Wang and M. Y. Bahadori, "Laser Diagnostics Applied to Combustion Studies," in *Twentieth Symposium (International) on Combustion* (The Combustion Institute, Pittsburgh, 1985), p. 1149.

5. K. J. Rensberger, M. J. Dyer and R. A. Copeland, "Time-Resolved CH ($A^2\Delta$ and $B^2\Sigma^-$) Laser-Induced Fluorescence in Low-Pressure Flames," Appl. Opt. 27, 3679 (1988).

6. A. M. Wodtke, L. Huwel, H. Schlüter, H. Voges, G. Meijer, and P. Andresen, "Predissociation of O_2 in the B state," J. Chem. Phys. 89, 1929 (1988).

7. G. Laufer and R. L. McKenzie, "Temperature Measurements in Hypersonic Air Flows using Laser-Induced O_2 Fluorescence," AIAA/NASA/AFWAL Conference on Sensors and Measurements Techniques for Aeronautical Applications, Atlanta, September 1988.

8. P. Andresen, A. Bath, S. Gröger, H. W. Lülf, G. Meijer, and J. J. ter Meulen, "Laser-induced fluorescence with tunable excimer lasers as a possible method for instantaneous temperature field measurements at high pressures: checks with an atmospheric flame," Appl. Opt. 27, 365 (1988).

9. A. C. Eckbreth, "Recent Advances in Laser Diagnostics for Temperature and Species Concentration in Combustion," in *Eighteenth Symposium (International) on Combustion* (The Combustion Institute, Pittsburgh, 1981), p. 1471.

10. W. R. Anderson, L. J. Decker and A. J. Kotlar, "Temperature Profile of a Stoichiometric CH_4/N_2O Flame from Laser Excited Fluorescence Measurements on OH," Comb. Flame 48, 163 (1982).

11. G. H. Dieke and H. M. Crosswhite, "The Ultraviolet Bands of OH," J. Quant. Spectrosc. Radiat. Transfer 2, 97 (1962).

12. C. R. Brazier, R. S. Ram, and P. F. Bernath, "Fourier Transform Spectroscopy of the $A^3\Pi$-$X^3\Sigma^-$ Transition of NH," J. Mol. Spectrosc. 120, 381 (1986).

13. C. E. Moore and H. P. Broida, "CH in the Solar Spectrum," J. Res. NBS 63A, 19 (1959).

14. J. M. Brown, J. T. Hougen, K. P. Huber, J. W. C. Johns, I. Kopp, H. Lefebvre-Brion, A. J. Merer, D. A. Ramsay, J. Kostas, and R. N. Zare, "The Labeling of Parity Doublet Levels in Linear Molecules," J. Mol. Spec. 55, 500 (1975).

15. M. B. Colket, "Spectroscopic Absorption Model for CN($X^2\Sigma \rightarrow B^2\Sigma$): Comparison of Experiments and Theory," J. Quant. Spectrosc. Radiat. Transfer 31, 7 (1984).

16. G. H. Mount, J. L. Linsky, and R. A. Shine, "One- and Multi-Component Models of the Upper Photosphere Based on Molecular Spectra," Solar Physics 32, 13 (1973).

17. R. N. Zare, A. L. Schmeltekopf, W. J. Harrop, D. L. Albritton, "A direct approach for the reduction of diatomic spectra to molecular constants for the construction of RKR potentials," J. Mol. Spectrosc. 46, 37 (1973).

18. B. M. Krupp, "A New Analysis of the $A^2\Delta$-$X^2\Pi$ System of CH," Astrophys. J. 189, 389 (1974).

19. I. Botterud, A. Lofthus, and L. Veseth, "Term Values and Molecular Parameters for CH and CH^+," Phys. Scr. 8, 218 (1973).

20. K. P. Huber and G. Herzberg, *Constants of Diatomic Molecules*, Van Nostrand and Reinhold, New York, 1979.

21. D. R. Crosley and R. K. Lengel, "Relative Transition Probabilities and the Electronic Transition Moment in the A-X System of OH," J. Quant. Spectros. Radiat. Transfer 15, 579 (1975).

22. I. L. Chidsey and D. R. Crosley, "Calculated Rotational Transition Probabilities for the A-X System of OH," J. Quant. Spectros. Radiat. Transfer 23, 187 (1980).

23. D. R. Crosley, "Semiquantitative Laser-Induced Fluorescence in Flames," Comb. Flame, in press, 1988.

24. G. P. Smith and D. R. Crosley, "Quantitative Laser-Induced Fluorescence in OH: Transition Probabilities and the Influence of Energy Transfer," in *Eighteenth Symposium (International) on Combustion* (The Combustion Institute, Pittsburgh, 1981), p. 1511; D. R. Crosley and G. P. Smith, "Rotational Energy Transfer and LIF Temperature Measurements," Comb. Flame 44, 27 (1982).

25. C. Chan and J. W. Daily, "Laser excitation dynamics of OH in flames," Appl. Opt. 19, 1357 (1980); R. P. Lucht, D. W. Sweeney and N. M. Laurendeau, "Time-resolved fluorescence investigation of rotational transfer in $A^2\Sigma^+$ (v = 0) OH," Appl. Opt. 25, 4086 (1986).

26. N. L. Garland and D. R. Crosley, "Energy Transfer Processes in CH $A^2\Delta$ and $B^2\Sigma^-$ in an Atmospheric Pressure Flame," Appl. Opt. 24, 4229 (1985).

27. R. J. Cattolica, D. Stepowski, D. Puechberty, and M. Cottereau, "Laser-Induced Fluorescence of the CH Molecule in a Low-Pressure Flame," J. Quant. Spectrosc. Transfer 32, 363 (1984).

28. R. G. Joklik and J. W. Daily, "LIF Study of CH $A^2\Delta$ Collision Dynamics in a Low Pressure Oxy-Acetylene Flame," Comb. Flame 69, 211 (1987).

29. (a) OH: K. R. German, "Direct measurements of the radiative lifetimes of the $A^2\Sigma^+$ (v' = 0) states of OH and OD," J. Chem. Phys. 62, 2584 (1975); J. Brzozowski, P. Erman, and M. Lyyra, "Precision Estimates of the Predissociation Rates of the OH $A^2\Sigma^+$ state ($v \leq 2$)," Phys. Scr. 17, 507 (1978); I. S. McDermid and J. B. Laudenslager, "Radiative lifetimes and quenching rate coefficients for directly excited rotational levels of OH ($A^2\Sigma^+$, v' = 0)," J. Chem. Phys. 76, 1824 (1982).

(b) NH: W. H. Smith, J. Brzozowski and P. Erman, "Lifetime studies of the NH molecule: New predissociations, the dissociative energy, and interstellar diatomic recombination," J. Chem. Phys. 64, 4628 (1976).

(c) CH: J. Brzozowski, P. Bunker, N. Elander and P. Erman, "Predissociation Effects in the A, B, and C States of CH and the Interstellar Formation Rate of CH via Inverse Predissociation," Astrophys. J. 207, 414 (1976).

30. (a) OH: R. A. Copeland, M. J. Dyer and D. R. Crosley, "Rotational-level-dependent quenching of $A^2\Sigma^+$ OH and OD," J. Chem. Phys. 82, 4022 (1985).

(b) NH: N. L. Garland and D. R. Crosley, "Rotational-Level-Dependent Quenching of the $A^3\Pi_i$, v' = 0 State of NH," J. Chem. Phys., submitted, 1988.

31. K. Kohse-Höinghaus, J. B. Jeffries, R. A. Copeland, G. P. Smith and D. R. Crosley, "The Quantitative LIF Determination of OH Concentrations in Low Pressure Flames," in *Twenty-Second Symposium (International) on Combustion* (The Combustion Institute, Seattle, 1988), in press; J. B. Jeffries, K. Kohse-Höinghaus, G. P. Smith, R. A. Copeland, and D. R. Crosley, "Rotational-level-dependent Quenching of OH ($A^2\Sigma^+$) at Flame Temperatures," Chem. Phys. Lett., in press, 1988.

32. K. J. Rensberger, R. A. Copeland, M. L. Wise, and D. R. Crosley, "NH and CH Laser-Induced Fluorescence in Low-Pressure Flames: Quantum Yields from Time-Resolved Measurements," in *Twenty-Second Symposium (International) on Combustion* (The Combustion Institute, Seattle, 1988) in press.

33. R. A. Copeland, M. L. Wise, K. J. Rensberger, and D. R. Crosley, "Time-Resolved Laser-Induced Fluorescence of the NH Radical in Low-Pressure N_2O Flames," Appl. Opt., submitted.

34. R. K. Lengel and D. R. Crosley, "Energy transfer in $A^2\Sigma^+$ OH. II. Vibrational," J. Chem. Phys. 68, 5309 (1978); G. P. Smith and D. R. Crosley, "Vibrational energy transfer in $A^2\Sigma^+$ OH in flames," Appl. Opt. 22, 1428 (1983); R. A. Copeland, M. L. Wise, and D. R. Crosley, "Vibrational Energy Transfer and Quenching of OH ($A^2\Sigma^+$, v' = 1)," J. Phys. Chem., in press, 1988.

35. K. H. Eberius, K. Hoyermann, and H. G. Wagner, "Experimental and Mathematical Study of a Hydrogen-Oxygen Flame," in *Thirteenth Symposium (International) on Combustion* (The Combustion Institute, Pittsburgh, PA 1971), p. 713.

36. N. Duric, P. Erman, and M. Larsson, "The Influence of Collisional Transfers and Perturbations on Measured A and B State Lifetimes in CN," Phys. Scr. 18, 39 (1978).

Figure Captions

1. Experimental LIF rotational excitation spectra of the Q-head region of the NH ($A^3\Pi_i$-$X^3\Sigma^-$) transition for a 13.8 Torr, $\phi = 1.04$, C_2H_2/N_2O flame. The spectra are obtained (top to bottom) at 1.1, 4.0, and 7.3 mm above the burner and are fit to temperatures of 1050, 2250, and 2670 K, respectively. The bottom trace is the residual of the fit at 2670 K. The transitions are labeled by the ground state total angular momentum quantum number J.

2. Experimental LIF spectrum of part of the CH ($A^2\Delta$-$X^2\Pi$) transition in a 6.8 Torr, $\phi = 1$, C_3H_8/O_2 flame. A fit to this spectrum yields a temperature of 1900 K. The residual to the fit is shown in the lower trace. The rotational transitions are relabeled to correspond to the notation suggested by Ref. 14.

3. Experimental LIF spectrum of part of the CN ($B^2\Sigma^+$-$X^2\Sigma^+$) transition in a 15 Torr, $\phi = 1.33$, C_3H_8/N_2O flame. A fit to this spectrum yields a temperature of 2575 K. The residual to the fit is shown in the lower trace.

4. Synthesized OH, NH, CN, and CH emission spectra at 2500 K. At this temperature, the transitions extend over many nanometers. The y-axis scale is different for each band shown.

5. Boltzmann plot of the OH ($A^2\Sigma^+$-$X^2\Pi_i$) normalized intensity divided by the line strength and degeneracy vs. rotational energy for a 7.2 Torr, $\phi = 1$, H_2/N_2O flame, in which the spectral bandpass preferentially detects the high rotational levels. The line corresponds to a temperature of 3770 K. The correct temperature of 2300 K is obtained by using the proper bandpass.

6. OH ($A^2\Sigma^+$-$X^2\Pi_i$) LIF spectrum (middle) and absorption spectrum (top) in the R-branch region in a 7.2 Torr, $\phi = 1$, H_2/N_2O flame. The LIF spectrum gives a temperature of 2250 K. The absorption spectrum gives a temperature of 1990 K, which is a concentration weighted average over the flame and its cooler boundary. The bottom trace is the residual to the fit for the LIF spectrum.

7. Temperature profiles for a 7.2 Torr, $\phi = 1$, H_2/N_2O flame (top) and H_2/O_2 flame (bottom). The triangles show the OH temperature and the circles the NH temperature in the H_2/N_2O flame. The boxes show the OH temperature in the H_2O_2 flame.

8. Temperature and LIF signal profiles for a 14 Torr, $\phi = 1.33$, C_3H_8/N_2O flame. The signal profiles are for CN, CH, and NH (top to bottom). The open boxes, diamonds, and solid boxes correspond to temperatures measured using CN ($B^2\Sigma^+$-$X^2\Sigma^+$), CH ($A^2\Delta$-$X^2\Pi$), and NH ($A^3\Pi_i$-$X^3\Sigma^-$) rotational excitation spectra, respectively.

9. Temperature and CH profiles for a 6.7 Torr, $\phi = 0.96$, C_3H_8/O_2 flame. The boxes and circles show temperatures determined from CH ($A^2\Delta$-$X^2\Pi$) and CH ($B^2\Sigma^-$-$X^2\Pi$) rotational excitation spectra, respectively. The bottom curve is the relative CH radical concentration. The line through the CH profile is synthesized from the parametrization data in Ref. 5.

Table I. Data for rotational excitation scans.

Radical	OH	NH	CH	CH	CN
System	$A^2\Sigma^+$-$X^2\Pi_i$	$A^3\Pi_i$-$X^3\Sigma^-$	$A^2\Delta$-$X^2\Pi$	$B^2\Sigma^-$-$X^2\Pi$	$B^2\Sigma^+$-$X^2\Sigma^+$
Band	(0,0)	(0,0)	(0,0)	(0,0)	(0,0)
Laser Dye	Sulforhodamine B (doubled)	PTP	Coumarin 120	QUI	QUI
Scan range[a]	306.71-307.06	335.70-336.20	429.76-430.48	387.10-387.77	387.37-387.78
Detector center position[a]	312	336	430	393	387
Number of significant lines	15	60	21	19	24
Range of N"	2-15	1-20	1-2,11-15	2-11	1-4,52-58
Thermal bandwidth[a] (2500 K)	20	18	25	20	8
Bandwidth of levels excited[a,b]	13	14	16	11	8
Significant transitions	R_1(2-4) R_1(14,15) R_2(6-13) $^RQ_{21}$(2-4)	Q_1(2-20) Q_2(2-20) Q_3(1-19)	R_1(1,2) R_2(1) Q_1(11-15) Q_2(11-15)	R_1(3-11) R_2(2-11)	R_1(0,1) R_2(1) P_1(1-4, 52-58) P_2(1-4, 52-58)

[a]Unit of wavelength is nm.

[b]Bandwidth needed to detect all fluorescence originating from excited levels, assuming no rotational energy transfer occurs.

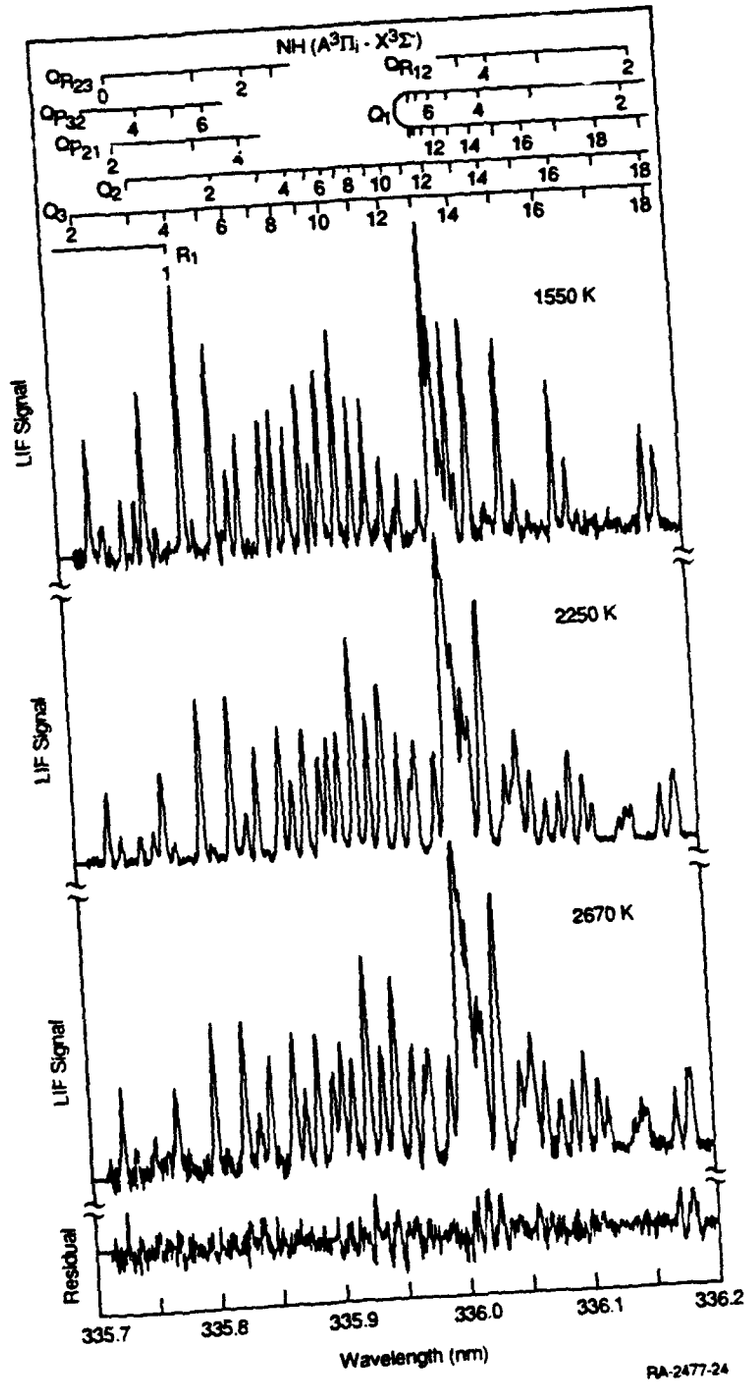
NH ($A^3\Pi_i$ - $X^3\Sigma^-$)
$^QR_{23}$
$^QP_{32}$
$^QP_{21}$
Q_2
Q_3
$^QR_{12}$
Q_1
R_1
1550 K
2250 K
2670 K
LIF Signal
LIF Signal
LIF Signal
Residual
335.7
335.8
335.9
336.0
336.1
336.2
Wavelength (nm)
RA-2477-24

Figure 1

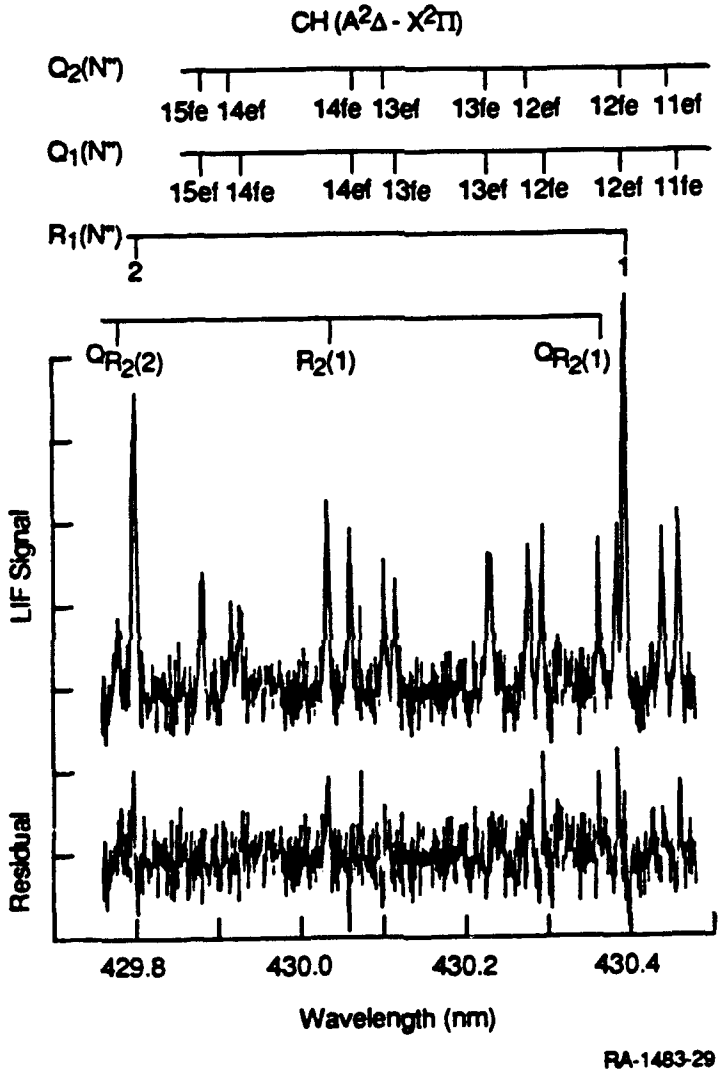
CH (A²Δ - X²Π)
Q2(N")
15fe 14ef
14fe 13ef
13fe 12ef
12fe 11ef
Q1(N")
15ef 14fe
14ef 13fe
13ef 12fe
12ef 11fe
R1(N")
2
1
QR2(2)
R2(1)
QR2(1)
LIF Signal
Residual
429.8
430.0
430.2
430.4
Wavelength (nm)
RA-1483-29

Figure 2

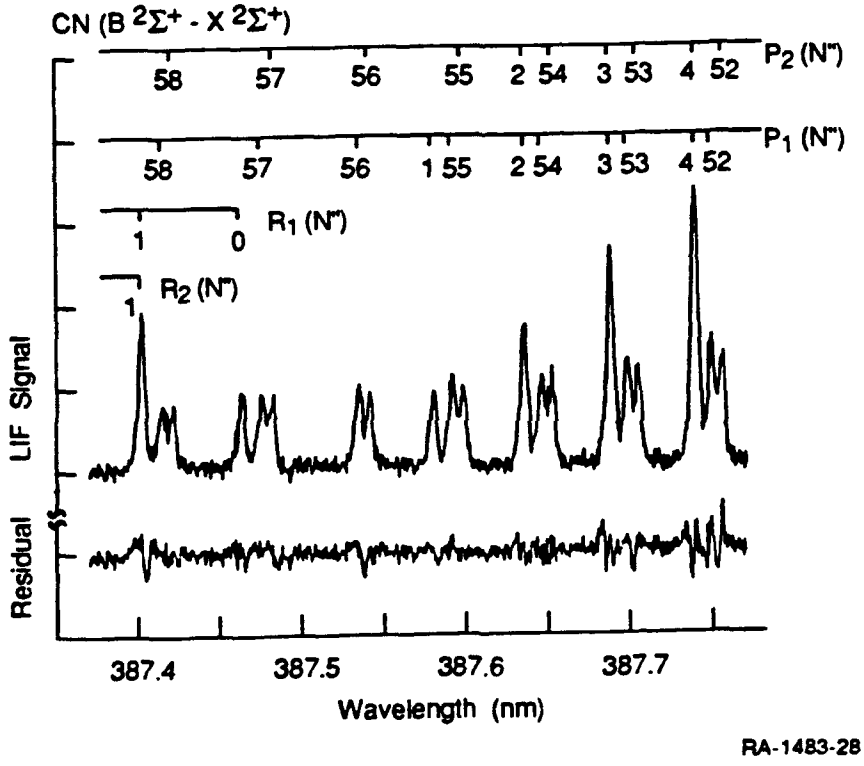
CN (B $^2\Sigma^+$ - X $^2\Sigma^+$)
58 57 56 55 2 54 3 53 4 52
P_2 (N")
58 57 56 1 55 2 54 3 53 4 52
P_1 (N")
1 0
R_1 (N")
1
R_2 (N")
LIF Signal
Residual
387.4 387.5 387.6 387.7
Wavelength (nm)
RA-1483-28

Figure 3

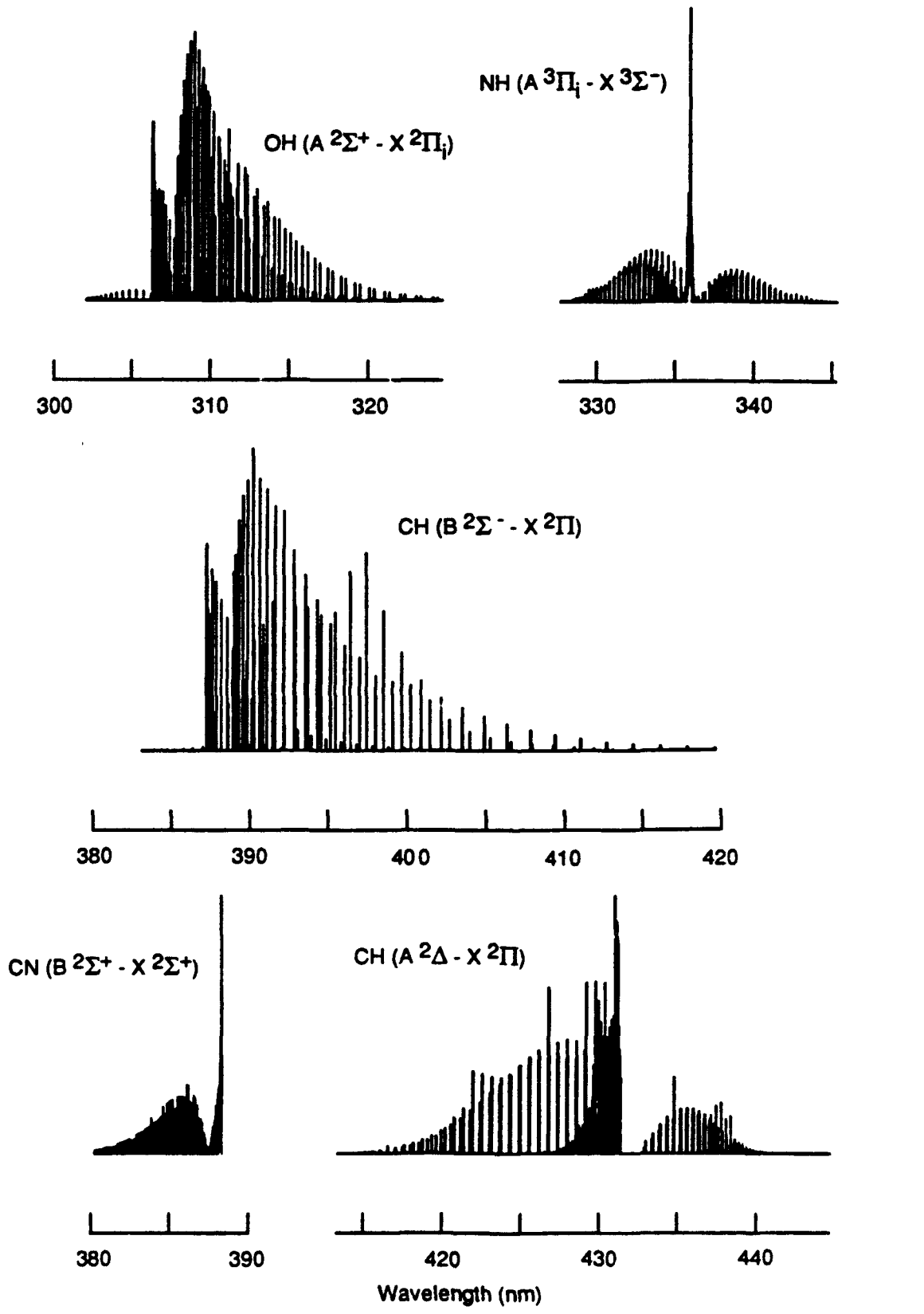
OH (A $^2\Sigma^+$ - X $^2\Pi_i$)
NH (A $^3\Pi_i$ - X $^3\Sigma^-$)
300
310
320
330
340
CH (B $^2\Sigma^-$ - X $^2\Pi$)
380
390
400
410
420
CN (B $^2\Sigma^+$ - X $^2\Sigma^+$)
CH (A $^2\Delta$ - X $^2\Pi$)
380
390
420
430
440
Wavelength (nm)
RA-2477-18

Figure 4

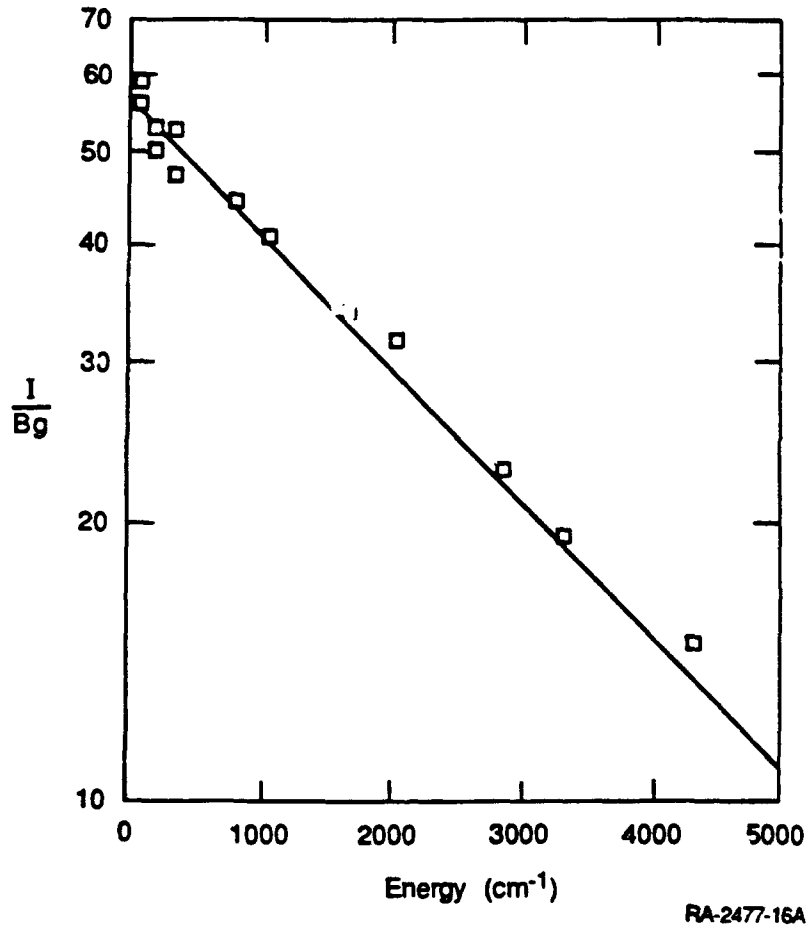
70
60
50
40
30
20
10
I
Bg
0
1000
2000
3000
4000
5000
Energy (cm-1)
RA-2477-16A

Figure 5

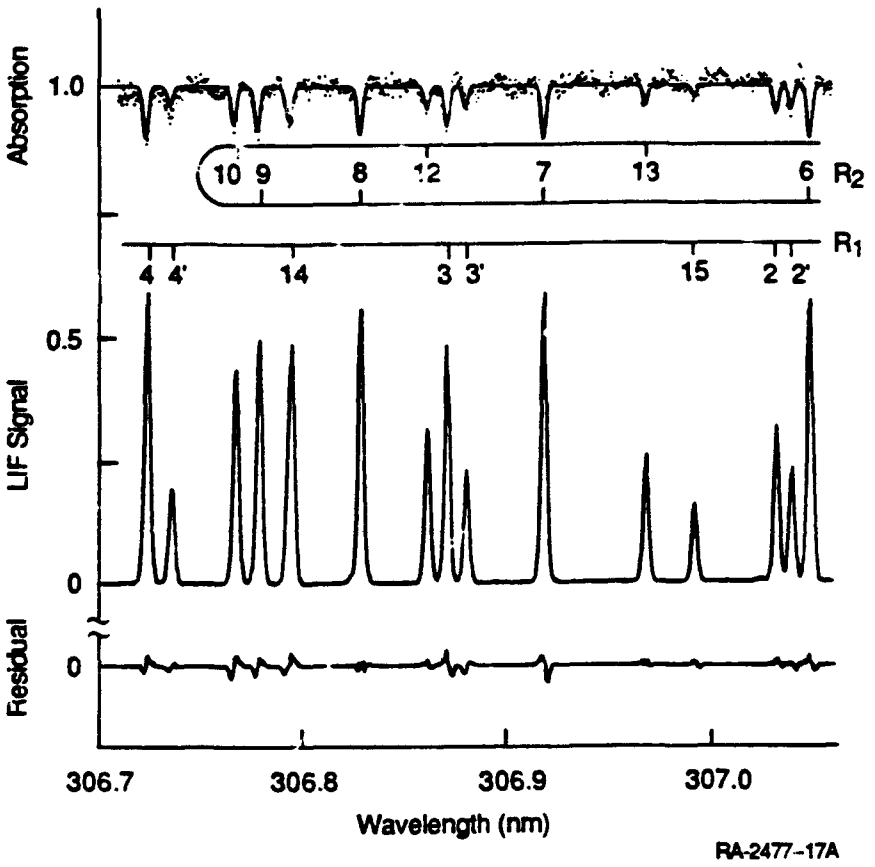
Absorption
1.0
10 9 8 12 7 13 6 R2
R1
4 4' 14 3 3' 15 2 2'
0.5
LIF Signal
0
Residual
0
306.7
306.8
306.9
307.0
Wavelength (nm)
RA-2477-17A

Figure 6

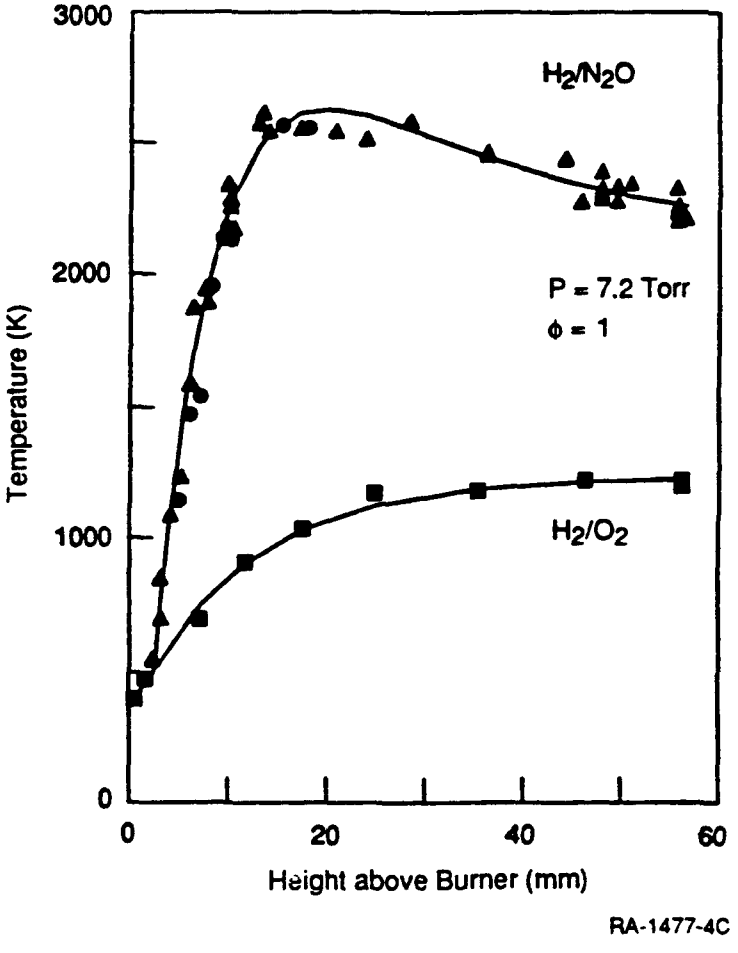
3000
2000
1000
0
Temperature (K)
H_2/N_2O
P = 7.2 Torr
ϕ = 1
H_2/O_2
0
20
40
60
Height above Burner (mm)
RA-1477-4C

Figure 7

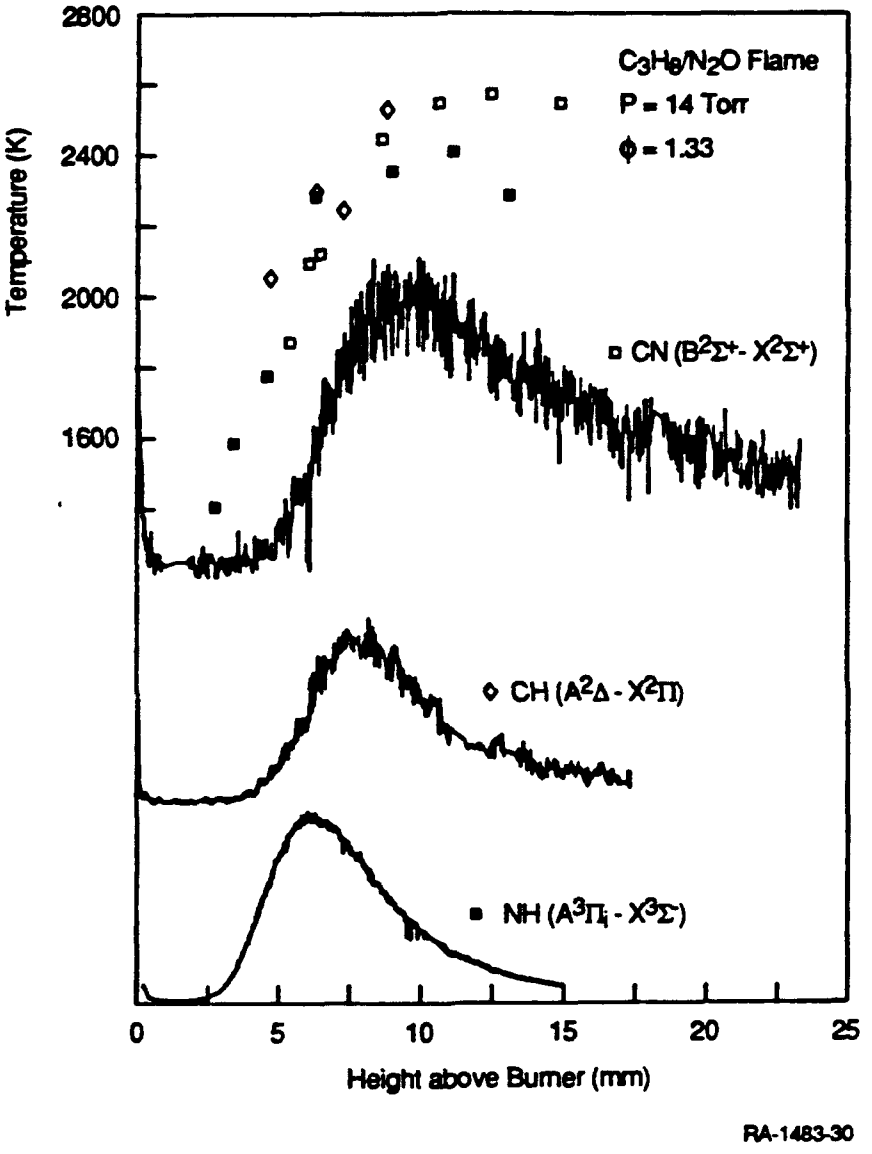
2800
2400
2000
1600
Temperature (K)
C3H8/N2O Flame
P = 14 Torr
ϕ = 1.33
CN (B2Σ+ - X2Σ+)
CH (A2Δ - X2Π)
NH (A3Πi - X3Σ-)
0
5
10
15
20
25
Height above Burner (mm)
RA-1483-30

Figure 8

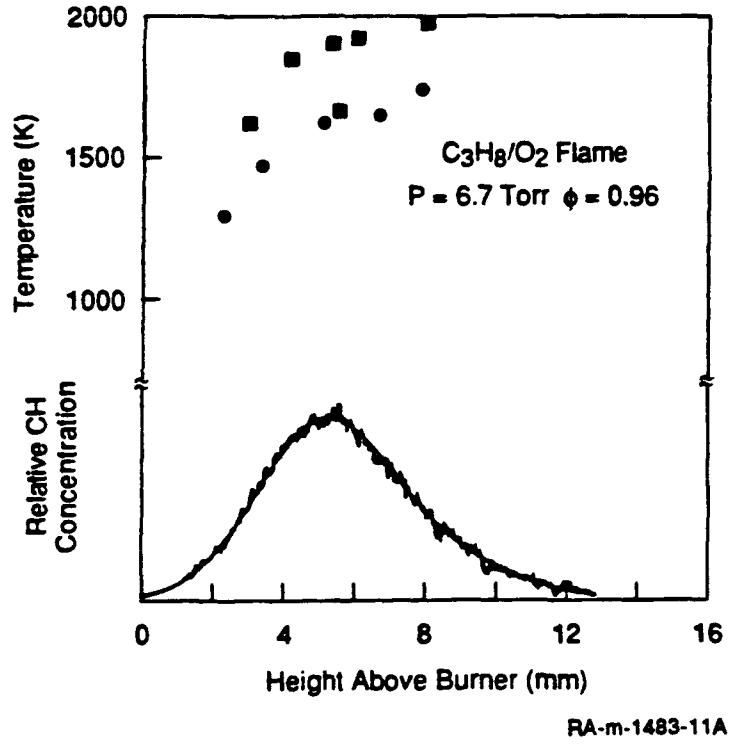
2000
1500
1000
Temperature (K)
C_3H_8/O_2 Flame
P = 6.7 Torr ϕ = 0.96
Relative CH Concentration
0
4
8
12
16
Height Above Burner (mm)
RA-m-1483-11A

Figure 9

Appendix G

ROTATIONAL AND TRANSLATIONAL EFFECTS IN COLLISIONS OF ELECTRONICALLY EXCITED DIATOMIC HYDRIDES

Reprinted from The Journal of Physical Chemistry, 1989, 93, 6273

Rotational and Translational Effects in Collisions of Electronically Excited Diatomic Hydrides

David R. Crosley

Molecular Physics Laboratory, SRI International, Menlo Park, California 94025
(Received: December 27, 1988)

Collisonal quenching and vibrational energy transfer proceed competitively with rotational energy transfer for several excited states of the diatomic radicals OH, NH, and CH. This occurs for a wide variety of molecular collision partners. This phenomenon permits the examination of the influence of rotational motion on the collision dynamics of these theoretically tractable species. Measurements can also be made as a function of temperature, i.e., collision velocity. In $OH(A^2\Sigma^+)$, both vibrational transfer and quenching are found to decrease with an increase in rotational level, while quenching decreases with increasing temperature. This behavior indicates that for OH anisotropic attractive forces govern the entrance channel dynamics for these collisions. The quenching of $NH(A^3\Pi_i)$ by many (although not all) collision partners also decreases with increasing rotational and translational energy, and $NH(c^1\Pi)$ behaves much like $OH(A^2\Sigma^+)$. However, the quenching of $CH(A^2\Delta)$ appears to decrease with increasing rotation but increases with increasing temperature, suggesting in this case anisotropic forces involving a barrier or repulsive wall. Such similarities and differences should furnish useful comparisons with both simple and detailed theoretical pictures of the appropriate collision dynamics.

Introduction

An ultimate goal of physical chemistry is to fully understand the outcome of some collisional encounter, be it a chemical transformation or the transfer of energy among the various degrees of freedom of the colliders. This requires an accurate knowledge of the potential surface(s) involved or at least those features of the potential that govern particular dynamic events. Currently, theoretical techniques are beginning to provide realistic surfaces for small systems. Tests of the quality of those surfaces, and an understanding of the influence of different regions or aspects of the surfaces, come from experiments designed to probe the collision events on a quantum-level-specific basis, selecting the initial state (or a small subset) and measuring the distribution over final states. Fully state resolved experiments are not always possible, but considerable information can still be gained with partial state selection in various modes. Diatomic hydrides provide an important class of molecules for study, presenting us with fortunate opportunities in two respects. First, at least with small collision partners, they are amenable to detailed calculation of potential surfaces and trajectories; such computations can be expected to be realistic even for excited electronic states. Second, due largely to their wide energy level spacing, they often afford good possibilities for achieving state-resolved experiments.

We consider here collisions of electronically excited states of the diatomic hydrides. For reasons of both fundamental and practical interest, these states, particularly for the hydroxyl radical, have been the subject of many studies by diverse means over a long period of time. With modern laser methods, individual vibrational and rotational quantum levels, or reasonably well defined distributions over such levels, can be initially selected within these excited states. In many cases the rates of quenching, vibrational and rotational energy transfer, and translational thermalization are all competitive; that is, they occur on similar time scales. This enables the study of the influence of one of these forms of energy on collisions involving relaxation of a different mode, e.g., the rotational level dependence of vibrational energy transfer. This situation stands in sharp contrast to that observed for ground electronic states, where rotational and translational thermalization typically take place some 100 times faster than vibrational transfer, thereby preventing such an examination. In collisional quenching, a special aspect of the potentials is also involved, the coupling between surfaces for different electronic states.

The first of such studies was that of downward vibrational energy transfer (VET) in the $A^2\Sigma^+$ state of the OH and OD radicals.[1,2] For the simple colliders H_2, D_2, and N_2, the VET cross sections were found to be on the order of gas kinetic and to decrease sharply with increasing rotational level. This rapid rate of transfer, together with other evidence discussed below, suggested that attractive forces and the formation of a transitory collision complex played a role in the VET process, while the dependence on rotational level indicated that those forces were anisotropic in nature. Because the A state of OH has a large dipole moment, 2.0 D, an anisotropic attractive interaction between it and a collision partner is not surprising. Subsequently, it was found that for the colliders N_2 and O_2 quenching of $OH(A^2\Sigma^+)$ varies with rotational level in a similar way[3] and that for many quenchers the cross sections decrease with increasing temperature (i.e., collision velocity).[4] Thus, anisotropic attractive forces appear important in this process as well. Investigations of quenching of the $A^3\Pi_i$ and $c^1\Pi$ states of NH, and the $A^2\Delta$ and $B^2\Sigma^-$ states of CH, show a dependence on rotational level, while quenching of both those states of NH, the $A^2\Delta$ state of CH, and the $A^3\Pi_i$ state of PH vary with temperature. However, for these radicals the interpretation is not as simple and, for CH at least, quenching appears to involve repulsive forces or a barrier.

This paper reviews the experiments investigating these effects of rotational and translational energy on VET and quenching in the diatomic hydrides and speculates on possible reasons for such behavior. Many of the ideas developed from experiments conducted on the OH radical, and the concepts thus involve the attractive forces noted above. One of the reasons for studying the other hydrides was an attempt to generalize from the findings on OH, but matters turned out to be more complicated and thus more interesting. The findings can be considered in terms of simple

(1) Lengel, R. K.; Crosley, D. R. *Chem. Phys. Lett.* **1975**, *32*, 261.
(2) Lengel, R. K.; Crosley, D. R. *J. Chem. Phys.* **1978**, *68*, 5309.
(3) McDermid, I. S.; Laudenslager, J. B. *J. Chem. Phys.* **1982**, *76*, 1824.
(4) Fairchild, P. W.; Smith, G. P.; Crosley, D. R. *J. Chem. Phys.* **1983**, *79*, 1795.

mechanistic pictures and eventually compared with realistic theoretical calculations. Thus, we can not only develop elementary concepts concerning these collisions but also use the results to test predictions from those sophisticated theories, particularly when we compare different electronic states of different hydrides.

This is not intended as a review of the field of diatomic hydride collisions as a whole but is specialized to the rotational and translational effects on quenching and VET and the information these effects convey concerning molecular interactions. Earlier work on OH and NH has been summarized in the reviews of Schofield[5] and Slanger,[6] respectively. Occasionally, large discrepancies among measurements reported from different laboratories can be seen; in at least some cases this can be attributed to unrecognized effects arising from the rotational and/or translational dependence. These interesting state-specific effects have immediate practical implications in determining fluorescence quantum yields for the large number of studies in which these radicals are detected in practical systems, using the method of laser-induced fluorescence (LIF). These include measurement of OH, NH, and CH for combustion applications[7] and monitoring of the OH radical in the troposphere[8] or stratosphere.[9]

Two conventions will be utilized throughout. First, the term quenching is used to denote total removal of the molecule from a given electronically excited state. This process, whose collisional rate is measured by the loss of fluorescent photons on either a time-dependent or steady-state basis, can include chemical reaction as well as conversion to the nonradiating ground state and/or other excited states. VET is considered a distinct and different process, occurring wholly within a particular electronic state. Second, from the pressure (density) dependence of a pseudo-first-order decay rate, one obtains a rate constant k in units of $cm^3\ s^{-1}$. This term contains an uninteresting dependence on mass and temperature through the collision velocity, $\langle v \rangle = (8kT/\pi\mu)^{1/2}$. We can better examine the effects of different colliders and the influence of collision energy on the effective interaction between the radical and collider through the "thermally averaged" cross section $\sigma = k/\langle v \rangle$, in units of cm^2, or as usually used here, $Å^2$. A subscript R, V, or Q on k or σ indicates the type of process: rotational energy transfer (RET), VET, or quenching.

Rotational Level Dependence and Collision Complex Formation in OH VET

The rotational dependence of collisions of a diatomic hydride was first apparent in experiments on VET in the $A^2\Sigma^+$ state of the hydroxyl radical.[1,2] These measurements were made using spectrally resolved fluorescence scans of laser-excited OH. The discharge flow system utilized is typical of those employed for many of these studies. Hydrogen atoms are produced by a microwave discharge in H_2 or H_2O; these are then reacted with NO_2 to form the OH molecules. Collision partners are added downstream of the radical production region and their densities monitored by pressure gauges and flowmeters. Enough time is allowed to permit the ground-state radicals and the colliders to mix and to reach translational and rotational thermalization with the cell walls, the latter condition checked by LIF excitation scans which measure the rotational population distribution within the ground state.

In these VET experiments, the beam from a pulsed tunable laser was directed into the cell, exciting the OH to the $v' = 1$ vibrational level of the A state. This ultraviolet transition, near 282 nm, requires the use of frequency-doubled dye laser radiation. Typical laser pulse durations in current LIF experiments of this type are 10 ns. The laser was tuned to a line sufficiently isolated spectrally that a single rotational level in the upper state was populated by the laser. The fluorescence at right angles was collected with a lens system, dispersed with a scanning monochromator, and detected with a photomultiplier. It was then processed with a gated integration system which recorded signals only during and shortly after the laser pulse, thereby avoiding background noise (dark current and light from the discharge) during the long period between laser pulses, which occur at typical repetition rates of tens of hertz.

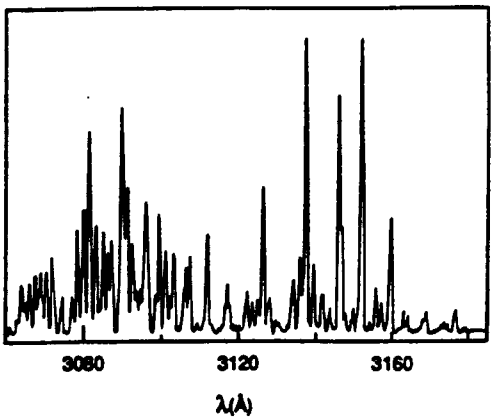

Figure 1. Fluorescence scan in the presence of 1 Torr of H_2 collider, exciting the $N' = 3$, $J' = 3^1/_2$ level of the $v' = 1$ vibrational level in $A^2\Sigma^+$ OH. Emission to the right of 3120 Å is the (1,1) band and consists mostly of five strong lines originating from the initially pumped rotational level, showing that little RET has occurred. Fluorescence at shorter wavelengths is the (0,0) band, emitted by OH molecules which have undergone VET from $v' = 1$ to 0. Comparison of the intensities shows that more VET has taken place than RET in $v' = 1$.

A fluorescence spectrum from this experiment is shown in Figure 1. Here, the electronic gate is set long enough to integrate in time over the entire time evolution of the fluorescence pulse which, in the presence of no added collider, occurs with a decay time of about 700 ns. This spectrum was obtained in about 1 Torr of added H_2 collider. The lines to the right of 3124 Å are primarily the (1,1) band, emitted by radicals in the initially pumped $v' = 1$ level, while the denser spectrum at shorter wavelengths is the (0,0) band, due to OH molecules in the $v' = 0$ level populated by VET collisions with the hydrogen. Note that the (1,1) band comprises five strong lines and a few much smaller ones. The strong lines all arise from the initially pumped rotational level $N' = 3$, and their predominance shows that little RET has occurred within $v' = 1$. However, the intensity of the (0,0) transition indicates that considerable VET has taken place. Because most of the OH molecules which remain in $v' = 1$ at this pressure are still in $N' = 3$, most of those which have undergone VET have come from $N' = 3$ as well, and the measured VET cross section, σ_V, will be specific to that particular level. This competition in which RET is slower than VET, illustrated clearly in Figure 1 for collisions with H_2, is the basis for the ability to determine rotational-state-specific cross sections for VET and quenching in the diatomic hydride radicals. The intensities of the fluorescence in the two bands seen in Figure 1 can be integrated to furnish the populations in the two vibrational levels, which are then readily analyzed to yield the VET cross sections.

For the colliders H_2, D_2, and N_2 the σ_V are large, 10–25 $Å^2$ for the lowest rotational level, $N' = 0$. Further, the σ_V were found to decrease sharply with increasing N', falling in the case of N_2 a factor of 2 between $N' = 0$ and 5. The results for H_2 and N_2 are given in Figure 2, plotted in the form $\ln [\sigma_V]$ vs $N'(N' + 1)$, a wholly empirical relationship discussed later. This phenomenon was attributed to the formation of a transitory collision complex with entrance channel dynamics dominated by anisotropic attractive forces.[1,2] The lifetime of this complex is not specified, but it is longer than a rotational period and lengthy enough to permit a significant amount of scrambling of energy among the

(5) Schofield, K. *J. Phys. Chem. Ref. Data* **1979**, *8*, 723.
(6) Slanger, T. G. In *Reactions of Small Transient Species*; Fontijn, A., Clyne, M. A. A., Eds.; Academic Press: London, 1983; p 231.
(7) Crosley, D. R., Ed. *Laser Probes for Combustion Chemistry*; American Chemical Society: Washington, DC, 1980; ACS Symp. Ser. No. 134. Eckbreth, A. C. *Laser Diagnostics for Combustion, Temperature and Species*; Abacus Press: Cambridge, MA, 1987.
(8) Crosley, D. R.; Hoell, J. M. Future Directions for H_xO_y Detection. NASA Conference Publication 2448, Dec 1986.
(9) Heaps, W. S.; McGee, T. J.; Hudson, R. D.; Caudill, O. *Appl. Opt.* **1982**, *21*, 2265. Stimpfle, R. M.; Anderson, J. G. *Geophys. Res. Lett.* **1988**, *15*, 1503.

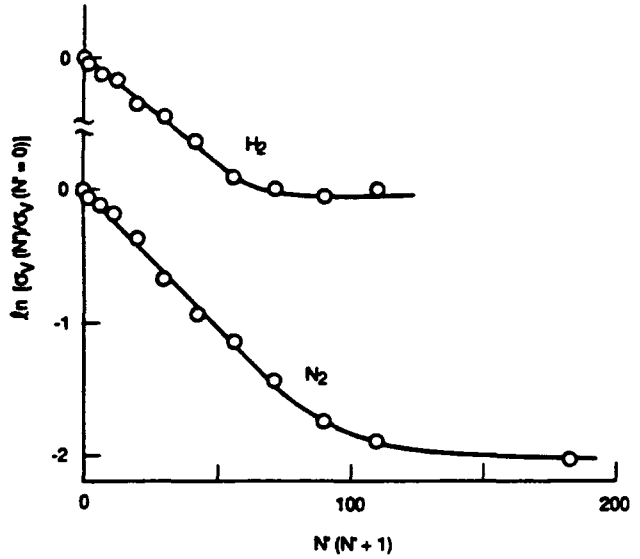

Figure 2. Cross sections for VET due to H_2 and N_2. The logarithm of σ_V is plotted vs $N'(N'+1)$, i.e., the rotational energy. This empirical correlation appears to work well for lower rotational levels but not for higher ones, as shown by the lines.

different vibrational, rotational, and translational degrees of freedom of both the OH and the collision partner.

The evidence for such a complex is as follows.[2] The first is simply the large size of the σ_V, with a range appropriate to interactions of a highly polar species like A-state OH. This is not caused by resonant energy exchange. This can be seen by comparing the VET cross section of 15 Å^2 by D_2, whose vibrational spacing matches that of OH within 4 cm^{-1}, with the σ_V of the 10 Å^2 for H_2 which has an energy mismatch of 1460 cm^{-1}. Similar arguments can be applied to N_2 relaxing OH and OD; further, the σ_V vary *smoothly* with N' (see Figure 2), not irregularly as might be expected for resonances dependent upon detailed vibrational–rotational level spacings. Altogether, the cross sections are not strongly dependent upon isotope, indicating that the internal level structure of the collision partner plays little role. (On the other hand, the complexes are not so long-lived as to facilitate chemical exchange, e.g., between D_2 and OH to yield excited OD.) The rotational population distribution in $v' = 0$, of OH molecules that have undergone VET, can be described by a temperature, albeit one which is hotter than the gas temperature: 600–700 K for H_2 and D_2 and 900 K for N_2. Further, this distribution appears independent of the N' initially excited in $v' = 1$. This suggests a partial conversion of OH vibrational energy into OH rotational energy, but in a statistical way as might be expected with rapid energy flow in the four-atom complex. Measurements were also made of the rate of transfer from $v' = 2$. Although less accurate because of poorer knowledge of the rotational distribution in $v = 1$ resulting from $2 \rightarrow 1$ transfer, they showed definitively for N_2 that $\sigma_V(2\rightarrow1) \sim \sigma_V(2\rightarrow0) \sim \sigma_V(1\rightarrow0)$. Relaxing 5800 cm^{-1} of vibrational energy as easily as 3000 cm^{-1} cannot be readily explained in conventional pictures of VET involving a purely repulsive interaction potential. Thus, there are several separate facts, all indicating the existence of a collision complex in VET of $A^2\Sigma^+$ OH molecules, a picture which underlies many of the subsequent concepts and postulates (though not always the results) concerning collisions of excited diatomic hydrides.

Within this framework of collision complex formation, the rotational level dependence was explained as follows.[1,2] The polar nature of the OH molecule leads to a highly anisotropic surface, having in some orientations deep attractive valleys which can lead to more efficient complex formation and thereby enhance the VET process. When the OH is not rotating, it and the collider can easily find these valleys and lock together to form the complex. As the OH rotates, however, it averages over the surface during the approach of the collision pair and washes out the influence of these particularly efficacious regions. Thus, the decrease in σ_V with increasing N' is due to a decrease in the cross section for complex

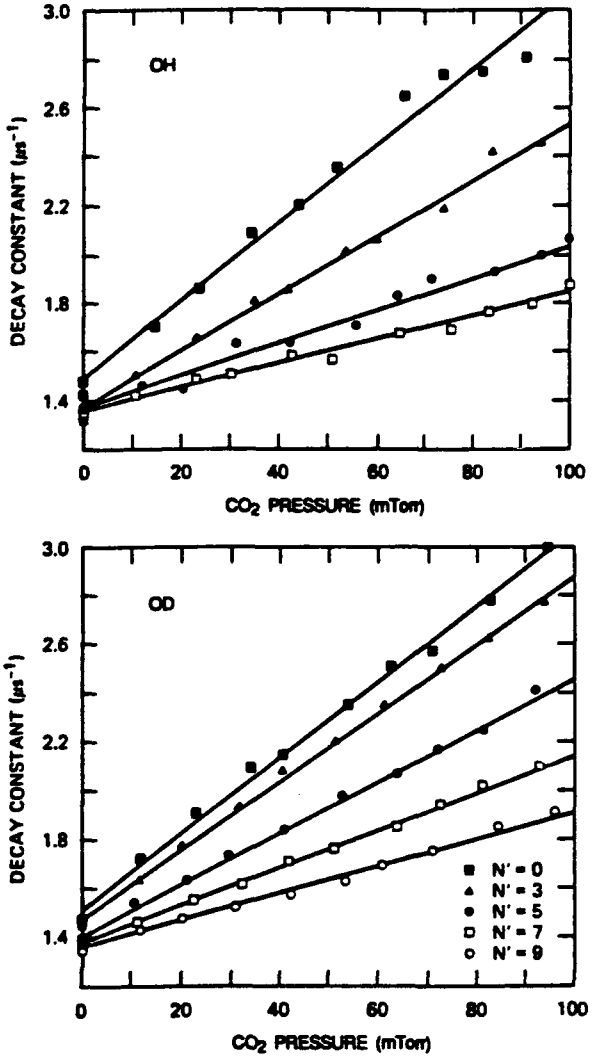

Figure 3. Decay constants for $v' = 0$ plotted vs pressure of added CO_2 collider, for several rotational levels of OH (upper panel) and OD (lower panel). The rate constant for quenching is obtained from the slope, and the intercept is the radiative rate. Note the striking variation of slope with N'.

formation. Trajectory studies[10] on vibrational transfer in HF–HF collisions indicated that such a mechanism could be operative, although no such state-specific experimental evidence is available on that system. The OH results are also in accord with the finding that σ_Q is independent of the fine structure level associated with each rotational level in ths $^2\Sigma$ state; that is, the effects are due to the mechanical rotation of the radical.

VET in A-state OH was further studied by German,[11] who at the same time investigated quenching by measuring the time dependence of the fluorescence signals. For this purpose, a signal integrator gate width of 50 ns was used and the time delay between the laser pulse and the gate varied to trace out the decay curve. With increasing collider density and collisional removal of the excited state, the decay constant becomes progressively faster; its slope when plotted vs density furnishes the rate constant for the removal process. Figure 3 shows such plots (taken from a later quenching study described below). The vibrationless $v' = 0$ level can decay only by quenching and radiation. $v' = 1$ can be collisionally removed by both quenching and VET; a combination of lifetime and fluorescence intensity measurements is necessary to determine both cross sections. German found that the total removal ($\sigma_V + \sigma_Q$) from $v' = 1$ decreased with increasing N' for the three colliders H_2, N_2, and O_2, in general agreement with the results of ref 1. A decrease of σ_Q for both $v' = 1$ and 0 with

(10) Berend, G. C.; Thommarson, R. L. *J. Chem. Phys.* **1973**, *58*, 3203.
(11) German, K. R. *J. Chem. Phys.* **1976**, *64*, 4065.

increasing N' was also indicated, although the reported variation is often less than the accompanying uncertainties.

In only two other studies, both of which are much more recent, has collider-specific VET of $A^2\Sigma^+$ OH (or any other radical) been studied in sufficient detail to permit an examination of the rotational level dependence. These studies again used combinations of fluorescence scans and time decay measurements. N_2, O_2, and H_2O, the important colliders for atmospheric monitoring purposes, were investigated by Burris et al.[12] while collisions with H_2O, NH_3, CO_2, CH_4, N_2O, N_2, SF_6, and CF_4 are described in ref 13. In general, the findings are in good agreement among all four of these collider-specific flow cell investigations. The total decay from the excited state decreases with increasing N' for all colliders (save the highly polar H_2O and NH_3, for reasons discussed below). A rotational distribution in $v' = 0$ described by a temperature of 750 K for N_2 collisions was found in ref 13, similar to that reported in ref 2. However, a close examination of the spectra for different initially excited N' in $v' = 1$ does reveal small differences (see also ref 14 for spectra under lower resolution), suggesting a weak memory.

The variation in σ_V and $\sigma_{Q,v=1}$ were separately determined for CO_2 (ref 13) and for N_2 and O_2 (ref 12). For all three colliders it appears that σ_V decreases less rapidly with N' than does $\sigma_{Q,v=1}$, although in each case 2-σ error bars are compatible with equal variation. If a collision complex is formed which then leads to both VET and quenching, the variation of the cross section with N' should be the same for each process. If different, the dependence for both processes cannot be governed solely by an anisotropic, attractive interaction. This point, although not outside the uncertainties in a difficult experiment, is a worrisome inconsistency in an otherwise understandable body of data on VET in $A^2\Sigma^+$ OH. It deserves further, more careful investigation for these colliders and others.

The rotational dependence of VET of OH has also been studied in a flame at atmospheric pressure,[15] using steady-state fluorescence intensity ratios. CH_4 was burned in air, and the OH was excited near the flame front region, so that a variety of collision partners were present and some temperature gradient was likely sampled. Spectrally resolved fluorescence furnished relative σ_V, which were found to decrease with N' similarly to the flow cell results.

Attractive Forces and Rotational Level Dependence in OH Quenching

McDermid and Laudenslager,[3] also motivated largely by quantum yield considerations for atmospheric monitoring of OH, used the time dependence of the decay of total, unfiltered fluorescence from the $v' = 0$ level to determine quenching cross sections σ_Q for the colliders N_2, O_2, H_2O, and H_2. A two-chamber flow cell with differential pumping maintained the background gas pressures from the OH production at very low values. A transient recorder was used to record the decay traces at different collider pressures. This work was the first in which a rotational level dependence of the quenching could be unambiguously discerned. It was observed for N_2 and, less markedly, for O_2. In addition, the measured cross sections are similar in size to the σ_V reported in ref 1, 2, and 11. This suggested that quenching too is governed by anisotropic, attractive forces.

A more extensive study of these effects was conducted in our laboratory. The cell was also differentially pumped, similar in design to that of McDermid and Laudenslager. A scanning gated integrator was used in the first set of measurements,[16] in which a larger set of rotational levels was studied for the same collision partners and for the deuterated species D_2 and D_2O. A later series of measurements[17] utilized a transient digitizer and included OD and a much larger set of colliders. The findings were largely in accord with expectations from the VET results: large cross sections for most colliders, varying in a manner consistent with attractive forces (this could also be anticipated from measurements of σ_Q at elevated temperature[4] as discussed below); identical behavior for deuterated and protonated species; and a nearly universal decrease of σ_Q with increasing N'.

We first consider the role which attractive forces play in the quenching process. Unlike VET, where we could examine cross sections for different v', a lack of resonance effects, etc., we have here only the variation in cross section among collider (and the temperature dependence discussed below). The lack of isotope dependence indicated that the quenching is governed not by internal levels but by electronic interactions, and prompted a simple theoretical examination in terms of attractive forces and collision complex formation.[4,17] One such picture, suggested by Parmenter and co-workers,[18] correlates the cross section with the well depth of the radical–collider interaction. The only experimental well depth for these excited radical colliders is from a recent study of $OH(A^2\Sigma^+)$–Ar van der Waals complexes.[19] A strongly attractive 700 cm^{-1} deep well and several bound vibrational levels were found. For the molecules studied here, the radical–collider well depths had to be estimated for correlation purposes by the square root of the collider–collider well depth, usually obtained from boiling point data. For OH some correlation can be found.[4]

However, more successful was an approach adapted from that used by Lee and co-workers[20] to describe quenching in SO_2. The model was formulated in terms of attractive interactions involving multipole moments between the excited OH and the collider. These r^{-2}, r^{-4}, and r^{-6} interactions arise from dipole–dipole, dipole–quadrupole, and dipole–induced dipole plus dispersion forces, respectively; they can be calculated from known (or reasonably estimated, if necessary) dipole and quadrupole moments, polarizabilities, and ionization potentials. In addition, the potential includes a repulsive centrifugal barrier $l(l+1)/r^2$, where the collisional angular momentum l can be expressed in terms of the collision energy and impact parameter. If, for a given energy, the impact parameter is small enough, the collision pair can surmount this barrier and form a complex; as it later dissociates, it will form $X^2\Pi_i$ OH part of the time (probability P) and form $A^2\Sigma^+$ OH the rest of the time. For this simple one-dimensional potential, trajectories can be readily calculated and integrated over a thermal velocity distribution (see ref 4) to yield a thermally averaged cross section σ_{CF} for complex formation. Then $\sigma_Q = P\sigma_{CF}$. There is no reason a priori to expect P to be the same for each collision partner, although a large variation among colliders would invalidate the idea of a collision governed predominantly by attractive force, entrance channel dynamics.

A plot of σ_Q vs σ_{CF} for $A^2\Sigma^+$ OH shows a good correlation for many colliders, with a value of $P = 0.5$ at room temperature.[17] Notable exceptions are CF_4 and SF_6, for both of which σ_{CF} is near 80 $Å^2$ but experimental upper limits give $\sigma_Q < 3$ $Å^2$. Also, N_2 has a conspicuously low P value near 0.1. It was suggested that each of these molecules is efficient at complex formation but inefficient at mixing the Σ and Π states during the lifetime of the complex. One would then expect them to be efficient at VET, which depends only on energy redistribution and not state mixing. N_2 was already known[1,11] to have a large σ_V, and this was later found to be true for the fluorinated species as well.[13] For large molecules, including an isomeric set of butenes, the model does not work.[21] Here, the quenching cross sections are larger than the calculated σ_{CF}, a result attributed to a breakdown in the ability

(12) Burris, J.; Butler, J. J.; McGee, T. J.; Heaps, W. S. *Chem. Phys.* **1988**, *124*, 251.
(13) Copeland, R. A.; Wise, M. L.; Crosley, D. R. *J. Phys. Chem.* **1988**, *92*, 5710.
(14) Crosley, D. R.; Copeland, R. A. *Proc. Soc. Photoinstrum. Eng.* **1987**, *742*, 6.
(15) Smith, G. P.; Crosley, D. R. *Appl. Opt.* **1983**, *22*, 1428.
(16) Copeland, R. A.; Crosley, D. R. *Chem. Phys. Lett.* **1984**, *107*, 295.
(17) Copeland, R. A.; Dyer, M. J.; Crosley, D. R. *J. Chem. Phys.* **1985**, *82*, 4022.
(18) Lin, H. M.; Seaver, M.; Tang, K. Y.; Knight, A. E. W.; Parmenter, C. S. *J. Chem. Phys.* **1979**, *70*, 5442.
(19) Berry, M. T.; Brustein, M. R.; Lester, M. I. *Chem. Phys. Lett.* **1988**, *153*, 17.
(20) Holtermann, D. L.; Lee, E. K. C.; Nanes, R. *J. Chem. Phys.* **1982**, *77*, 5327.
(21) Smith, G. P.; Crosley, D. R. *J. Chem. Phys.* **1986**, *85*, 3896.

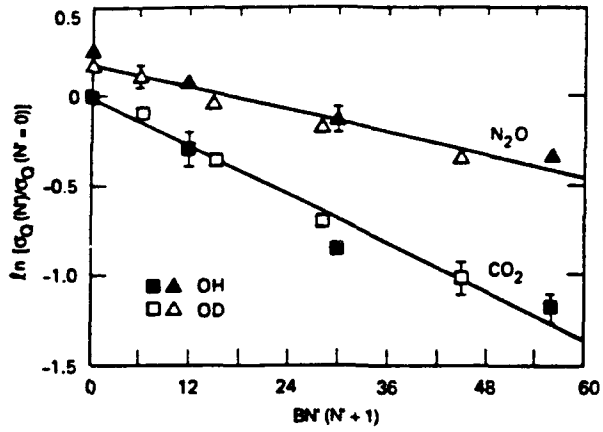

Figure 4. Cross sections for quenching $v' = 0$ plotted in logarithmic form vs the rotational energy, for OH and OD with the two colliders N_2O and CO_2. Both isotopes fit on the same curves when plotted in this way.

to describe these molecules by simple pointwise multipole moments. In spite of these exceptions, it appears safe to conclude that the quenching of $A^2\Sigma^+$ OH, like VET in the same state, is often controlled by attractive forces, which depend on interactions among the electronic wave functions but not strongly on the internal vibration–rotation level structure of the collider pair.

The simple model considered only a one-dimensional potential, with the nonrotating OH and its collision partner aligned in the most favorable orientation. All of the attractive forces except dispersion involve the direction of the dipole moment of the OH so that one expects a high degree of anisotropy. Attractive forces with distinctive anisotropy are evident in an ab initio calculation[22] of the potential for $OH(A^2\Sigma^+)$ interacting with $CO(X^1\Sigma^+)$. Thus, one does indeed expect valleys in the potential surface, along which the approach is especially favorable. Huo[23] assembled a simple model potential with dipole–dipole interactions in two different directions, elaborating on our qualitative picture. These trajectory calculations showed a 25% decrease in σ_Q as N' increased from 0 to 5.

A plot of decay constant vs pressure of added CO_2, for both OH and OD in $v' = 0$, adapted from ref 17, is shown in Figure 3. The slope, i.e., value of σ_Q, clearly varies strongly with rotational level. Cross sections were measured for 19 colliders, and a significant rotational level dependence was found for all but the rapid quenchers C_2H_6, C_2H_4, C_2H_2, and CCl_4, for which σ_Q is between 80 and 120 Å^2. The rotational effects were studied for both isotopes with CO_2 (Figure 3) and N_2O, the colliders exhibiting the largest N' dependence, in the hopes that some mechanistic insight might be gained. The cross sections are plotted in Figure 4 in the form $\ln [\sigma_Q(N')]$ vs the variable $BN'(N'+1)$, i.e., the rotational energy. Both isotopic forms fit on the same plot; plots vs BN', that is, the rotational frequency, do not show as good a correlation. Cross sections with other collision partners, plotted as in Figure 4, also produce straight lines. The results of ref 2, for $v' = 1 \rightarrow 0$ VET, for collisions with N_2 and H_2 are examined in the same way in Figure 1. It appears that the mechanism producing the rotational dependence is the same for both quenching of $v' = 0$ and VET from $v' = 1$.

This correlation, however, does not reveal the details of this mechanism for there is yet no theoretical basis for this or any other type of dependence on rotational energy. Conclusions may be drawn by fitting data to some established relationship; however, an unknown relationship cannot be proven in this manner. We stress that, although this correlation with the rotational energy is reminiscent of an energy gap law, that simple picture is not applicable here. In the process of VET or quenching of $A^2\Sigma^+$ OH, some 3000 cm^{-1} of vibrational or 30000 cm^{-1} of electronic energy, respectively, is converted into other forms. The OH internal energy thus changes considerably, much more than the maximum value of 500 cm^{-1} of rotational energy variation involved here. Perhaps the relationship illustrated in Figures 1 and 4 can be explained in simple theoretical terms; perhaps insight into its meaning requires investigation through complex numerical trajectory computations on realistic surfaces. We believe that it does reflect the behavior of the collision partners sampling the entrance region to the potential surface(s) on which both quenching and VET take place and hope that such state-specific results will provide detailed, useful comparison with theory.

Rotational Level Dependence of Quenching in NH

The first direct investigation of the rotational level dependence of quenching in a hydride other than OH was performed by Hofzumahaus and Stuhl[24] on the $A^3\Pi_i$ state of the NH radical. Sequential multiphoton photolysis of NH_3 by an ArF laser at 193 nm produced the NH directly in the excited state; the nascent rotational distribution was nonthermal but well-defined with a maximum population between $N' = 8$ and 13. Quenching was then determined from the pressure dependence of the time decays of the resulting fluorescence emission following the photolysis laser pulse. A monochromator dispersed the fluorescence, with a wide exit slit to detect all Q-branch lines of the (0,0) band. This avoided potentially complicating effects in the observed time (and pressure) dependence due to RET among the A-state levels.

Although the translational energy was not measured directly in this experiment, there is little available from the dissociation process, so the collision temperature is likely near 300 K. (Because σ_Q can depend on both rotation and translation, it is important that both distributions be specified when comparing results. This is often not possible and has caused confusion in the past; see ref 25 for a discussion of this point concerning various NH quenching measurements.) Addition of ~100 Torr of N_2, found to be a very inefficient quencher of A-state NH, cools the rotational levels to a 300 K distribution. In this way, σ_Q were determined for distributions over both high and low rotational levels for the colliders H_2 and NH_3; σ_Q was higher by 50% for the lower N'. A subsequent study[26] included CO and O_2 quenchers and Ar relaxer, with similar results. The cross sections are about half those measured for $A^2\Sigma^+$ OH with the same colliders and suggest at least for NH_3 a significant role of attractive forces. Thus, the same mechanism probably governs the rotational level dependence in both hydrides. For CO_2 no dependence on rotational level was found.[26,27] However, the cross section for this collider is much smaller, only 1 Å^2 compared with 70 Å^2 for OH in $N' = 0$, and rotational thermalization likely occurs before quenching thus preventing the observation of any rotational-level-dependent σ_Q.

Quenching of single rotational levels was investigated by using LIF excitation of NH produced in a discharge flow system;[25] the experimental method and apparatus were the same used for the OH measurements of ref 17. Nine collision partners were investigated; of these, all but CO_2 and N_2O showed a rotational level dependence. With the exception of these last two colliders, the cross sections are between 7 and 100 Å^2 and show some though not impressive correlation with either the well depth or multipole model calculations. σ_Q for H_2O and D_2O are the same (as are those for H_2 and D_2 measured for a thermal distribution at high temperature[28]), indicating again that the internal levels of the collider are unimportant. From these rotational-level-specific results[25] one can calculate an effective σ_Q for a 300 K rotational distribution to compare with the values measured directly for a thermal distribution. The calculated cross sections are between 10% and 20% larger than those of ref 24 and 26 for H_2, CO, O_2,

(22) Vegiri, A.; Farantos, S. C.; Papagiannakopoulos, P.; Fotakis, C. In *Selectivity in Chemical Reactions*; Whitehead, J. C., Ed.; Kluwer: Dordrecht, 1988; NATO ASI Ser. C245, p 393.
(23) Huo, W. Private communication.
(24) Hofzumahaus, A.; Stuhl, F. *J. Chem. Phys.* **1985**, *82*, 3152.
(25) Garland, N. L.; Crosley, D. R. *J. Chem. Phys.* **1989**, *90*, 3566.
(26) Kenner, R. D.; Heinrich, P.; Pfannenberg, S.; Stuhl, F. Manuscript in preparation.
(27) Browarzik, R. Thesis, Ruhr-Universität, Bochum, 1988.
(28) Garland, N. L.; Jeffries, J. B.; Crosley, D. R.; Smith, G. P.; Copeland, R. A. *J. Chem. Phys.* **1986**, *84*, 4970.

C_2H_6, H_2O, and NH_3, and the same for CO_2, constituting reasonable agreement between two very different methods of determining the same quantity. Recently,[29] sequential multiphoton photolysis of NH_3 to produce ground-state NH has been followed by single-level LIF excitation, to directly measure $\sigma_Q(N')$ for NH_3 collider. Line width measurements[30] indicate a translational temperature below 900 K. The results from the Bochum and SRI laboratories again differ uniformly by this same 20%.

Contrasting with the results from both the photolysis and the LIF measurements for NH_3 collider, however, are findings from a quite different method.[31] Here, the NH was formed from dissociation of NH_3 by a beam of 2-keV electrons, and the time decay of the resulting emission was monitored through a high-resolution monochromator. The authors report finding smaller rate constants for lower rotational levels, noting that this is contrary to the results of Hofzumahaus and Stuhl. Many rotational levels are produced in this process although only one fine-structure component of one rotational level was monitored for each decay measurement. Thus, RET by the NH_3 could affect the results, through simultaneous filling and depletion of the level detected. However, RET like quenching proceeds more slowly for higher N', as shown by a comparison of the results of ref 24 for $N' = 13$ ($\sigma_R/\sigma_Q \sim 0.5$) and ref 29 for $N' = 3$ ($\sigma_R > \sigma_Q$), so the reason for this discrepancy is not known.

The cross sections reported in ref 25 exhibit acceptably straight lines when plotted in the form $\ln [\sigma_Q(N')]$ vs $N'(N'+1)$. From these plots and also an examination of the results for OH, one finds that the more efficient quenchers show a smaller variation with rotational level. An explanation for this is as follows. An especially efficient quencher like polar NH_3 forms strong attractive interactions over the entire potential surface, so the complex can form readily regardless of approach angle. Thus, the additional attraction at preferred orientations adds little, and the cross section is not enhanced for rotationless or slowly rotating radicals, as it is in the case of a less efficient collider.

The N' dependence has also been examined in measurements[32,33] conducted in low-pressure flames of H_2 and hydrocarbons burning in N_2O. Although quite different from discharge flow cell conditions, this is a convenient way to study higher rotational levels. At 14-Torr total pressure, the time decay of LIF following single-level excitation was monitored. The quenching rate was determined from measurements at a fixed pressure by subtracting the known radiative contribution and dividing by the total gas density. The collisional environment where the NH could be found ranged from fuel plus N_2O near 1400 K to H_2O plus N_2 near 2200 K. A decrease in the total quenching rate of about 5% was found when N' was varied from 2 to 12. This result may be due to a small N' dependence of σ_Q for the species involved (recall that N_2O exhibits none) or a diminished N' dependence at higher temperature (as seen for OH–H_2O collisions described below).

The rotational level dependence of quenching of the $c^1\Pi$ state of NH has also been investigated. The c state can be produced by multiphoton photolysis of some precursor or by LIF. In the latter method, excitation is from the metastable $a^1\Delta$ state, formed in turn by photolysis or in a discharge flow system. Rohrer and Stuhl[34] used ArF photolysis of HN_3 to determine cross sections for many collision partners. The nascent, hot c-state distribution was cooled to 300 K by addition of Ar. The cross sections are very close to those for $A^2\Sigma^+$ OH (and quite unlike those for $A^3\Pi_i$ NH) for nearly all the colliders studied. Additionally, ab initio calculations for NH(c)–H_2 collisions[35] show a distinctly anisotropic surface. Thus, one might expect a rotational level dependence like that for OH.

Little N' dependence has been found, however. Intersystem transfer, c → A, was investigated for four colliders in both the absence and presence of added Ar relaxer.[36] O_2 and NO were found to have smaller cross sections for the 300 K rotational distribution than for the hot initial distribution. For O_2, this was attributed to resonant energy exchange involving metastable states of the collider, but no such explanation could be given for NO. Quenching by Xe showed no N' dependence, while that by N_2O was smaller for the higher N' distribution.

Umemoto et al.[37] made quenching measurements by LIF, exciting single levels of $c^1\Pi$ from the $a^1\Delta$ state, which was produced in the multiphoton XeCl laser photolysis of HN_3. The a-state NH was formed with a large amount of translational energy, equivalent to a temperature of 10 500 K; exciting the c-state promptly after the photolysis pulse ensures it has this same high collision velocity. The authors report cross sections for nine colliders, with 1-σ error bars of 17%. No rotational level dependence between $N' = 2$ and 8 could be discerned within this uncertainty. (The results are compatible with those of ref 36 for N_2O, given the error limits in each experiment.) The authors also describe a large series of σ_Q measurements at a translational temperature of 300 K, using He relaxer; however, this produces at the same time a thermal rotational distribution so that N'-specific cross sections could not be determined. Therefore, the lack of an observed N' dependence in NH($c^1\Pi$) quenching at high temperature may be inherent to this state or may reflect a decreased N' dependence at higher collision energy. In either event, the $c^1\Pi$ state should provide useful comparisons with theoretical models (e.g., ref 35 for H_2 collisions). Rotational-level-specific quenching at room temperature, through discharge flow production of $a^1\Delta$ or $b^1\Sigma^+$ and LIF time decay measurements, is highly deserving of study.

Rotational Level Dependence of Quenching of CH

The rotational dependence of quenching in the CH radical has been investigated very little, although quenching studies have been made on both the $A^2\Delta$ and $B^2\Sigma^-$ states. Each can be produced either by multiphoton photolysis of a suitable precursor or by LIF from the ground $X^2\Pi$ state. In view of the fact that the quenching of CH(A) appears to be governed by repulsive, not attractive, forces (see below), its rotational level dependence is of particular interest.

Nokes and Donovan[38] used multiphoton ArF photolysis of acetone and bromoform to produce CH in $A^2\Delta$. A series of colliders were examined by using the pressure dependence of the time decay of the emission following the excimer pulse, as in the NH studies described above. Helium was added to produce rotational and translational thermalization in most of the experiments. However, one set of measurements[39] was conducted on quenching by H_2, in the presence and absence of helium. The hot initial distribution was found to be quenched more slowly than the 300 K distribution.

The rotational level dependence of quenching of both the B and A states was investigated in the same low-pressure hydrocarbon/nitrous oxide flames described above for NH quenching, as well as flames burning in oxygen.[32,40,41] In these experiments the pressures of the flames were varied between 4 and 14 Torr to determine the quenching rate from LIF time decays. Again, the collisional environment is far from fully characterized although

(29) Kaes, A.; Stuhl, F. *Chem. Phys. Lett.* **1988**, *146*, 169.
(30) Kaes, A.; Stuhl, F. To be submitted for publication.
(31) Gustafsson, O.; Kindvall, G.; Larsson, M.; Olsson, B. J.; Sigray, P. *Chem. Phys. Lett.* **1987**, *138*, 185.
(32) Rensberger, K. J.; Copeland, R. A.; Wise, M. L.; Crosley, D. R. *Twenty-Second Symposium (International) on Combustion*; The Combustion Institute: Pittsburgh, in press.
(33) Copeland, R. A.; Rensberger, K. J.; Wise, M. L.; Crosley, D. R. *Appl. Opt.*, in press.
(34) Rohrer, F.; Stuhl, F. Presented at the Ninth International Symposium on Gas Kinetics, Bordeaux, France, July 1986.
(35) Staemmler, V.; Pöhlchen, M. To be submitted for publication.
(36) Rohrer, F.; Stuhl, F. *J. Chem. Phys.* **1987**, *86*, 226.
(37) Umemoto, H.; Kikuma, J.; Tsunashima, S.; Sato, S. *Chem. Phys.* **1988**, *120*, 461; **1988**, *125*, 397.
(38) Nokes, C.; Gilbert, G.; Donovan, R. J. *Chem. Phys. Lett.* **1983**, *99*, 491. Nokes, C. J.; Donovan, R. J. *Chem. Phys.* **1984**, *90*, 167.
(39) Donovan, R. J. Private communication.
(40) Crosley, D. R.; Rensberger, K. J.; Copeland, R. A. In *Selectivity in Chemical Reactions*; Whitehead, J. C., Ed.; Kluwer: Dordrecht, 1988; NATO ASI Ser. C245, p 543.
(41) Rensberger, K. J.; Dyer, M. J.; Copeland, R. A. *Appl. Opt.* **1988**, *27*, 3679.

the quenching rate was found to vary little with position in the flame (i.e., with temperature and composition). The $A^2\Delta$ quenching rate decreases 9% and 16% when N' increased from 2 to 12 for the fuels C_3H_8 and C_2H_2, respectively. A slightly larger decrease was found for the $B^2\Sigma^-$ quenching rate in each flame. Flames burning CH_4 showed no N' dependence. Earlier steady-state fluorescence intensity measurements[42] in atmospheric pressure flames had indicated a decrease in σ_Q with N', whereas no N' dependence was discerned for VET or B → A transfer.

KrF laser photolysis of acetone was also used to generate and measure the quenching of $CH(A^2\Delta)$ by that same parent molecule.[43] Rotationally resolved emission spectra indicated a distribution over vibrational and rotational levels of $A^2\Delta$ and an approximately equal amount of $B^2\Sigma^-$. The R-branch lines show a smoothly decreasing σ_Q between $N' = 4$ and 8, and the Q-branch, which also includes $N' = 2$ and 3, a somewhat larger value. Although the overlap of emission from the (1,1) and (0,0) bands in both branches and the possibility of B → A transfer complicate the interpretation in terms of A-state quenching alone, there appears a definite dependence on rotational level.

Other Diatomic Hydrides

To our knowledge, in only three other cases involving diatomic hydrides has the rotational level dependence of quenching been considered. Nedelec and co-workers have studied quenching and RET in a large number of metal hydrides, using spectrally and time-resolved LIF in hot discharge cells. The species have included BH, NaH, KH, AlH, CdH, MgH, ZnH, and HgH. Only for the $A^1\Sigma^+$ of the NaH molecule[44] was any rotational effect on quenching investigated. The authors made measurements with H_2 collider on $N' = 6$ and 12 in $v' = 11$ and report that σ_Q "did not depend appreciably" on rotational level. The RET cross sections are similar to those for quenching, not only for this molecule but also[45] for $KH(A^1\Sigma^+)$. Thus, if a rotational level dependence exists, perhaps for other v' or another collision partner, it should be observable. This could be very interesting in that these pseudo-two-electron molecules may be amenable to simple theoretical treatment.

LIF time decay measurements have also been performed on quenching of the $A^2\Sigma^+$ state of the LiH molecule.[46] The collider was Li, present in the heat pipe used for formation of the hydride. The rotational level dependence of σ_Q in the $v' = 5$ and 6 levels which were investigated is quite marked, owing to sharp resonant transfer producing Li atoms in the 2^2P level and not the type of collision dynamics postulated for OH, NH, and CH. However, the theoretical tractability of this small species makes it a most attractive candidate for further study in other v' and with other collision partners.

The $B^2\Sigma^+$ state of the OH molecule can be made to fluoresce[47] by means of laser excitation from high-lying levels of the ground state, for example $v'' = 8$ or 9 produced in a discharge system by the H + O_3 reaction. Collisional removal of the excited state by Ar and He varies markedly with N', but this has been attributed to rotational transfer into and out of rotational levels which rapidly predissociate.

Rotational and Temperature Dependence of Quenching of OH by H_2O

Quenching of $A^2\Sigma^+$ OH by the water molecule is an important subject for study from a practical standpoint, i.e., quantum yields in combustion and atmospheric processes, as well as for fundamental reasons. Considering only LIF experiments with single-level excitation made on $N' = 0$, one finds one pair of measurements[3,11] reporting $\sigma_Q = 65$ Å^2 and another pair[16,48] where a value of 90 Å^2 was found. The pressure of H_2O is notoriously difficult to control and measure accurately in flow systems, and so values this diverse are not surprising.

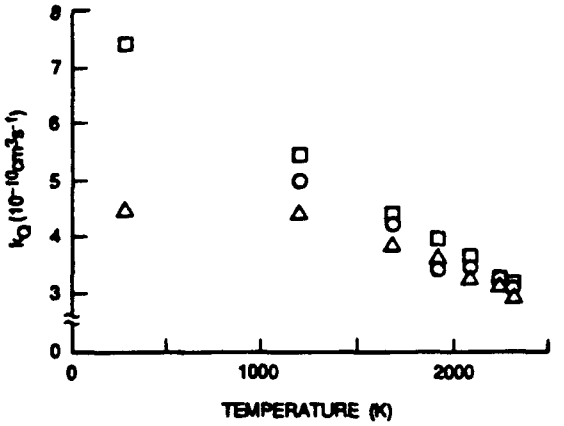

Figure 5. N'-dependent quenching rate constants for $v' = 0$ over a large temperature range: squares; $N' = 3$; circles, $N' = 8$; triangles, $N' = 16$. The points at 300 K are for H_2O collider (from ref 48). Those at higher temperature are from flame studies (ref 52). At the highest temperatures the quenching is due to H_2O, although hydrogen atoms contribute significantly at 1200 K. Comparing the points at highest and lowest temperature shows that the rotational level dependence present at 300 K has disappeared at 2300 K.

Cleveland and Wiesenfeld[48] photolyzed O_3 to product $O(^1D)$ atoms which react with H_2O to produce OH in high rotational levels of both $v'' = 0$ and 1 of $X^2\Pi_i$. A tunable laser was then used to excite the OH to specific N' of both $v' = 0$ and 1 in the A state; time decay measurements as a function of H_2O density furnished σ_Q for each vibrational level. (Recall that for H_2O $\sigma_Q \sim 10\sigma_V$.) The results agree excellently with those of ref 13, 16, and 17, which were made between $N' = 0$ and 7. These measurements continue to much higher N', showing a further drop in σ_Q to $N' = 12$ and then a constant value up to $N' = 19$. This is very much like the behavior of σ_V at high N' for H_2 and N_2 colliders (see Figure 1). Apparently, for sufficiently fast rotation the averaging of the surface becomes complete, and a further increase in N' causes no further decrease in efficiency.

Unfortunately, the OH translational energy in this experiment is not known accurately. The $O(^1D)$ + H_2O reaction forms OH with an effective translational temperature[49] of 3500 K. The quenching measurements were performed with 1.25 Torr of added He, 2 μs after the photolysis laser. At this delay, 8 Torr of He thermalizes low rotational levels[50] and surely translation too, but the effects for higher N'' and at the lower pressure were not measured directly.

Quenching of OH has also been investigated[51,52] in low-pressure flames of H_2 burning in mixtures of O_2 and N_2O. The method, as for NH in flames, was LIF time decay at a fixed pressure (here 7 Torr) with subtraction of the radiative component. In the reaction zone[51] a noticeable dependence of the quenching rate on N' was found. The degree varied with position and thus with collider and temperature in this complicated environment. In the burnt gases,[52] the use of mixtures of the two oxidants permitted the temperature to be adjusted between 1200 and 2300 K. The σ_Q for three N' from this experiment are shown in Figure 5. Also included are the H_2O quenching results of Cleveland and Wiesenfeld, assuming a 300 K translational temperature for their measurements. Because the gas composition in the flames varies

(42) Garland, N. L.; Crosley, D. R. *Appl. Opt.* **1985**, *24*, 4229.
(43) Hontzopoulos, E.; Vlahoyannis, Y. P.; Fotakis, C. *Chem. Phys. Lett.* **1988**, *147*, 321.
(44) Nedelec, O.; Giroud, M. *J. Chem. Phys.* **1983**, *79*, 2121.
(45) Giroud, M.; Nedelec, O. *J. Chem. Phys.* **1982**, *77*, 3998.
(46) Wine, P. H.; Melton, L. A. *J. Chem. Phys.* **1976**, *64*, 2692. Ibbs, K. G.; Wine, P. H.; Chung, K. J.; Melton, L. A. *J. Chem. Phys.* **1981**, *74*, 6212.
(47) Sappey, A. D.; Crosley, D. R.; Copeland, R. A. *J. Chem. Phys.* **1989**, *90*, 3484.
(48) Cleveland, C. B.; Wiesenfeld, J. R. *Chem. Phys. Lett.* **1988**, *144*, 479.
(49) Gericke, K.-H.; Comes, F. *J. Chem. Phys.* **1982**, *65*, 113.
(50) Cleveland, C. B.; Jursich, G. M.; Trolier, M.; Wiesenfeld, J. R. *J. Chem. Phys.* **1987**, *86*, 3253.
(51) Kohse-Höinghaus, K.; Jeffries, J. B.; Copeland, R. A.; Smith, G. P.; Crosley, D. R. *Twenty-Second Symposium (International) on Combustion*; The Combustion Institute: Pittsburgh, in press.
(52) Jeffries, J. B.; Kohse-Höinghaus, K.; Smith, G. P.; Copeland, R. A.; Crosley, D. R. *Chem. Phys. Lett.* **1988**, *152*, 160.

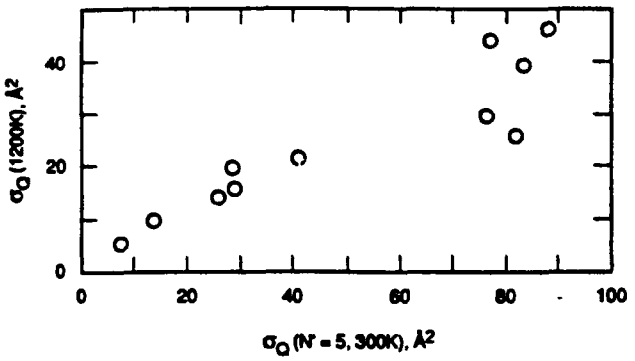

Figure 6. Cross sections for quenching of OH $A^2\Sigma^+$, $v' = 0$, showing a decrease with temperature. For each of the 11 colliders studied at both temperatures, the elevated temperature cross section at 1100–1200 K (ref 4 and 21) is plotted vs the 300 K value (ref 17). The room-temperature value for $N' = 5$ is plotted to minimize effects due to the rotational dependence; at 1200 K, the most probable value of N' is 4.5.

along with the temperature, a flame chemistry model is needed for interpretation, and even then ambiguities remain. However, three important conclusions can be drawn. First, the average σ_Q for H_2O decreases between 300 and 2300 K; second, quenching by H atoms is significant, with an average $\sigma_Q = 16$ Å² at 1200 K. Finally, the magnitude of the N' dependence for H_2O quenching diminishes with increasing temperature: at 300 K, $\sigma_Q(N'=3)/\sigma_Q(N'=16) = 1.7 \pm 0.2$ while at 2300 K the ratio is 1.02 ± 0.04.

This variation is consistent with our hypotheses about the collision dynamics. The σ_Q for each N' should decrease with temperature due to the governance by attractive forces (see below). However, that for low N' should decrease faster than for high N'. This is because, at a higher collision velocity, the enhancement due to the preferred orientations is less effective, in the same way that it is inhibited by faster rotation.

A separate measurement[53] of the N' dependence of quenching of OH by H_2O is in conspicuous disagreement with the results of Cleveland and Wiesenfeld (see Figure 3 of ref 48) and the mechanistic interpretation above. Multiphoton photolysis of H_2O at 248 nm produced $A^2\Sigma^+$ OH, and rotationally resolved emission was monitored. Time decay as a function of pressure was used to obtain σ_Q for $N' = 6$–17. The results show nearly constant σ_Q, within quoted error bars, for H_2O, N_2, and CO colliders, although the authors suggest that for H_2O there is a significant increase with N' for high N'.

Temperature Dependence of Quenching in OH

Collisional processes governed by attractive forces and complex formation have cross sections that decrease with increasing approach velocity. In contrast, when a potential barrier or repulsive wall dominates, the cross section will increase. Therefore, a determination of the velocity or temperature dependence provides important evidence regarding the nature of these intermolecular forces.

This connection, which had been considered for quenching of glyoxal,[18,54] was the motivation for the initial measurements of σ_Q for OH $A^2\Sigma^+$ at elevated temperatures.[4] These were performed in a laser pyrolysis/laser fluorescence (LP/LF) system.[55] A mixture containing SF_6, H_2O_2, and the collider was irradiated with a pulsed CO_2 laser. The infrared radiation is absorbed by the SF_6 and rapidly thermalized, thereby flash heating the system to temperatures as high as 1400 K; OH is formed by the pyrolysis of the peroxide. With proper attention to gas-dynamic processes following the initial heating, one has a homogeneous sample at high temperature in which to perform quenching studies using the time decay of LIF signals. The SF_6 is (fortunately!) a very

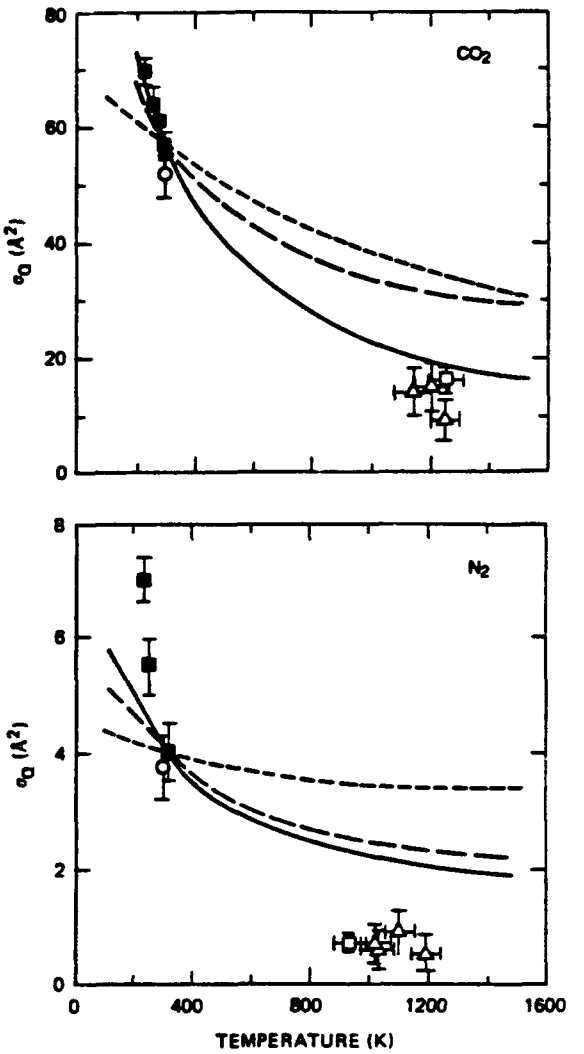

Figure 7. Experimental and calculated temperature dependence of quenching cross sections for $v' = 0$ for collisions with CO_2 (upper panel) and N_2 (lower panel): triangles, ref 4; open squares, ref 21; circles, 300 K thermal average calculated from the results of ref 17; filled squares, ref 56. The calculated temperature dependence arising from the shift in the N' distribution together with the N' dependence of σ_Q at 300 K is given by the short dashes. The calculated temperature dependence predicted by the multipole interaction model is shown by the long dashes. The solid line exhibits the combination of the both effects.

inefficient quencher but quite effective at RET. Therefore, the LP/LF results are for a thermal distribution in the excited state at the experimental temperature (obtained from excitation scans yielding $T_{rotational}$ in the ground state of the OH), and N'-specific cross sections cannot be determined.

In ref 4, σ_Q are reported for 11 quenchers at temperatures near 1100 K; some redeterminations and extensions to larger hydrocarbons are given in ref 21. For a proper comparison of these thermally averaged σ_Q with those at lower T, one must consider also the rotational dependence which, however, is known only at 300 K. In Figure 6, the thermally averaged σ_Q at 1100–1200 K, determined by LP/LF, is plotted vs $\sigma_Q(N'=5)$ measured at room temperature; this is the rotational level most highly populated at the elevated temperature. σ_Q decreases in all cases.

The temperature dependence of quenching was also investigated[56] at lower temperatures, 230–310 K, for the colliders H_2, N_2, O_2, and CO_2, by cooling with dry ice the flow cell described earlier. Argon was added at a pressure of 8–10 Torr so a thermal excited-state rotational distribution was always maintained. σ_Q for NH_3 was measured[57] over this range in the flow cell and also

(53) Papagiannakopoulos, P.; Fotakis, C. *J. Phys. Chem.* **1985**, *89*, 3439.
(54) Parmenter, C. S.; Seaver, M. *Chem. Phys.* **1980**, *53*, 333.
(55) Smith, G. P.; Fairchild, P. W.; Jeffries, J. B.; Crosley, D. R. *J. Phys. Chem.* **1985**, *89*, 1269.
(56) Copeland, R. A.; Crosley, D. R. *J. Chem. Phys.* **1986**, *84*, 3099.
(57) Jeffries, J. B.; Copeland, R. A.; Crosley, D. R. *J. Chem. Phys.* **1986**, *85*, 1898.

between 800 and 1450 K, using the LP/LF system. The results for CO_2 and N_2 (including the other LP/LF results[4,21]) are shown in Figure 7.

As T increases, the thermally averaged σ_Q decreases due to two effects. First, the attractive nature of the forces causes an inherent decrease for any N'; second, the distribution shifts to higher N' which have lower σ_Q at any T. The lines with long dashes in Figure 7 show the change from the first cause, calculated by use of the one-dimensional multipole interaction model. The lines with short dashes show the amount of decrease from the shifting distribution, assuming (perhaps incorrectly, as discussed above) the N' dependence does not vary with T; the solid lines represent the combined effect. In each case, the calculated values are matched to the experiments at 300 K. It appears that, even with these simple ideas, we understand reasonably well the attractive interactions for CO_2 collider. Other gases, save N_2, also fit this picture; see Figure 6 and ref 21, 56, and 57.

N_2 exhibits a much sharper decrease than the other colliders, which can be explained as follows. Nitrogen also quenches anomalously weakly; that is, a complex is formed but the $\Sigma-\Pi$ state mixing is not strong for N_2. At low T and thus lower collision energy the complex lives longer, allowing the collider-induced state mixing perturbation to last longer, but there is not enough time to effect sufficient mixing at the higher temperature. That is, for N_2 the probability P for quenching decreases with decreasing complex lifetime and with increasing T. In contrast, CO_2 and other colliders are so efficient that the $\Sigma-\Pi$ mixing is complete even for the shortest lived complex, and P is independent of T.

As one approaches much higher collision energies, and less effective quenching due to the attractive force interactions, the repulsive wall of the potential may begin to play a role in the quenching. For such a mechanism, σ_Q will become constant and eventually begin to increase with further increase in T. A constant or nearly constant value of σ_Q at high T is consistent with the combined LP/LF and flame results for H_2O quencher,[52] and an increase is hinted at in quenching by NH_3 at elevated temperature.[57]

The temperature dependence of VET in excited OH (or the other hydrides) has not been investigated. Besides its fundamental interest, it has practical significance for LIF monitoring of OH for both combustion and atmospheric chemistry. From the picture developed thus far, we expect a variation in σ_V similar to that in σ_Q for most colliders. For N_2, where the vibrational-state mixing is efficient in contrast to the ineffective electronic-state mixing, we anticipate a much smaller temperature variation in σ_V than was found for σ_Q.

Temperature Dependence of Quenching in NH, PH, and CH

LIF decay measurements[28] in the LP/LF system were also used to study quenching of the $A^3\Pi_i$ state of NH at 1400 K; the radical was produced by addition of small amounts of NH_3, which reacted with F atoms formed by pyrolysis of the SF_6. The rotational population is thermal, with $N' = 5$ most highly populated at this temperature, and so comparison should be made with the room-temperature values of σ_Q for this level.[25] As for OH quenching, NH_3 shows a large decrease, from 80 to 26 Å^2. There are also decreases for CH_4, CO, and O_2, but CO_2, N_2O, and H_2 exhibit no temperature dependence. For H_2O collider, comparison can be made between the room-temperature results and the flame measurements:[33] $\sigma_Q(N'=6)$ at 300 K is about twice the upper limit of 17 Å^2 measured at 2300 K. Thus, for the colliders that have evident dipole–dipole attractive interactions and large cross sections, increasing the temperature produces a decrease in σ_Q. This is in accord with the picture constructed for OH quenching. For nonpolar colliders, however, the behavior is varied, and the mechanism must involve more than simple complex formation with a constant $\Pi-\Sigma$ mixing interaction. This does not invalidate the explanation developed to describe the N' dependence, however. The initial stage of the collision could still consist of entrance channel dynamics on an anisotropic attractive surface, with the probability P of quenching controlled by subsequent, partner-dependent state mixing within that complex.

Quenching of thermal $NH(A^3\Pi_i)$ has been studied[40] at 300 and 415 K, for the same set of colliders listed above plus C_2H_6. The excited state was formed by photolysis of NH_3 in the presence of 100 Torr of Ar which produces thermalization but not quenching. Between these temperatures σ_Q decreased 10–25%, depending on collider, except for CO_2. The shift in rotational distribution between these two temperatures can account for only a 2–5% decrease.

The $A^3\Pi_i$ state of the PH radical is similar that of the isovalent NH. It too has been studied[58] at these same temperatures, 300 and 415 K, using 193-nm photolysis of PH_3 in the presence of Ar as the rotational relaxer. Individual σ_Q are similar though not identical with those for $NH(A^3\Pi_i)$, including small values for both N_2O and CO_2. For other molecules there is a 20–30% drop in σ_Q between these two temperatures. N_2 is especially interesting. It did not quench NH ($\sigma_Q < 0.006$ Å^2) but does quench PH with a small σ_Q of 0.6 Å^2 at 300 K. However, at 415 K, this has dropped to 0.36 Å^2, as for OH, quenching by this inefficient collider exhibits an especially large temperature dependence. One would then expect σ_Q to be much larger at cold temperatures and also to find a measurable value for NH in a sufficiently cold cell.

The $c^1\Pi$ state of NH has a collider specificity of σ_Q which mimics that of $A^2\Sigma^+$ OH, as noted above, and one might well expect a similar collision energy dependence. Two sets of LIF measurements have been made,[37] one exciting from $a^1\Delta$ at an equivalent translational temperature of 10 500 K and the other thermalized at 300 K, using Ar relaxer with a time delay following the photolysis laser. Recall that no rotational level dependence could be discerned at the higher temperature; if true for all T, a direct comparison is possible. For all nine colliders investigated, σ_Q was smaller at the higher energy; the amount of decrease ranged from 60% to 80%.

The temperature dependence of the quenching of $A^2\Delta$ CH is, however, quite different. Several investigations at different temperatures have included enough common colliders to form comparisons. In those at room temperature, excimer laser photolysis formed the excited state directly, and decay time measurements in the presence of a thermalizing rare gas furnished σ_Q. Results are available from ArF photolysis of acetone[59] and acetone or bromoform[38] and from KrF photolysis[60] of CH_2Br_2. The results from these three studies, tabulated in ref 60, spread over about a factor of 2 for common colliders; this is nonetheless suitable for an examination of the temperature dependence. Excimer laser dissociation of acetone and thermalization by Ar were also used[26] to measure σ_Q for several colliders at the elevated temperature of 415 K.

Quenching of this state has also been studied at higher temperature. The LP/LF method[61] was used for measurements at 1300 K, producing the radical by the reaction of added CH_4 with F atoms formed in the SF_6 pyrolysis. In addition, upper limits for σ_Q have been obtained near 1800 K in the low-pressure flame system[32,41] for H_2O, N_2, and CO_2. (These replace earlier values[40] where the ability to obtain only limits from these flames had not been recognized.)

Altogether, one has cross sections at different temperatures available for those three colliders and for H_2, O_2, CO, N_2O, and NH_3. For polar NH, σ_Q decreases slightly between 300 and 415 K and 30% further by 1300 K. The temperature dependence of σ_Q for CO, O_2, and H_2O is ambiguous; possible differences are smaller than error bars, and the interpretation depends on the choice of σ_Q at 300 K from among ref 38, 59, or 60. The other four colliders, however, show an increase in σ_Q as the temperature increases. The changes are dramatic: σ_Q doubles between 300 and 415 K and increases another factor of 5–20, depending on collider, going to 1300 K. The cross section limits at 1800 K are yet higher. This behavior is that expected for a collision governed by a potential barrier or repulsive wall. Assuming that barrier

(58) Kenner, R. D.; Pfannenberg, S.; Stuhl, F. Manuscript in preparation.
(59) Heinrich, P.; Kenner, R. D.; Stuhl, F. *Chem. Phys. Lett.* **1988**, *147*, 575.
(60) Becker, K. H.; Wiesen, P. *Z. Phys. Chem. (Munich)*, in press.
(61) Garland, N. L.; Crosley, D. R. *Chem. Phys. Lett.* **1987**, *134*, 189.

is responsible, its height may be obtained through an Arrhenius plot; the results of such an analysis[26] show activation energies ranging from 2 to 4 kcal/mol.

The temperature dependence for quenching $A^2\Delta$ CH is thus very different from that of the other radicals. For all colliders investigated, $A^2\Sigma^+$ OH and $c^1\Pi$ NH show a decrease in σ_Q with increasing T, and a decrease is found in most cases for quenching the $A^3\Pi_i$ states of both NH and PH. This indication of the role of attractive forces makes sense, at least for the A states of OH and NH, in view of their dipole moments, 2.0 and 1.3 D, respectively. However, the A state of CH has a comparable dipole moment of 0.9 D. Thus, if a mechanism involving long-range attractive forces and complex formation is responsible for quenching of the other radicals, a simple view would suggest it should be for CH as well. This appears true for the polar collider NH_3 but not H_2O, while in most other cases the quenching seems to be governed by a barrier, even though the cross sections are fairly large, a few Å^2. Therefore, the collision must involve more complicated interactions than only long-range attractive forces. We do know that such an extension of these simple collision complex ideas breaks down in another case for these same species, the comparison of VET in the excited and ground[62] electronic states of OH. For the polar colliders NH_3 and H_2O, σ_V for the $X^2\Pi_i$ and $A^2\Sigma^+$ states are quite similar. However, for other colliders, VET proceeds 100–1000 times more slowly in the ground state. Both states have comparable dipole moments (that of the X state is 1.7 D), so in this case more than just the long-range part of the potential must be involved.

Recall that, like NH and OH, CH exhibited a decrease in σ_Q with increasing N'. Therefore, it appears that in CH the surface is also anisotropic. Perhaps a complex is indeed involved, with entrance channel dynamics controlling its formation, but if so, then the Δ–Π state mixing within the complex must be governed by some repulsive interaction occurring on a different region of the potential surface.

Summary

We have reviewed experiments investigating the rotational level and translational energy dependence of collisions of electronically excited states of simple diatomic hydrides. For processes of quenching and VET that proceed more rapidly than rotational thermalization, the cross section decreases with increasing N', suggesting an anisotropic potential surface. For $A^2\Sigma^+$ OH, there exists considerable evidence suggesting the role of long-range attractive forces, including a decrease in σ_Q with increasing temperature, and it appears that collisions of this molecule are relatively well described by such a simple picture. For NH and CH matters are more complex. The N' dependence again suggests orientational effects, but the variation with temperature is not uniform and clearly indicates repulsive forces for CH. Such variations in behavior among otherwise similar radicals, between two excited states of the same radical (NH), and for various collision partners are not simply explained. They should therefore provide good tests of more detailed theoretical treatments of the collisions of these small, computationally tractable species. Several useful future experiments are immediately evident, such as the N' dependence of quenching of $NH(c^1\Pi)$ at room temperature and the temperature dependence of VET in $OH(A^2\Sigma^+)$. As more information becomes available, these unusual effects in these interesting excited diatomic hydride species should continue to enhance our knowledge of molecular collision dynamics.

Acknowledgment. That part of this research performed in my laboratories has involved many colleagues, whose roles in both the experiments and the continually evolving interpretations has been essential. I am pleased to acknowledge Richard Copeland, Mark Dyer, Paul Fairchild, Nancy Garland, Jay Jeffries, Katharina Kohse-Höinghaus, Russell Lengel, Karen Rensberger, Gregory Smith, and Michael Wise for their participation. Different portions were supported at various times by various agencies; I am grateful for funding from the National Aeronautics and Space Administration, the National Science Foundation, the Army Research Office, the Department of Energy, the Gas Research Institute, the Air Force Wright Aeronautical Laboratories, and the Air Force Office of Scientific Research. This review was written while on leave at the Ruhr-Universität in Bochum, Federal Republic of Germany. I thank Professor Fred Stuhl and his research group for their kind hospitality and many interesting and helpful discussions and the Deutsche Forschungsgemeinschaft (SFB 42) for providing financial support for this visit.

Registry No. OH, 3352-57-6; NH, 13774-92-0; CH, 3315-37-5.

(62) Rensberger, K. J.; Jeffries, J. B.; Crosley, D. R. *J. Chem. Phys.* **1989**, *90*, 2174.

Appendix H

LASER-INDUCED FLUORESCENCE AND DISSOCIATION OF ACETYLENE IN FLAMES

CONFERENCE PROCEEDINGS **191**

OPTICAL SCIENCE AND ENGINEERING SERIES 10

RITA G. LERNER
SERIES EDITOR

ADVANCES IN LASER SCIENCE–IV

PROCEEDINGS OF THE FOURTH INTERNATIONAL LASER SCIENCE CONFERENCE

ATLANTA, GA 1988

EDITORS:

JAMES L. GOLE, PROGRAM CHAIR
GEORGIA INSTITUTE OF TECHNOLOGY

DONALD F. HELLER, PROGRAM VICE-CHAIR
LIGHT AGE, INC., MT. BETHEL, NEW JERSEY

MARSHALL LAPP, CONFERENCE CHAIR
SANDIA NATIONAL LABORATORIES AND
LAWRENCE LIVERMORE NATIONAL LABORATORIES

WILLIAM C. STWALLEY, ADMINISTRATIVE VICE-CHAIR
UNIVERSITY OF IOWA

AIP
American Institute of Physics **New York**

LASER-INDUCED FLUORESCENCE AND DISSOCIATION OF ACETYLENE IN FLAMES

George A. Raiche, David R. Crosley and Richard A. Copeland
Molecular Physics Laboratory, SRI International
Menlo Park, California 94025

ABSTRACT

Laser-induced fluorescence and photoinduced dissociation of acetylene is observed in both room temperature cells and low-pressure flames. Acetylene is excited via the $\tilde{A}$-$\tilde{X}$ electronic transition between 210 and 230 nm. The fluorescence exhibits long vibronic progressions due to the different equilibrium geometries; acetylene is trans-planar in the $\tilde{A}$ state and linear in the $\tilde{X}$ state. Intense fluorescence from electronically excited carbon radicals (C_2^*) is also observed upon resonant excitation of C_2H_2 at room and flame temperatures. In addition, a non-resonant laser-induced production of C_2^* is observed in the flame. The effects of C_2H_2 pressure (i.e., electronic quenching) and laser fluence on fluorescence are examined.

INTRODUCTION

Acetylene is an important chemical intermediate in hydrocarbon combustion and is likely a key species in soot formation. Although its fundamental spectroscopy and photophysics have been well studied,[1] its optical detection in the high temperature environment of flames has proven difficult.[2] Acetylene absorbs at many discrete wavelengths in the 210-240 nm region and fluoresces throughout the ultraviolet in the $\tilde{A}$-$\tilde{X}$ electronic system. In multiphoton experiments at 193 nm C_2H_2 photodissociates into electronically excited C_2^* and CH* radicals that emit throughout the visible.[3] We report here on the detection of C_2H_2 in both low-pressure flames and a room temperature flow cell via laser-induced fluorescence (LIF) and photodissociation methods. In these experiments the output of a frequency-doubled excimer-pumped dye laser (210 to 240 nm) excites C_2H_2, and the resulting fluorescence is dispersed by a monochromator and monitored with a photomultiplier tube. The amplified signals are then captured by a transient digitizer or a boxcar integrator.

ACETYLENE FLUORESCENCE AND PHOTODISSOCIATION

We have observed strong fluorescence signals from both acetylene and C_2^* following resonant excitation of rotationally resolved vibronic bands in the C_2H_2 $\tilde{A}$-$\tilde{X}$ electronic system. The ultraviolet and visible emissions resulting from excitation of the $\nu_3 = 4$ level of the A-state at 215.9 nm are depicted in Figure 1, which has not been corrected for the wavelength response of the detection setup. The dominant features in the spectrum are emissions from the C_2 Swan ($d^3\Pi_g$-$a^3\Pi_u$) and Deslandres-d'Azambuja ($C^1\Pi_g$-$A^1\Pi_u$) systems, although C_2H_2 $\tilde{A}$-$\tilde{X}$ LIF is also observed. The C_2^* emission signals rise promptly with the laser pulse, indicating a unimolecular mechanism for formation of both excited states. Higher resolution emission scans reveal vibrational structure and show population up to $v = 3$ in the C state and $v = 6$ in the d state.

The apparent ratios of the C_2^* to $C_2H_2^*$ signal intensities are the result of three experimentally controlled parameters: C_2H_2 pressure, laser fluence, and excited vibrational level in the $\tilde{A}$ state. From the temporal evolution of fluorescence for the different emissions, individual decay constants are determined by fitting the decay to a

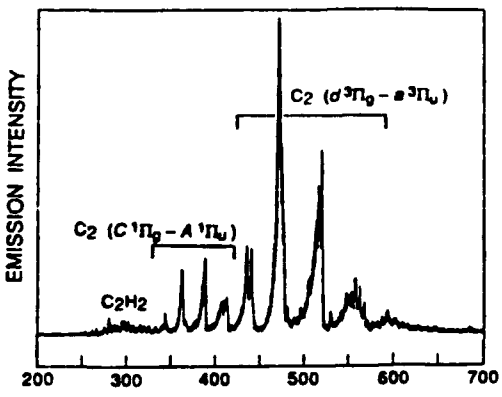

Figure 1

single exponential, while phenomenological total removal rate constants are taken from the slope of the line relating these decay constants to C_2H_2 pressure. The intercepts correspond to the radiative lifetime. We find that the emission from C_2H_2 is rapidly quenched ($\sim 5 \times 10^{-10}$ cm^3 s^{-1} for $\nu_3 = 3$) while quenching of the C and d states of C_2^* is approximately two and four times slower, respectively. At the ~1 Torr pressure of Fig. 1, the C_2^* d-state signal is enhanced relative to the other emissions and probably will be stronger in higher pressure flame conditions.

Another contribution to this ratio is the non-linear nature of the C_2^* production mechanism. While a detailed mechanism has not been isolated, the energetic requirements of the dissociation of C_2H_2 to C_2^* (C, d) dictate that at least one additional photon must be absorbed by the $\tilde{A}$ state in order to photodissociate to electronically and vibrationally excited C_2. In this wavelength region, we observe C_2^* production only with resonant excitation of the $\tilde{A}$ state. In fact, dissociation through a 1+1 mechanism would require the concerted elimination of H_2, an unlikely event. A more likely scenario involves absorption of one photon to the $\tilde{A}$ state and two more photons by the $\tilde{A}$ state (or a rapid predissociation product, possibly C_2H) to allow sequential elimination of hydrogen. Our power dependence studies indicate that the C_2^* signal scales approximately as the laser power squared, while the C_2H_2 signal is slightly less than linear between ~0.2 and 2.0 GW cm^{-2}. Because of these different laser power functions, the C_2^* signals are strongly enhanced at high power and tight focusing (Fig. 1, ~5 GW cm^{-2}).

The ratio also strongly depends on the C_2H_2 excitation wavelength. For a fixed laser power C_2^* signal intensity increases with increasing ν_3' in the $\tilde{A}$ state. At ~1.4 GW cm^{-2}, the C_2^* signal varies from approximately five times the C_2H_2 LIF signal to negligible, as excitation in ν_3 varies from 3 to 1 quanta. An apparent threshold for C_2^* production, observed between $\nu_3' = 1$ and $\nu_3' = 2$ (231.0 and 225.6 nm, respectively), is consistent with an excitation mechanism that involves a rapid predissociation from C_2H_2 $\tilde{A}$ to a C_2^* precursor, possibly C_2H. *In summary, high pressures, high laser fluence, and shorter excitation wavelengths all favor the production of C_2^* emission over C_2H_2 LIF.*

ACETYLENE FLAME STUDIES

All of the above-mentioned factors determine that C_2^* emission may be a very suitable diagnostic for C_2H_2 flame concentrations. Our studies have shown that the excitation spectrum of acetylene, useful as a "fingerprint" in room temperature experiments, can also be used to identify acetylene in the flame environment with rotational resolution. Using C_2^* laser-induced emission as the acetylene diagnostic, and tuning to a known C_2H_2 transition, we measure a one-dimensional spatial distribution

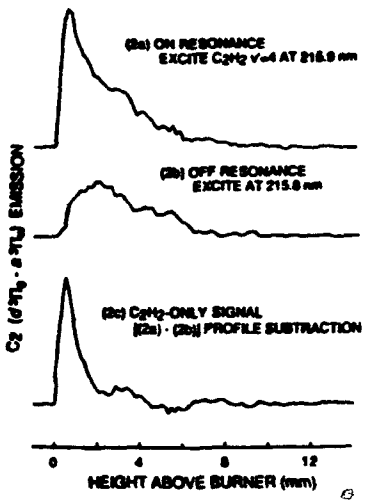

Figure 2

of C_2^* signal in a stoichiometric, 3 Torr C_2H_2/O_2 flame. Figure 2a is such a profile of C_2^* emission intensity as a function of the height of the laser beam above the burner surface. These profiles are useful as maps of acetylene concentrations in flames only to the extent that the C_2^* emission signal can be directly related to C_2H_2 concentration. Room temperature C_2^* production is strictly a resonant process through C_2H_2; however, the laser-correlated production of C_2^* in flames is observed even when the excitation laser is tuned off a C_2H_2 resonance, as shown in Fig. 2b. This nonresonant C_2^* excitation constitutes an interference to its use as a diagnostic for acetylene. In Fig. 2a note the sharp rise and slower decay of the signal over ~5 mm. In Fig. 2b note the slow signal rise, which we also attribute to C_2^* emission. Since the non-resonant background signal is not a strong function of laser wavelength, it also contributes to the Fig. 2a signal which therefore represents the sum of the resonantly and nonresonantly produced C_2^* emissions. A subtraction, representing the emission directly attributable to C_2H_2 excitation, is shown in Fig. 2c. Note the sharp rise and decay of the emission signal, indicating the rapid consumption of acetylene in the flame front. Clearly, some of the C_2^* laser-induced emission observed in the flame cannot be directly attributed to C_2H_2 excitation. The emission spectrum of the nonresonant excitation is identical with that of the resonantly-produced emission, suggesting a common excitation pathway following thermal or laser-induced dissociation of C_2H_2. In most flames this interference has not hampered our detection of C_2H_2, and upon further investigation should prove interesting in its own right.

ACKNOWLEDGEMENT

This work is supported by the Aero Propulsion Laboratory of the Air Force Wright Aeronautical Laboratories and the Physical Sciences Department of the Gas Research Institute.

REFERENCES

1. J.K.G. Watson, M. Herman, J. C. Van Craen, and R. Colin, J. Mol. Spectrosc. 95, 101 (1982); J. C. Stephenson, J. A. Blazy, and D. S. King, Chem. Phys. 85, 31 (1984); J. C. Van Craen, M. Herman, R. Colin, and J.K.G. Watson, J. Mol. Spectrosc. 111, 185 (1985); M. Fujii, A. Haijima, and M. Ito, Chem. Phys. Lett. 150, 380 (1988).

2. R. L. Farrow, R. P. Lucht, W. L. Flower, and R. E. Palmer, Proceedings of the Twentieth International Symposium on Combustion, p. 1307, The Combustion Institute, 1984.

3. J. R. McDonald, A. P. Baronarski, and V. M. Donnelly, Chem. Phys. 33, 161 (1978); H. Okabe, R. J. Cody, and J. E. Allen, Jr., Chem. Phys. 92, 67 (1985).

Appendix I

LASER-INDUCED FLUORESCENCE DETECTION OF SINGLET CH_2 IN LOW-PRESSURE METHANE/OXYGEN FLAMES

LASER-INDUCED FLUORESCENCE DETECTION OF SINGLET CH_2 IN LOW-PRESSURE METHANE/OXYGEN FLAMES

Andrew D. Sappey, David R. Crosley, and Richard A. Copeland
Molecular Physics Laboratory
SRI International
Menlo Park, California 94025

ABSTRACT

Methylene, CH_2, is a chemically important intermediate in hydrocarbon combustion but has previously eluded optical detection in a combustion environment. The CH_2 signal as a function of height above the burner surface in a premixed, laminar, methane/oxygen flame (5.6 Torr and fuel equivalence ratio = 0.88) is measured by laser-induced fluorescence (LIF) in the $\tilde{b}^1B_1$-$\tilde{a}^1A_1$ electronic system. The $\tilde{a}$ state which lies ~3165 cm^{-1} above the ground state is populated at the high temperatures of the flame (800-1800 K). Although less than one photon for each laser pulse is detected, we can unambiguously attribute the LIF features in the region 450 to 650 nm to CH_2 by both scanning the excitation laser and dispersing the fluorescence. LIF temperatures and CH and OH LIF concentration profiles are also obtained for the flame. The CH_2 radical concentration maximum occurs closer to the burner than that of either OH or CH, as expected from models of methane combustion chemistry.

Paper 89-48 Fall Meeting of the Western States Section of the Combustion Institute, Livermore, California, October, 1989.

MP 89-193
October 9, 1989

INTRODUCTION

The methylene radical, CH_2, is generated during the early stages of hydrocarbon fuel ignition and decomposition. Although many reactions of CH_2 have been studied at room temperature,[1] the precise role of methylene in the combustion process remains uncertain due to a lack of information on high temperature rate constants. Even so, methylene has been implicated in the buildup of higher hydrocarbons and ultimately the formation of soot.[2,3] Methylene is fundamentally interesting because of the relationship between electronic structure and reactivity. It has two low-lying electronic states, the triplet ground state, $\tilde{X}^3B_1$, and the metastable $\tilde{a}^1A_1$ singlet state, which lies ~3165 cm^{-1} above the $\tilde{X}$ state[4] and is more reactive.[5] These two states may act independently; therefore, the kinetics and energy transfer of the two states may need to be individually considered in reaction kinetic mechanisms.

Clearly, detection of methylene in a well characterized combustion environment is a highly desirable goal. Unfortunately, the only known triplet excited state of CH_2 lies at such high energy[6] (~88,000 cm^{-1}) that excitation with lasers from the ground state is not feasible under combustion conditions. However, in room temperature cell experiments, laser-induced fluorescence (LIF) has been observed in the $\tilde{b}^1B_1$-$\tilde{a}^1A_1$ system of singlet CH_2 created directly in the $\tilde{a}$ state by the photodissociation of either acetic anhydride or ketene.[7-10] This system is observed throughout the visible region of the spectrum. Approximately 1% of the CH_2 molecules will be in the metastable $\tilde{a}$ state at combustion temperatures if the singlet and triplet states equilibrate.

We report the first optical detection of singlet CH_2 in a combustion system. We excite the (0,14,0)-(0,0,0), (0,16,0)-(0,0,0), and (0,20,0)-(0,0,0) vibrational bands

[(v_1',v_2',v_3')-(v_1'',v_2'',v_3'')] of the $\tilde{b}$-$\tilde{a}$ electronic system in a 5.6 Torr, $\phi = 0.88$ methane/oxygen flame. The fuel equivalence ratio, ϕ, is defined as the mole ratio of fuel to oxidizer taking into account flame stoichiometry. The largest signal is obtained by exciting the Σ-Π Q bandhead of the (0,16,0)-(0,0,0) vibrational transition at 18597 cm^{-1} and observing fluorescence with a filtered phototube centered on the (0,16,0)-(0,1,0) band. Even this signal only amounts to one CH_2 fluorescence photon every 3 to 5 laser pulses. Factors influencing the signal are discussed. Methylene signal levels decrease as a function of increased pressure and/or increased fuel equivalence ratio. We observe many unassigned transitions at least one of which is larger than the assigned (0,16,0)-(0,0,0) features, underscoring the need for a thorough understanding of the spectroscopy of this complicated, highly perturbed molecule for diagnostic purposes. Relative concentration profiles of OH, CH, and CH_2 for this flame are obtained, and the flame temperature gradient is probed via rotationally resolved OH excitation scans. Finally, we estimate the absolute signal sizes of CH_2 relative to CH. The data show unequivocally that the CH_2 concentration peaks before CH and OH in the flame, consistent with longstanding models of hydrocarbon combustion.

CH_2 SPECTROSCOPY

Before describing the experiments, we briefly summarize the important spectroscopic properties of the methylene radical. The visible spectrum of singlet methylene in the region from 11,000 to 22,000 cm^{-1} has been studied extensively and partially assigned by Herzberg and Johns,[6] Ashfold et al.,[10] and Petek et al.[11] The spectrum is due to a $^1B_1$-$^1A_1$ transition between two electronic states which correlate with the degenerate $^1\Delta$ state in the linear representation. The degeneracy is removed by strong coupling between electron orbital and vibronic angular momentum. Also known as the

Renner-Teller effect, this coupling produces a strongly bent $^1A_1$ lower state and a nearly linear $^1B_1$ excited state.[6] Accurate potential energy curves have been determined for the two states.[12] The assigned bands of the visible spectrum correspond to a progression in the excited state bending mode, ν_2, i.e., $(0,\nu'_2,0)$-$(0,0,0)$ with $\nu'_2 = 12$-20. Each member of the progression is composed of multiple subbands, the strongest of which are similar to Σ-Π bands of a linear molecule for ν'_2 = even ($K'_a = 0 \leftarrow K''_a = 1$) and Π-Σ for ν'_2 = odd ($K'_a = 1 \leftarrow K''_a = 0$). Here K_a is the projection of the sum of rotational, vibrational, and electronic angular momenta on the principal symmetry axis. Weaker subbands corresponding to excitation of $K'_a = 2,3,4,...$, occur to the red of the strong Σ-Π and Π-Σ subbands. The primary selection rules[6,11] are: $\Delta J = 0, \pm 1$, $\Delta K_a = \pm 1$, and $\Delta K_c = 0, \pm 2$, although recent stimulated emission pumping experiments[13] show abnormally strong $\Delta K_a = \pm 3$ bands. Each subband consists of six main branches for $K'_a > 0$ while only three branches exist for $K'_a = 0$ excited states. Methylene contains two identical hydrogen nuclei of spin 1/2 (similar to H_2O); the lower state nuclear spin degeneracy is three for antisymmetric levels and one for symmetric levels. This results in a pronounced intensity alternation in the CH_2 spectrum.

Thus, in theory, the spectroscopy of CH_2 is understood. In practice, the CH_2 $\tilde{a}$ and $\tilde{b}$ states are highly perturbed by the triplet ground state and by each other. In an elegant study by Petek et al.[11] of CH_2 produced by photodissociation of ketene, 10000 transitions are observed from 15000-18000 cm^{-1}, only 477 of which are readily assignable; the translational temperature of singlet methylene is estimated to be 355 K from the Doppler width of the transitions. At the elevated temperatures in a flame (1500-2000 K), we expect the spectrum to be considerably more complex.

Figure 1 is a schematic vibronic energy level diagram of the relevant levels of the $\tilde{X}$ and $\tilde{a}$ states of methylene. The lowest vibrational level of the $\tilde{a}$ state lies at slightly higher energies than the (1,0,0) and (0,0,1) vibrational states of the triplet. The details of the

interaction of these vibrational states have been characterized.[14] In order to avoid some of the complications of unassigned lines and new features, we excite definitively assigned transitions of the Σ-Π subbands of (0,14,0) and (0,16,0) bands. In an attempt to understand how the Franck-Condon overlaps change as a function of the excited v'_2 level, we also excite CH_2 in the vicinity of the (0,20,0)-(0,0,0) Σ-Π Q branch bandhead. This vibrational bandhead is observed by Ashfold et al.[10] but not assigned rotationally.

EXPERIMENTAL APPARATUS

These experiments are performed in a low-pressure flat-flame combustion apparatus which has been described in detail previously.[15] Briefly, a McKenna Products flat-flame porous-plug burner is translated vertically on a motor-driven translation stage. The premixed laminar flat flame is scanned through the stationary laser beam to obtain LIF signal profiles of various combustion species. The burner and translation stage are mounted in a stainless steel vacuum chamber evacuated by a mechanical pump. The burner and exhaust manifold are water cooled to maintain stable operating conditions. Gases are introduced into the burner via a series of calibrated mass flow meters and fine metering valves. The premixed methane/oxygen flame is held at 5.6-6.0 Torr and has a fuel equivalence ratio, ϕ, of 0.88. The flows of CH_4 and O_2 are 428 and 970 standard cubic centimeters per minute, respectively. No gas flows through the flame shroud in the burner head.

Optical access for the excitation laser is provided by two Brewster windows. For the observation of fluorescence, light is collected using either a two-lens collection system as described previously[15] or a three-lens system with a depth-of-field limiting aperture which effectively reduces the amount of background flame emission. The first lens (4"

focal length, 2" diameter) collimates the light and the second lens (2" f.l., 2" dia.) focuses the image of the laser beam on a variable width rectangular slit (nominally 1 mm wide) which serves as a field stop. The strongly diverging light coming through the slit is collected by the third lens (2" f.l., 2" dia) and focused on to the slit of a monochromator or a filtered phototube approximately 25 cm from the third lens. We align the collection optics by maximizing the signal from Raman shifted laser light in air. Calibration of the light collection system including reflection losses, collection solid angle, photocathode quantum efficiency, photomultiplier tube gain, and preamplifier gain is achieved by Raman scattering in H_2 utilizing the method of Bischel , Bamford and Jusinski.[16]

CH_2 EXCITATION AND FLUORESCENCE SPECTRA

For most diatomic molecules enough information is available to determine the best excitation and detection wavelengths for LIF detection in a flame. For methylene such information is not complete. Unfortunately, little quantitative data is available on the relative strengths of the different vibrational bands. In the flame, we examine the excitation of the (0,14,0)-(0,0,0), (0,16,0)-(0,0,0) and (0,20,0)-(0,0,0) vibrational bands and the wavelength dependence of the resulting fluorescence. Under all conditions the CH_2 LIF signals are weak with the signal to noise ratio peaking at about 5 to 1 for our averaging of 250 shots at each wavelength position. The small signals limit the quality and quantity of spectroscopic data that we can obtain from the flame.

Many of the rotational features in the excitation spectra cannot be assigned to known transitions; extreme care must be exercised in their assignment. The dispersed fluorescence spectra are easier to understand; consequently we describe them first. To our knowledge, the only fluorescence spectrum in the literature is obtained by Feldmann et al.[7]

for excitation of the (0,14,0) level. The fluorescence spectrum which we obser ' for the (0,14,0) level is qualitatively similar to their published spectrum. With 4.0 nm monochromator resolution, we observe a feature near 642 nm assigned as the (0,14,0)-(0,1,0) band and a significantly weaker feature near 713 nm due to fluorescence to the (0,2,0) and (1,0,0) vibrational levels. For the ã state of CH_2, the ν_1 symmetric stretch mode is nearly resonant with two quanta of the bend; therefore, for weak signals, we cannot distinguish between (0,2,0) and (1,0,0), or (0,3,0) and (1,1,0) with 4 nm monochromator resolution. Because of a background due to scattered laser light we cannot observe fluorescence to the (0,0,0) level. Grimley and Stephenson[9] state the Franck-Condon factors for the (0,14,0)-(0,0,0) and (0,14,0)-(0,1,0) bands are similar in magnitude. Fluorescence from the (0,16,0) level is shown in Figure 2(a). Not correcting for monochromator and photomultiplier tube response, we find the (0,16,0)-(0,1,0) feature to be about three times larger than the combination of the (0,16,0)-(0,2,0) and (0,16,0)-(1,0,0) bands. From the position of this combination feature, we believe most of the fluorescence is in the (0,16,0)-(0,2,0) band. In order to examine the effect of vibrational excitation in the b̃ state on the fluorescence pattern, we excited the Q head of the (0,20,0)-(0,0,0) band.[10] Interestingly, we observe that the maximum in the fluorescence signal shifts further away from the excitation wavelength in changing from the (0,16,0) to the (0,20,0) band. The maximum shifts from fluorescence terminating on the (0,1,0) level to the (0,2,0) and (1,0,0) combination (about twice as large) while the (0,3,0) and (1,1,0) combination is only slightly smaller than the (0,1,0) peak. No evidence for fluorescence to the (0,4,0), (1,2,0) and (2,0,0) grouping is seen.

For the discussion of excitation spectra we focus our attention on the (0,16,0)-(0,0,0) vibrational band. We choose this band because it is largely unperturbed,[11] rotational distributions have been obtained in the past,[9] and it furnishes the largest signal of all the bands studied. Figure 3 is an excitation spectrum in the region of

the $^PQ_{1,J}$ branch bandhead of the (0,16,0)-(0,0,0) band. The notation $^PQ_{1,J}$ is defined as follows. The Q indicates that the J quantum number does not change in the transition; the p superscript denotes a ΔK_a change of -1. The subscript, 1, is the value of K_a'', and the subscript J is the value of K_c'' which here is the same as J". Also visible on the blue end of the spectrum is the region of the $^PR_{1,J-1}$ branch. The assignments are taken directly from Petek et al.[11] This spectrum is obtained by collecting fluorescence with a phototube equipped with filters which pass light in the region from 570-600 nm ((0,16,0)-(0,1,0) band). Many of the peaks are not assignable. The large number of unassigned features is typical of the CH_2 flame spectra. We find these unassigned rotational features have about the same signal profile as a function of height above the burner as the assigned CH_2 features, disappear at the same time on changing flame conditions, and exhibit the same fluorescence decay times. We therefore conclude that they are due to CH_2.

Petek et al.[17] observe at least 100 distinct but unassigned transitions in the same wavelength region. With the exception of one very large peak at 18633.49 cm^{-1}, all of the unassigned transitions in their data in this region are of much lower intensity than the assigned transitions. This is not the case with our data. The majority of unambiguously observed but unassigned transitions are at least as intense as the assigned transitions. This is most likely due to the elevated rotational temperature (1200-1800 K) at which our data is taken although the higher peak power of our laser system may contribute through saturation effects. In contrast, Petek et al. calculate the translational temperature in their experiments to be 355 ± 25 K (the vibrational temperature is much hotter ~1500 K).[11] Apparently, some of our transitions can be attributed to absorption of CH_2 in high angular momentum quantum levels of the $\tilde{a}$ (0,0,0) vibronic state.

Both Petek et al. and we observe an anomalously large unassigned peak at 18633.49 cm^{-1}; in the higher resolution data[17] (0.07 cm^{-1} bandwidth), the feature appears as a single peak. This feature is an example of the complexity of CH_2 spectroscopy and

demonstrates the extreme care that must be exercised in assigning features in the spectrum. (Initially, we assigned this feature to the (0,16,0)-(0,0,0) vibrational band.) In our lower resolution data (0.3 cm^{-1}), we also slightly overlap the (0,16,0)-(0,0,0) 3_{03}-2_{11} transition as shown in Figure 3. Figure 2 compares dispersed fluorescence spectra obtained by pumping the $PQ_{1,J}$ bandhead at 18597.5 cm^{-1} (upper trace) and the unassigned feature at 18633.49 cm^{-1} (lower trace). Excitation via the assigned bandhead gives a fluorescence spectrum with two peaks corresponding to (0,16,0)-(0,1,0) and (0,16,0)-(0,2,0)+(1,1,0) fluorescence at the anticipated wavelengths (583 and 629 nm, respectively). Excitation of the unassigned feature at 18633.49 cm^{-1} also gives rise to fluorescence at the wavelengths of the (0,16,0)-(0,1,0) and (0,2,0) bands, but additional peaks are present at 558 and 607 nm. Although we overlap very slightly the 3_{03}-2_{11} transition of the (0,16,0)-(0,0,0) band $PR_{1,J-1}$ branch when tuned to the unassigned feature, it is not sufficient to account for the large amount of fluorescence observed at 583 and 629 nm. Although the unidentified fluorescence peaks at 558 and 607 nm roughly correspond in wavelength to the positions of the (0,17,0)-(0,1,0) and (0,17,0)-(0,2,0)+(1,0,0) Π-Σ bands, we cannot explain fluorescence at all these wavelengths based on (0,16,0) or any other upper state energy level.

Figure 4 shows two excitation scans of the 18622-18642 cm^{-1} region. The upper trace is obtained by monitoring 583 nm fluorescence and the lower trace by monitoring the 607 nm fluorescence. A scan similar to the lower trace is obtained by monitoring 558 nm fluorescence. The lower trace shows absolutely no evidence of (0,16,0)-(0,0,0) $PR_{1,J-1}$ features, but at least two features, one quite large, are present. On the other hand, scanning the same region by detecting 583 nm fluorescence, one observes (0,16,0)-(0,0,0) $PR_{1,J-1}$ features and the two features which appear by themselves when monitoring the unassigned fluorescence features.

Because of the poor signal to noise, the flame is not the ideal environment to examine this interesting spectroscopic mystery in detail; however the preceding discussion does point out that a correct assignment of CH_2 features is essential to understanding both the concentration and fluorescence pattern of CH_2. Even though spectroscopic complications do persist, we have identified many of the features in this excitation region and for CH_2 concentration profiles, excite only features that correspond to the positions of lines in published spectra with identities confirmed by resolved fluorescence scans.

FLAME SELECTION AND RADICAL PROFILES

The CH_4/O_2 flame was initially selected for simplicity in modeling and lack of possible interfering higher hydrocarbons; however, tests of CH_2 signal size versus the identity of the fuel and oxidizer reveal that the initial choice was judicious. We find that the magnitude of the peak CH_2 signal decreases approximately linearly with the pressure, so the signal is reduced by about a factor of two increasing the pressure from 6 to 14 Torr. In addition, the peak of the CH_2 signal moves noticeably closer to the burner surface for the same change in pressure. The signal size also decreases for higher ϕ (richer flames). The CH_2 signal is no larger in ethane and acetylene/oxygen flames, and the acetylene flame suffers from increased C_2 flame emission interference. Finally, N_2O oxidizer created an extremely large non-resonant spurious LIF signal, perhaps from NO_2, that made any CH_2 signal unobservable. For this study, we choose to examine the lowest pressure CH_4/O_2 flame that can be stably and reproducibly operated in the low-pressure burner. The fuel equivalence ratio is adjusted to produce the largest signal. The flame pressure is 5.6-6.0 Torr with $\phi = 0.88$.

To characterize the experimental flame, we obtain LIF signals from CH_2, CH, and OH as a function of height above the burner surface. For the CH_2 and CH data, we capture over 90% of the fluorescence signal inside a boxcar gate of width 55 ns. In addition, we measure rotationally resolved OH LIF excitation scans to determine the flame temperature profile. For these, a 10 ns gate is set on the peak of the time dependent fluorescence signal to minimize the effect of collisions on the temperature measurement.[18] Figure 5 is a composite picture of these four profiles where the signals have been converted to concentration by the procedure outlined below. The CH radical profile is obtained by exciting the $P_{1ef}(7)$ rotational line in the $A^2\Delta$-$X^2\Pi$ (0,0) band.[15] Fluorescence is observed on the (0,0) band. The OH profile is obtained by pumping the $Q_1(6)$ line of the $A^2\Sigma^+$-$X^2\Pi_i$ (0,0) band.[19] Fluorescence in the (0,0) band is monitored. The CH_2 profile is obtained by exciting the (0,16,0)-(0,0,0) $PQ_{1,J}$ bandhead (see Fig. 2) with ~5 mJ of unfocussed light at 18597 cm^{-1} which excites molecules mostly from the 4_{14} and 2_{12} levels of the $\tilde{a}$(0,0,0) state. The profile is adjusted for background Raman scattering by subtracting a profile obtained by moving the excitation laser wavelength off a CH_2 resonance feature. In most cases the background signal is small (<10%) relative to the CH_2 LIF. The OH temperatures are obtained by fitting excitation scans of the R_2 bandhead region of the A-X (0,0) band.[18] Details of measuring CH, OH, and temperature profiles can be found in Refs. 15, 18, and 19, respectively. Only the quantitative aspects of CH and CH_2 results are discussed in this work. The OH profile is corrected for temperature but not collisional effects and no attempt has been made to make these measurements fully quantitative.

The absolute signal intensity for CH is approximately 30 times larger than the CH_2 signal for the flame tested. To convert LIF signal profiles to ground state radical concentration profiles, several factors must be addressed. These are: 1) calibration of the fluorescence collection system including photomultiplier and monochromator response; 2)

fluorescence quantum yield of the excited state; 3) the partition function for the molecules in the ground state; and 4) spectral considerations such as Franck-Condon factors and rotational line strengths for the excitation and fluorescence transitions. Although we are not able to quote final values for CH_2 and CH number densities, we will discuss the information we have obtained toward this goal.

The determination of the absolute density of a particular species from LIF requires an accurate calibration of the fluorescence collection system. A convenient means of calibration has been described by Bischel, Bamford and Jusinski.[16] The calibration involves spontaneous Raman scattering of a laser of known power flux by a known density of H_2. The procedure leads to a constant which includes effects such as geometrical factors, reflection losses, gain and quantum efficiency of the photomultiplier and gain of the electronics. However, one must use this procedure with special attention to the conditions of optical saturation, because the effective beam cross sectional area can be different for spontaneous Raman and saturated LIF. This problem prevents us from obtaining a CH and CH_2 number density in these experiments.

The fluorescence quantum yield of the excited state determines how many of the excited molecules fluoresce before they are lost to non-radiative processes. In the flame for the radicals considered here, the dominant loss process is electronic quenching via collisions with the other flame species. For CH, these quenching processes have been previously examined for a variety of flames as a function of height above the burner.[15] From these measurements, the fluorescence quantum yield for CH was found to be almost independent of position in the flame. No information is available for the quenching of CH_2 at high temperatures; therefore, we measured the time dependence of the LIF in the flame. This is complicated by the extremely rapid decay of the fluorescence. Using a 10 ns/point transient digitizer, we observe the temporal evolution of the CH_2 fluorescence following excitation of the (0,16,0)-(0,0,0) Q branch bandhead at several positions in the flame. We

fit the fluorescence signals to a single exponential from 90 to 10% of the peak of the signal. We find that the lifetimes are independent of position and equal to 45 ± 8 ns; the uncertainty is two standard deviations from the average value for six measurements throughout the flame. This value may be slightly affected by the response time of the detection electronics and the finite pulse width of the excitation laser. Therefore, the actual value may be slightly faster. Since the error introduced by neglecting this effect is smaller than many other approximations that would go into these measurements, a detailed deconvolution analysis is not warranted at this time.

The fluorescence decay time in the flame is significantly shorter than the radiative lifetime[10] of 3000 ns indicating substantial quenching of the excited CH_2. The average quenching rate constant in the flame is 5×10^{-10} cm^3s^{-1} assuming a temperature of 1500 K. Ashfold et al.[10] have measured quenching rate constants of the CH_2 $\tilde{b}$ state with various colliders such as O_2 and CH_4. Values of $2\text{-}4 \times 10^{-10}$ cm^3s^{-1} were obtained at room temperature. Considering the unknown identities of the collider species in the flame and possible changes in the collisional quenching cross section with temperature, the average observed quenching rate constant is quite reasonable. This value is faster than for the diatomic radicals CH,[15] NH,[20] and OH[19] under similar conditions. From these data, we estimate the fluorescence quantum yield for CH_2 to be 0.015 ± 0.004. The quantum yield estimate[15] for the A state of CH in the experimental flame is ~0.30 ± 0.10. The uncertainties are estimates based on our confidence in the input parameters.

The raw signal profiles are analyzed by taking into account population changes of the excited level due to the temperature gradient in the flame by normalizing to the Boltzmann population of the excited level as a function of height. The temperature profile is parametrized using a simple functional form to interpolate between the discrete temperature points.[15, 20] This temperature normalization is a trivial exercise for CH and OH, but much more complicated for CH_2. For CH_2 we choose to divide the partition

function into a vibronic part (both electronic and vibrational) and a rotational part. This assumes the rotational constants of the singlet and triplet level are the same and do not change with vibrational level. This approximation introduces only a small error in the partition function. The vibronic part is relatively simple to calculate. Figure 1 shows some of the important vibrational levels. The partition function is calculated by counting all possible vibrational levels of the ground state triplet and singlet excited states as though they belong to a single state except that the degeneracy of the triplet levels is three. The (0,0,0) level of the ã state lies ~3165 cm^{-1} higher in energy than the (0,0,0) level of the ground state and the calculation of the partition function follows straightforwardly.[4] Vibrational constants for the two states are obtained from Ref. 21. One caveat should be mentioned. Jensen, Bunker and Hoy[22] note that the energy level structure of the triplet is complicated by a low barrier to linearity which extensively mixes the bending vibration with rotation. This causes the vibrational levels of the triplet state to be poorly described by the harmonic oscillator approximation. However, we still use that approximation. We find 1.3% of the CH_2 molecules are in the (0,0,0) level of the ã state.

The calculation of the rotational partition function proceeds straightforwardly given the assumption of vibronic and rotational separability. We approximate the energy levels of CH_2 by the symmetric top formula which gives energies in the absence of asymmetry doubling. These energies approximate closely the average energy of an asymmetry doubled pair given in Ref. 11. Therefore, this approximation introduces almost no error. The K doubling, 2J+1 degeneracy, and nuclear spin statistics are included explicitly. These energies and degeneracies are used to calculate the denominator of the partition function. The numerator is calculated by using the actual energy of the excited level from Ref. 11 and the degeneracy of that level. The result of the calculation is that approximately 0.6% of the molecules in ã (0,0,0) are in the 4_{14} and 2_{12} levels at 1250 K. The total partition function increases quickly from 0.0001% at the burner surface (~500 K) to

0.0065% at 14 mm above the burner surface (~1550 K) and then stays nearly constant to 60 mm at ~1900 K.

Quantifying absolute ground state CH and CH_2 number densities from the number of photons collected also requires accurate vibrational band transition probabilities and rotational line strengths. This can be done accurately for CH because of the availability of the pertinent data;[15] however, that is not the case for CH_2. The radiative lifetime[10] of the Σ levels of the (0,16,0) is 3.0 μs. However, we can only make an intelligent guess of the relevant vibrational band transition strengths from the fluorescence intensity data. We also lack accurate rotational line strengths, although Grimley and Stephenson[9] have calculated and used rotational line strength factors for the (0,16,0)-(0,0,0) Σ-Π P branch lines to determine a rotational distribution. As stated in Ref. 11, calculated rotational line strengths could differ from the experimental values due to singlet-tripet mixing and the presence of other perturbations. Nonetheless, an estimate of the number density of singlet CH_2 can be extracted from these. To obtain a number density for total CH_2 in this flame, thermal equilibrium between the singlet and triplet must be assumed. Based on preliminary modeling of this flame,[23] we believe that equilibrium is not attained between singlet and triplet CH_2.

Preliminary attempt to quantify absolute CH and CH_2 concentrations failed because the Raman scattering light collection system calibration is not directly applicable to LIF measurements made under conditions of optical saturation. The laser conditions used to excite CH and CH_2 (17 μJ/pulse in 1.3×10^{-3} cm^2 and 5 mJ/pulse in 7.9×10^{-3} cm^2 respectively) saturate their respective transitions. Unfortunately, for saturated LIF, the wings of the laser beam can contribute to the signal as much as the peak. Thus, the effective cross sectional area of the laser beam is much larger than the area for the unsaturated Raman calibration measurement by at least a factor of 10. This uncertainty is directly transferred to the final concentration. This precludes the determination of absolute

concentrations. Future work will attempt to solve this problem. We are able, however, to make a direct comparison of signal sizes for CH and CH_2 excitation. The excitation parameters for each laser are as given in the preceding paragraph. Under these conditions, we observe a CH_2 signal of 850 mV at the peak of the CH_2 profile; all the fluorescence on the (0,16,0)-(0,1,0) band is captured in the 4 nm bandwidth of the monochromator to yield this signal. With the same optical train, we observe a CH signal of 3100 mV at the peak of the CH profile. However, not all CH (0-0) fluorescence is captured in the bandwidth of the monochromator and the boxcar scale is a factor of 4 less sensitive than for the CH_2 measurements. When this is taken into account, the actual CH signal is 23 volts. Other conditions such as phototube voltage are the same for the two measurements. Thus, one can expect approximately a factor of 30 larger signals from CH excitation the CH_2 excitation under our laser and flame conditions.

DISCUSSION

We have unambiguously detected CH_2 via LIF in the $\tilde{b}$-$\tilde{a}$ electronic system; however, the signals are extremely weak. Detection of polyatomic radicals in a combustion environment can be difficult, but the added complication of LIF excitation from an electronic state that is populated at the 1% level increases the difficulty considerably. For many combustion applications, CH_2 detection will not be feasible with this technique. However, in low-pressure flames, concentration profiles suitable for comparison with combustion models for singlet CH_2 can be obtained. Before discussion of this comparison, we discuss possible interferences with CH_2 detection and recommended transitions for excitation and fluorescence observation.

Briefly, CH_2 LIF signals are very different in character from those typically seen for diatomic molecules. For the diatomics, each laser pulse results in a large number of fluorescence photons in the bandwidth of the detector. For CH_2, we obtain less than one photon per pulse. Most of the noise in the spectra is due to the statistical variation in the number of photons detected. This can be improved by longer averaging. This also implies the larger the number of fluorescence photons from a given excitation and fluorescence combination the better the signal. In most cases this is correct; however, several important sources of interference need to be considered.

There are two major types of background interferences in the experiment, those created by the flame itself and those caused by the laser light. Chemiluminescent reactions in the flame generate visible continuous emission which is primarily composed of CH $B^2\Sigma^-$-$X^2\Pi$ and $A^2\Delta$-$X^2\Pi$ bands at 390 and 430 nm respectively and C_2 $d^3\Pi_u$-$a^3\Pi_g$ emission (the Swan system) at 470 ($\Delta v = +1$), 515 ($\Delta v = 0$), and 555 ($\Delta v = -1$) nm in the

spectral region of interest for CH_2 detection. If a monochromator is used, possible second order OH $A^2\Sigma^+$-$X^2\Pi_i$ emission near 620 nm can be eliminated by use of appropriate long pass filters. Many electronic and optical techniques can be applied to discriminate against this emission; for example, detection optics that limit the depth of field observing only the volume near the laser beam can be used.[26] In this initial study, we find that chemiluminescent emission causes some noise; however, its effects can be minimized. It is not the limiting noise source for these CH_2 signals.

Raman scattering from the major species of the flame is the largest background signal induced by the laser light in our experiments. Raman scattering from CH_4, O_2, and flame intermediates becomes stronger as the excitation wavelength is decreased because of the λ^{-4} dependence of the Raman cross section.[27] This makes Raman scattering a significant problem exciting the (0,20,0) transition but less of a problem on either the (0,14,0) or (0,16,0) levels. All of the Raman scattered photons are detected during the laser pulse within the nominal 50-ns boxcar gate used in this investigation, making it the dominant laser-induced noise source. We did not attempt to discriminate against the Raman signal by time-delaying the detection gate until after the laser pulse. For our experimental signal level (~0.2 photons/pulse) such gating would have resulted in a drastic decrease in the signal to noise ratio for the same averaging time, due to photon statistics. At low pressures, for excitation of the (0,16,0) vibrational transition, Raman scattering is less than 10% of the CH_2 signal; however as the pressure is increased, it becomes a greater problem. In addition, the CH_2 signal decreases at higher pressure. The Raman shifts for the major species CH_4, O_2, CO, CO_2, and H_2O are 2915, 1556, 2145, 1388, and 3657 cm^{-1}, respectively.[26] The resulting Raman spectrum is broad and relatively featureless, and on-resonance/off-resonance, subtractions can be used to minimize its effect. Rayleigh and Mie scattering preclude observation at the excitation wavelength. We also observe a background consisting of a very broad fluorescence to the red of the laser wavelength.

Under our experimental conditions this is a minor interference, but at higher pressures or for richer conditions such broad fluorescence might become significant. Possible origins and a discussion of this type of laser-induced signal can be found in Ref. 27.

Even with the interferences discussed above, the primary limit on signal to noise remains the photon statistics. Signal to noise ratio can be improved with greater patience; however, eventually a point is reached at which the stability of the burner system or the excitation laser becomes a problem. Therefore, the primary selection criterion is simply to choose the transition producing the greatest number of fluorescent photons (subject to the caveat that the interferences do not increase significantly). For CH_2 the radiative lifetimes decrease with increasing vibrational level from 4.6 μs for (0,12,0) to 2.5 μs for (0,20,0) indicating that excitation of the higher vibrational levels is better. However, the difference is only twofold and no information is available on the vibrational level dependence of quenching. Clearly, more work is needed to make the choices quantitative.

We find that excitation of the (0,16,0)-(0,0,0) band and detection of the (0,16,0)-(0,1,0) band provides the best signals with our excitation laser, optical detection system, and flame conditions. We also observe signals exciting (0,14,0) and (0,20,0) from the vibrationless level of the singlet state. For (0,20,0) excitation, Raman processes become a significant noise source and a rotational assignment of the excitation transition is lacking. Excitation of the (0,14,0) level results in smaller signals, and the (0,14,0) vibrational level is quite perturbed. We believe little difference should be seen exciting vibrational levels 15-17, and all of these levels could be used. In any case, extensive averaging will have to be undertaken to obtain signals.

Even if intense CH_2 LIF signals could be obtained, several approximations must be made to convert the measurement to total CH_2 concentration. Perhaps the most suspect assumption is that the singlet and triplet states of CH_2 are in chemical equilibrium. Indeed, a preliminary modeling study of this flame,[23] using reported reactivities for the two

electronic states, indicates that the singlet and triplet are not in equilibrium. With this in mind, it is interesting to make some general observations about the radical profiles. Note that none of these observations would change significantly for even large deviations of the singlet and triplet from chemical equilibrium. In fact, analysis of the CH_2 profile assuming thermal equilibrium of only the singlet state moves the peak of the CH_2 signal from ~9 mm to ~11 mm. Therefore, regardless of how the analysis of the CH_2 profile is performed, the CH_2 profile always peaks before the CH and OH profiles. This is the expected result as methane oxidation involves stepwise removal of hydrogen from carbon. This is the first optical experimental demonstration of the expected concentration profiles for CH and CH_2 in methane oxidation. The CH_2 profile is very noisy within about 5 mm of the burner surface due to temperature normalization; the small signal is divided by the partition function, which is a very small number at this position in the flame. Finally, one further caveat should be mentioned. These profiles are not obtained using a shroud flow around the flame[15]. Under the low pressure conditions of this experiment, the shroud causes the flame to blow off the burner. As a result, the gases have a tendency to diverge or mushroom. Thus, the flow speed is somewhat less than calculated from mass flow rates and the burner area, and the profiles are probably slightly altered as a result.

CONCLUSION

Although LIF detection of CH_2 in a high temperature environment is feasible as demonstrated by this work, the general applicability of the technique may be limited because of the low signal levels. The number densities of CH and CH_2 are probably similar, but the fraction of CH_2 molecules in the excited level is much lower, and the CH_2 $\tilde{b}$ state is rapidly quenched causing low signal levels. The CH_2 concentration peaks before CH in the flame, confirming longstanding theories of methane combustion; this conclusion is independent of chemical equilibrium and partition function assumptions. The possibility of chemical disequilibrium between singlet and triplet CH_2 needs to be addressed theoretically before this technique can be made truly quantitative for ground state CH_2. Experimentally, reliable vibrational band transition probabilities are needed as well as experimental rotational line strengths in a well characterized system. In addition, more accurate means of fluorescence collection system calibration must be devised. Future investigations will focus on these quantitative questions.

ACKNOWLEDGEMENTS

We thank Jay Jeffries and Greg Smith for many helpful discussions on the combustion chemistry of CH_2. We also thank Brad Moore for copies of unpublished spectra from Ref. 11. We gratefully acknowledge support for this research by the Aero Propulsion and Power Laboratory of the U.S. Air Force Wright Research and Development Center.

FIGURE CAPTIONS

Figure 1. Energy level diagram for the vibrational levels of singlet and triplet CH_2.

Figure 2. Fluorescence scans following excitation of CH_2 in a low-pressure methane/oxygen flame. These are uncorrected for the response of the detection system.

(a) Signal after excitation of the Q head of the (0,16,0)-(0,0,0) band near 18598 cm^{-1}.

(b) Signal after excitation of an unassigned CH_2 feature near 18633 cm^{-1}.

Figure 3. CH_2 excitation scans in which the energy of the photon is varied between 18600 and 18640 cm^{-1}. The fluorescence is detected at wavelengths between 570 and 600 nm. This corresponds to the position of the (0,16,0)-(0,1,0) band.

Figure 4. Excitation scans near the (0,16,0)-(0,0,0) R head monitoring fluorescence centered 582 nm (top) and 607 nm (bottom) with 4 nm bandwidth. Most features in the top spectrum have been assigned to known rotational transitions in the (0,16,0)-(0,0,0) band in Refs. 6 and 11.

Figure 5. Relative concentration and temperature measurements on the 5.6 -Torr, ϕ = 0.88 methane oxygen flame. In the top panel, OH rotational temperatures are plotted as a function of height above the burner surface as the squares. The solid line is a fitted parameterization of the profile as described in Ref.

15. The bottom panel shows the relative concentration profiles of the three species CH_2, CH, and OH. The CH_2 profile peaks closest to the burner surface. The CH profile peaks near 15 mm, while the OH concentration persists out into the burnt gases.

REFERENCES

1. Laufer, A. H. Rev. Chem. Intermed. **1981**, 4, 225.

2. Homann, K. H.; Schweinfurth, H. Ber. Bunsenges. Phys. Chem. **1981**, 85, 569.

3. Homann, K. H.; Wellmann, Ch. Ber. Bunsenges. Phys. Chem. **1983**, 87, 609.

4. McKellar, A. R. W.; Bunker, P. R.; Sears, T. J.; Evenson, K. M.; Saykally, R. J.; Langhoff, S. R. J. Chem. Phys. **1983**, 79, 5251.

5. Böhland, T.; Temps, F.; Wagner, H. Gg. Ber. Bunsenges. Phys. Chem. **1986**, 90, 468.

6. Herzberg, G.; Johns, J. W. C. Proc. R. Soc. London Ser. A **1966**, 295, 106.

7. Feldmann, D.; Meier, K.; Schmiedl, R.; Welge, K.H. Chem. Phys. Lett. **1978**, 60, 30.

8. Danon, J.; Filseth, S. V.; Feldmann, D.; Zacharias, H.; Dugan, C. H.; Welge, K. H. Chem. Phys. **1978**, 29, 345.

9. Grimley, A. J.; Stephenson, J. C. J. Chem. Phys. **1981**, 74, 447.

10. Ashfold, M. N. R.; Fullstone, M. A.; Hancock, G.; Ketley, G. W. Chem. Phys. **1981**, 55, 245.

11. Petek, H.; Nesbitt, D. J.; Darwin, D. C.; Moore, C. B. J. Chem. Phys. **1987**, 86, 1172.

12. Duxbury, G.; Jungen, Ch. Mol. Phys. **1988**, 63, 981.

13. Xie, W.; Ritter, A.; Harkin, C.; Kasturi, K.; Dai, H.-L. J. Chem. Phys. **1988**, 89, 7033.

14. Petek, H.; Nesbitt, D. J.; Moore, C. B.; Birss, F. W.; Ramsay, D. A. J. Chem. Phys. **1987**, 86, 1189.

15. Rensberger, K. J.; Dyer, M. J.; Copeland, R. A. Appl. Opt. **1988**, 27, 3679.

16. Bischel, W. K.; Bamford, D. J.; Jusinski, L. E. Appl. Opt. **1986**, 25, 1215.

17. Petek, H.; Nesbitt, D. J.; Darwin, D. C.; Moore, C. B. unpublished results.

18. Rensberger, K. J.; Jeffries, J. B.; Copeland, R. A.; Kohse-Höinghaus, K.; Wise, M. L.; Crosley, D. R. Appl. Opt. **1989**, 28, 3556.

19. Kohse-Höinghaus, K.; Jeffries, J. B.; Copeland, R. A.; Smith, G. P.; Crosley, D. R. Twenty-Second International Symposium on Combustion; p. 1857; 1988.

20. Copeland, R. A.; Wise, M. L.; Rensberger, K. J.; Crosley, D. R. Appl. Opt. **1989**, 28, 3199.

21. Comeau, D.C.; Shavitt, I.; Jensen, P.; Bunker, P.R. J.Chem. Phys. **1989**, 90, 6491.

22. Jenson, P.; Bunker, P. R.; Hoy, A. R. J. Chem. Phys. **1982**, 77, 5370.

23. Smith, G. P. private communication

24. Garland, N. L.; Crosley, D. R. J. Quant. Spectrosc. Radiat. Transfer **1985**, 33, 591.

25. Cross, P.C.; Hainer, R.M.; King, G.W. J. Chem. Phys. **1944**, 12, 210.

26. Dyer, M. J.; Pfefferle, L. D.; Crosley, D. R. Appl. Opt., in press, **1989**.

27. Eckbreth, A.C. "Laser Diagnostics for Combustion Temperature and Species," Abacus; Cambridge, **1988**, Chapter 5.

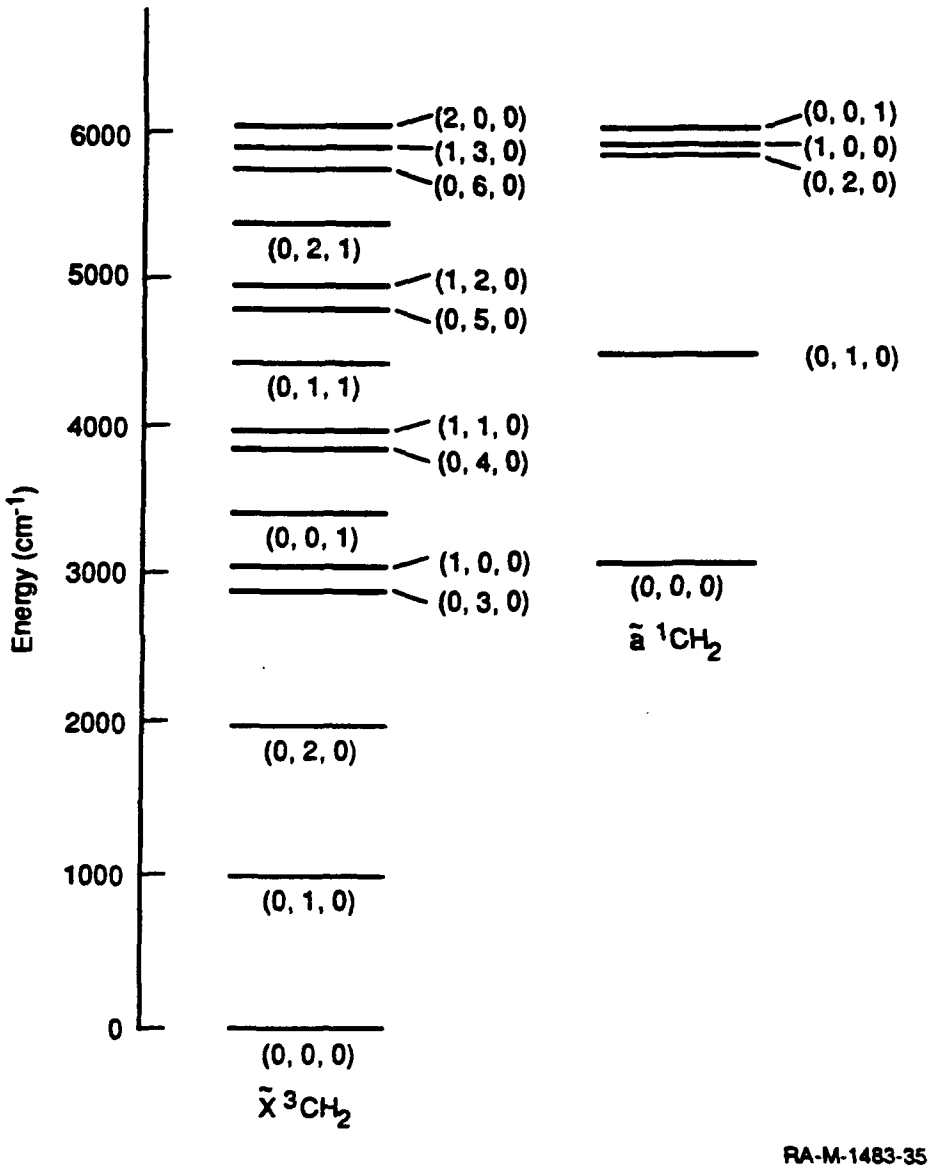
Energy (cm⁻¹)
6000
5000
4000
3000
2000
1000
0
(2, 0, 0)
(1, 3, 0)
(0, 6, 0)
(0, 2, 1)
(1, 2, 0)
(0, 5, 0)
(0, 1, 1)
(1, 1, 0)
(0, 4, 0)
(0, 0, 1)
(1, 0, 0)
(0, 3, 0)
(0, 2, 0)
(0, 1, 0)
(0, 0, 0)
X̃ ³CH₂
(0, 0, 1)
(1, 0, 0)
(0, 2, 0)
(0, 1, 0)
(0, 0, 0)
ã ¹CH₂
RA-M-1483-35

Figure 1

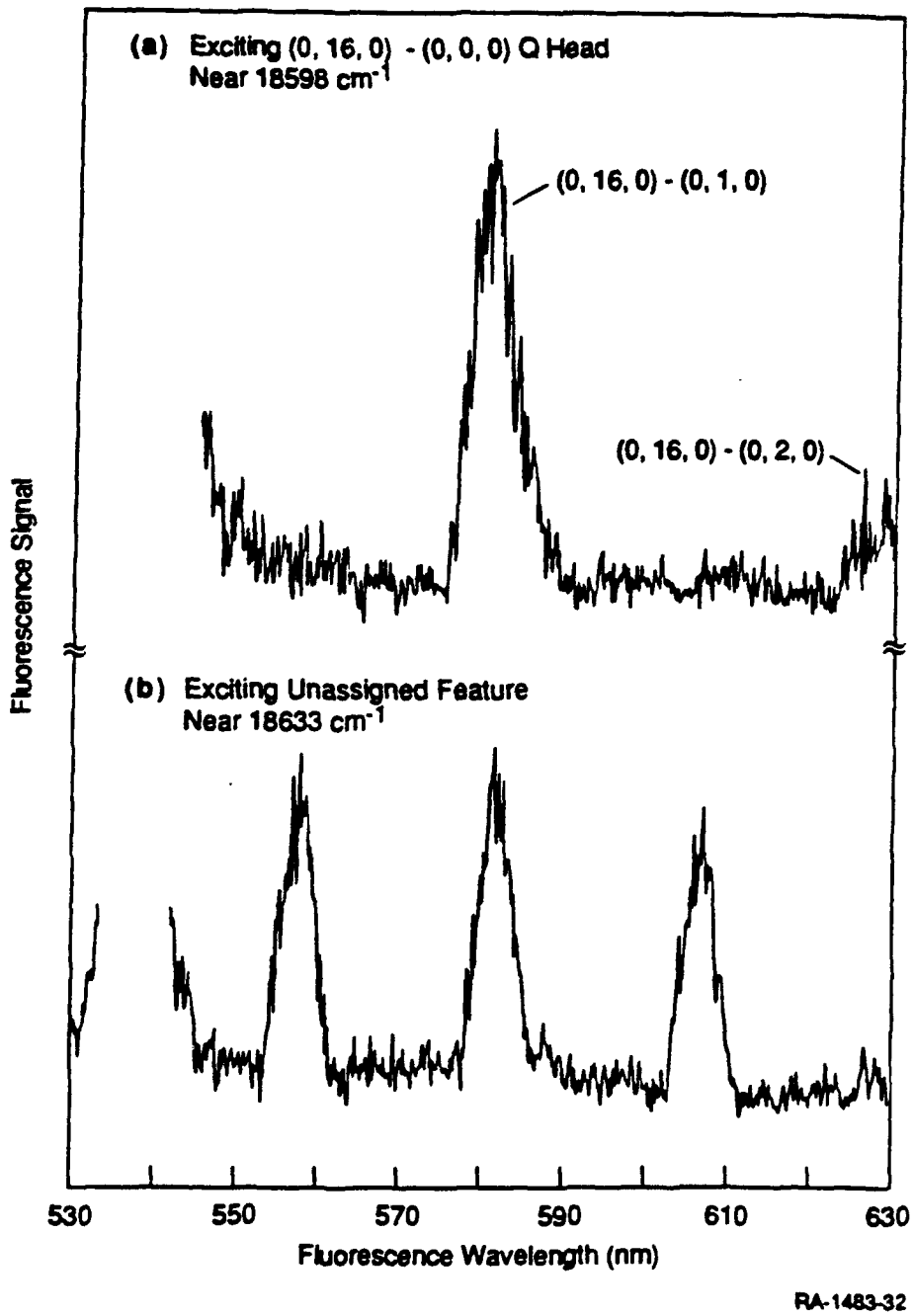
(a) Exciting (0, 16, 0) - (0, 0, 0) Q Head
Near 18598 cm-1
(0, 16, 0) - (0, 1, 0)
(0, 16, 0) - (0, 2, 0)
(b) Exciting Unassigned Feature
Near 18633 cm-1
Fluorescence Signal
530
550
570
590
610
630
Fluorescence Wavelength (nm)
RA-1483-32

Figure 2

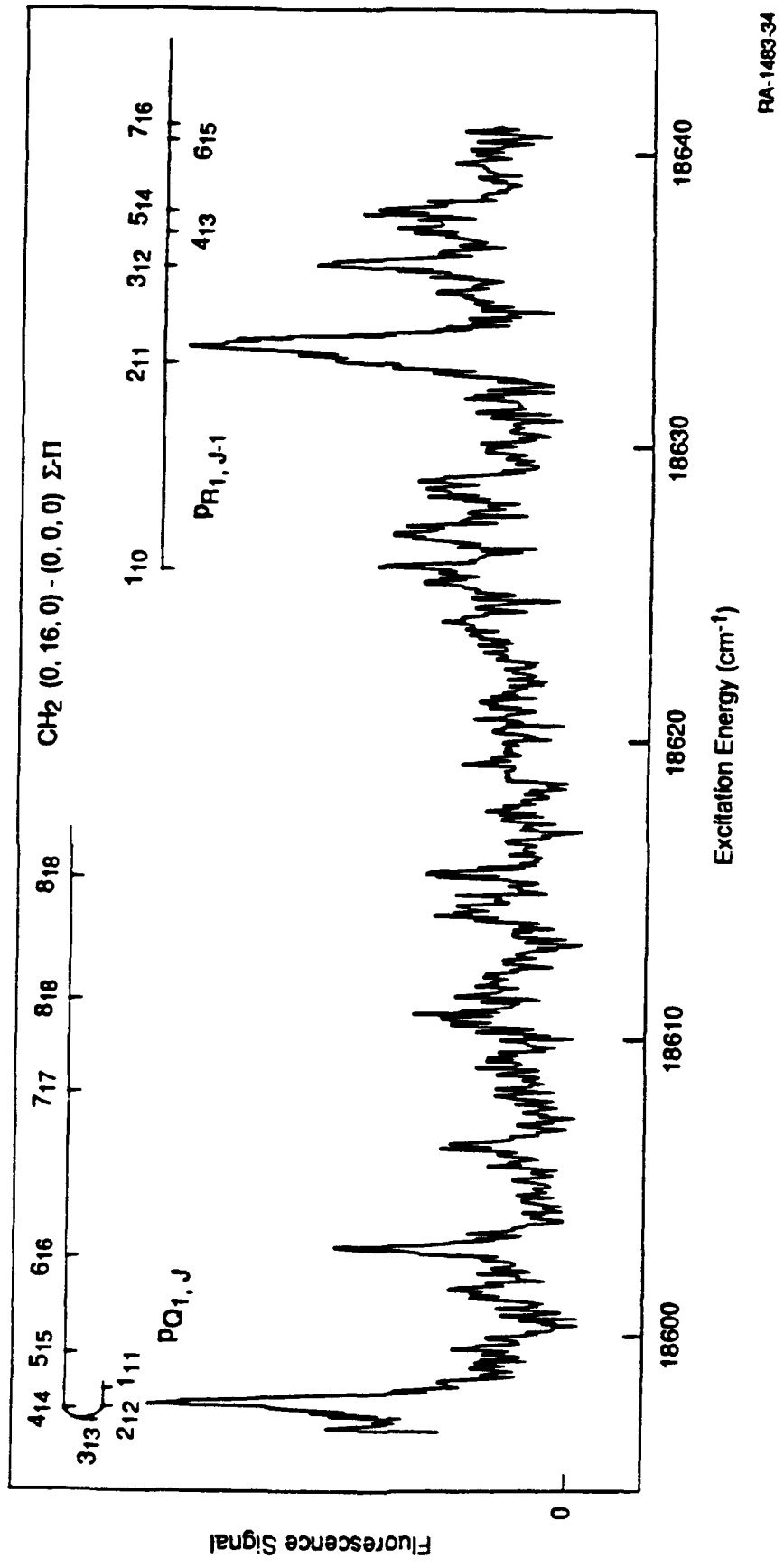
CH_2 (0, 16, 0) - (0, 0, 0) Σ-Π
$^pQ_{1, J}$
$^pR_{1, J-1}$
4_{14} 5_{15} 6_{16} 7_{17} 8_{18} 8_{18}
3_{13} 2_{12} 1_{11}
1_{10} 2_{11} 3_{12} 5_{14} 7_{16}
4_{13} 6_{15}
18600 18610 18620 18630 18640
Excitation Energy (cm^{-1})
Fluorescence Signal
0
RA-1483-34

Figure 3

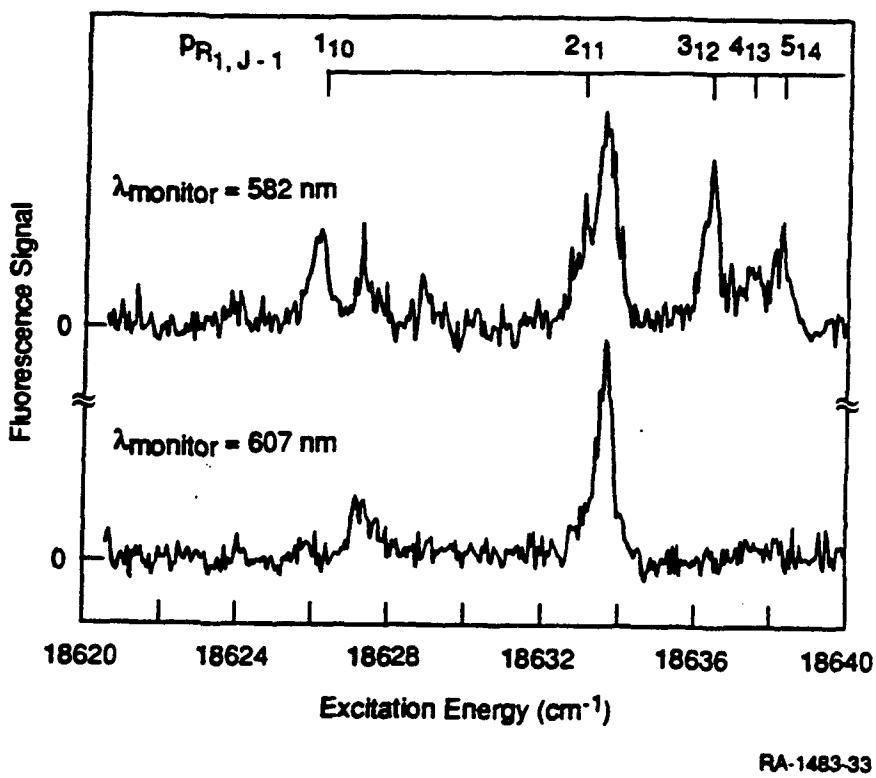
$P_{R_{1,J-1}}$
1_{10}
2_{11}
3_{12} 4_{13} 5_{14}
$\lambda_{monitor}$ = 582 nm
$\lambda_{monitor}$ = 607 nm
Fluorescence Signal
0
0
18620
18624
18628
18632
18636
18640
Excitation Energy (cm^{-1})
RA-1483-33

Figure 4

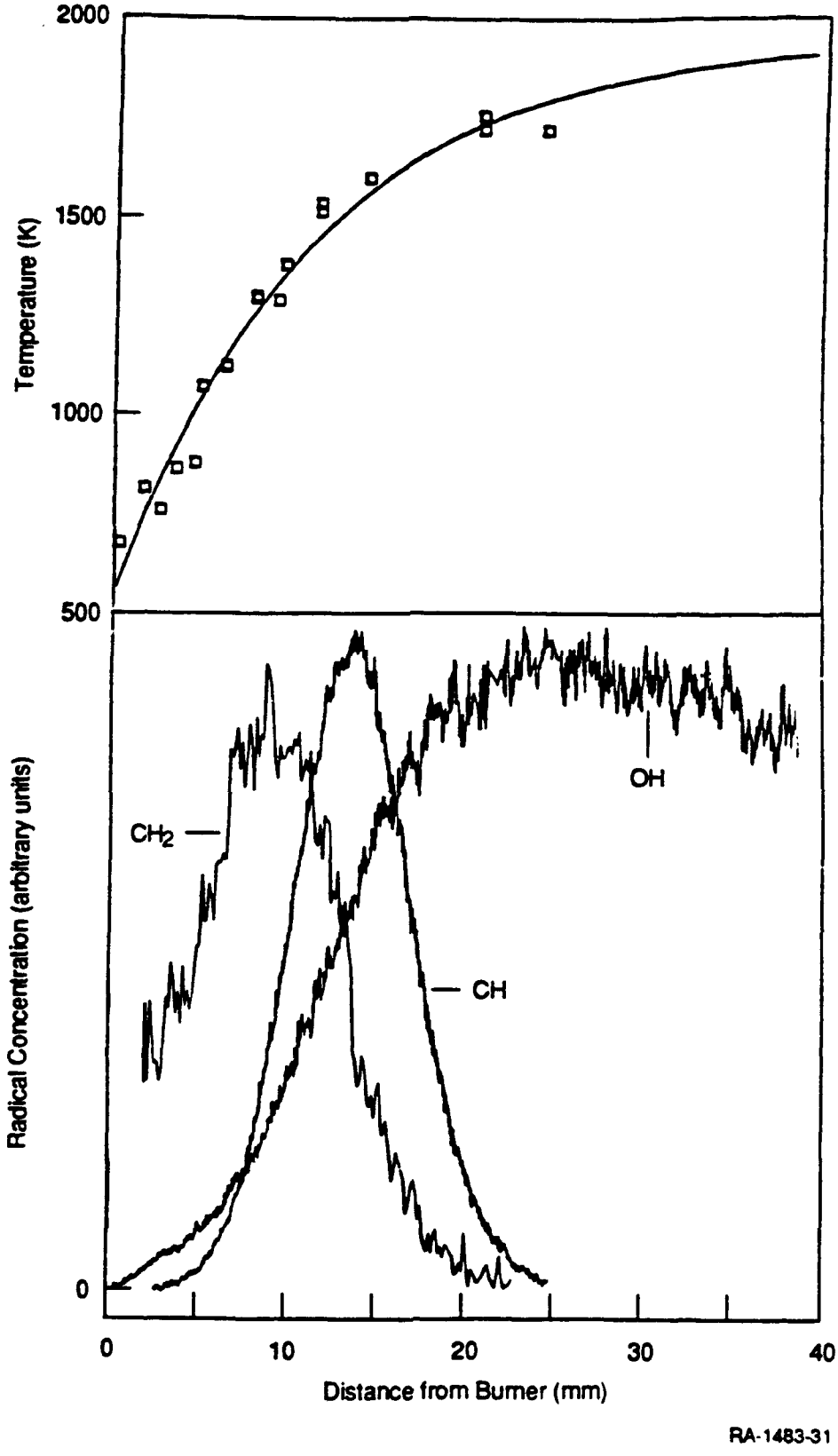
2000
1500
1000
500
Temperature (K)
Radical Concentration (arbitrary units)
CH2
OH
CH
0
0
10
20
30
40
Distance from Burner (mm)
RA-1483-31

Figure 5

Appendix J

RESONANCE ENHANCED MULTIPHOTON PHOTODISSOCIATION OF C_2H_2

RESONANCE-ENHANCED MULTIPHOTON PHOTODISSOCIATION OF C_2H_2

George A. Raiche, David R. Crosley and Richard A. Copeland
Molecular Physics Laboratory, SRI International
Menlo Park, California 94025

ABSTRACT

Emission from the $C^1\Pi_g$ and $d^3\Pi_g$ electronic states of C_2 is observed following resonant excitation of several vibrational levels in the $\tilde{A}\ ^1A_u$ electronic state in the acetylene molecule. Acetylene is excited via the $\tilde{A}$–$\tilde{X}$ electronic transition with the output of a frequency-doubled excimer-pumped dye laser (210-230 nm), and the fluorescence is dispersed with a monochromator. At low laser pulse energies laser-induced fluorescence in the C_2H_2 $\tilde{A}$–$\tilde{X}$ system dominates the emission spectrum; as the energy is increased, emission from the C and d states of C_2 becomes more important. At the highest laser powers investigated (~1 GW cm^{-2}), the C_2 photofragment fluorescence is the strongest signal. The temporal, spectral, laser fluence and pressure dependence of the various fluorescence signals are examined for excitation of different vibrational levels in the C_2H_2 $\tilde{A}$ state. Possible applications of C_2 fluorescence techniques to detection of C_2H_2 in combustion environments are discussed.

MP 89-195
October 10, 1989

INTRODUCTION

Acetylene is an important chemical intermediate in hydrocarbon combustion and is likely a key species in soot formation. Under conditions typical of flames, i.e. high temperatures and the presence of other interfering species, acetylene detection is difficult because of its complex spectroscopy, small transition moment, and the small fractional population in individual rovibronic levels. Such difficulties can limit the precision of flame diagnostic measurements. Even under these adverse conditions, acetylene has been observed in atmospheric-pressure flames using coherent anti-Stokes Raman spectroscopy[1] and, in low-pressure flames in our laboratory,[2] via a laser-induced emission scheme monitoring electronically excited C_2 photofragment (C_2^*) emission. Preliminary studies indicate that measurement of C_2^* laser-induced emission is a sensitive and selective laser method for detection of C_2H_2 in the harsh combustion environment. In order to make such studies quantitative, however, the acetylene dissociation mechanism and energy transfer properties of the photofragments, as well as the spectroscopy, must be understood. This room-temperature investigation examines these phenomena.

Acetylene absorbs light at many discrete ultraviolet wavelengths (210-240 nm), exciting individual rovibronic levels in the $\tilde{A}\ ^1A_u$ electronic state. A detailed rotational assignment and analysis of these transitions has been performed using absorption spectroscopy.[3,4] Laser-induced fluorescence (LIF)[5-8] and resonance-enhanced multiphoton ionization[8] studies have achieved rotational state specificity using tunable lasers as an excitation source. The dominant aspect of acetylene's $\tilde{A}\ ^1A_u$ - $\tilde{X}\ ^1\Sigma_g^+$ spectroscopy is the effect of the change of geometry in going from the ground to the excited state; because the $\tilde{A}$ state is trans-planar while the ground state is linear, both absorption and emission spectra are characterized by poor Franck-Condon overlap at small Δv.

Emission spectra therefore exhibit long progressions, and the absorption spectrum has relatively strong $\tilde{A}$–$\tilde{X}$ transitions from vibrational levels above the ground state. The non-diagonal nature of the transitions has been exploited in stimulated-emission pumping experiments, where highly excited ground state vibrational levels can be efficiently prepared.[9]

The photodissociation of acetylene is also a subject of considerable fundamental interest. Since C_2H_2 is a "simple" polyatomic molecule and photodissociates readily at ultraviolet wavelengths, its photolysis following excitation at 193 nm has been studied by several groups.[10-16] This excitation, which probably occurs through vibrationally excited levels of the $\tilde{A}$ state,[12] results in the production of C_2H and a hydrogen atom as the primary dissociation channel.[10] The dissociation energy of this process has been measured using a molecular time of flight method with mass-spectrometric detection[10] and Fourier transform infrared (FTIR) emission[12] of the C_2H fragment. A recent study using Stark anticrossing spectroscopy by Green et al.[17] obtained an upper limit lower than the currently accepted value. The exact location of the onset of this dissociation is uncertain.[17] At higher laser fluences, subsequent absorption of one or more photons results in the production of both C_2 and CH in various electronic states.[13-16] These pathways have been observed either by detecting the fluorescence of the photofragment directly[13-15] or by probing the C_2 product state distributions via LIF.[16] In addition, non-resonant photolysis of C_2H_2 has been observed following 266 nm excitation.[18] This mechanism must involve an initial multiphoton absorption step, since the single photon energy is insufficient to access the $\tilde{A}$ state.

In this manuscript, we report recent experiments on the ultraviolet photophysics and collision dynamics of acetylene. The fundamental difference between the preceding investigations and the current study is that we use narrowband tunable radiation to resonantly excite rovibronically-resolved features of the $\tilde{A}$–$\tilde{X}$ electronic transition, inducing

photodissociation. We have observed the efficient production of the C_2 $C^1\Delta_u$ and $d^3\Pi_u$ states as the laser tuned through the various C_2H_2 $\tilde{A}$-state resonance features. The ratio of C_2^* to C_2H_2 emissions is observed to be strongly dependent upon both laser power and photon energy; C_2^* signal intensity is quadratically dependent on laser energy at the experimentally accessible values, indicating a multiphoton process. Large (near gas-kinetic) cross sections for the quenching of photolysis products by acetylene are measured. If the C_2H fragment is energetically inaccessible at the wavelength of the first photon (an open question given the uncertainty of dissociation energy for acetylene), then the mechanism for resonantly-enhanced production of C_2^* must be different from the decomposition into C_2H and subsequent excitation process recently proposed for photolysis at 193 nm.[16] We discuss possible mechanisms for the C_2H_2 photolysis that are consistent with these observations and the thermochemistry of the C_2H_2/C_2 system.

EXPERIMENTAL APPROACH

The experimental approach is straightforward. Acetylene molecules are excited by the output of a pulsed, frequency doubled, tunable dye laser, and the resulting fluorescence is monitored at a right angle to the incoming excitation beam. We generate ultraviolet radiation by frequency-doubling the (430-460 nm) output of an excimer-pumped dye laser (Lambda-Physik FL2002) in a β-barium borate SHG crystal. Aceylene (Matheson), which is used directly from the cylinder without further purification, is slowly flowed through the fluorescence cell at pressures between 0.1 and 2.0 Torr. Up to 400 μJ of light near 220 nm can be delivered in a ~ 15 ns pulse to the center of the flow cell. In most of the experiments a 175 mm focal length quartz lens focuses the light to a 50 μm beam waist, giving a local power density approaching 1 GW/cm^2. The focal area is imaged onto the slit of a 0.3 m Heath monochromator and the dispersed fluorescence is monitored by a photomultiplier tube (EMI 9558). A transient digitizer (10 ns per channel) or a boxcar integrator captures the amplified photomultiplier output while a CAMAC based computer controls the experiment. The relative output power of the laser is monitored using a photodiode, and absolute energy measurements are made using a calibrated energy meter (Laser Precision Corp., RJP-735 head). For some studies, we use a small helium flow onto the entrance and exit windows to prevent the buildup of carbon deposits on the interior surfaces. These deposits can result in a 50% reduction of delivered laser energy over the course of several minutes.

RESULTS

We have observed strong fluorescence signals from both acetylene and C_2^* following resonant excitation of rotationally resolved vibronic bands in the C_2H_2

$\tilde{A}\ ^1A_u$ - $\tilde{X}\ ^1\Sigma_g^+$ electronic system. We characterized this fluorescence by dispersing the fluorescence, varying the laser power, changing the total pressure, and exciting different vibrational bands in the $\tilde{A}$ state. Before proceeding with a detailed discussion of these experiments, we should explain the spectroscopic nomenclature we will follow in this work. Because the electronic transition is from a linear state ($\tilde{X}$) to a bent state ($\tilde{A}$) the labeling of the normal modes is different in the two systems. We adopt the notation of Watson et al.[3], who label the transition from $\tilde{X}\ ^1\Sigma_g^+$, $v_4'' = 0$, $\ell'', = 0$ to $\tilde{A}\ ^1A_u$, $v_3' = 4$, $K' = 1$ as the $V_0^4K_0^1$ vibrational band. Both v_4'' and v_3' correspond to bending modes in the acetylene molecule; the other vibrational quantum numbers follow conventional labeling and are described in Ref. 3.

Excitation and Fluorescence Spectra

Excitation spectra of acetylene are acquired throughout the ultraviolet region between 213 and 223 nm. Most bands in this region have a similar shape, with a strong R head and Q and P branches marching out to longer wavelengths. The band shapes are similar to those plotted in Ref. 6 and 8. One of the more interesting regions is that near the $V_0^4K_0^1$ vibrational band. An excitation spectrum from 213 to 223 nm, using a filtered (UG-11, 3 mm) phototube to detect fluorescence from approximately 250 to 320 nm, shows an abrupt decrease in the fluorescence intensity at excitation wavelengths above ~46500 cm^{-1}. Qualitatively this decrease in fluorescence efficiency confirms a recent result of Fujii et al.[8], who compare the intensity of absorption and laser-induced fluorescence spectra. They attribute this falloff to a dissociation threshold for HCC–H production near this energy.[8]

Figure 1 is the fluorescence emission spectrum, at 2 nm resolution, corresponding to the excitation of the R-head of the $V_0^4K_0^1$ vibrational band. Surprisingly, the spectrum is dominated by C_2 emission in the 350-600 nm range (Fig. 1, top), although the C_2H_2 $\tilde{A} \rightarrow \tilde{X}$ LIF is also observed in the 290-340 nm region (Fig. 1, bottom). These spectra are not corrected for the response of the detection system, which is expected to decrease

markedly for our detection system below ~ 350 nm. Our C_2H_2 LIF spectra for $\nu_3' = 4$ and $\nu_3' = 3$ are qualitatively similar to those obtained by Stephenson et al.[6] for $\nu_3' = 0$ to 3, although we observe the C_2^* emission at longer wavelengths. As will be discussed below, the ratio of C_2^* emission to C_2H_2 $\tilde{A}$-state LIF is strongly dependent on both excitation wavelength and laser intensity.

The dominant features of the acetylene LIF emission spectrum, the series of large peaks extending from 340 to 570 nm, are attributed to the C_2 Deslandres-d'Azambuja (DdA) ($C\ ^1\Pi_g \rightarrow A\ ^1\Pi_u$, 340-420 nm) and Swan ($d^3\Pi_g \rightarrow a^3\Pi_u$, 430-570 nm) systems. This is the first observation of the production of C_2 emission from resonant photodissociation of C_2H_2 using tunable light. With sufficient laser intensity (~1.5 MW/cm^2 at 1 Torr of acetylene) these emissions can be seen with the naked eye. The spectrum of Figure 2 is acquired with a 30 ns integration gate at the peak of the temporal evolution of the fluorescence in order to minimize the effects of collisional relaxation on the emission. These higher resolution spectra show population into v' = 4 of the d state, and v'=2 of the C state. When we tune off C_2H_2 features, both the C_2H_2 LIF and the C_2^* signals disappear. The production of CH radical, reported in studies of acetylene excited by 193 nm radiation,[13,15] is not observed.

Time and Pressure Dependence of the Fluorescence Signals

The time and pressure dependences of the acetylene and C_2 emission signals provide information about the source of the C_2^*. If the C_2^* signal rises promptly with the laser pulse at low pressures then the C_2^* is probably a photodissociation product, while a slow or pressure dependent rise might be attributed to a chemiluminescent bimolecular reaction. In these experiments we carefully examine the rise of the C_2^* fluorescence signals and find them both independent of the C_2H_2 pressure, and also faster than the response of the detection system (~10 ns). Therefore, both the DdA and the Swan system are produced

by the absorption of photons by C_2H_2 or one of its photodissociation products. We see no evidence for a chemiluminescent or other bimolecular chemical reaction.

The effect of acetylene pressure on the temporal evolution of the fluorescence is examined following excitation of the R bandheads of the $V_0^3K_0^1$ (220.6 nm) and $2_0^1V_1^2K_0^1$ (221.6 nm) vibronic bands. We observe the fluorescence with a monochromator of 2.0 nm bandpass set to several wavelengths which correspond to emission from the $\tilde{A}$ state of C_2H_2, and the C and d states of C_2. This bandpass for C_2H_2 covers a number of vibrational features which we do not attempt to assign. We sum 1000 laser shots to obtain a fluorescence decay curve, and fit the temporal evolution to a single-exponential from 90 to 10% of the peak signal. The fitted decay constants are than plotted versus the C_2H_2 pressure to obtain a phenomenological collisional removal rate constant, k, from the slope of the line. The intercept, under ideal circumstances, would be the reciprocal of the radiative lifetime. Results for the collisional removal and lifetimes of both C_2H_2 and C_2^* species are summarized in Table I.

Before discussing the quantitative aspects of these results, we must first describe exactly the quantity we are measuring. We are recording the time dependence of the fluorescence within a certain bandpass of the monochromator. In these measurements the monochromator bandpass has a triangular shaped response function with a 4 nm full width at half height. If C_2H_2 collisions only remove molecules from the excited electronic state and cause no rotational and vibrational energy transfer, the value obtained from the slope would be the electronic quenching decay constant. We have little or no information about the relative magnitude of these processes in either C_2H_2 or the excited states of C_2. Pending more detailed investigations we will consider the values in Table 1 simply as phenomenological removal rate constants, given for the detected fluorescence wavelength.

Following excitation of C_2H_2 $v_3' = 3$, we measure a total removal rate constant of $(5.2 \pm 0.4) \times 10^{-10}$ cm^3 s^{-1}, while for the $v_2' = 1$, $v_3' = 2$ vibrational level we measure

$k = (6.5 \pm 0.7) \times 10^{-10}$ cm^3 s^{-1}. The uncertainty given is two standard deviations of the fit of the decay constant versus pressure to a line. We find the level with one quantum of vibration in the ν_2 mode is removed slightly faster than the pure ν_3 level; however, the difference is just outside the respective error bars of the two measurements. Such small differences could easily be caused by vibrational energy transfer as described above. Our results agree well with the studies of Abramson et al.[5] for $\nu_3' = 3$ and are slightly faster than those of Stephenson et al.[6] for $\nu_3 = 0,1$, and 2. From comparison with these studies we observe that the removal rate by C_2H_2 tends to increase with more vibrational excitation in the $\tilde{A}$ state, and only small differences are found for different modes at similar energies.

The collisional quenching of the C_2 C and d states by acetylene is studied in the same manner as for the C_2H_2 $\tilde{A}$ state. Removal rate constants for the C state are (3.5 ± 0.3) and $(4.3 \pm 0.2) \times 10^{-10}$ cm^{3}s^{-1} following excitation of the $V_0^3K_0^1$ and $2_0^1V_1^2K_0^1$ bands of acetylene, respectively. For the d state, excitation of both vibrational levels yield values of $(1.0 \pm 0.1) \times 10^{-10}$ cm^{3}s^{-1}. For Swan emission the observation window covers the several vibrational levels in the $\Delta v = +1$ series (~470 nm), while for the DdA observations the $v' = 0,1$ levels of the $\Delta v = 0$ series (~385 nm) are selected.

Regardless of the resolution used to detect emitting product species or the details of the state specific energy transfer, time dependent measurements on C_2 fluorescence should yield the same result for different excitation methods, if the resulting distribution over electronic and vibrational states is the same for each excitation scheme: Such is the case for our d state measurements, in which Swan emission is generated by exciting both the acetylene $V_0^3K_0^1$ and $2_0^1V_1^2K_0^1$ transitions. The comparable magnitude of the k's and zero-pressure fluorescence lifetimes indicate that the vibronic distributions of C_2^* produced at each wavelength are similar. On the other hand, the k's and zero-pressure lifetimes measured for the C state under the same conditions are different for the two excitation wavelengths. Therefore, different C state product distributions result from exciting

acetylene features with photons that differ in energy by only ~ 200 cm^{-1}, whereas the d state distribution is pump-wavelength independent. This conclusion is corroborated by fluorescence spectra acquired as a function of excitation wavelength, in which the C state emissions resulting from pumping the $V_0^3K_0^1$ and $2_0^1V_1^2K_0^1$ transitions have different intensity distributions, while the d emissions are nearly identical (Figure 2). Examining Figure 2 C state spectra carefully, we note stronger emission from v' = 1 than from v' = 0 following excitation of the $2_0^1V_1^2K_0^1$ transition. This implies a larger fraction of v' = 1 is generated from pumping the combination feature as opposed to pumping the pure feature. For time resolved studies we observe emission from v' = 1 and v' = 0 together, following excitation of features separately. Since the rate constant for removal of the combination band emission is faster than that for the pure band (Table I) we may conclude, therefore, that the v' = 1 level of the C state is depleted faster than the v' = 0 level.

Zero-pressure intercepts for C_2 presented in Table I are similar in magnitude to the existing data for the d (Refs. 16,19 and 20) state and differ slightly from the only previous C state fluorescence lifetime (Ref. 20). Our measurements do not resolve individual rotational and vibrational levels but represent an average over the distributions created by the photodissociation process. Our C-state measurement of ~ 50 ns is slower than the ~ 30 ns measurement of Ref. 20. Curtis et al.[20] report little variation in the lifetime with vibrational level in the C state, so the vibrational averaging cannot explain the differences. This difference requires further investigation. The zero pressure intercepts we measure for C_2H_2 for the two excitation transitions are similar, both being slightly faster than those of Stephenson et al[6] for lower vibrational levels. The large variations in lifetimes between different rotational levels, attributed by Scherer et al.[7] to a Fermi interaction within $V_0^3K_0^1$ make a detailed examination of our rotationally unresolved results impossible. Rotational level specific results are required for a complete understanding.[7]

To determine the relative yield of C_2^* as a function of vibrational excitation in the C_2H_2 $\tilde{A}$ state, emission spectra were acquired by pumping the R-heads of the V_0^4, V_0^3, V_0^2, and V_0^1 bands near 215.9, 220.6, 225.6, and 231.0 nm, respectively, at constant (~50 μJ/pulse) laser energy. These spectra are shown in Figure 3. The ratio of C_2 to C_2H_2 emission in the spectra are strongly dependent upon both the laser intensity and the C_2H_2 A state vibrational level. Specifically, the ratio increases with both increasing vibrational excitation and laser intensity. In the $v_3' = 1$ spectrum, for example, the emission is dominated by that of C_2H_2 features seen in second order between 540-600 nm; only a trace of the Swan emission at ~ 520 nm is seen. In the $v_3' = 2$ spectrum, however, the C_2^* and C_2H_2 emissions are similar in magnitude and by $v_3' = 3$ the C_2^* signals dominate the emission. A phenomenological threshold for the production of C_2 Swan emission therefore appears between excitation to $v_3' = 1$ and $v_3' = 2$ of the C_2H_2 $\tilde{A}$ state.

The dependence of emission product ratios on laser intensity suggests that the pathways to C_2H_2 and C_2^* differ with respect to photon order. We undertook power dependence measurements for the C_2 signals at 385 nm (DdA) and 470 nm (Swan), and for C_2H_2, at several pump wavelengths. A typical series is depicted in Figure 4. Here the C_2 Swan signal exhibits a quadratic power dependence (circles) under conditions in which the C_2H_2 LIF appears to be a slightly saturated 1-photon process (squares). The C_2 DdA emissions also show a quadratic power dependence. At lower laser intensities, the C_2H_2 LIF signal is linearly dependent on laser power. Because of the differences in photon order for the C_2^* and C_2H_2 emissions, the ratio of C_2 to C_2H_2 signals are strongly dependent upon the experimental laser power. Simple spectral normalization for laser power is not useful in the case of mixed photon orders. Care must be taken to assure that laser power during the course of an emission scan remains constant if meaningful comparisons of C_2 and C_2H_2 emission strengths are to be made.

DISCUSSION

The production of excited C_2^* from acetylene is of interest for both fundamental photophysical considerations and as a combustion diagnostics tool. The strength and spectral location of the C_2^* emissions, coupled with the apparent efficiency of its production from C_2H_2 using a frequency-doubled dye laser, are promising for application to the monitoring and imaging of C_2H_2 in flames. In addition, the C_2 radical itself is a major hydrocarbon flame emission source. To properly apply C_2^* signals as a diagnostic for C_2H_2 in flames, therefore, requires characterization of its production and removal mechanisms. We will describe several mechanisms for the production of excited C_2 from acetylene photolysis which are consistent with its resonant production through the C_2H_2 $\tilde{A}$ state, the observed photon dependence of the C_2^* and C_2H_2 emission signals, and the pertinent thermochemical and photon energies.

While the production of C_2^* has been observed in earlier 193 nm acetylene photolyses, the role of the C_2H_2 $\tilde{A}$ state (and higher states) is unclear. Emission from both CH (A) and C_2 (C, d, A) has been reported in these studies.[13,14] The first step of the photolysis at 193 nm is thought to be a transition to one or several highly excited levels of C_2H_2 $\tilde{A}$ which persist for 10^{-10}-10^{-12} s prior to subsequent absorption or predissociation.[14] The predissociation yield to C_2H has been estimated at 15%.[10] Recent studies that probe the C_2 fragment via LIF also implicate C_2H as an important intermediate in the 193 nm photodissociation.[16] Since we excite the C_2H_2 lower on the $\tilde{A}$ potential energy surface with 215-230 nm photons, however, the fluorescence quantum yield is substantial with $\tilde{A}$ state radiative lifetimes on the order of 10^{-7}s. Dissociation to C_2H must thus be significantly slower at the wavelengths we use in our study compared to 193 nm.

Our experiments clearly demonstrate that resonant transitions to the $\tilde{A}$ state are necessary for production of C_2^* at these photon energies. The processes that the $\tilde{A}$ state can subsequently undergo determine the production mechanism for C_2^*. We see indications (C_2 C state k's, emission intensity distributions) that the distributions of some but not all photolysis products depend on the vibrational mode excited in C_2H_2, confirming that the overall photolysis mechanism is sensitive to the nature of the $\tilde{A}$ state. However, the energetics of the reasonable unimolecular processes for this system indicate that the $\tilde{A}$ state cannot be the direct precursor to the excited C_2. A higher state of acetylene optically coupled to the $\tilde{A}$ state, or a chemical species to which C_2H_2 $\tilde{A}$ promptly evolves, must be the intermediate through which we form C_2^*.

Our discussion of the mechanism of C_2^* production is dominated by a consideration of the relevant thermochemical and photon energies for the "reasonable" processes. Having measured a quadratic dependence of C_2^* signal intensity on laser energy, we attribute production of C_2^* to either a two-photon process, *or* a three-photon process in which one step is saturated. Bimolecular and other collisional chemiluminescent processes are ruled out by the prompt rise time of the C_2^* emission. Given these constraints, we briefly consider the processes that can occur following the absorption of each photon by C_2H_2 or its photodissociation products.

After the resonant absorption of the first photon acetylene can undergo several processes. It can fluoresce, change electronic state via collisions or nonradiative processes, absorb another photon, or dissociate. Little direct experimental information is available on the fraction of molecules along each pathway; however, the time dependence of the fluorescence places a limit on the rates of these processes. At low pressures only a small fraction of the molecules excited to the $\tilde{A}$ state have time during the laser pulse (~10 ns) to either dissociate or change electronic state since the fluorescence lifetimes of these states are ~ 200 ns.[5,6] This differs significantly from excitation at 193 nm where dissociation is

much faster than fluorescence and no emission from the $\tilde{A}$ state is observed[13,16]; the pathways for the production of C_2 and CH at 193 nm[13-16] may differ from those applicable to this study. From the energetics we know at least one more photon must be absorbed during the laser pulse by the excited species to generate C_2^* emission. Although a relatively slow process, the carbon-hydrogen bond could be broken at these energies to form C_2H. The exact energy of this dissociation threshold is currently under debate. Recent experiments place the dissociation of threshold somewhere between 520 and 570 KJ mol^{-1} above the $\tilde{A}$ state.[17] This corresponds to between 1 and 5 quanta in the bending mode ν_3. We observe a large increase in C_2^* production as we tune the excitation laser through this region. This C_2^* emission could result from the absorption of two more photons by C_2H with subsequent ejection of another H atom. The opening of the dissociation channel between $\nu_3' = 1$ and $\nu_3' = 2$, as indicated by the most recent determination of the threshold,[17] could explain the abrupt increase observed in C_2^* signal following excitation higher than $\nu_3' = 1$. However, considering the small fraction of C_2H which could be produced during the laser pulse and subsequently excited, a process in which the C_2H_2 itself is excited may be a more likely pathway. Rapid v-dependent intersystem crossing to nearby triplet states of C_2H_2 and subsequent excitation through the triplet manifold could also be important in C_2^* production. But, as with C_2H dissociation, this must be a minor pathway to be consistent with the time dependence of the fluorescence.

A probable scenario is that the $\tilde{A}$ state molecules themselves absorb another photon to states of C_2H_2 lying just below the ionization potential at ~11.4 eV.[7] Little is known about this region. One photon vacuum ultraviolet experiments show a long progression of electronic states that are very structured and dissociate to C_2H.[2] This might explain the differences in efficiency of C_2^* production between different vibrational levels. Although

symmetry restrictions dictate that the same states cannot be accessed as in the one photon spectrum, we believe the two photon spectrum might have similar structure. A two-photon transition through C_2H_2 is of sufficient energy to yield electronically and vibrationally excited C_2 and is obviously consistent with the quadratic power dependence. This transition energy is insufficient, however, to access CH (A), which could account for our failure to observe the CH A→X emission reported in 193 nm dissociation studies. The energetics of the two-photon transition require that molecular H_2 be eliminated from C_2H_2 in a concerted fashion. Such a process is thermochemically favored relative to $C_2 + 2H$. The potential surface to which C_2H_2 must be excited, symmetry $\Sigma_g^+ \leftarrow A_u \leftarrow \Sigma_g^+$ for a parallel transition,[22] correlates to A_1 symmetry in the C_{2v} point group appropriate for cis-bent C_2H_2.[23] However, the corresponding spatial arrangement of C_2 C $^1\Pi_g$ or d $^3\Pi_g$ + H_2 ($^1\Sigma_g^+$) correlates to A_2+B_2 in C_{2v}. A smooth correlation to the molecular elimination products therefore does not exist. Even if the potential curves are such that an avoided crossing allows correlation from C_2H_2 to $C_2 + H_2$, potential barriers for such symmetry-forbidden processes in related molecules[24] are estimated to be on the order of 4 eV, well above the excess energy available (~1 eV) in our hypothetical two-photon transition. Therefore, unless the barrier to symmetry-forbidden H_2 elimination in C_2H_2 is unusually small, this dissociation mechanism appears unlikely in our case.

At these energies (two photons above the C_2H_2 ground state) decomposition to $C_2H + H$ could be extremely rapid. Either highly excited C_2H_2, or the resulting C_2H, could serve as an intermediate for absorption of a third ultraviolet photon. This third photon, if absorbed by C_2H_2, would take the acetylene to a region above the ionization threshold where it could dissociate to a variety of fragments, including C_2^*. This energy region has been investigated in a one photon study in which electronically excited photofragments are also generated.[25] Alternatively, C_2H produced following the two-photon absorption might dissociate directly to C_2^* upon absorption of a third photon.

Unfortunately, our single laser experiment in incapable of distinguishing between these processes and we cannot determine a mechanism unambiguously. Two-wavelength, time delayed, two-laser experiments would be useful to unravel the mechanism. On the other hand, the importance of the $\tilde{A}$ state as an intermediate for photodissociation of C_2H_2 is clearly established, and the $\tilde{A}$ state can provide a stepping stone to examine the dynamics and spectroscopy of C_2H_2 and C_2H in highly excited states.

CONCLUSIONS

We have observed the unimolecular production of (emitting) singlet and triplet excited states of C_2, as well as C_2H_2 $\tilde{A}$–$\tilde{X}$ LIF, from the resonant excitation of the C_2H_2 near-UV $\tilde{A} \rightarrow \tilde{X}$ transition. The power dependence of the C_2^* emission signal is found to be quadratic, in the power regime where the one-photon C_2H_2 transition appears to be saturated. While zero-pressure lifetimes are consistent with previous measurements, the quenching rate constants measured as a function of v' in C_2H_2 $\tilde{A}$ are significantly larger than those previously measured for smaller values of v'. In addition, an apparent threshold for the production of C_2^* has been observed. The fluorescence yield ratio of C_2H_2 to C_2 is found to be strongly dependent on both laser intensity and vibrational level in the $\tilde{A}$ state.

These results are consistent with a model for the unimolecular photolysis of C_2H_2 involving a resonant single-photon excitation to the $\tilde{A}$ state, followed by photon absorption by the highly excited C_2H_2 or the dissociation product C_2H. The timescale of the photodissociation is < 10 ns, excluding bimolecular processes from consideration as mechanisms for C_2^* production. Our data, and the uncertainty in dissociation threshold for HCC-H,[17] does not allow us to unambiguously choose one mechanism as more likely in the resonantly enhanced photolysis.

Preliminary flame studies in this laboratory indicate that the laser-induced C_2 Swan emissions are useful as a diagnostic for acetylene. If the mechanism for C_2^* production involves only transitions in the C_2H_2 manifold, then application of this diagnostic in flame studies should be straightforward. If a mechanism involving C_2H is operative, however, a

significant interference might be present in flame systems where C_2H itself is a combustion intermediate.

ACKNOWLEDGEMENTS

The authors thank David M. Golden, Peter G. Green, and Jay B. Jeffries for useful discussions, and the authors of Ref. 17 for a preprint of their work. We thank Mark J. Dyer for technical assistance. This research was sponsored by the Aero Propulsion and Power Laboratory of the Air Force Wright Research and Development Center, and the Physical Sciences Department of the Gas Research Institute.

REFERENCES

1. R. L. Farrow, R. P. Lucht, W. L. Flower, and R. E. Palmer, in Twentieth (International) Symposium on Combustion, p. 1307 (Combustion Institute, Pittsburgh, 1984).

2. G. A. Raiche, D. R. Crosley, and R. A. Copeland, in Advances in Laser Science-IV, in press.

3. J. K. G. Watson, M. Herman, J. C. van Craen, and R. Colin, J. Molec. Spectrosc. 95, 101 (1982).

4. J. C. van Craen, M. Herman, R. Colin, and J. K. G. Watson, J. Molec. Spectrosc. 111, 185 (1985) and references therein.

5. E. Abramson, C. Kittrell, J. L. Kinsey, and R. W. Field, J. Chem. Phys. 76, 2293 (1982)

6. J. C. Stephenson, J. A. Blazy, and D. S. King, Chem. Phys. 85, 31 (1984).

7. G. J. Scherer, Y. Chen, R. L. Redington, J. L. Kinsey, and R. W. Field, J. Chem. Phys. 85, 6315 (1986).

8. M. Fujii, A. Haijima, and M. Ito, Chem. Phys. Lett. 150, 380 (1988).

9. E. Abramson, R. W. Field, D. Imre, K. K. Innes, and J. L. Kinsey, J. Chem. Phys. 83, 453 (1985).

10. A. M. Wodtke and Y. T. Lee, J. Phys. Chem. 89, 4744 (1985).

11. F. Shokoohi, T. A. Watson, H. Reisler, F. Kong, A. M. Renlund, C. Wittig, J. Phys. Chem. 90, 5685 (1986).

12. T. R. Fletcher and S. R. Leone, J. Chem. Phys. 90, 871 (1989).

13. H. Okabe, J. Chem. Phys. 62, 2782 (1975).

14. J. R. McDonald, A. P. Baronavski, and V. M. Donnelly, Chem. Phys. 33, 161 (1978).

15. H. Okabe, R. J. Cody, and J. E. Allen Jr., Chem. Phys. 92, 67 (1985).

16. R. S. Urdahl, Y. Bae, and W. M. Jackson, Chem. Phys. Lett. 152, 485 (1988).

17. P. G. Green, J. L. Kinsey, and R. W. Field, J. Chem. Phys., in press.

18. B. B. Craig, W. L. Faust, L. S. Goldberg, and R. G. Weiss, J. Chem. Phys. 76, 5014 (1982).

19. C. Naulin, M. Costes and G. Dorthe, Chem. Phys. Lett. 143, 496 (1988) and references therein.

20. L. Curtis, B. Engman, and P. Erman, Physica Scripta 13, 270 (1976).

21 M. Suto and L. C. Lee, J. Chem. Phys. 80, 4824 (1984).

22. C. K. Ingold and G. W. King, J. Chem. Soc. 1953, 2702 (1953).

23. G. Herzberg, Electronic Spectra of Polyatomic Molecules, D. van Nostrand Co., Inc. (New York, 1966).

24. K. Raghavachari, J. J. Frisch, J. A. Pople, and P. von R. Schleyer, Chem. Phys. Lett. 85, 145 (1982).

25. J. C. Han, C. Ye, M. Suto, and L. C. Lee, J. Chem. Phys. 90, 4000 (1989).

Table I. Slopes and intercepts from plots of the fluorescence decay constants versus C_2H_2 pressure.

Excite	Slope, k (10^{-10}cm^3 s^{-1})	Intercept (ns)	Emitting Species	Detected Wavelength (nm)
$V_0^3K_0^1$	5.19 ± 0.43	205 ± 37	$C_2H_2(\tilde{A})$	291.5
	3.53 ± 0.29	49.3 ± 1.4	$C_2(C)$	381.5
	1.06 ± 0.04	132 ± 12	$C_2(d)$	466.5
$2_0^1V_1^2K_0^1$	6.50 ± 0.72	162 ± 23	$C_2H_2(\tilde{A})$	291.5
	4.25 ± 0.26	55.2 ± 1.5	$C_2(C)$	381.5
	1.03 ± 0.19	127 ± 6.4	$C_2(d)$	466.5

FIGURE CAPTIONS

Figure 1. Fluorescence emission spectrum resulting from excitation of the acetylene $V_0^3K_0^1$ R-head near 215.9 nm. The acetylene pressure is ~ 1 Torr and the monochromator bandpass is 4.0 nm. The spectrum has not been corrected for detection wavelength response, which should peak near 500 nm and decrease toward the ultraviolet and infrared. Detection gating was set to observe prompt emission following the laser pulse. The upper spectrum is dominated by C_2^* C→A and d→a emissions. A 15× magnification of the upper spectrum is given below. It shows C_2H_2 $\tilde{A}\rightarrow\tilde{X}$ unassigned vibronic transitions.

Figure 2. C_2^* emission spectra (left panels: C→A $\Delta v=-1$; right panels: d→a $\Delta v=-1$) following photolysis through C_2H_2 $\tilde{A}$. We excite the R-heads of the $2_0^1V_1^2K_0^1$ (top) and $V_0^3K_0^1$ (bottom) band. All spectra are acquired under identical conditions and are plotted on the same vertical scale. Note that while the d→a emission profiles are nearly identical for both pump wavelengths, the C→A emissions following excitation are more intense, and suggest greater vibrational excitation after pumping $2_0^1V_1^2K_0^1$ than from $V_0^3K_0^1$. This suggests that the mechanism for production of C_2^* is very sensitive to the nature of the C_2H_2 $\tilde{A}$ state intermediate vibrational levels.

Figure 3. Fluorescence emission spectra resulting from excitation of acetylene $v_3' = 3$, $v_3' = 2$, and $v_3' = 1$ R-heads near 220.6, 225.6, and 231.0 nm, respectively. The laser energy is approximately 50 μJ/pulse. Note the near absence of C_2^* Swan emission near 520 nm in $v_3' = 1$ spectrum. Maximum C_2^* yield is obtained at high laser energy and high v_3'. The finger-like structure to the red of 550 nm is C_2H_2 $\tilde{A} \rightarrow \tilde{X}$ emission in second order, while the off-scale peak is scattered laser light.

Figure 4. Intensities of C_2^* (Swan) emission and C_2H_2 LIF as a function of laser energy at 215.9 nm ($V_0^4K_0^1$). The C_2^* emission scales approximately quadratically with laser energy, while the C_2H_2 LIF is apparently a saturated single-photon process at the laser energies necessary to induce strong C_2^* emission. At lower laser energies, C_2H_2 LIF scales linearly.

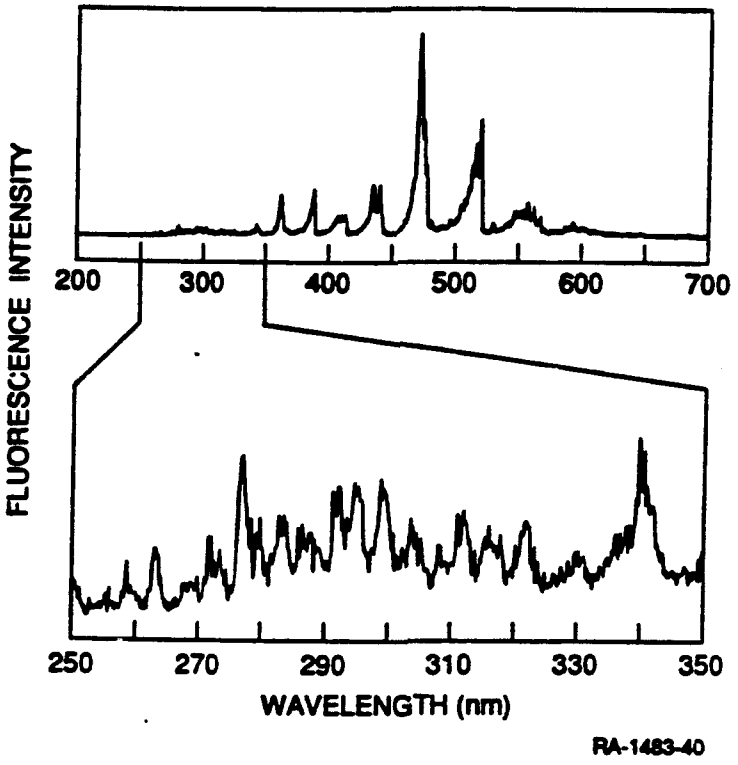
FLUORESCENCE INTENSITY
200
300
400
500
600
700
250
270
290
310
330
350
WAVELENGTH (nm)
RA-1483-40

Figure 1

J-27 and J-28 MISSING FROM DOCUMENT

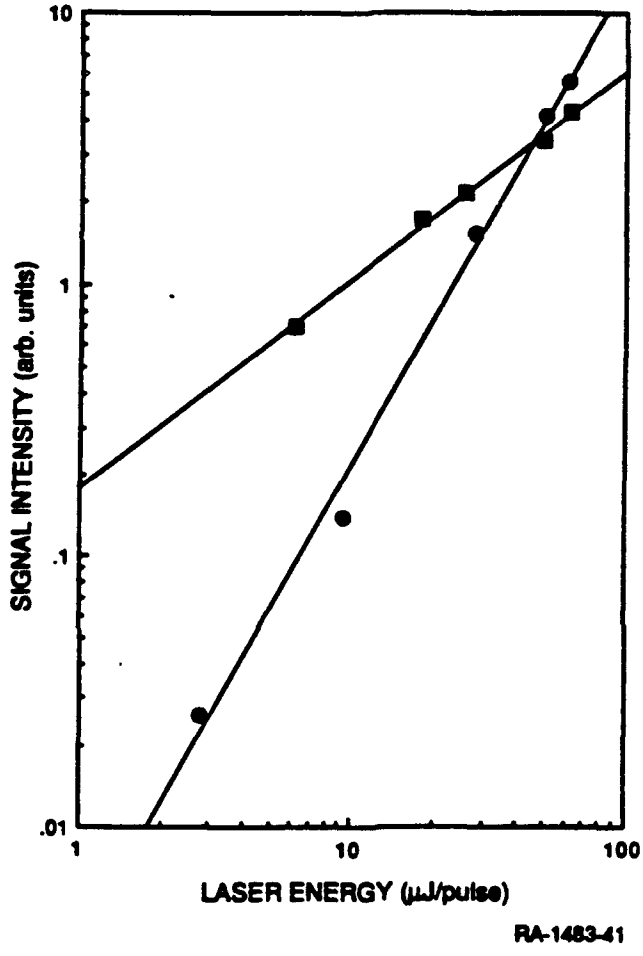
10
1
.1
.01
SIGNAL INTENSITY (arb. units)
1
10
100
LASER ENERGY (μJ/pulse)
RA-1483-41

Figure 4